universität wien

MAGISTERARBEIT

Titel der Magisterarbeit

„The Determination of Element Abundances in Cool Giants. Häufigkeitsbestimmung in kühlen Riesen."

Verfasser

Bernhard Wenzel Ing. Bakk.rer.nat.

angestrebter akademischer Grad

Magister der Naturwissenschaften (Mag. rer. nat.)

Wien, April 2012

Studienkennzahl laut Studienblatt: A 066 861
Studienrichtung laut Studienblatt: Magisterstudium Astronomie
Betreuer: Doz. Dr. Thomas Lebzelter

This thesis was done with data from the European Southern Observatory

Für Barbara

Contents

Chapter 1

Introduction

1.1 AGB-stars

A good introduction into the topic of AGB-stars is the book "Asymptotic Giant Branch Stars" of Habing and Olofsson (Habing and Olofsson, 2003). The introduction of this thesis is mainly based on this book, on the very good introduction of the PhD-thesis of Michael Lederer (2009) and a conference paper from A. I. Karakas (Karakas, 2011).

All common stars, with an initial mass range from 0.8 to 8 $M_\odot$ will become AGB-stars. This will also be the fate of our own Sun in approximately $4.5 \cdot 10^9$ years. The AGB-phase is only a brief moment, about 1% of the lifetime of the star on the main sequence. As one can see in the HRD presented in Fig. 1.1, AGB-stars are evolved objects with high luminosities and low temperatures. The temperature range is typically from 2500 K to 4000 K. AGB-stars have passed core hydrogen (H) and core helium (He) burning. They prevent gravitational collapse with H-shell and He-shell burning processes (Karakas, 2011).

As mentioned, the asymptotic giant branch (AGB) phase of a star is a rather short episode in its lifetime. When the nuclear burning process of a medium to intermediate mass star stops, it ends as a white dwarf along with a planetary nebula which may be visible after a few thousand years. Before this happens, the star will grow to a very large diameter, and it has also a very high luminosity. As a consequence of the bigger star radius, the effective temperature T_{eff} will become lower than it was before. Therefore, these stars are also seen in other galaxies, which are further away than e.g. the Local Group (Rejkuba, 2004). The structure of an AGB-star already contains a

degenerate C/O-core in its center, which will later become the white dwarf. (Habing and Olofsson, 2003).

Red giant branch stars (RGB-stars) are quite similar to AGB-stars. In the "E-AGB"-phase (early AGB phase), the stars are bluer than RGB-stars during their last phase, an AGB-star begins "thermally pulsing" (TP-AGB). The "thermally pulsing phase" is the reason the star ejects mass at high rates. This leads to the stopping of nuclear reactions and finally to a transition to a white dwarf. Evolved stars like AGB-stars also tell us about the star formation history in other galaxies. Because of their mass-loss, they play a role in the enrichment of new elements or s-process nuclei in the Interstellar Medium (ISM). (Habing and Olofsson, 2003).

1.2 A brief sketch of history

The HR-Diagram (HRD) was introduced between 1911 and 1914 by Hertzsprung and Russel and compares the stars temperatures (colours) with their luminosities. The HRD (Fig. 1.1) is dominated by the main-sequence (MS) of stars, corresponding to the longest phase of H-burning, in the stellar life. In addition, we find in the HRD, red giants which are located above the MS and dwarfs which are located below the MS. Russel suggested that these giants and dwarfs may have an incorrect spectral type, but it turned out to be correct. It is a funny fact in astronomy and physics that results which are not in the expected range, which are often seen as false data, bad errors, or false interpretation, are leading to new scientific discoveries. In our case to RGB, AGB, and white dwarf stars. (Habing and Olofsson, 2003).
Many AGB-stars belong to the group of long periodic variables (LPVs). In 1596 the disappearance of a 3rd magnitude star in Cetus, was noticed by the astronomer Fabricius. He thought it was a "Stella Nova" like the one reported by Tycho Brahe 1572. But the Dutch astronomer Holwarda observed the reappearance of Fabricius star in 1638. Since then, the dis- and reappearance of the star was observed periodically. Later, many stars of this type were found. They were named "Stellae Mirae", the miraculous or Mira stars (Habing and Olofsson, 2003). The analysis of the radial velocities of Mira stars showed that they are different for stars with a different period. This lead to the conclusion that Miras with shorter periods have less mass and are older than Miras with longer periods (Feast, 1963). Glass and Evans (1981) found a linear relation between the K-magnitude and the period of Mira variable stars.

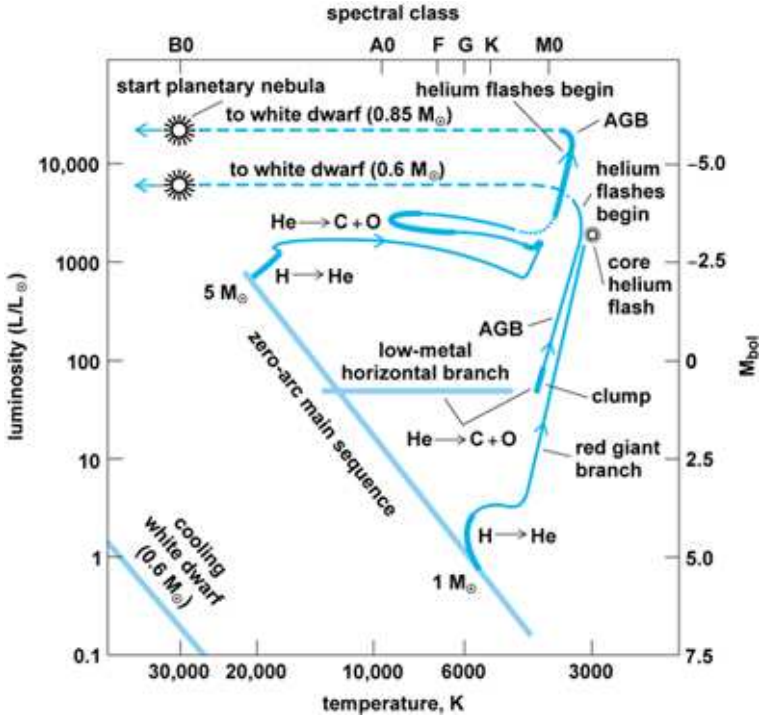

Figure 1.1: The HR-Diagram from McGrow-Hills Access Science web page. This HRD shows the evolution of intermediate mass stars from (1 to 5) $M_\odot$. AGB-stars have masses from (0.8 to 8) $M_\odot$. (After J. B. Kaler, Stars, W. H. Freeman, 1992, 1993, from work of I. Iben, Jr.)
`http://www.accessscience.com/figID=654000FG0030`

1.2.1 Planck equation

The physical origin of the different colours of the stars, clearly visible in the HRD, became clear with the connection between thermodynamics and the electromagnetic radiation. The ultimate result is the Planck equation, which was found by Max Plank in 1900.

$$B_\lambda(T) = \frac{2hc^2}{\lambda^5} \frac{1}{e^{hc/(\lambda k_B T)} - 1} \tag{1.1}$$

The Planck-law describes the energy which is emitted by the spectral radiance of a black body. B is the spectral radiance, T is the absolute temperature, k_B is the Boltzmann constant, h is the Planck constant, c is the speed of light and λ is the wavelength. In Fig. 1.2 the radiation of the Sun and a black body are compared together. Due to the Plank Equation we understand

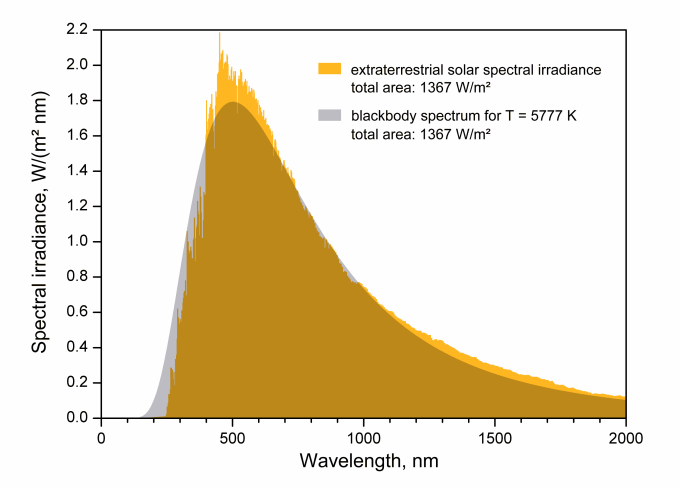

Figure 1.2: The Sun is a good example for a black body. The effective temperature is 5777K with a solid angle of 6.8e-5 steradian. (c) Wikipedia (c) GNU Free Documentation License, Version 1.2 `http://en.wikipedia.org/wiki/File:EffectiveTemperature_300dpi_e.png`

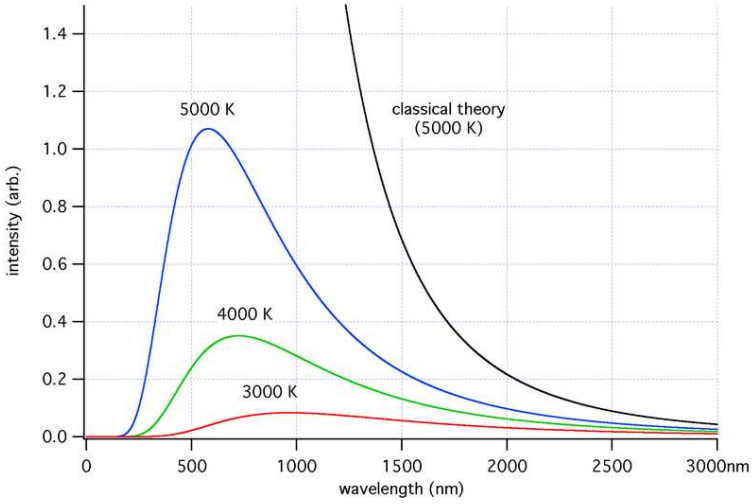

Figure 1.3: The coloured curves represents the Planck-law. They describe a black body radiation. The electromagnetic radiation is emitted in discrete quanta. The black curve at the right, represents the ultraviolet catastrophe, which was resolved by the Planck-law. (c) Wikipedia, (c) Wikimedia Commons: `http://en.wikipedia.org/wiki/File:Blackbody-lg.png`

why red stars are cooler than blue or white stars in the HRD, as one can see in Fig. 1.3. Also the temperature range from 2500 K to 4000 K of AGB-stars, are in the red area of the Plank Curve in Fig. 1.3.
AGB-stars do have a different spectrum from that of a black body.

1.3 Stellar evolution

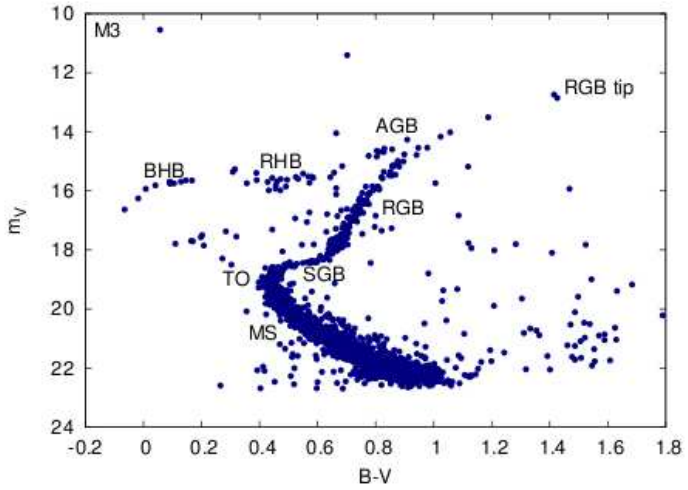

Figure 1.4: A color magnitude diagram of the cluster M3 with data from Rey (2001). It shows stars at many stages of their evolution corresponding to different masses at approximately the same age. Namely the main sequence (MS), the turn-off point (TP), the sub-giant branch (SGB), the red giant branch (RGB), the asymptotic giant branch (AGB), the RGB-tip, and the red horizontal branch (RHB) and the blue horizontal branch (BHB). For a detailed description see the text. Taken from the PhD-thesis of M.Lederer (Lederer, 2009).

In this chapter the focus is set to the evolution of low-mass stars. Star formation begins in the interstellar medium (ISM) when molecular clouds become unstable corresponding to the Jeans criterion (Jeans, 1928). Smaller parts of the cloud are fragmented into clumps. These clumps will grow larger and larger, and become according to their initial mass, mostly low-mass stars (Chabrier, 2005). When the clumps are contracting, the temperature will rise up until it is high enough to ignite hydrogen burning. The star is contracting as long as it is in thermal and hydrostatic equilibrium. Then the contraction stops. In other words, the pressure inside the star prevents the gravitational

collapse of the outer envelope. This is the beginning of the life of a star. It has now reached the zero age main sequence (ZAMS) as shown in the HRD in Fig. 1.1.

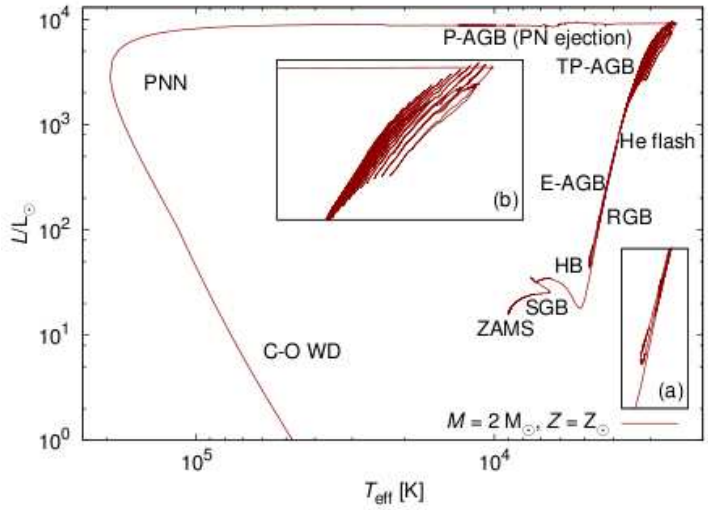

Figure 1.5: HRD with the theoretical evolutionary track for a star with 2 $M_{\odot}$ and solar metallicity. Sub-figure (a) zooms into the horizontal branch and sub-figure (b) zooms into the TP-AGB phase. Data from Herwig (2005). For a detailed description see the text. Taken from the PhD-thesis of M. Lederer (Lederer, 2009).

1.3.1 Main sequence

Stars begin their nuclear-burning process on the ZAMS and begin to evolve along the main sequence (MS), see Fig. 1.1. They burn hydrogen into helium in their cores. The H core contracts and H-burning is established in a shell (Karakas, 2011). Due to the fact that stars live most of their life on the MS, we can see in the CMD of M3 in Fig. 1.4, that most of the stars observed, are indeed located on the MS. Low-mass stars are burning hydrogen to helium via the proton-proton chain (pp). The time scale of H exhaustion for the pp chain lasts around 10^{10} years.

1.3.2 Turn off point

When the stars are evolving to the turn-off point (TOP) in the stellar evolutionary track, the nuclear reactions in their cores have consumed all of

the hydrogen, within the core so the fusion of hydrogen proceeds in a shell around the star centre (see Fig. 1.4).

1.3.3 Sub giant branch

After the TOP, the stars evolve onto the sub giant branch (SGB). The remnants of the hydrogen burning process form a helium core. If this helium core exceeds the Schönberg-Chandrasekhar limit (Schönberg and Chandrasekhar, 1942), it will collapse on a thermal time scale. Therefore, it will heat up and release energy. Because of the temperature increase of the base of the H-burning shell, the CNO cycle takes place and becomes the main burning process.

1.3.4 Red giant branch

When the stars reach the red giant branch (RGB)[1] in the HRD, the stars have higher luminosities and lower temperatures. At this time the convective mantle has expanded and cooled down. This explains the cooler temperatures in the HRD. At the RGB, the convective envelope moves inward and reaches regions from where H-burning elements can be mixed with the stellar surface (see Fig. 1.6). These elements are: ^{3}He, ^{4}He, ^{13}C, and ^{14}N. The ^{12}C/^{13}C ratio changes from the solar value of about 89 to about 20. The *first dredge-up* occurs! While the star rises on the RGB, the He cores of low mass stars are contracting and heat up. The cores can also become electron-degenerate. The FGB-phase is terminated when the temperature reaches about 100 million Kelvin and the triple alpha reactions are ignited (Karakas, 2011).

Core helium flash

Temperature and density in the degenerate core are decoupled at the end of an RGB-star life. A violent He ignition is the outcome of this fact and is called a core helium flash. The maximum initial mass for the occurrence of a core He-flash is about 2 $M_{\odot}$ at a solar composition (Karakas, 2011). In more detail, the core is contracting and therefore heating up thus at some point helium burning can ignite when the temperature is high enough. Then, the degenerate cores of low mass stars endure a thermonuclear runaway due to a feedback[2] between the temperature and the nuclear reaction rate. The

[1] An alternative term for the RGB in the literature is *first giant branch* (FGB).

[2] The nuclear reaction rate rises with higher temperatures, but the pressure remains constant.

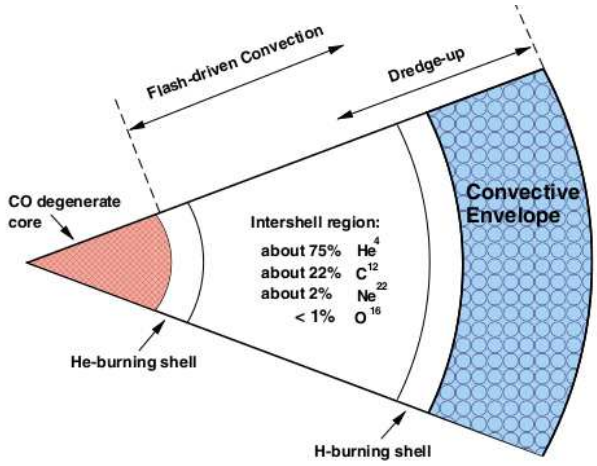

Figure 1.6: A schema of an AGB-star structure. It shows a degenerate C-O core, the He-burning shell above the core. Below a convective envelope is the H-burning shell. The inter-shell region becomes enriched by s-process elements. This figure is not to scale (Karakas et al., 2002).

helium flash is located at the tip[3] of the RGB. It marks the end of the RGB phase.

1.3.5 Horizontal branch

The journey proceeds onto the horizontal branch (HB), (see Subfigure (a) in Fig. 1.5). Depending on the mass-loss on the RGB and the metallicity, the stars can enter either the blue horizontal branch (BHB) or the red horizontal branch (RHB). Stars at the HB, are burning helium in their cores. This leads to the production of ^{12}C and ^{16}O. Hydrogen burning continues in a shell around the helium core. When the helium in the centre is exhausted, an inert C-O core is formed from the ashes of the helium burning process. The star now has the configuration of a double shell burning phase as seen in Fig. 1.6. The mantle of the star again expands and the star moves to the upper right of the HRD, onto the asymptotic giant branch (AGB).

[3]To be seen at the upper right in the CMD in Fig. 1.4.

1.3.6 Asymptotic giant branch

E-AGB

In the early AGB phase a H-burning shell and a He-burning shell are established. The star has a core consisting of carbon and oxygen (C-O core), which is supported by the pressure of degenerated electrons. The C-O core is surrounded first by the He-burning shell, and above it the H-burning shell. Due to the degeneracy of the C-O core, no carbon burning can occur in its center, because of neutrino emissions which have a cooling effect. The fact that the C-O core has to be degenerate, sets the upper mass limit for AGB-stars at about 8 $M_{\odot}$. (Lattanzio and Wood, 2003).

The largest part of the luminosity comes from the He-burning shell, with a contribution from the gravitationally contracting electron degenerate C-O core. The hydrogen burning shell, which is placed above the He-shell, instead provides only minimal energy input for the total luminosity. The He burning shell becomes thinner and, as a result of this, the luminosity decreases. This thin He burning shell begins oscillating due to a thermal instability. The hydrogen burning shell takes over being the main luminosity generator. Its energy output can vary periodically.

TP-AGB

The He-shell on the AGB is susceptible to thermal instabilities. Therefore the energy output of the He-burning shell is very sensitive to changes in the temperature (Schwarzschild and Härm, 1965; Weigert, 1966). In general, He-burning provides most of the energy input to the luminosity at low luminosities. The He shell burns in a thick He-layer which is the remnant of the upper H-burning shell. The H-burning shell becomes more dominant when the He inter-shell becomes thinner. Therefore the He-burning shell declines in luminosity. The He-burning contribution to the luminosity can start to oscillate, increase in luminosity again and as a result a simultaneous decline in the contribution of H-burning to the total luminosity occurs. These oscillations in the burning shells are the beginning of the thermally pulsing AGB-the TP-AGB phase.

Thermal pulses (TP) are the repetitive activation of the He-burning shell. Again, most of the luminosity is produced by the He-burning shell during a TP. The H-burning shell breaks down periodically and therefore produces only a little amount of luminosity. This TP is the reason for a periodical

variation in the stellar luminosity of an AGB-star[4]. The TP-AGB phase occurs for some 10^6 years. The number of TPs are dependant on the stellar parameters. The duration of a single TP is very short compared to the entire TP-AGB phase, so the possibility of observing an AGB-star during a TP is very low. The two related phenomena dredge-up and mass-loss will be described in later chapters.

P-AGB

The AGB phase is terminated by strong mass-loss. A stellar wind[5] removes the hydrogen-rich mantle and drives it into the ISM. The core of the AGB-star remains unaffected by the removal of the mantle. Therefore, the nuclear burning reactions can continue and the star moves to higher temperatures in the HRD while the luminosity will remain constant. The stellar wind creates a planetary nebula (PN) around the remaining nucleus. This fast transition from an AGB-star to the PN phase is called *Post-AGB* phase (P-AGB). When the nuclear burning processes come to an end, the remains of the core will become a white dwarf (WD). The white dwarf will cool down on time-scales of some 10^9 years.

[4]The time scale of the variations induced by the thermal pulses is much larger than the time scale caused by stellar pulsation.

[5]The outflow velocity of the stellar wind is around 10-20 km s^{-1}.

1.4 AGB internal structure

AGB-stars are stars, which have initial masses between 0.8 $M_\odot$ and 8 $M_\odot$ and are now close to the end of their evolution.

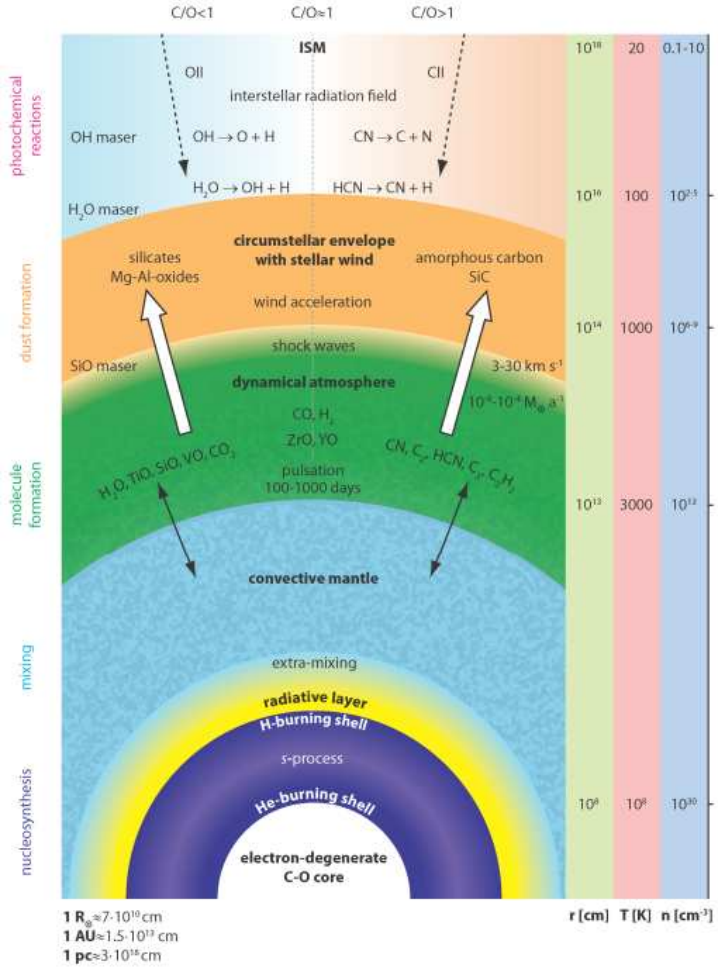

Figure 1.7: AGB structure by Michael Lederer (2009). One can see the typical features of an AGB-star: the electron degenerate C/O-core, the He and H burning shell, the convective mantle, the dynamical atmosphere where the molecules are formed, and the circumstellar envelope, which is the interface to the ISM.

As one can see in Fig. 1.7, an AGB-star consists from the inside out of:

- A small degenerate[6] core consisting of oxygen and carbon, which has a very high temperature and is also very dense.
- A He-burning shell and above a H-burning shell, with an intershell region in-between.
- A convective mantle (stellar envelope).
- A thin atmosphere.
- A circumstellar envelope (CSE), which is very large, cool and thin, which is created by pulsation, mass-loss and dust formation. It is also the layer which interacts with the ISM.

(Habing and Olofsson, 2003)

The structure of an AGB-star consists of:

- Ten orders of magnitude in size.
- Thirty orders of magnitude in density.
- Seven orders of magnitude in temperature.

(Habing and Olofsson, 2003).

1.4.1 The core and stellar envelope

When there is no more helium in the center of the core, the He-burning shell moves outward. The core consisting of C and O, which have been produced, contracts. If the core has reached the density of a white dwarf, the contraction stops due to electron degeneracy pressure. Size and temperature are now about 10^8 cm and 10^8 K respectively. The core contracts, the envelope expands and the luminosity will increase. This is the start of the E-AGB phase[7]. The stellar envelope is now about 10^{13} cm in size, and the effective temperature is now about 3000 K. The envelope can also become pulsationally unstable. The characteristic time scale for the pulsation al instability is around some one hundred days (see Fig. 1.7). (Habing and Olofsson, 2003).

[6]The core has no active nuclear reactions.
[7]He-burning in the shell produces most of the energy at the moment.

1.4.2 Double-shell burning and thermal pulses

When the star has reached a very high luminosity[8], approximately around $3000\,L_\odot$ or M_{bol} = -4, it can burn both hydrogen and helium in shells. The thin He-burning shell around the core produces carbon at a high rate. This carbon is added to the mass of the core. This short episode is called a "thermal pulse" or "He-shell flash". A modulation in the luminosity is the consequence. Between these thermal pulses, the star is able to burn hydrogen again. The phase of alternating H and He burning is called: "TP-AGB phase". (Habing and Olofsson, 2003).

1.4.3 Thermal pulses and dredge-up

Thermal pulses (TP) can cause a dredge-up of nuclear processed material to the surface of the star. During TPs, convection can reach into the deep layers where nuclear burning is happening. Therefore the stellar surface becomes enriched with nuclear-burning-processed elements, especially carbon. (Habing and Olofsson, 2003). The nature of TPs and the first, second and third dredge-up will be discussed in Chapter 1.5 - *Nucleosynthesis and dredge-up* in greater detail.

1.4.4 Hot bottom burning

In TP-AGB-stars with high masses like $M_i \simeq 3.5\,M_\odot$, the main zone of the convective stellar envelope can reach into high-temperature regions at $T > 20 \cdot 10^6 - 40 \cdot 10^6\,K$ of the core, so that H-burning via the CNO-cycle can occur. This process called "hot bottom burning" (HBB), is also refereed to as "envelope burning" (Groenewegen and Marigo, 2003).

In the case of *hot bottom burning*, the conversion from O-rich to C-rich chemistry may not happen. If there is enough mass, carbon will burn into nitrogen before it reaches the surface. In the case of stars at the low mass end of the AGB the amount of matter between the core and surface is too low to drive a dredge-up. Therefore, the conversion cannot occur. (Habing and Olofsson, 2003).

[8]Similar to the luminosity of the tip of the RGB.

1.4.5 The role of molecules in the atmosphere

Most of the starlight comes from the atmosphere of a star. An exact definition of where an atmosphere begins and ends is difficult because it has no exact boundaries. Habing and Olofsson (2003) characterize the atmosphere of an AGB-star with low temperatures, low gravities and low densities. The atmosphere usually has a large extension and is the interface to the surrounding ISM. Another characteristic is that the AGB-stars have a very dynamic atmosphere. It is pulsating, creating shock waves, producing dust and last but not least, it is connected to the huge mass-loss of an AGB-star. Gustafsson (2007) discusses the physical processes[9] in AGB-stellar atmospheres which are dominated by dynamical processes, which have no spherically symmetry, which have deviations from thermal equilibrium, which are sources of dust formation, and which have uncertain outer boundaries.

Molecules

The molecules can be formed in the atmosphere and in the circumstellar envelope of AGB-stars, since these regions are cool enough. Molecules have more inner degrees of freedom[10] compared to atoms. The energy levels of electrons can split into many rotational and vibrational states and their electronic energy levels have a high number of transitions. Therefore, the molecules leave their characteristic features in the spectral energy distribution. This is the reason we can observe many *rotation-vibration bands* in AGB-star spectra, like the CO 3-0 band, the CO 4-1 band, or the CO 5-2 band with second overtone transition. For greater details of the theory of molecular spectra see e.g. the books *Spectra of atoms and molecules* (Bernath, 2005) or *Molecular spectra and molecular structure* (Herzberg, 1950).

The molecules determine also the spectral and photometric appearance of an AGB-star atmosphere (Tsuji, 1966). Due to its high bond energy, the CO-molecule has an important role in the spectra of AGB-stars. Less abundant species are bound in CO molecules. This explains the important role of the C/O-ratio of AGB-star atmospheres. The C/O-ratio can be oxygen-rich when $C/O < 1$. In this case, surplus oxygen atoms are available, which can form oxygen-rich molecules like TiO. In the carbon rich case $C/O > 1$, the oxygen is bound up in CO molecules and there are surplus carbon atoms available. These carbon atoms can form molecules like CN or C_2 (Lattanzio and Wood, 2003).

[9] In order to improve model atmospheres for comparison to AGB-star atmospheres.
[10] The degrees of rotation and vibration.

Molecules in the oxygen-rich case with high partial pressures are:

- H_2O, TiO, SiO, OH, VO

The most abundant molecules in the carbon-rich case are:

- CN, CH, C_2, C_3, HCN, C_2H_2

CO is present in both the oxygen- and carbon-rich case. (Lattanzio and Wood, 2003; Habing and Olofsson, 2003).

1.4.6 Mass-loss mechanism

Due to pulsation, the star can deposit mechanical energy in the outer parts of the atmosphere. These outer parts are only weakly bound by gravity. So the atmosphere can become very extended in comparison to a hydrostatic one. At high altitudes, grain condensation will take place in the post-shock gas. It is then possible that gas particles reach escape velocity, because of the mechanical energy input or by radiation pressure which interacts on grains or molecules. This is basically the mass-loss mechanism. (Habing and Olofsson, 2003).

1.4.7 The M, S and C-stars

Luminous cool AGB-stars cover the spectral classes of M, S and C.
In Table 1.1 the main spectral characteristics of AGB-stars are shown. As

Spectral type	Optical spectra	IR spectra
M	TiO	TiO, SiO, H_2O, OH, CO
late M	VO + TiO	VO, TiO, SiO, H_2O, OH, CO
MS	TiO + ZrO	ZrO, TiO, SiO, H_2O, OH, CO
S	ZrO	ZrO, CO
C	carbon compounds CO, C_2, CN, no metallic oxides	CN, CO, C_2, C_3, HCN, C_2H_2

Table 1.1: Spectral types for M, S and C (Habing and Olofsson, 2003).

mentioned before, the distinction between M and C-stars is related to the value of the C/O-ratio. Is the ratio greater than one, we have C-stars, is the ratio smaller than one we have M-stars. The optical spectra of M-stars are dominated by TiO while those of the carbon stars are dominated by C_2 and CN. The importance of C-stars is that C/O >1 indicates that this particular

star has added some extra carbon to its envelope, which is an indicator of the third dredge-up.

Another class are the S-stars which have molecules and are often enriched with ZrO. Generally s-process elements are created by slow irradiation with neutrons at temperatures of some T = 10^8 K. The third dredge-up can explain the observed overabundance of s-processed elements, which are brought up from deep regions of the star. MS-stars have TiO and ZrO molecules. (Lattanzio and Wood, 2003).

1.4.8 The circumstellar envelope

The circumstellar envelope (CSE) is formed by a slow wind at velocities of about 15 kms^{-1}. The CSE is made of escaping molecular gas which is dominated by H_2, CO and particles of dust. The molecules are much more fragile to UV photons than dust grains, which can survive much further away from the star. The properties of grains and molecules are strongly dependent on the C/O-ratio. The CSE merges with the interstellar medium where temperatures are about 10 K and the particle densities are less than 10 cm^{-3}. This can occur at distances of about 10^{16} m away from the star, which corresponds also to the outer limit of an AGB-star. (Habing and Olofsson, 2003).

1.4.9 Termination of the AGB

The mass-loss process determines the duration of the evolution, because that the growth rate of the core is smaller than the rate of ejection of matter. At the end of the AGB evolution the post-AGB evolution begins. This is when all the matter around the core of the star is ejected and the mass of the remaining stellar envelope is less than 0.01 $M_\odot$. The mass-loss rate in the final AGB stages is around $10^{-4} M_\odot yr^{-1}$. The post-AGB phase lasts only some thousand years, and after it the star may form a planetary nebula (PN). While the PN expands, the core remains as a white dwarf. (Habing and Olofsson, 2003).

1.5 Nucleosynthesis and dredge-up

In an AGB-star, different nucleosynthesis processes occur in the active double shell configuration (see Fig. 1.7): hydrogen burning via the CNO cycle, helium burning (triple alpha process), and the s-process. The processed

elements are mixed throughout the active area, due to the instability of the configuration. The primary burning products of an AGB-star are: ^{4}He, ^{12}C, ^{14}N, ^{16}O, ^{19}F, ^{22}Ne, ^{23}Na, ^{25}Mg, ^{26}Al and ^{27}Al. Other species are the result of hot bottom burning. (Lattanzio and Wood, 2003).

1.5.1 Initial composition and dredge-up

When the star enters the AGB stage, it has initially an oxygen-rich atmosphere. Due to the occurrence of thermal pulses, the abundance of carbon can exceed the abundance of oxygen on the surface. The atmosphere of the star will change from its initial oxygen-rich state to carbon-rich. This is the second dredge-up (SDU) episode for low-mass stars and the third one for intermediate mass stars. However any dredge-up during the TP-AGB phase is called "third dredge-up" (3DUP).

The reaction rate of $^{12}C(\alpha,\gamma)^{16}O$ determines the composition of the small, dense, degenerate ^{12}C and ^{16}O core. Atop the core is the He-burning shell located, which is separated from the above H-burning shell by a very thin intershell layer. Above the H-burning shell is the radiative buffer zone which separates the convective envelope from the nucleosynthesis burning shells (see Fig. 1.7). The composition of the stellar surface of an AGB-star is a reflection of the initial composition and the first dredge-up (FDU), and for more massive stars than 4 $M_{\odot}$, also the second dredge-up (SDU). Dredge-ups are convective mixing processes that bring inner material of the star to the surface (Herwig, 2005). Both the FDU and SDU are mixing regions that have experienced H-burning[11] to the surface. The FDU is mixing up regions that have experienced only partial H-burning, and the SDU is mixing regions which have burned all of its hydrogen. Therefore the SDU has a greater impact on the change of the surface abundances. As a result of the FDU and SDU, the abundances of ^{13}C and ^{14}N and a bit of ^{4}He are increasing and inherent, the abundances of ^{12}C,^{16} O, and ^{18}O are decreasing. (Lattanzio and Wood, 2003). When the H-shell is proceeding into the envelope, it is burning H into ^{4}He and most of the CNO processed elements are ending up as ^{14}N. ^{14}N is also the prime component of the intershell region (see Fig.1.6). The He-shell is burning in triple-alpha reactions ^{4}He into ^{12}C. Most of the ^{14}N cores are capturing two α-particles, forming ^{22}Ne. (Lattanzio and Wood, 2003).

[11] Mainly via the CNO cycle.

1.5.2 First dredge-up

When the star reaches the giant branch, the inward movement of the convective envelope mixes partial H-burned products to the surface. The changes in the abundance by the FDU are depending on the mass and the composition of the star.
The characteristic abundance changes are:

- Decrease of 30% of ^{12}C.
- Increase of ^{13}C by a factor of about 2-3.
- Increase of ^{14}N by a factor of about 3-4.
- Decrease of ^{15}N by a factor of about 2.
- Decrease of 30% of ^{18}O.
- A weak increase of ^{17}O.

Typical isotopic ratios are:

- $^{12}\mathrm{C}/^{13}\mathrm{C} \approx 20$.
- $^{16}\mathrm{O}/^{18}\mathrm{O} \approx 600$.

(Lattanzio and Wood, 2003). Models from various groups are in a good agreement for stars of about $2.5\,\mathrm{M}_{\odot}$. Below this mass there are some uncertainties. The ratio $^{12}\mathrm{C}/^{13}\mathrm{C} \approx 10$ is lower as predicted. Extra mixing (Charbonnel, 1995; Sweigart and Mengel, 1979) due to rotation (Zahn, 1992; Sweigart and Mengel, 1979) below the convective envelope can be the cause. Extra mixing affects only stars with masses of $\mathrm{M} \leq 2.5\,\mathrm{M}_{\odot}$

1.5.3 Second dredge-up

A second dredge-up is possible for stars with $\mathrm{M} > 4\,\mathrm{M}_{\odot}$. It occurs after the exhaustion of the central helium (Becker, 1981; Becker and Iben, 1980). The convective envelope reaches down into a region where all hydrogen was used up and the resulting He material is added to the envelope. The oxygen isotopes would not change much. But since to the CNO cycle has produced a lot of ^{14}N in this region, the isotopic abundances of $^{14}\mathrm{N}/^{15}\mathrm{N}$ will change by a factor of about 6 (Lattanzio and Boothroyd, 1997).

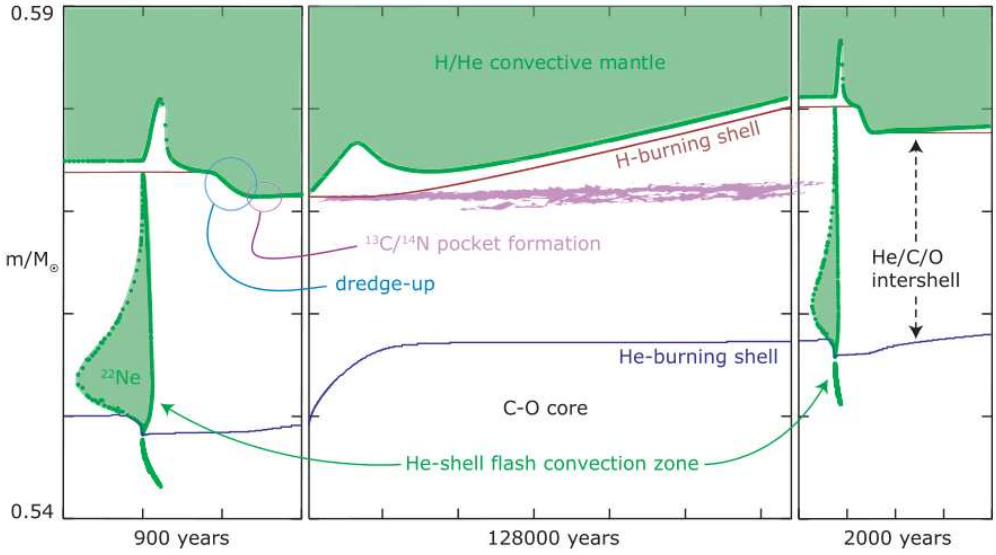

Figure 1.8: Kippenhahn diagram of a thermal pulse sequence and third dredge-up. It shows the phase of TPs and convective regions of the 3DUP and also the time evolution of the H- and He-burning shells. The time scale of reoccurring TPs are not necessary the same. The Figure has been adapted from Herwig (2005) with data from a model with $M = 2\,M_{\odot}$, $Z = 0.01$ (Herwig and Austin, 2004) and was taken from Lederer (2009).

1.5.4 Third dredge-up

The third dredge-up (3DUP) occurs during the evolution of an AGB-star, when it reaches the TP-AGB phase. The often repeated third dredge-up (3DUP) enriches the stellar envelope with He-burning products and s-processed elements. By increasing the number of C atoms, the bands of molecular oxides fade out and disappear. This is because the existing excess of oxygen is now locked in the CO molecule. This generates the so called S-stars where $C/O \approx 1$. After the S-stars stage, further enrichment will generate C-stars. Molecular bands of carbon-rich stars appear. So called SC-stars are possible, if s-process elements are more dominant in the spectra. (Lattanzio and Wood, 2003).

Thermal pulses

Before a thermal pulse (TP) happens, the H-burning shell provides most of the stellar luminosity. The H-burning shell also leaves its burning ashes onto

the quiescent He-shell, which does not provide much input for the luminosity at the moment. Therefore the mass of the He-shell is growing up and also the temperature is rising. Triple-alpha reactions are maybe triggered and a thermonuclear runaway[12] of the He-shell occurs. A pulse-driven convection zone (PDCZ) mixes the burning products of He throughout the intershell (see Fig. 1.8). The expansion of the inter-shell region into the H-burning shell terminates it. Due to the missing H-burning shell and its radiative layer, the mantle from above can now penetrate the former H-shell and reach into regions with fresh nuclear processed materials. Protons which are brought here by convection have the possibility to form a ^{13}C-pocket (see violet markers in Fig. 1.8). The ^{13}C-pocket provides neutrons for the s-process. The reaction rate is: $^{12}\mathbf{C}(\mathbf{p},\gamma)^{13}\mathbf{N}(\beta^+,\nu)^{13}\mathbf{C}(\alpha,\mathbf{n})^{16}\mathbf{O}$. A 3DUP phase ends when the H-burning shell and its radiative layer is re-established. The phase of a TP is only 1/100 of the time of the interpulse phase. The TPs stop when the mass-loss process has used up all the star mantle.

Chemical composition

Due to the repeating occurrence of the 3DUP, the chemical composition of the stellar atmosphere changes. Initially the low-mass AGB-stars are oxygen-rich. They have the spectral type M. If the atmosphere was enriched with s-process elements and has the ratio of C/O ≈ 1, the object is called S-star[13], and if C/O < 1, they are called MS-stars. If the ratio is C/O > 1, the star is called carbon-star or C-star. Notice that it is possible for stars to become also carbon rich without the 3DUP. Herwig showed that at very low metallicities the star can become carbon enriched immediately after the first dredge-up (Herwig et al., 2000).

1.5.5 Triple-alpha process and the production of carbon

The nuclear reactions in AGB-stars are known for the production of carbon. The carbon isotope ^{12}C is formed by triple-α reactions[14] (Salpeter, 1952) of burning ^{4}He into ^{12}C. Due to convection, new ^{4}He from the outer shell is mixed down, while fresh processed ^{12}C is mixed outward.

[12] He-shell flash.
[13] This classification has some exceptions, see e.g. Lebzelter et al. (2008a).
[14] Which is also called Salpeter process.

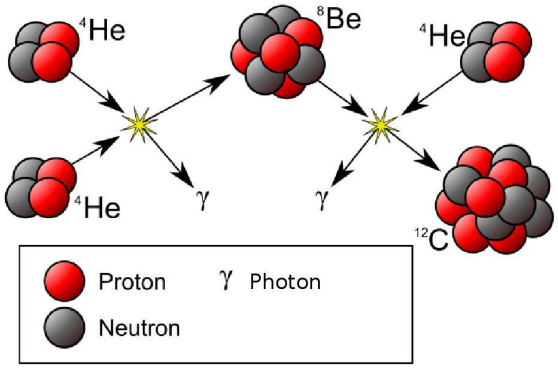

Figure 1.9: Triple-alpha-process: Two ^{4}He are merged into ^{8}Be, and the ^{8}Be is merges with one ^{4}He to a ^{12}C nucleus, releasing energy. Figure adapted after: `http://en.wikipedia.org/wiki/File:Triple-Alpha_Process.png` (C) Wikimedia Commons, Creative Commons Attribution-Share Alike 3.0 Unported license.

1.5.6 Extra mixing

Observations on element and isotopic abundances in red giants indicate (Busso et al., 2007) another mixing process beside the convective ones like the 3DUP. This additional process should transport matter from the convective mantle to the top of the H-burning shell and back. The interesting part is, that this process is able to transport material through the radiative layer between the convective mantle and the H-burning shell. Applying the Schwarzschild criterion (Schwarzschild, 1958) we do not expect convection in the radiative layer. The schema of the extra-mixing[15] zones is shown in Fig. 1.10. Extra-mixing has effects on the abundance ratios of C/O, N/O and the isotopes ^{18}O/^{16}O,^{17} O/^{16}O,^{14} N/^{15}N,^{26} Al/^{27}Al (Nollett et al., 2003) and also on ^{12}C/^{13}C (Busso et al., 2007). Two parameters are crucial to model the extra-mixing process. The mass circulation rate[16] $\dot{M}$ and the maximum temperature T_{max} to which the material being circulated is exposed. So the parameters ($\dot{M}$, T_{max}) are crucial for the amount of material being exposed to partial hydrogen burning and the changes in the abundances due to it. The physical processes of extra-mixing on the AGB are still not understood

[15]Other terms in the literature for extra-mixing are: deep-mixing, slow-mixing and cool-bottom-processing (Wasserburg et al., 1995).

[16]This is the rate at which material is being transported between the radiative layer and the convective mantle.

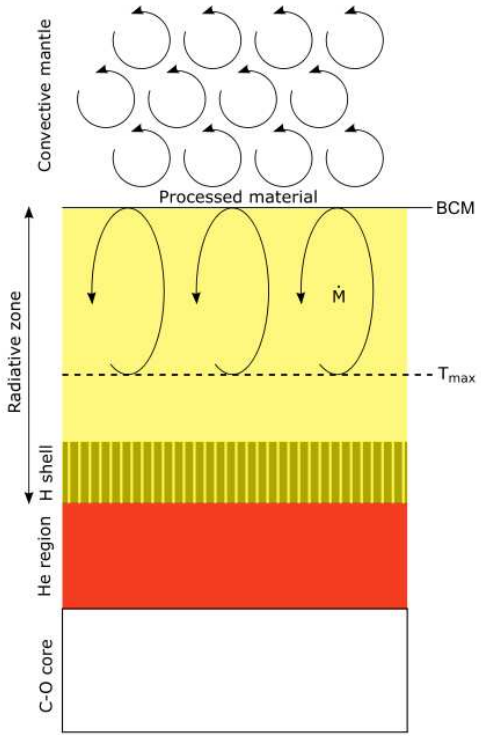

Figure 1.10: A not to scale schema of extra mixing. A non convective mixing process is suggested to transport material from the bottom of the convective mantle (BCM), to regions with higher temperatures up to T_{max}. The schema is after an idea from Nollett et al. (2003) and was taken from the PhD thesis from Lederer (2009).

well and the topic is under active research. See e.g. (Zahn, 1992; Maeder and Zahn, 1998; Herwig, 2000; Palacios et al., 2006; Cantiello et al., 2007; Stancliffe and Glebbeek, 2008; Eggleton et al., 2008; Talon and Charbonnel, 2008; Denissenkov et al., 2008; Lebzelter et al., 2008b).

1.6 Mass-loss process

In the early days (before 1980), of stellar evolution calculations, assumed that the mass of a star did not change. Biermann (1951) found the first observational evidence of a mass loss. He observed a comet and its tail. He found out that solar photons do not have enough momentum, to give the comet tail its form and shape. Biermann proposed that the alignment of the

comet tail was due to solar matter particles. (Habing and Olofsson, 2003). The mass-loss rate of our Sun is very low. It is about

$$\frac{\mathrm{dM}}{\mathrm{dt}} = 3 \cdot 10^{-14}\,\mathrm{M_{\odot}yr^{-1}} \tag{1.2}$$

At this rate, the Sun will not loose very much mass in its entire lifetime. It will be around a total mass of $4 \cdot 10^{-4}\mathrm{M_{\odot}}$. A theoretical problem at this time was, that it was unclear if the particles could even leave the Sun, because of the gravitational field of the Sun.

Circumstellar envelope

A bit later, Deutsch (1956) observed the binary system α Her. He found out that circumstellar gas (circumstellar envelope: CSE) was visible around an M-giant. The gas was located up to $2 \cdot 10^5\,\mathrm{R_{\odot}}$ away from the star. The circumstellar gas had an outflow velocity of about 10 km $\mathrm{s^{-1}}$. Thus it could leave the gravitational field of the star. Deutsch calculated a mass loss rate of about $\dot{\mathrm{M}} = 3 \cdot 10^{-8}\mathrm{M_{\odot}yr^{-1}}$ for the binary system α Her. Reimers (1975) derived an empirical relation for low mass-loss rates of red giant stars.

$$\frac{dM}{dt} \propto \frac{L \cdot R}{M} \tag{1.3}$$

L is the stellar luminosity, R the radius and M the mass. But AGB-stars have dense CSEs around them, so this fact requires much higher mass-loss rates than the *Reimers-equation* predicts. RGB-stars experience a stellar wind. In the last TP-AGB phase it becomes a dense superwind which drives the mass-loss (Renzini and Voli, 1981; Habing and Olofsson, 2003).

So the life of a red giant star ends by a heavy mass loss on the AGB. The mass-loss is very important for the stellar evolution, because mass-loss leads to the termination of the evolution of a star on the AGB. The mass-loss process is driven by pulsation and radiation pressure acting on dust grains. (Habing and Olofsson, 2003).
The mass-loss rate increases rapidly with increasing luminosity of a star. As a consequence the main mass-loss of a star occurs at the end of the AGB evolution (Vassiliadis and Wood, 1993). AGB-stars have mass-loss rates of about $\dot{\mathrm{M}} = 10^{-5}\mathrm{M_{\odot}yr^{-1}}$ with outflow velocities of about 10 km $\mathrm{s^{-1}}$ (Karakas, 2011). A pulsation-enhanced dust-driven wind (Wood, 1979), which has terminal velocities of about 10 to 20 km $\mathrm{s^{-1}}$, increases the mass-loss up to $\dot{\mathrm{M}} = 10^{-7}...10^{-4}\mathrm{M_{\odot}yr^{-1}}$ (Höfner et al., 2003; Höfner, 2008) and will effectively deplete all the remaining mass of an AGB-star.

1.6.1 Detection of AGB-stars

AGB-stars can be detected best in the infrared. Space observatories like the infrared camera of the Hubble-Telescope (HST), ISO, IRAS, and MSX, or the big ground based telescopes as the Very Large Telescope (VLT) play an important role for gaining data on AGB-stars. In databases like DENIS and 2MASS which cover IJHK-photometry data one can obtain first basic information on the stars. Also the (sub)-mm wavelength is an important window to observe AGB-stars. Finally the optical surveys like OGLE, EROS and MACHO provide data on the variability of AGB-stars.

1.6.2 The circumstellar medium (CSM)

The mass-loss process forms an expanding CSE which affects the circumstellar medium (CSM) around the AGB-star. At low mass-loss rates, the CSE can be observed as a weak IR-excess. At high mass-loss rates the star is obscured and appears as a low-temperature and high-luminosity object, almost like a protostar. There are also features of solid particles and microscopic grains. In M-stars silicate grains appear and in C-stars amorphous carbon grains can be found. (Habing and Olofsson, 2003).

1.7 Thesis outline

With a data sample from the globular cluster NGC 1783 in the LMC, we want to derive constraints for AGB-star models. Especially we want to test if the first, second or third dredge-up had occurred. We achieve this by measuring the abundances and isotopic ratios in the atmosphere of the AGB-stars, using the software *AGB*StarViewer which was written for this task. Some stellar parameters, like the metallicity and the mass dependence are well defined for this globular cluster (see Chapter 2 - *Observed data from NGC 1783*). The methods of this approach are presented in Chapter 3 - *Synthetic spectra* and Chapter 4 - *Data analysis*, on which the software *AGB*StarViewer is based. The results are presented in Chapter 6 and are discussed in Chapter 7 - *Conclusions*.

Chapter 2

Observations

2.1 NGC 1783

Because of the presence of intermediate age clusters in the Large Magellanic Cloud (LMC), where the stars have masses from 1.5 to 2 $M_\odot$ (Girardi et al., 1995), the third dredge-up (3DUP) is very likely to occur. The LMC globular cluster NGC 1783 was selected because it has a homogeneous level of age, metallicity, mass and distance. The globular clusters (GC) in our own Milky-Way (MW) are too old for the 3DUP. On the other hand, most of the intermediate up to high-mass stars, have already evolved beyond the AGB-phase, so it is difficult to gain accurate results for the constraints of AGB-models in our own Galaxy. The star cluster NGC 1783 was observed with the Very Large Telescope (VLT) with the Infrared Spectrometer And Array Camera (ISAAC)[1] instrument. There were observed sixteen AGB-stars and two stars for calibration.

2.1.1 Intermediate age cluster

The age of NGC 1783 was determined to 1.1 Gyrs (Frogel et al., 1990) but recently it was re-determined by Mucciarelli et al. (2007) to $\tau = 1.4 \pm 0.2$ Gyr using photometry from the HST-telescope (see Fig. 2.1). The metallicity was determined to [Fe/H] = -0.45 (Cohen, 1982; Frogel et al., 1990).

[1] ESO-VLT1/ISAAC

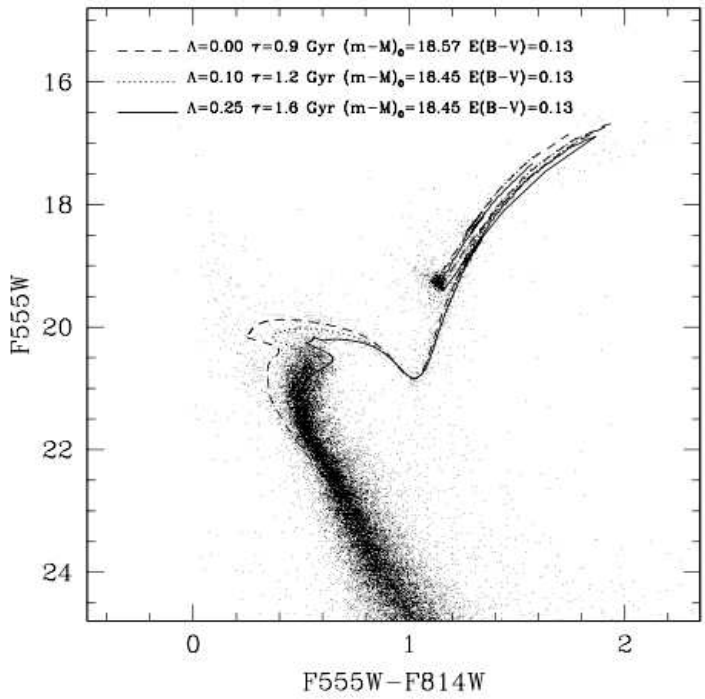

Figure 2.1: The age of NGC 1783 determined by photometry. The data were obtained with the HST-Advanced Camera for Surveys (ACS) and HST-Wide Field Channel (WFC). Here, the best fit of the theoretical Pisa Evolutionary Library (PEL) (Castellani et al., 2003) isochrones is overplotted to the colour magnitude diagram. Also models with different assumptions for the overshooting efficiency (Λ_{os}) and the best fit age, distant modulus and reddening for each Λ_{os} are shown. Taken from Mucciarelli et al. (2007).

ICRS coord. (ep=J2000)	04 59 08 -65 59.3 (Optical)
FK5 coord. (ep=J2000 eq=2000)	04 59 08 -65 59.3 (Optical)
FK4 coord. (ep=B1950 eq=1950)	04 58 59 -66 03.7 (Optical)
Gal coord. (ep=J2000)	276.606 -35.942 (Optical)
Angular size (arcmin)	5.30 4.70 60 (∼) (Opt)
Fluxes (2)	B 10.9 [∼] D ∼ ,V 10.93 [∼] D ∼

Table 2.1: Basic coordinates of the globular cluster NGC 1783. ICRS, FK5, FK5 and Gal coordinates are based on Bica et al. (2008). The angular size is based on Bonatto and Bica (2010). Other object names are GlC (), Cl* (KMHK,[SL63]), * (CD,HD), G (ESO). Taken from the Simbad database.

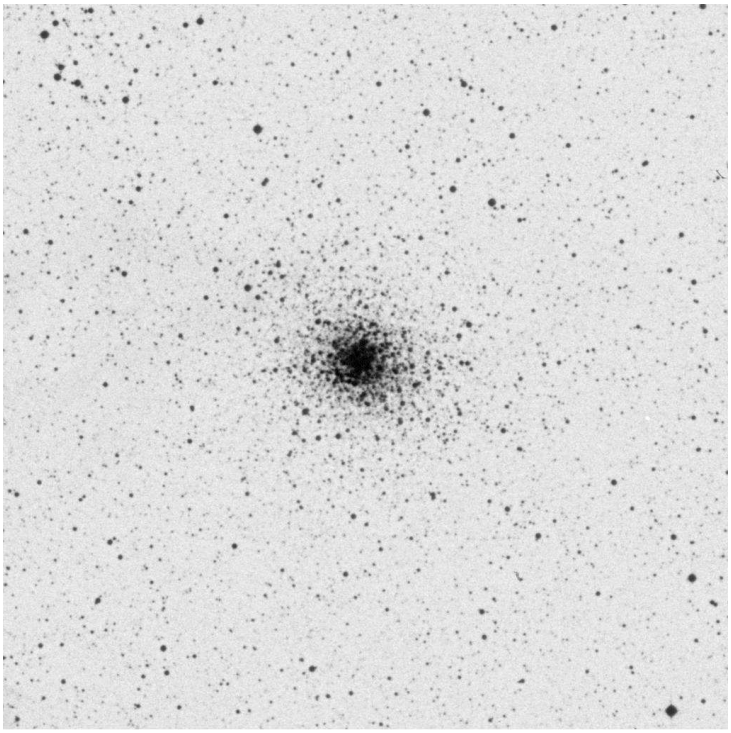

(a) NGC 1783

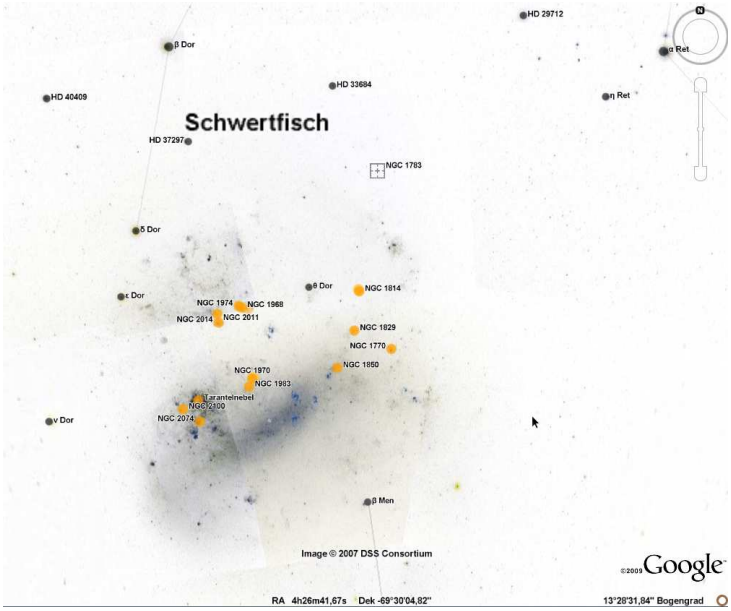

(b) LMC

Figure 2.2: (a) The globular cluster NGC 1783 is shown. Taken from the Simbad database. (b) The LMC is shown in the square, a little beneath and right apart from the letters “Schwertfisch”. Taken from Google-Earth (c). In both diagrams the colours were inverted.

LMC Cluster Stars: Observed Indices
A. Low-Dispersion Data

Cluster (NGC)	Star	$(V-K)_0$	Ca II (Å)	Ca I (Å)	Fe (Å)	Mg (Å)	Na (Å)	Notes
1783	G39	3.53	...	10.1	9.9	11.0	2.6	13, 4
	G40	4.0	M star	...	...	...	...	3, 4
	G13	4.25	M star	...	...	...	...	3, 4
	G32	4.75	M star	...	...	...	...	3, 4

(a) Observed indices of NGC 1783

Abundances of LMC Clusters

NGC	$[Z/Z_\odot]$ (dex)	σ (dex)	No. Stars	SWB Class	Notes
		Low Dispersion			
1652	−1.1	0.2	2	(V)	
1783	−0.45	0.3	1(3)	V	
1841	−2.3	0.4	3	VII	1
1846	−1.1	0.4	3	VII	
1978	−0.5	0.2	2	VI	
2121	−0.95	0.4	2	VI	
2173	−0.75	0.4	4	V-VI	
2193	≥ -0.8	...	(2)	(V-VI)	
2210	−1.7	0.4	1	VII	
2257	−1.4	0.2	2	VII	

(b) Metallicities of LMC clusters

Figure 2.3: (a) Observed indices of various bright stars in NGC 1783. Note that three stars are marked as M-stars. (b) Metallicities of LMC clusters. NGC 1783 is listed with [Fe/H] = -0.45. Taken from Cohen (1982).

Cluster (1)	# (2)	Class (3)	Mem (4)	I.D. (5)	Class (6)	K (7)	J-K (8)	H-K (9)	K_0 (10)	$(J-K)_0$ (11)	$(H-K)_0$ (12)	m_{bol} (13)	Source (14)	Notes (15)
N1783	1	M	Y	TLE 2		...	...	...	11.24	1.07	0.23	14.19	D,H	G7
V	2	M	Y	TLE 8		11.49	1.08	0.20	11.46	1.02	0.18	14.35	B,H	
	3	M	Y	TLE 7		...	...	...	11.56	1.01	0.20	14.20	D,H	G14
	4	M	Y	TLE 6	M4 (8)	...	...	...	11.31	1.02	0.20	14.20	D	G13
	5		Y			12.95(3)	0.95(3)	0.17(3)	12.92	0.89	0.15	15.54(M)	B	
	6	M	Y	TLE14		12.73(3)	0.96(3)	0.16	12.70	0.90	0.14	15.35	B	G4
	7	C	Y	TLE10		11.36	1.06	0.21	11.33	1.00	0.19	13.95	B,E	
	8	C	Y	G6 (9)		13.17	0.80	0.13	13.17	0.74	0.11	15.44	C,G	21
	9	M	Y	TLE15	M1 (8)	11.78	1.00	0.18	11.75	0.94	0.16	14.49	A,D	G40,LPV?(9)
	10	C	Y	TLE 1	C (2)	10.26	1.93	0.77	10.23	1.87	0.75	13.47	B,H	
	11	M	Y	TLE11		11.51	1.00(3	0.18(3)	11.48	0.94	0.16	14.21	A,H	
	12	M	Y			11.84	0.97(3	0.18	11.81	0.91	0.16	14.47	A	
	13	M	Y	TLE 9	S (2)	10.93	1.11	0.27	10.90	1.05	0.25	13.83	B,E,	
	14	M	Y	TLE 5	S (2)	11.23	1.09	0.23	11.20	1.03	0.21	14.11	B,H	
	15	C	Y	TLE 3	C (2)	...	...	...	10.33	1.54	0.57	13.41	C,D	G30
	16	M	Y	TLE 4	M4 (8)	...	...	...	11.07	1.03	0.22	13.98	D,H	G32
	17	C	Y?		C (10)	10.09	1.46	0.49	10.06	1.38	0.47	13.05	A	V2

(a) Observed indices of NGC 1783

ADDITIONAL PHOTOMETRY FOR AGB STARS[a]

Cluster	#	sp	*J–K*	*H–K*	M_{bol}	*K–L*	H_2O	CO
N1783	1	M	1.07	0.23	14.19		0.10 3	0.24
V	3	M	1.01	0.20	14.20		0.08	0.15
	4	M	1.02	0.20	14.20		0.06	0.19
	9	M	0.94	0.16	14.49		0.06	0.15
	10	C	1.87	0.75	13.47	0.67 6	...	...
	15	C	1.54	0.57	13.41		0.14 4	-0.01 3

(b) Additional photometry of NGC 1783

Figure 2.4: Observed indices of (a) red giants in NGC 1783 and additional photometry for AGB-stars (b). TLE gives the identifictions from Tom Lloyd Evans (1980a; 1980b; 1983; 1984). The Table is taken from Frogel et al. (1990).

INTEGRATED CLUSTER PARAMETERS[a]

Cluster	SWB	m_{bol}	Cluster colors minus AGB		AGB fraction of m_{bol}		GB color: $J-K$ at $K=$		age	[Fe/H]
			$J-K$	$H-K$	C	C and M	12.8	12.0		
Kron 3	6.5	11.60	0.49	0.06	0.05	0.05	0.88	...	8.	-1.20
N121	7.0	10.77	0.71	0.13	0.00	0.05	0.83	0.96	12.	-1.40
N152	4.0	12.05	0.56	0.10	0.36	0.36	...	0.96	2.2	-0.80
N220	3.0	12.68	0.49	0.14	0.00	0.00	...	...	...	...
N231	2.5	...	...	...	0.00	0.00	...	...	...	...
N265	3.0	11.79	0.23	-0.01	0.00	0.16	...	...	...	...
N269	3.5	11.60	0.48	0.06	0.00	0.16	...	...	...	...
N299	1.0	10.95	0.81	0.13	0.00	0.26	...	...	...	...
N306	3.0	...	...	...	...	...	...	...	...	...
N339	7.0	12.45	0.55	0.07	0.00	0.00	...	...	...	...
N361	0.0	12.16	...	...	...	...	0.85	0.92	...	...
N411	5.5	12.35	0.74	0.10	0.20	0.20	...	...	1.8	-0.90
N416	6.0	10.94	0.61	0.13	0.03	0.03	...	...	2.5	...
N419	5.0	9.98	0.66	0.13	0.37	0.37	0.85	0.91	1.2	...
N1651	5.0	...	...	...	...	...	0.90	0.98	2.5	-0.50
N1652	6.0	...	...	...	0.00	0.00	0.88	0.96	...	-1.10
N1751	5.0	10.88	0.82	0.22	0.23	0.44	...	...	...	...
N1783	5.0	10.51	0.65	0.10	0.04	0.15	0.89	0.95	1.1	-0.45
N1806	5.0	10.38	0.60	0.07	0.11	0.25	0.88	0.93	...	...
N1841	7.0	13.38	0.66	0.15	0.00	0.00	0.79	0.91	...	-2.30
N1846	5.0	10.40	0.63	0.06	0.22	0.40	0.88	0.96	...	-1.10
N1850	2.0	8.81	0.52	0.11	0.00	0.03	0.61	0.73	0.05	...
N1854	2.0	9.95	0.44	0.14	0.00	0.17	0.62	0.69	0.04	...
N1866	3.0	9.44	0.48	0.09	0.00	0.06	...	0.79	0.12	-0.1
N1978	6.0	10.06	0.74	0.18	0.13	0.17	0.88	1.01	2.1	-0.70
N1987	4.0	11.18	0.11	-0.21	0.14	0.38	0.85	0.95	...	...
N2058	3.0	10.86	0.43	0.01	0.00	0.24	0.60	0.73	0.09	...
N2107	4.0	10.88	0.56	0.16	0.00	0.16	...	...	...	...
N2108	5.0	11.40	0.80	0.39	0.20	0.28	0.81	...	...	...
N2121	6.0	11.37	0.65	0.19	0.13	0.24	0.91	0.99	2.7	-1.00
N2136	3.0	10.20	0.56	0.11	0.00	0.06	0.71	0.80	0.05	...
N2154	5.0	11.25	0.68	0.16	0.28	0.28	0.85	0.95	...	...
N2173	5.5	12.25	0.73	0.29	0.22	0.57	0.92	0.98	2.1	-0.75
N2209	3.5	12.74	0.49	0.08	0.58	0.58	...	...	1.0	-1.00
N2213	5.5	11.61	0.12	-0.15	0.31	0.39	0.88	0.95	1.6	-0.50
N2214	2.0	10.42	0.11	0.04	0.00	0.21	...	...	0.05	...
N2231	5.0	12.85	1.20	0.23	0.46	0.46	0.86	...	1.56	...
N2257	7.0	14.51	0.56	0.09	0.00	0.00	0.83	0.98	15.9	-1.80

[a] The AGB in this table refers to all stars with $M_{bol} \leq -3.6$. The GB colors for SMC clusters have been determined after adjusting its distance modulus by -0.3 mag to correspond to that of the LMC. The values of m_{bol} tabulated have not been so adjusted: they are the observed values.

Figure 2.5: Integrated parameters of LMC clusters. Note that the metallicity of NGC 1783 is [Fe/H] = -0.45 and the age is 1.1 Gyrs. The other cluster ages differ from 0.04 to 15.9 Gyrs. Taken from Frogel et al. (1990).

The stars are named from NGC 1783-01 to NGC 1783-15 following the numbering of TLE. In a shorter notation the label is star01 to star15. Meaning star01 is the object NGC 1783-01.

Stars	Instrument	$\alpha(J2000)$	$\delta(J2000)$
NGC 1783-01	ISAAC	04 58 54	-65 58 45.6
NGC 1783-02	ISAAC	04 59 02	-65 59 52.5
NGC 1783-03	ISAAC	04 59 16	-65 58 38.0
NGC 1783-04	ISAAC	04 59 22	-65 58 58.1
NGC 1783-05	ISAAC	04 59 16	-65 59 15.0
NGC 1783-06	ISAAC	04 59 03	-65 59 22.8
NGC 1783-07	ISAAC	04 59 01	-65 59 17.5
NGC 1783-08	ISAAC	04 59 00	-65 58 35.5
NGC 1783-09	ISAAC	04 59 09	-65 59 49.6
NGC 1783-11	ISAAC	04 59 07	-65 59 01.9
NGC 1783-12	ISAAC	04 59 15	-66 00 29.0
NGC 1783-13	ISAAC	04 59 25	-65 58 17.1
NGC 1783-14	ISAAC	04 59 02	-66 00 10.5
NGC 1783-15	ISAAC	04 59 12	-66 00 26.9
NGC 1783-IR1	ISAAC	04 59 01	-65 58 30.5
HD33322	ISAAC	05 04 36	-65 45 45.7
HD33895	ISAAC	05 09 04	-65 56 28.4

Table 2.2: Coordinates of the observed stars in NGC 1783 with ISAAC (ESO-VLT1/ISAAC).

Stars	Spectral type	Temperature [K]	$L_{\odot}$	Fe/H
NGC 1783-01	C	2477	10766	-0.45
NGC 1783-02	MS	3500	4800	-0.45
NGC 1783-03	C	3500	-	-0.45
NGC 1783-04	MS	3500	-	-0.45
NGC 1783-05	M	3500	5100	-0.45
NGC 1783-06	M	3500	-	-0.45
NGC 1783-07	M	3600	-	-0.45
NGC 1783-08	M	3600	-	-0.45
NGC 1783-09	M	3900	-	-0.45
NGC 1783-11	-	-	-	-0.45
NGC 1783-12	M	-	-	-0.45
NGC 1783-13	-	-	-	-0.45
NGC 1783-14	-	4000	1570	-0.45
NGC 1783-15	-	-	-	-0.45
NGC 1783-IR1	-	-	-	-0.45
HD33322	-	-	-	-0.45
HD33895	-	-	-	-0.45

Table 2.3: First results of temperature and $L_{\odot}$ after the sample stars derived by Thomas Lebzelter. The temperature was obtained from NIR colours. The metallicity and the spectral types of the stars were taken from Frogel et al. (1990), Frogel et al. (1980), and Cohen (1982).

2.2 VLT/ISAAC

With the Infrared Spectrometer And Array Camera (ISAAC) (Moorwood et al., 1998), near-infrared spectra with a medium spectral resolution of

$$R = \lambda/\Delta\lambda = 10000 \tag{2.1}$$

of the stars were obtained. The application for observing time was done in period 74A. The setup used was SWS-MR with 1.62 μm and 2.3 μm.

2.2.1 Overview of ISAAC

ISAAC is mounted on the Nasmyth A focus. The infrared is covered from the range 1 μm to 5 μm with two arms.

Hawaii Rockwell array

- 1024 x 1024 array
- Wavelength: 1 - 2.5μm

InSb Aladdin array

- 1024 x 1024 InSb
- Wavelength: 3 - 5μm
- For short wavelengths broad band filters are needed

Instrument Mode	$\lambda/\Delta\lambda$	Scale (pixel)	Limit magnitude range
SW LRes Spectroscopy	500	0.147	18 - 20.5
SW MRes Spectroscopy	3000	0.147	17.5 - 19.5
LW LRes Spectroscopy	500	0.147	11 - 14
LW MRes Spectroscopy	2000	0.147	10 - 13

Table 2.4: Spectroscopic modes of ISAAC. Short wavelength (SW), long wavelength (LW), S/N = 5 per resolution element (continuum per hour), seeing FWHM of 0.65 arc seconds, and using a 1.0 arc seconds slit. (c) ESO `http://www.eso.org/sci/facilities/paranal/instruments/isaac/overview.html`

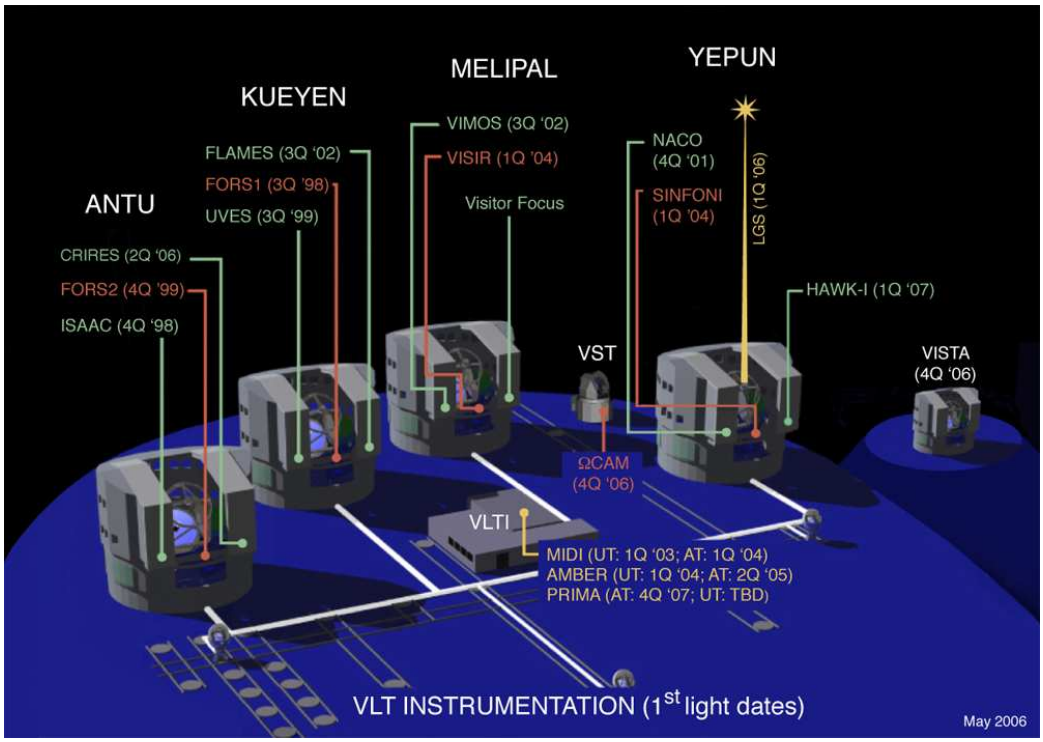

(a)

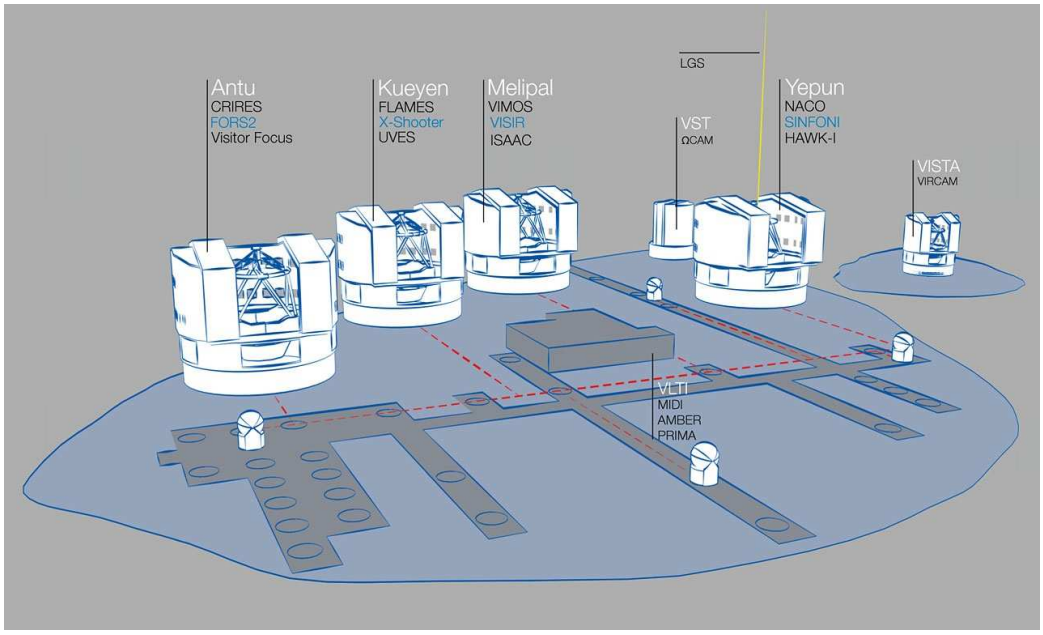

(b)

Figure 2.6: Subfigure (a) Instrumentation during May 2006. The obtained data for this thesis was gathered when the Infrared Spectrometer And Array Camera (ISAAC) was at the VLT1-Antu. Subfigure (b) Actual instrumentation on the VLT from the year 2011. ISAAC has moved to the VLT3. (c) ESO.

2.3 Data reduction

The original data were in the fits file format, standard infrared data reduction (Joyce, 1992), was applied by Thomas Lebzelter using IRAF.

2.4 Radial velocity

The radial velocities of the stars had to be determined. They were obtained from the observed spectra of the stars. In the middle of each obtained spectrum a prominent bandhead was taken to obtain the radial velocity at a given wavelength[2] λ_c. In case of the K-band, the ^{12}CO 3-1 bandhead was taken, and in the H-band the ^{12}CO 5-2 bandhead was taken.

2.4.1 Doppler-shift correction

The wavelength grid of the stars data files must be copied to the COMA08-file *wavin.dat* and with this input file, a COMA08 calculation run must be performed. In the file *sphread.ctr*, the Doppler-shift value RVEL is initially set to 0.0 km s^{-1}. So the computed synthetic spectra of COMA08 had a Doppler-shift of initially 0 km s^{-1}. The synthetic spectra were now shifted with the software *AGB*StarViewer until the two spectra overlapped 100% at the deepest point of the given bandheads in the middle of the spectra. With the obtained radial velocity value from *AGB*StarViewer, the value RVEL in the control-file *sphread04.ctr* was set. Then the program Sphread04 was called to re-calculate the correct Doppler-shift for the synthetic spectra.

The involvement of Sphread04 is necessary because it re-calculates the flux with the new Doppler-shift at a given wavelength, which *AGB*StarViewer does not. (Of course one can estimate the radial velocity only by editing RVEL and calling the program Sphread04 iteratively several times. The advantage with *AGB*StarViewer is, that one can estimate the correct Doppler-shift directly in the plot-window of *AGB*StarViewer, which Sphread04 cannot.)

[2]H-band: λ_c= 15995.948 Å, and for the K-band: λ_c = 23247.179 Å.

Star	H-band v_r [km s^{-1}]	K-band v_r [km s^{-1}]	Mean v_r [km s^{-1}]
NGC 1783-01	198.00	200	199.00
NGC 1783-02	222.54	-	222.54
NGC 1783-03	193.98	218.35	206.17
NGC 1783-04	208.89	202.75	205.82
NGC 1783-05	239.00	243.63	241.32
NGC 1783-06	193.59	187.31	190.45
NGC 1783-07	220.00	217.75	218.88
NGC 1783-08	185.00	217.75	201.38
NGC 1783-09	222.70	233.39	228.05
NGC 1783-11	-	-	-
NGC 1783-12	209.00	129.00 $*^1$	-
NGC 1783-13	-	-	-
NGC 1783-14	-	-	-
NGC 1783-15	-	-	-
NGC 1783-IR1	218.00	217.84	217.92
HD33322	-	-	-
HD33895	-	-	-
Mean:	**210.06 ± 16.19**	**206.78± 31.72**	**213.15 ± 15.33**

Table 2.5: Radial velocities of the AGB-stars in NGC 1783. The Radial velocities were measured at the prominent bandheads for the H-band at: λ_c= 15995.948 Å, and for the K-band at: λ_c = 23247.179 Å. The total mean of the radial velocities is 213.15 ± 15.33 km s^{-1}.

$*^1$ The measured radial velocity of star12 in the K-band cannot be correct because all other stars are within the same range of v_r. Due to the reason, that all bandheads are at the correct positions in the K-band spectrum of star12, it must be a reduction problem, of unknown origin.

Chapter 3

Synthetic spectra and abundances

In order to calculate synthetic spectra for a comparison with the observations we used model atmospheres, which were compared to the spectra of the stars. We used the COMARCS code (Aringer, 2000; Aringer et al., 2009). COMARCS is a modified version of the MARCS code from Gustafsson et al. (1975), based an older version of Jørgensen (1992). The MARCS code was updated recently by Gustafsson et al. (2008).

MARCS stands for *Model Atmospheres in a Radiative Convective Scheme*. In the MARCS code, the temperature and the pressure structure are calculated under the assumption of a one-dimensional spherical configuration with a hydrostatic and local thermal equilibrium (LTE). The LTE also implies a chemical equilibrium (CE). COMARCS uses updated atomic and molecular opacities, which were calculated with COMA08[1]. The COMA08 package (Aringer 2000, Aringer et al. 2009) , was also used to compute the synthetic spectra which ensures the same opacity input for model construction and radiative transfer for synthetic spectroscopy.

COMA stands for *Copenhagen Opacities for Model Atmospheres* (Aringer, 2000). The model spectra were calculated with spherical radiative transfer routines based on common structures (Windsteig et al., 1997). VALD-2 (Kupka et al., 2000) was used for the atomic line data. The molecular data were taken from many other sources. An overview is given in Aringer et al. (2009) and Cristallo et al. (2007). Corrected line position data for CO (Goorvitch and Chackerian, 1994) and CN (Jørgensen, 1997) were used.

[1]COMA08 is the eight version of COMA.

3.1 Atmospheric models and spectral synthesis

About 1238 MARCS[2] model atmospheres with [Fe/H] = -0.4 and a temperature range from 2300 K to 3900 K were taken from Lederer et al. (2009). These model atmospheres are qualified for rather cool C, M and MS stars (Loidl et al. 2001, Aringer et al. 2002). It should be pointed out that the metallicity in NGC 1783 is [Fe/H] = -0.45. In order to save computing time, a small discrepancy[3] was accepted and the models with a metallicity of [Fe/H] = -0.40 were used. Because of the cluster age of 1.4 Gyears (Mucciarelli et al., 2007), which results in an approximate turn-off mass of 1.5 $M_\odot$, we have accepted the latter value for the models, and the mass and the metallicity were kept constant at M = 1.5 $M_\odot$ and [Fe/H] = -0.40. The microturbulent velocity was set to[4] at ξ= 2.5 km s^{-1}, which is a valid velocity for atmospheres for low-mass AGB-stars (Aringer et al., 2002; Gautschy-Loidl et al., 2004). The initial solar abundances were set to an element composition, where the value for the C/O-ratio is C/O = 0.48 (Grevesse and Noels, 1993). The initial solar value for the carbon isotopic ratio was set to $^{12}C/^{13}C = 89.9$ (Anders and Grevesse, 1989). Hill found out an oxygen over-abundance for many of the clusters in the LMC (Hill et al., 2000). So we calculated an additional over-abundance of oxygen with +0.2 dex for the model atmospheres.

3.1.1 Parameters

The computed model atmospheres have the following parameters:

1. The effective temperature: T_{eff} [K]
2. The surface gravity: log (g [cm s^{-2}])
3. The C/O-ratio
4. The mass: M [$M/M_\odot$]
5. The metallicity: [Fe/H]
6. The micro-turbulent velocity ξ [km s^{-1}]

[2]Labelled with the version number "mxcom03" which was also used in Lederer et al. (2009).

[3]A difference of 0.05 in the metallicity is smaller than a realistic error of an abundance determination.

[4]Although we had models available with ξ= 2.5 km s^{-1} or ξ=3.5 km s^{-1}.

Constant parameters

The following parameters were kept constant (Lederer et al., 2009).

- Mass: M = 1.5 $M_{\odot}$
- Metallicity: [Fe/H] = -0.40
- Micro-turbulent velocity: ξ= 2.5 km s^{-1}

Parameter variations

The following parameters were fitted (Lederer et al., 2009).

- Temperature [K]
- Log (g [cm s^{-2}])
- C/O-ratio
- Isotopic abundance of $^{12}C/^{13}C$

The grid for the temperature covers a range from 2300 K to 3900 K with a stepsize of ± 50 K. The range for the logarithm of the surface gravity was set to -0.50 to 0.50 with a stepsize of ± 0.25. The C/O-ratio was calculated with a stepsize of ± 0.05, and the isotopic abundance of $^{12}C/^{13}C$ was calculated with a stepsize of ± 1. Some papers also predict an over-abundance for Oxygen with +0.2 dex (Hill et al., 2000). In a second computing run, the oxygen over-abundance value was varied from 0 to + 0.2 dex.

Error bars

The error is determined from the stepsize of the parameters.

- Δ T = 50 K
- Δ Log(g) = 0.25
- Δ(C/O) = 0.05
- Δ ($^{12}C/^{13}C$) = 1
- Δ O = 0.2 dex

3.1.2 O-rich case

If the C/O ratio is smaller than one (C/O < 1), the star is of oxygen-rich type. This means that the major opacity contributors are:

- H_2O, TiO, CO and CN (Loidl et al. 2001, Aringer et al. 2002).

But there are also:

- OH, SiO, TiO_2, VO, ZrO, ScO, YO, LaO (Jørgensen, 1994; Jørgensen, 1995).

3.1.3 C-rich case

If the C/O ratio is greater than one (C/O > 1), the star is of carbon-rich type. This means that the major opacity contributors are:

- C_2H_2, C_2, C_3, HCN, CN and CH (Loidl et al., 2001; Aringer et al., 2002).

3.1.4 Molecule selection for M-stars

Since we had only calculated spectra for the M-stars and MS-stars, the main opacity contributors for the C-rich case namely HCN, C_2H_2, C_3, and C_2, were excluded in order to save computing time. Included were the following molecules:

- CO, CH, SiO, CN, TiO, H_2O, OH, VO, CO_2, SO_2, HF, HCI, FeH, CrH, ZrO, YO and CS.

3.2 Spectral synthesis with COMA08

3.2.1 Calculated star spectra

We have calculated nearly 4000 stellar spectra for the H-band and 8000[5] for the K-band. The range for the H-band was 6381.62 to 6053.26 cm^{-1} (15692.09 to 16507.96 Å) and for the K-band the range was 4415.01 to 4177.12 cm^{-1} (22680.56 to 23919.13 Å)

[5]The first 4000 calculations were made for both H-band and K-band, the second 4000 calculations were only for the K-band with variations of the isotopic abundance of $^{12}C/^{13}C$ in a dense grid around the previous best fitted spectra (see Chapter 4.5.1).

The spectra were calculated with a high resolution of

$$R = \Delta\lambda/\lambda = 300000 \tag{3.1}$$

in order that they describe line profiles smoothly and that they can be compared with future observed spectra, which may have a different resolution. The program *Sphread04* which is included in the COMA08 package, convolved these spectra via a Gaussian

$$G(\Delta\lambda, \sigma) = \frac{1}{\sqrt{2\pi} \cdot \sigma} \cdot \exp\left(-\frac{(\Delta\lambda/\sigma)^2}{2}\right) \tag{3.2}$$

to match the medium resolution of 10 000 of the observed stars.

$$\sigma = \sigma_R + \sigma_{v_t} \tag{3.3}$$

$$\sigma_R \equiv \frac{\lambda}{2R} \tag{3.4}$$

σ_{R} reduces the effective resolution to a given R, and

$$\sigma_{v_t} \equiv \frac{\lambda}{2} \cdot \frac{v_t}{c} \tag{3.5}$$

$\sigma_{\mathrm{v_t}}$ accounts for the macroturbulent velocity $\mathrm{v_t}$.

3.2.2 Computers

The synthetic spectra were computed on three computers. Mainly at the two servers: AGB and MIRA of the Institute for Astronomy in Vienna and for a small part on my computer at home[6]. The servers have dual-core cpus. The Fortran software COMA08 was installed and configured in the same way on all computers. A certain spectrum was computed on all computers for testing reasons. The resulting files of the computed spectra were compared and they were identical.

The difficulty in the software setup is that the atomic and molecular linelists have to be installed on all computers. The compressed data on a DVD have about 6 GB. Unpacked, the data have about 20 GB. A future application will be to have the atomic data on one server, and several other servers can access the data over the network interface in order to setup a parallel computing configuration.

[6]AMD64 +3.5 GHz

3.2.3 COMA08 files

Wavin.dat

To get good results for a comparison, the wavelength of the synthetic spectra should be exactly[7] the same as in the observed data. Therefore one has to copy the column of the wavelength from the observed data, e.g.: star01K.dat and put it in a file called *wavin.dat*. The format of *wavin.dat* has to be only one column of wavelength data and the unit must be μm. The program Sphread04 can now produce data at exactly the same wavelength-points which were observed. This is necessary to get good fitting results from a chi-square fit.

Control files

The spectral resolution can be selected different from the wavelength grid. The resolution of the computed synthetic spectra should be the same as the resolution from the observed data. We used the COMA08 control files: *coma08.ctr* and *sphread.ctr*, for manipulating the calculation. A good starting point for the calculation of the grid would be to calculate the H-band and K-band with a high resolution, like 300 000. Then, afterwards, these pre-calculated spectra will be convolved to the specific observed wavelength-points for every star. These wavelength-points must be copied to the file *wavin.dat* for every star. The program Sphread04 can produce an unique spectrum for every star, with the input of *wavin.dat* of the specific star. Sphread04 also re-calculates the flux of the new wavelength-points from the file *wavin.dat*. A script can be used to match the computed high resolution spectra, which output is in the *.spe files, with every star *wavin.dat* file. This needs only some minutes to compute the spectra for every star instead of hours of computing time, if COMA08 calculates each star spectrum from the scratch. The value INPTYP of *sphread.ctr* must be set to SPE, so COMA08 takes the data from each pre-calculated *.spe file. Also the specific Doppler-shift of each star will be taken into account, with the variable RVEL in the program Sphread04.

[7]Meaning at the exact wavelength-points.

Chapter 4

Data analysis

4.1 H-band 1.62 μm

In the H-band, the wavelength range from 6381.62 to 6053.26 cm^{-1} (15692.09 to 16507.96 Å) was observed. It it possible to derive the temperature and the C/O-ratio in the H-band and then use the found parameters to investigate the K-band. With CN lines and metal lines like the ones of Fe, Ti and Si, the effective temperature and other parameters can be estimated. A common advantage is that the H-band is mostly free of telluric lines. The C/O-ratio of a stellar atmosphere can be determined by comparing the intensities of the $^{12}C^{16}O$ 3-0 bandhead with those of the OH lines (Lederer et al., 2009). We have selected mostly the same set[1] of model atmospheres to produce spectra for both bands. From the H-band the stellar parameters and the C/O-ratio were derived. Oxygen abundances were derived also from OH lines[2].

4.2 K-band 2.3 μm

In the K-band the wavelength range from 4415.01 to 4177.12 cm^{-1} (22680.56 to 23919.13 Å) was observed. Because the K-band spectrum is sensitive to the isotopic abundances of $^{12}C/^{13}C$, the carbon isotopic ratio of $^{12}C/^{13}C$ was derived in this wavelength band. Although the K-band is not very sensitive to the effective temperature, we tried to determine the temperature from there, too, and compared[3] it with the results from the H-band.

[1] Meaning the 4000 model-atmospheres were calculated each for the H-band and K-band.

[2] See Table 4.3

[3] See result tables, Chapter 6.

4.3 Signal to noise

The signal to noise (S/N) of some stars was determined by Thomas Lebzelter. For every spectrum we have two observations taken at different slit positions. These are normalised by dividing them through the corresponding median. After that we calculated a mean spectrum and the deviations for each pixel. Then we computed (spectra 1 - mean)^2. The standard deviation is used to determine the signal to noise ratio and the squared differences give the chi-square.

The results of some stars are:

Star H-band	S/N	χ^2	Number of pixels
05 H	96	0.23	986
07 H	70	0.49	987
09 H	23	2.56	1001
12 H	72	0.61	1009

Table 4.1: Signal to noise (S/N) of some stars, determined by Thomas Lebzelter.

4.4 Overview plots

The overview of the H-band and the K-band sorted by the star names is shown in Fig 4.2.

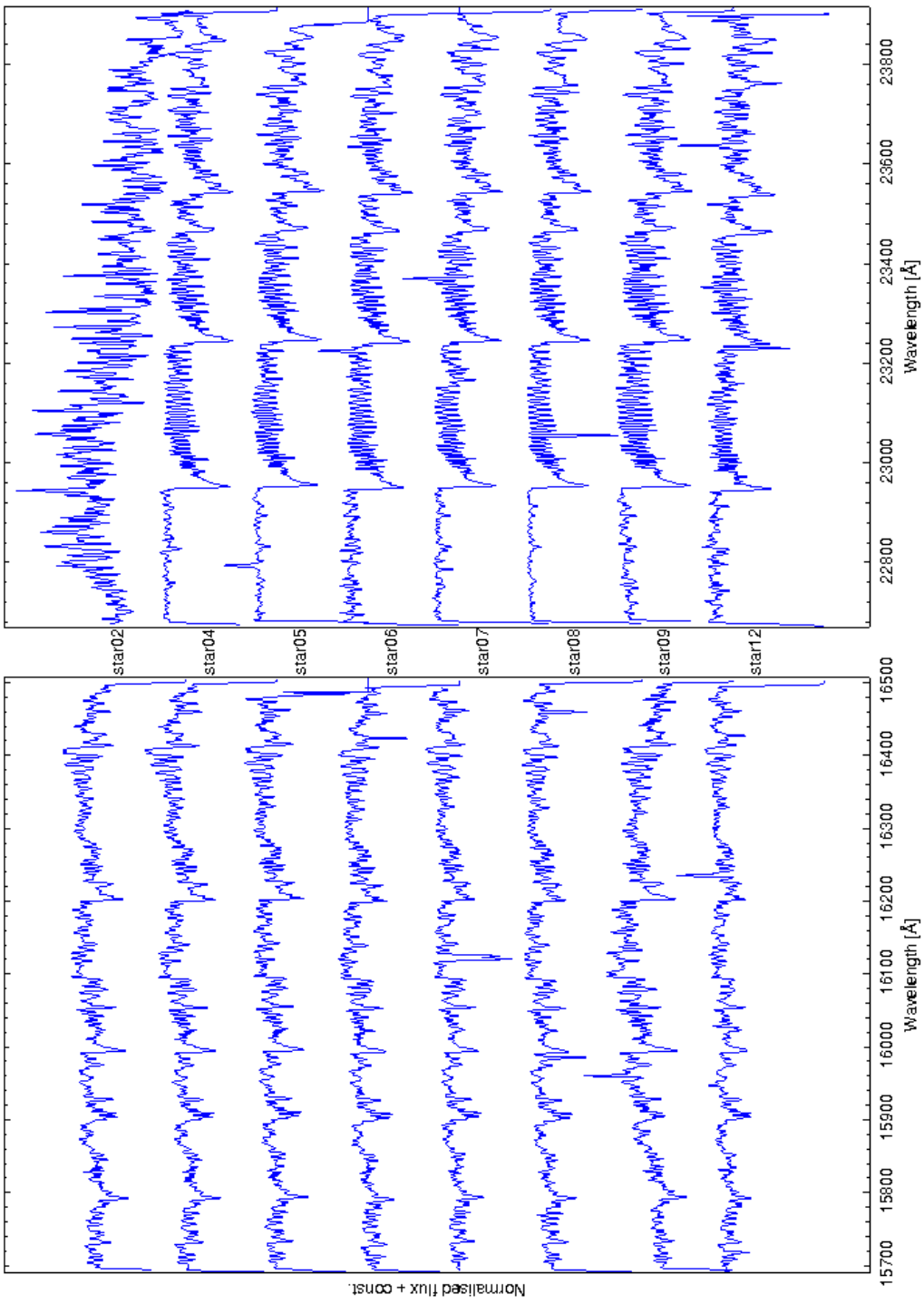

Figure 4.1: Overview of the M-type AGB-stars with normalised flux in the H-band (1.6 nm) and K-band (2.3 nm). Note the bad spectra from star02K. It was excluded from the investigations.

4.5 Model parameters

The grid of the MARCS models was calculated by Michael Lederer (2009). The ranges of the physical parameters are:

- Temperature: 2300 to 3900 K with Δ T = 50 K
- Log(g[cm s^{-2}]): -0.50 to 0.50 with Δ log(g) = 0.25
- C/O: 0.10 to 3.00 with Δ C/O = 0.05

In Fig. 4.2, Fig. 4.3 and in Fig. 4.4 the parameter space of the synthetic spectra calculations are shown. In Fig. 4.3 one can see that for the C/O-ratio the grid range was limited. For lower temperatures, from 2300 K to 3300 K, there are only C/O values above 1 because all cooler stars in the cluster are expected to be carbon-rich. So there were no COMARCS models calculated below a C/O-ratio of 1.0. From a temperature range from 3400 K to 3900 K the C/O values vary mostly from 0.10 to 1.1. In almost all investigated stars we found C/O-ratios smaller than 1.0, i.p. they are oxygen-rich, see the final result tables at Chapter 6.

4.5.1 A denser grid for $^{12}C/^{13}C$

After determining the values of temperature, the surface gravity and the C/O-ratio, the grid[4] for the isotopic abundance of $^{12}C/^{13}C$ was calculated. It should be noted that the $^{12}C/^{13}C$-ratio has almost no influence on the atmospheric structure.

The grid for the isotopic abundance of $^{12}C/^{13}C$ was calculated from 4 to 50 in steps of one with $\Delta\, ^{12}C/^{13}C = 1$ and from 51 to 100 mostly in steps of five with $\Delta\, ^{12}C/^{13}C = 5$. This was possible because the best model fits for the $^{12}C/^{13}C$-ratio were found at values below 50.

In the H-band there are no prominent ^{13}C features or ^{13}CO bandheads, so a safe estimation of the isotopic abundance of $^{12}C/^{13}C$ is uncertain in the H-band. Only one single $^{13}C^{12}O$ feature in the H-band was found[5] but it is blended with Fe and V.

[4] The first grid has the initial standard solar value of $^{12}C/^{13}C = 89.9$.
[5] See Table 4.6.

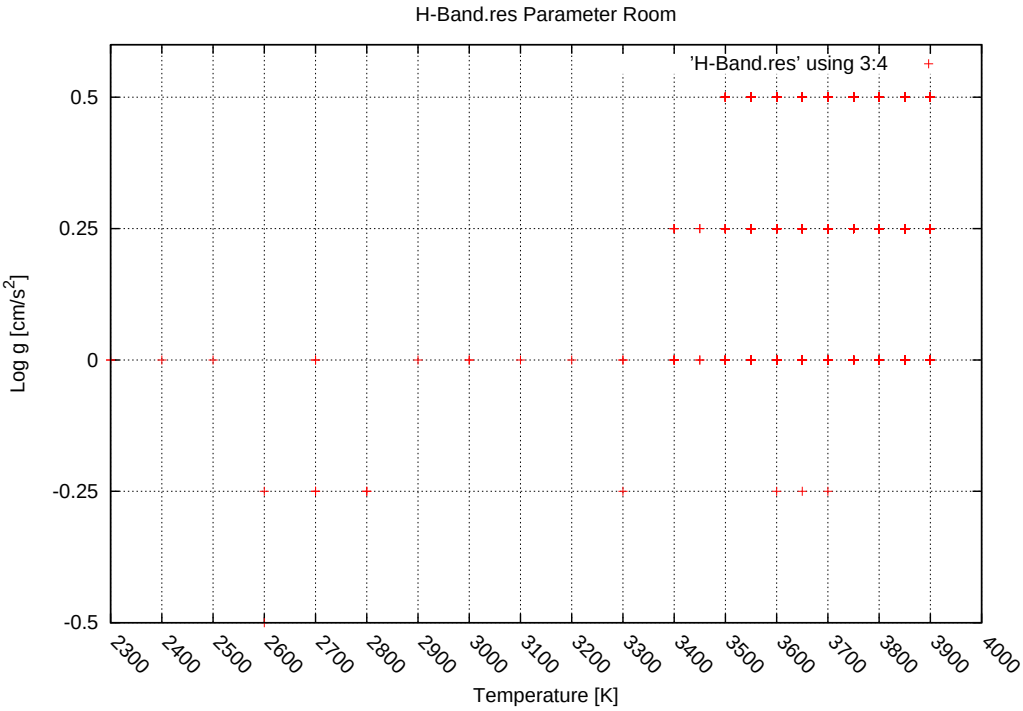

(a) H-band

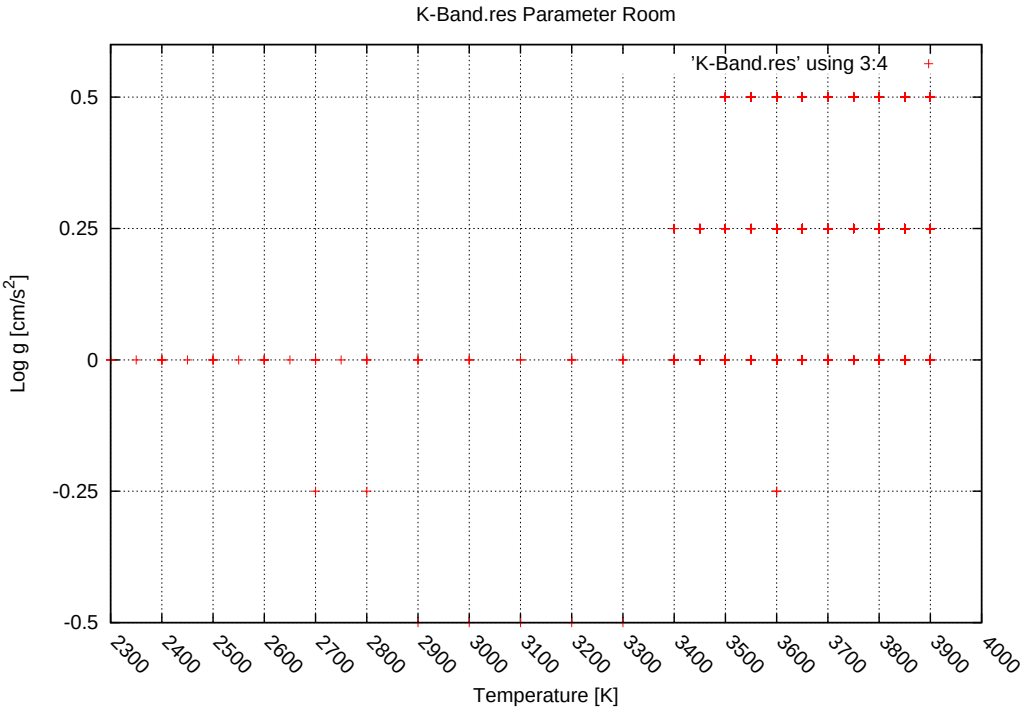

(b) K-band

Figure 4.2: Overview of the parameter space of the synthetic model calculations for the logarithm of the surface gravity.

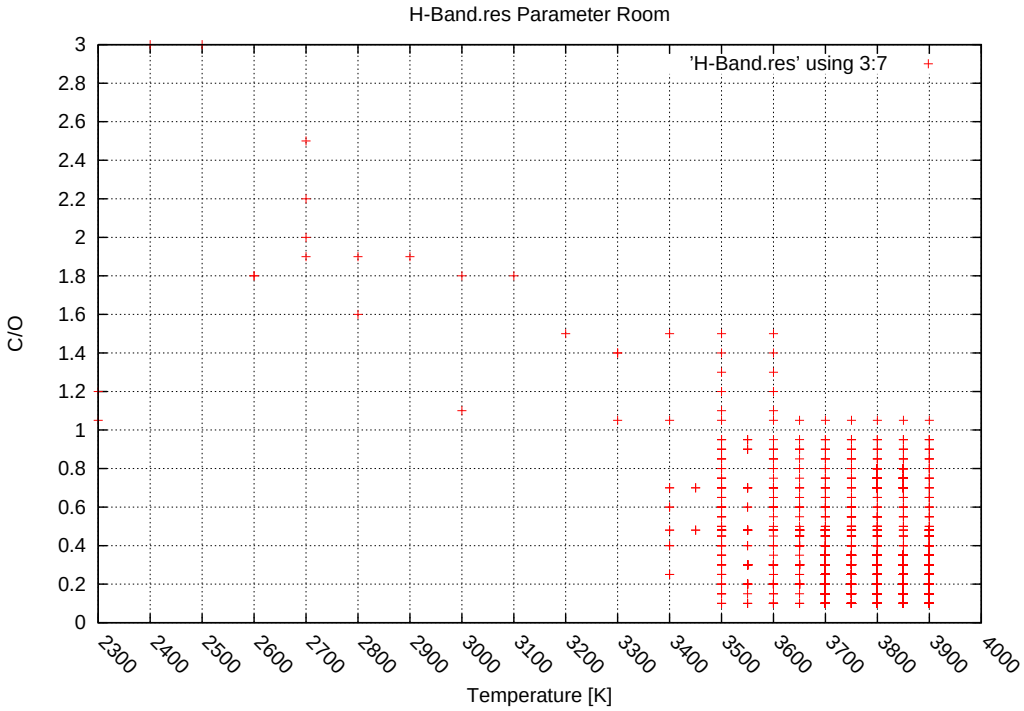

(a) H-band

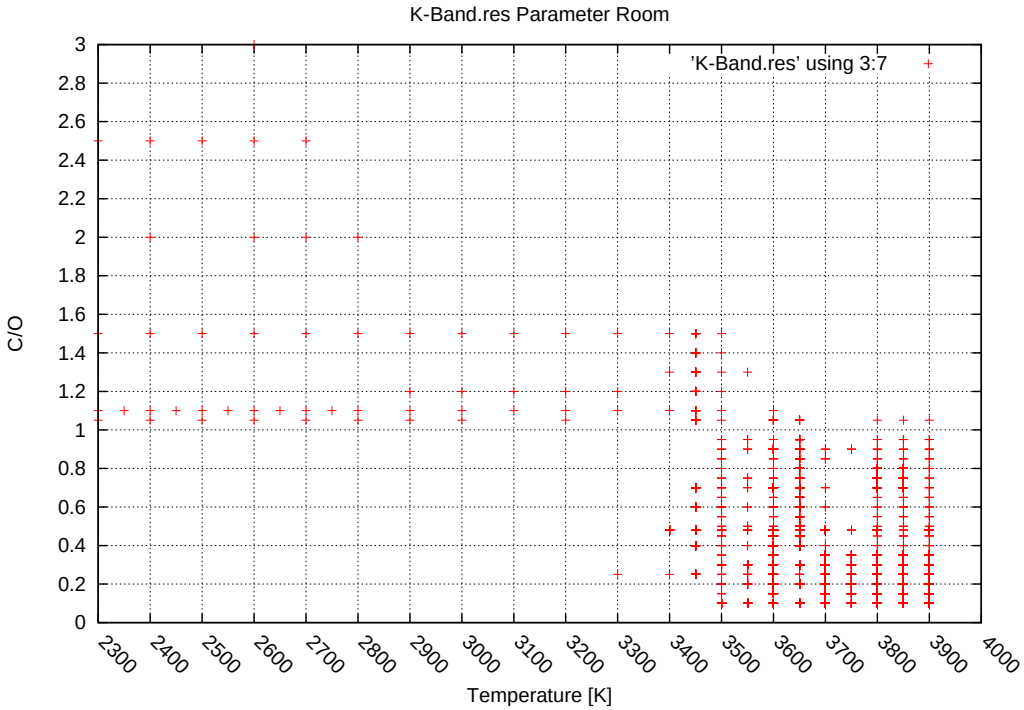

(b) K-band

Figure 4.3: Overview of the parameter space of the synthetic model calculations for the C/O-ratio. The gap at 3750 K in the K-band is not dramatic, because the final C/O-ratio was derived from the H-band.

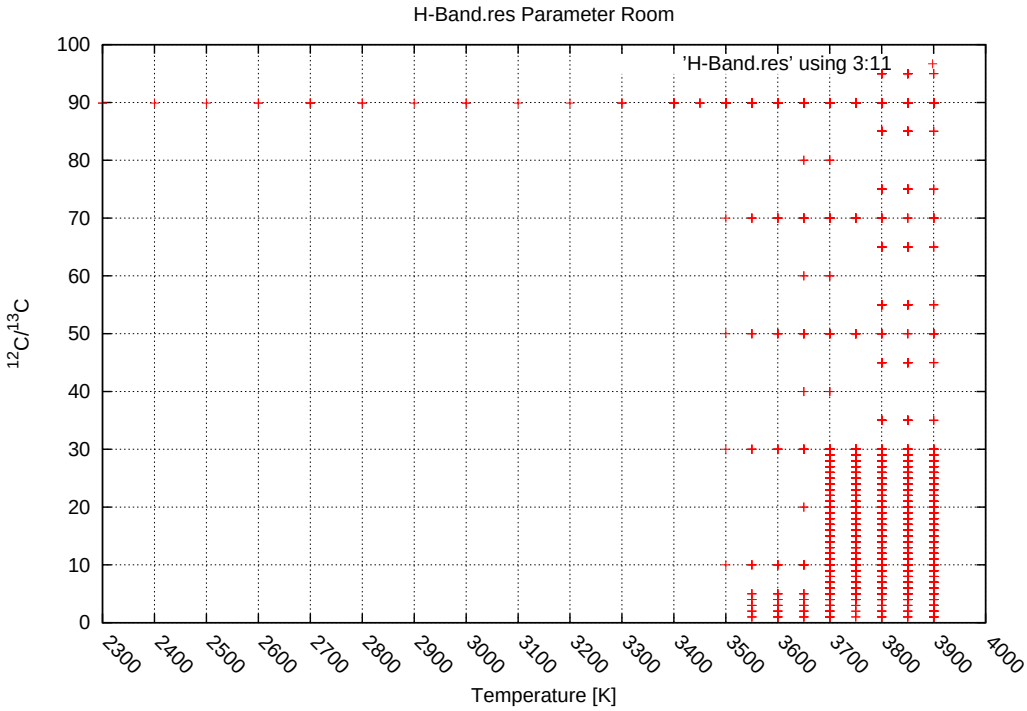

(a) H-band

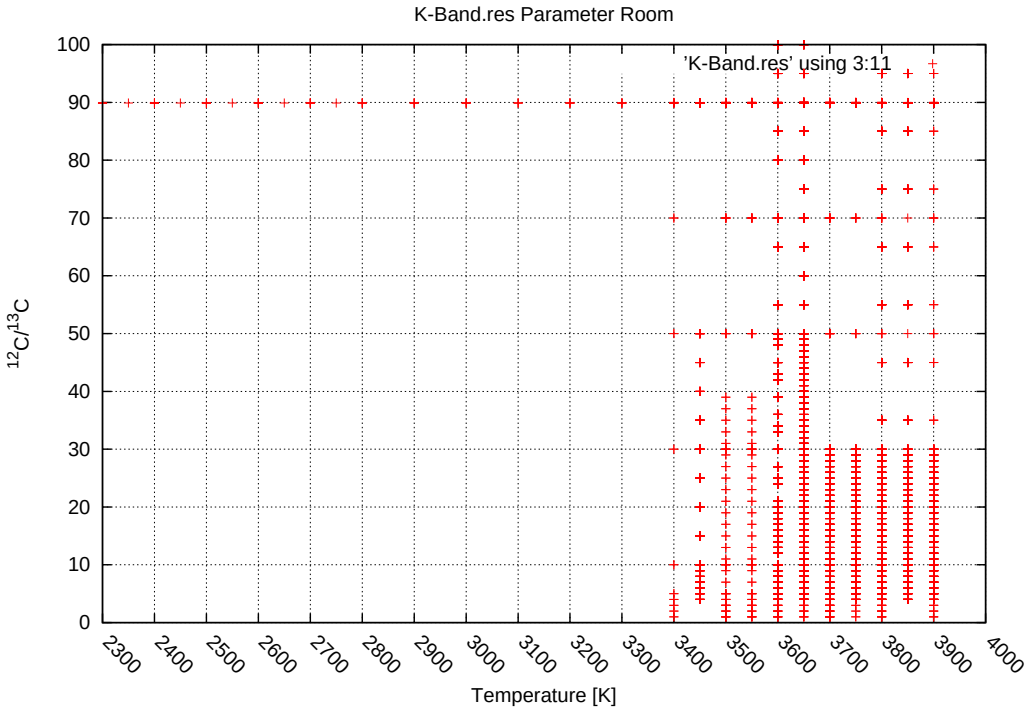

(b) K-band

Figure 4.4: Overview of the parameter space of the synthetic model calculations for the isotopic abundances of $^{12}C/^{13}C$ (IACO). The gap at 3500 K to 3650 K in the H-band is not dramatic because the $^{12}C/^{13}C$-ratio was derived in the K-band.

4.6 Included bandheads and features

Features	Lower limit [Å]	Upper limit [Å]	Sum [Å]
^{12} CO 4-1 head	15780.62	15810.92	-30.31
V, Fe,^{13}C^{12}O	15938.00	15946.00	-8.00
^{12} CO 5-2 head	15992.76	16029.44	-36.69
OH 2-0 P 13.5	16077.29	16083.00	-5.71
CO 6-3 head	16200.91	16228.83	-27.91
^{12} CO 7-4 head	16340.00	16345.00	-5.00
OH 3-1 P10.5	16363.61	16377.96	-14.35
Fe & ^{12}CO 7-4 head	16412.00	16418.00	-6.00

Table 4.2: General overview of features in the H-band. A small single ^{13}C^{12}O feature was found in the H-band, but it is blended by V and Fe features. V is vanadium. Total: 133.97 Å.

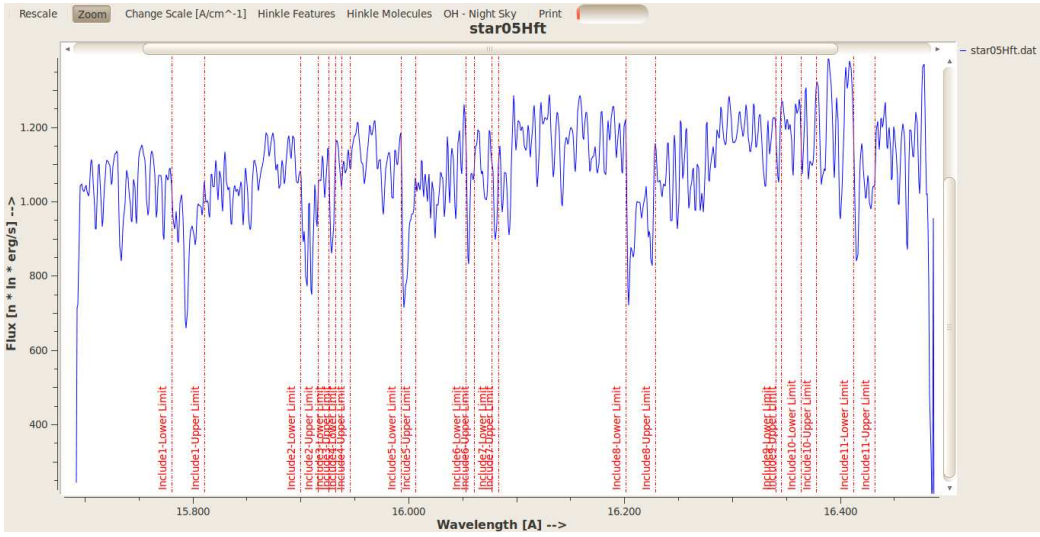

(a) star05 H-band

Figure 4.5: *AGB*StarViewer inclusions: The included bandheads and features in the H-band of star05 are shown. They correspond to Table 4.3.

Features	Lower limit [Å]	Upper limit [Å]	Sum [Å]
^{12} CO 4-1 head	15780.62	15810.92	-30.31
OH 2-0 P1e 13.5 OH 2-0 P1f 13.5 OH 2-0 P2f 12.5	15900	15916	-16
OH 3-1 P1e 8.5 OH 3-1 P1f 8.5	15926	15932	-6
^{13}C^{12}O, V and Fe	15938	15946	-8
^{12} CO 5-2 head	15992.76	16006.32	-13.56
OH 3-1 P2e 8.5 OH 3-1 P2f 8.5	16052	16061	-9
OH 2-0 P2e 13.5 OH 2-0 P2f 13.5	16077.29	16083	-5.71
CO 6-3 head	16200.91	16228.83	-27.91
OH 3-1 P2e 10.5 OH 3-1 P2f 10.5 OH 4-2 P1e 5.5 OH 4-2 P1f 5.5	16340	16345	-5
OH 3-1 P2f 10.5 OH 3-1 P2e 10.5 OH 4-2 P1e 5.5 OH 4-2 P1f 5.5	16363.61	16377.96	-14.35
Fe + ^{12}CO 7-4 head	16412	16432	-20

Table 4.3: Included Ranges in the H-band. Total: 154.844 Å. A small single ^{13}C^{12}O feature was found in the H-band, but it is blended by V and Fe features.

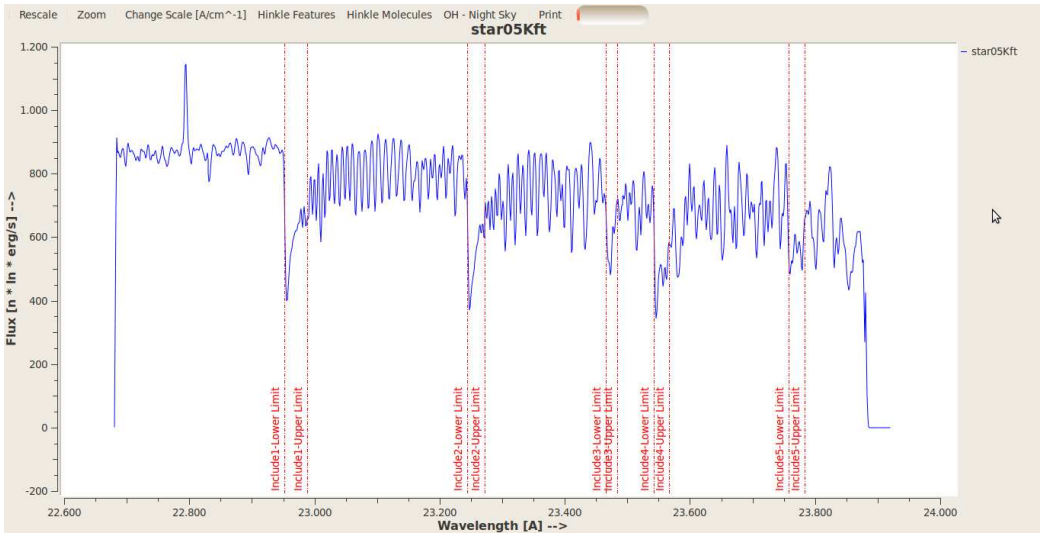

(a) star05 K-band

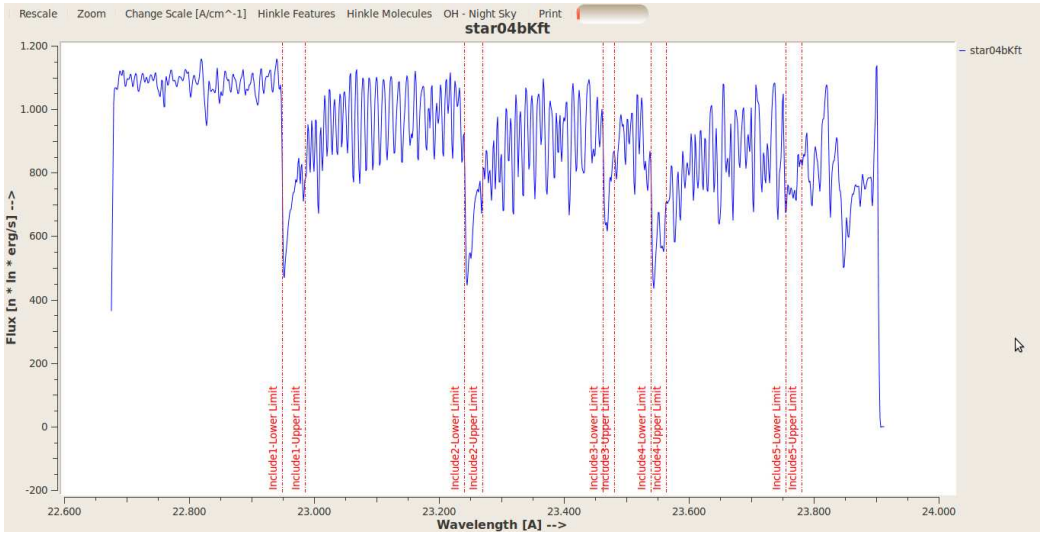

(b) star04 K-band

Figure 4.6: *AGB*StarViewer inclusions: Included bandheads and features in the K-band. Star05 has a radial velocity of 243 km s^{-1} and star04 has a radial velocity of 203 km s^{-1}. The shifts of the inclusion ranges were corrected via the SW *AGB*Starviewer.

Bandhead	Lower limit [Å]	Upper limit [Å]	Sum [Å]
^{12}CO 2-0 head	22951.762	22988.084	-36.322
^{12}CO 3-1 head	23243.546	23272.604	-29.058
^{13}CO 2-0 head	23465.109	23483.270	-18.161
^{12}CO 4-2 head	23542.595	23566.810	-24.215
^{13}CO 3-1 head	23758.104	23783.529	-25.425

Table 4.4: Included bandheads in the K-band. Total: -133.181 Å.

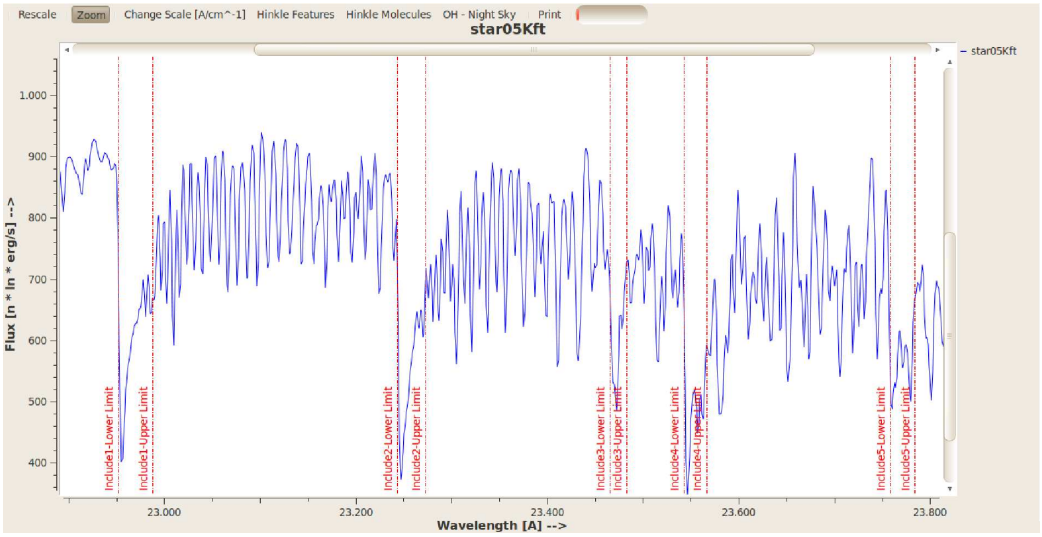

(a) star05 K-band

Figure 4.7: *AGB*StarViewer inclusions: Here the K-band of star05 is shown, zoomed into the included bandheads.

4.7 Excluded ranges

If there are any bad data regions in the spectra of a star, and one wants to do a fit, it must be guaranteed that these wavelength ranges are excluded in all other stars too. Then the fits of all stars become statistically comparable. In the following tables these excluded regions are listed. They are valid for star02, star04, star05, star06, star07, star08, star09 and star12.

Lower limit [Å]	Upper limit [Å]	Sum [Å]
15687.000	15697.000	10.000
15958.403	15962.363	3.960
16115.703	16129.274	13.571
16233.433	16236.618	3.185
16480.047	16507.96	27.913

Table 4.5: Excluded ranges for all stars in the H-band. This is necessary because of cosmics or bad data in the marked ranges. The excluded ranges cover a total sum of 58.629 Å.

Lower limit [Å]	Upper limit [Å]	Sum [Å]
22672.750	22686.735	13.985
22789.000	22799.000	10.000
23051.842	23057.871	6.029
23221.843	23232.720	10.877
23366.542	23371.365	4.823
23634.072	23640.080	6.008
23816.720	23919.130	102.41

Table 4.6: Excluded ranges for all stars in the K-band. This is necessary because of cosmics or bad data in the marked ranges. The excluded ranges cover a total sum of 154.132 Å

4.7.1 A peculiar descent in the stellar spectra

The part above 23800 Å of the observed wavelength range in the K-band was excluded totally. The reason of this was that the flux of the observations of all stars was not comparable to the synthetic spectra. The normalised flux of the synthetic spectra were nearly at one, while the observed spectra had a significant descent, so they were not comparable to a chi-square fit. Possible reasons for this peculiarity could be an error of the instrumentation, or missing features (molecules) in COMA08 which were not activated for the calculations, or which were not implemented at all. Or the pipeline of the reduction and flux calibrating process is not working properly for this wavelength range above 23800 Å.

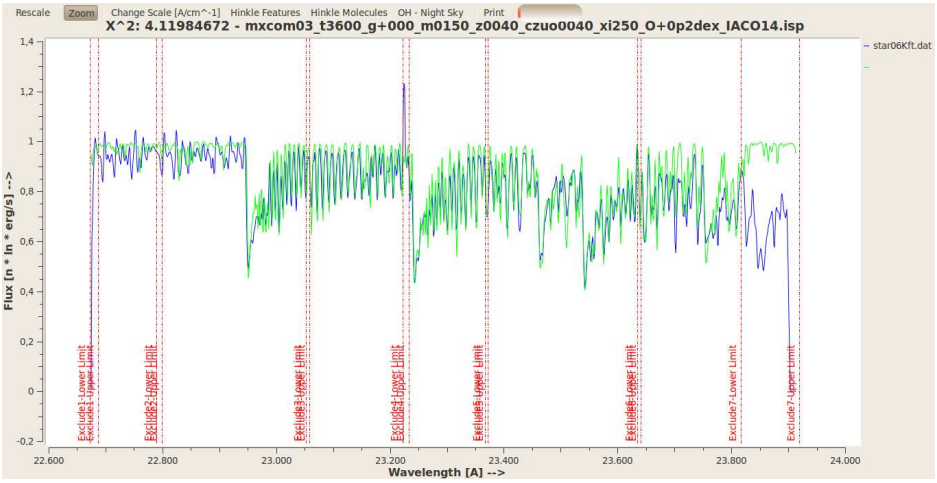

(a) Excluded K-band regions

Figure 4.8: Here the best fit of star06 is shown. The excluded ranges are marked by the red vertical lines. Beneath the peak in the middle of the spectra, note the peculiar descent of the observed (blue) spectra greater than 23800 Å. This descent appears in all other stars, too.

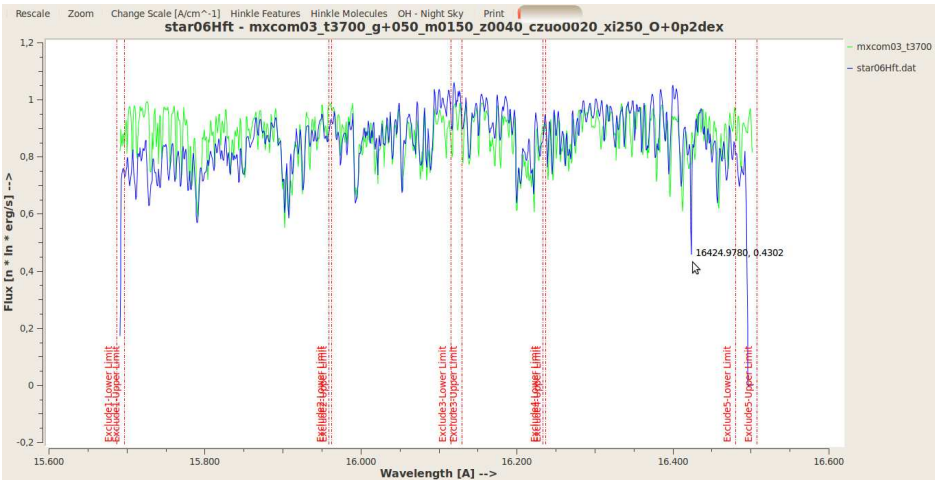

(a) Excluded H-band regions

Figure 4.9: Here the best fit of star06 is shown in the H-band. The excluded ranges are marked by the red vertical lines. While the most right part is not a big problem, the most left part of the spectra has a descent from 15700 Åto 15800 Å. There is also an interesting feature at 16424 Å, in the observed (blue) spectra next to the mouse arrow.

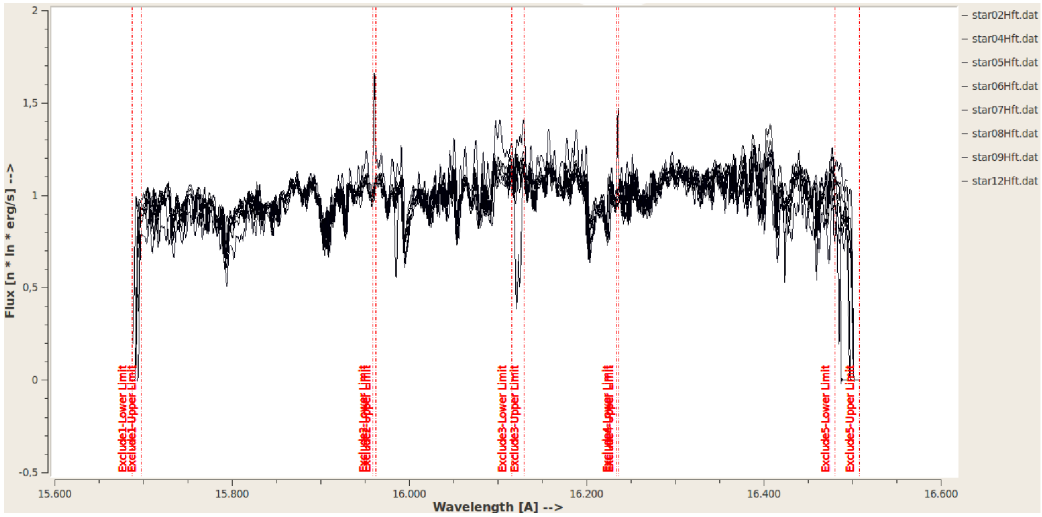

(a) H-band excluded ranges

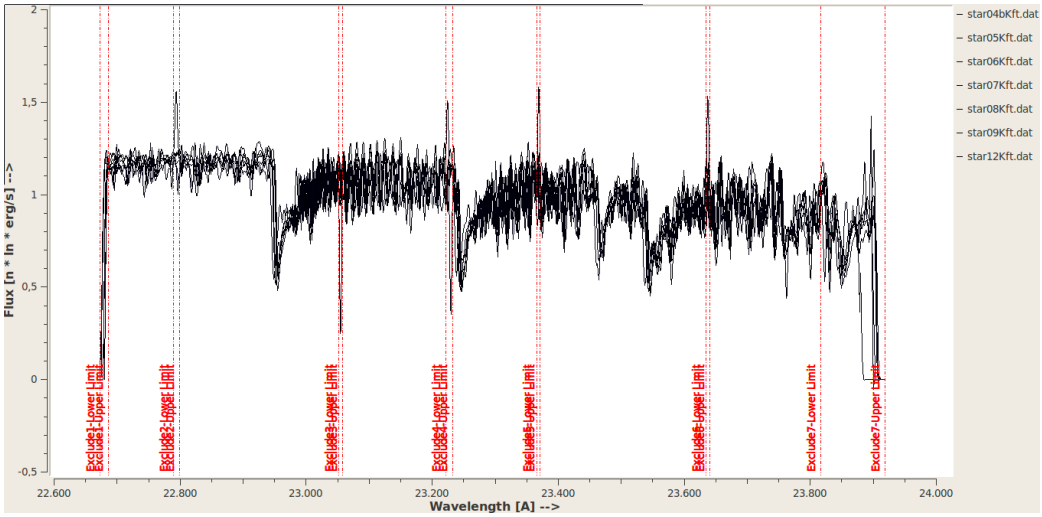

(b) K-band excluded ranges

Figure 4.10: *AGB*StarViewer with excluded ranges marked. Here all stars are shown in the H-band and K-band. Note the several peaks due to cosmics.

4.8 Data fitting

4.8.1 Flux normalisation

In order to perform a chi-square fit, the data have to be normalised first. With the flux normalisation the two fluxes of the synthetic and observed spectra become comparable. There are three common methods to do this: the mean, the median and the least squares. In this thesis the observed flux was normalised to the synthetic flux via least-squares. But let's discuss the methods briefly.

Mean

The first and simplest approach is to divide the observed flux through its mean value.

$$\overline{x} = \frac{1}{n} \sum_{i=1}^{n} x_i \tag{4.1}$$

(Bartsch, 2004). The disadvantage with this method is, that the resulting flux is not in the range from zero to one. It has values which are larger than one. E.g. $x = 1.2$ or $x = 1.4$ something. This depends on the flux of the observed star. Using the mean, one has to calculate the mean of the synthetic flux also. So both the synthetic and the observed data have to be divided with the mean value. Using the mean is problematic if the observed data have high peaks like cosmics[6]. These high peaks will falsify or distort the value of the mean and should not be taken into account.

Median

The median, or central-value, is very similar to the mean, but it does not have the problem with the peaks, because the median sorts high data peaks statistically out. But still, the observed and the synthetic flux have to be divided by the median, and the resulting curves can be higher than the limit from zero to one. The central-value is the mid-value of a series of variations $\mathrm{x}_1 \leq \mathrm{x}_2 \leq ... \leq \mathrm{x}_\mathrm{n}$.
If n is odd

$$\mathrm{x}_{0.5} = \mathrm{x}_{\frac{\mathrm{n}}{2}+1} \tag{4.2}$$

If n is even

$$\mathrm{x}_{0.5} = \frac{\mathrm{x}_{\frac{\mathrm{n}}{2}} + \mathrm{x}_{\frac{\mathrm{n}}{2}+1}}{2} \tag{4.3}$$

[6]High energetic particles.

with

$$P(X < \ x_{0.5}) \leq \frac{1}{2} \leq \mathrm{P}(\mathrm{X} \leq \mathrm{x}_{0.5}) \tag{4.4}$$

(Bartsch, 2004).

Least squares

Finally, the least square approach was chosen. The computed (synthetic) flux from COMA08, with a range from zero to one was taken unchanged. The total range of the observed spectra was divided into ten equal regions. For each region, the maximum value of the flux was taken to determine the maximum value for the least square analysis. Then the flux was normalised to the synthetic flux via the found least-square value.

Least square - rules

- Select bandwith in ten equal ranges.
- Find the maximum of each range.
- Sum each found maximum to a value.
- Calc the least square sum with the observed sum divided through the synthetic sum.
- Divide the flux with the least square sum.

Stars	Max flux H-band	Max flux K-band
NGC 1783-02	801.00	-
NGC 1783-04	1398.82	1158.24
NGC 1783-05	1353.00	**913.00**
NGC 1783-06	714.46	**754.00**
NGC 1783-07	975.61	**1118.00**
NGC 1783-08	1096.86	1239.28
NGC 1783-09	**323.00**	1464.68
NGC 1783-12	**1551.00**	**430.00**

Table 4.7: The maximum fluxes of the stars. Bold ones have an artificially limited flux because of high data peaks like cosmics. The data of star02K were not good enough for the evaluation.

Stars	Least-square H-band	Least-square K-band
NGC 1783-02	737.889	-
NGC 1783-04	1201.199	1125.045
NGC 1783-05	1246.269	**902.386**
NGC 1783-06	671.742	**716.743**
NGC 1783-07	887.921	**1085.343**
NGC 1783-08	1040.354	1228.999
NGC 1783-09	**290.328**	1424.523
NGC 1783-12	**1484.998**	**417.523**

Table 4.8: The least square sum of the stars for each band.

4.8.2 Chi-square

To determine the best model for the observations, the chi-square test of K. Pearson was done.

$$\chi^2 = \sum_{i=1}^{n} \frac{(O_\mathrm{i} - E_\mathrm{i})^2}{E_\mathrm{i}} \tag{4.5}$$

χ^2 is the cumulative number of the chi-square, it asymptotically approaches the χ^2-distribution. O_i are the observed wavelength points, E_i is an expected (computed) wavelength point, n is the number of the total wavelength points.

Absolute chi-square

Alternatively a variation of K. Pearsons chi-square test, which is used by Stefan Uttenhtaler, was implemented in the SW *AGB*StarViewer. It allows to test star data with very small fluxes.

$$\chi^2 = \sum_{i=1}^{n} \frac{(O_\mathrm{i} - E_\mathrm{i})^2}{(O_\mathrm{i} + E_\mathrm{i}) \cdot \frac{1}{2}} \tag{4.6}$$

With the term $(O_\mathrm{i} + E_\mathrm{i}) \cdot \frac{1}{2}$, the chi-square value cannot become negative, which in case will falsify the chi-square value and may happen at small fluxes. Accordingly to Stefan Uttenthaler it is called an absolute chi-square test. In this thesis the chi-square of K. Pearson was used.

Discussion of the chi-square

One problem during the chi-square analysing process is, that there are often several physical values in the mathematical parameter space of the solution. But in reality only one e.g. temperature of the star could be the correct one. An example is the temperature in star05H (Fig. 6.9) and star06H (Fig. 6.10). The temperature differs in star05H from 3700 to 3900 K. While the only models with T=3900 K (number 14) and T = 3850 (number 17) have a log(g) of zero instead of log(g) = 0.5 like the rest of the models, and therefore could be identified as statistical outliers, the model number 27 has also 3850 K but a log(g) = 0.5. On the other hand, the model numbers 13 and 15 have also a temperature of 3800 K like the eigth best fitting models, while their log(g) = 0.25 instead of log(g) = 0.5 like the other models. The temperature range still differs about more than 100 K from 3750 K to 3850 K. This is more than the predicted accuracy of ± 50 K for the temperature.

The situation in star06H is quite similar. If one is looking at the log(g) of the ten best fitting models, they have a log(g) = 0 and log(g) = 0.5! The log(g) is no help here to determine which temperature is the best approximation to the physical reality. So for star06H the best fit result for the temperature is T=3850 K but also T=3900 K could be a reliable result.

So a single best fit chi-square model is no guarantee for a reliable final result. But which models do represent the best physical solution? By taking simply the best fitting model, one has to make the sure, that this best model is under no circumstances a statistical outlier.

Some kind of mean of the best solutions would be nice to have, especially, if there are several models with a chisquare value close to the best fit value but with quite different stellar parameters. Therefore, the need of a *Fair Mean* was necessary. It is the mean between the best fitting model, the normal mean of the 30 best fitting models and the weighted mean of the 30 best fitting models. In the result tables it is called the *Final Mean*.

4.9 Parameter and abundance determination

Lebzelter et al. (2008b) and Lederer et al. (2009) did investigate the H-band to determine the temperature and then, take the found temperature to investigate the physical parameters of the K-band. This method saves computing time because not all synthetic spectra must be calculated for both bands.

In this thesis, contrary to the method described before, there was calculated the whole set[7] Having the very same calculations for both bands, a better statistical investigation is possible. The goal was to determine if there is a general shift in the temperature from the H-band versus the K-band.

Then the results from the chi-square were analysed with three methods:

- Via the best fitting model
- Via the mean of the best fitting models
- Via the weighted mean of the best fitting models

4.9.1 The best fitting model

One option is to simply take the best fit[8] of a model. Although this is a good starting point, it is not safe against statistical outliers. The results can be seen Chapter 6, in the section *Result tables*.

4.9.2 The mean of the best models

But a single mathematical number, as produced by the chi-square, does not always comply to the physical reality. A more robust strategy would be to take some kind of a mean of the best fitting models. Less than one percent of the best fitting model calculations were taken for determining the mean. This were the 30 best fitting spectra of the about 4000 total calculated spectra.

4.9.3 The weighted mean of the best models

To support the entity of the chi-square, a weighted mean in order of the descending numbers of the chi-square, would be better. This means the best

[7] The basis calculations for both bands have the same ∼4000 synthetic models.
[8] The best fit has the smallest chi-square value

chi-square results should have more weight in the total mean. The data set of the best chi-square descending looks like:

$$\vec{x} = (0, 1, ..., n, ..., N_{total}) \tag{4.7}$$

N_{total} is the number of the best models which were taken for the investigation. In our case $N_{total} = 30$.
The weighted chi-square of the X-axis should be a linear relation like

$$\vec{x}_{weight}(n) = (100\% - \frac{100\%}{N_{total}} n) \tag{4.8}$$

so the best chi-squares have a weight as shown in Fig. 4.11. The weighted mean would be

$$Mean_{weighted}(n) = \frac{1}{n} \sum_{i=1}^{n} x_i \cdot x_{weight,i} \tag{4.9}$$

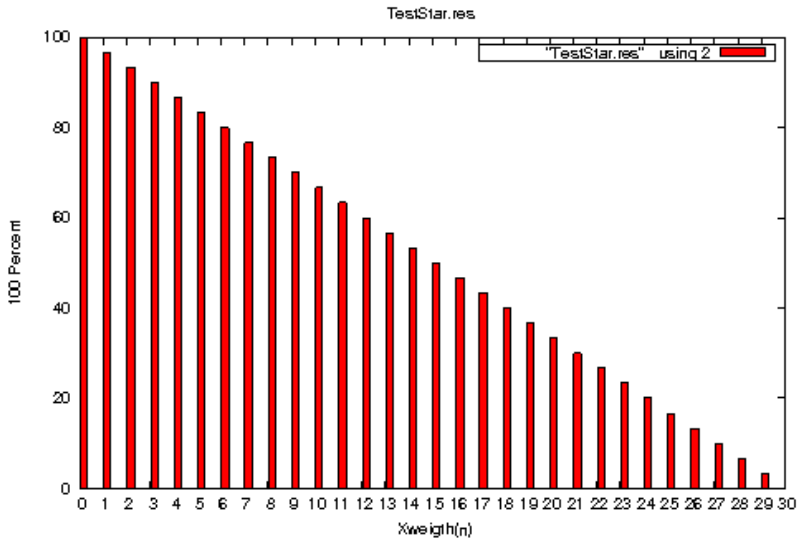

Figure 4.11: The function $\vec{x}_{weight}(n)$ shows the weight of the linear fit, corresponding to the numbers of the X-Axis. So the best chi-square at n=0 has more weight than chi-square at n=1, n=2, and so on.

A Gnuplot visualisation problem:
The x-range for all plots should be 1 to 30. The equivalent command in Gnuplot is *set xrange [1:30]*. But since Gnuplot has the internal values listed

like an array in the language C, e.g. like *double Results[30]* it reads the values from position 0 to position 30. So the first item is adressed with zero, e.g. *print(Results[**0**]);* In Gnuplot the command *set xrange [1:30]* has the side effect, that the first entry, in our cast the best fit, will be ignored! Therefore the x-range was set from 0 to 30 with *set xrange [0:30].* This means the best fit is addressed with zero in all plots. This looks not beautyfull but the internal calculations will be done correct.

Testing the weighted mean

Fig. 4.11 shows the weight which will be applied to the thirty best model fits. It is a linear relation, which decreases from 100 % to 1 % in N_{tot} steps. In this thesis the best thirty fitting models were used. The following Figures are showing some test cases for the weighted mean[9]. Fig. 4.12 shows a constant value of 3000 K. The mean and the weighted-mean have the same result of 3000 K. Fig. 4.13 shows a similar situation. The first eight and the last eight models have the same temperature. The mean and the weighted-mean have nearly the same result of 3067 K and 3065 K. The difference is due to rounding errors. In Fig. 4.14, the last eight models have a temperature of 4000 K while the others have 2000 K. Therefore the weighted-mean is about 383 K smaller than the mean. In Fig. 4.15 the opposite situation is shown. The first eight models have a temperature of 4000 K while the others have 2000 K. The difference between the mean and the weighted-mean is 380 K. Fig. 4.16 shows a linear decrease from 4000 K to 2250 K. The weighted-mean is about 243 K higher than the mean. And in Fig. 4.17 the opposite situation is shown. An increase from 2250 K to 4000 K in steps of 50 K is resulting in a weighted-mean which is 244 K lower than the mean. These tests ensure that the concept of the weighted-mean is working properly.

[9]Although they are rather unlikely for a star, they fulfil the test scenarios for the weighted mean.

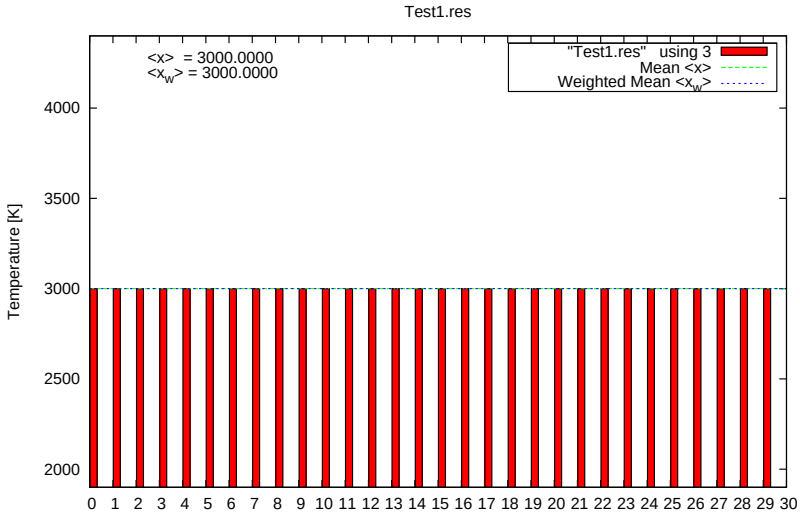

Figure 4.12: Test 1 of the weighted mean. The temperatures of all of the test models are constant at 3000 K. The mean and the weighted mean are showing the same results.

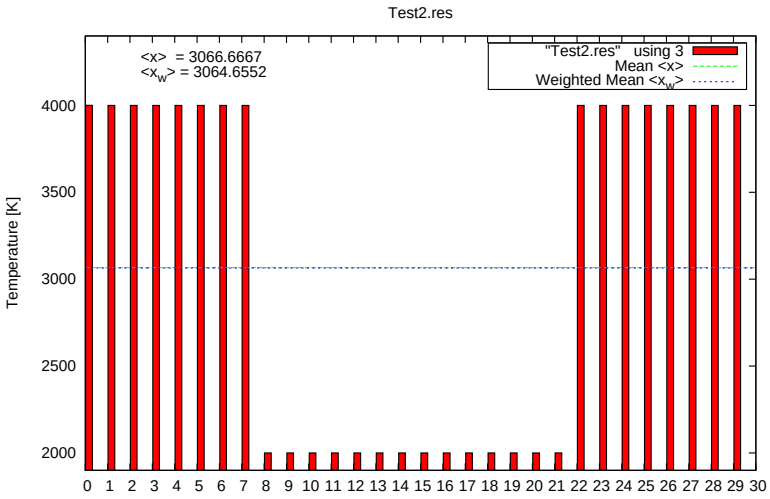

Figure 4.13: Test 2 of the weighted mean. The first eight and the last eight models have a temperature of 4000 K. The fourteen models in the middle have all 2000 K. The mean is 3067 K and the weighted-mean is 3065 K.

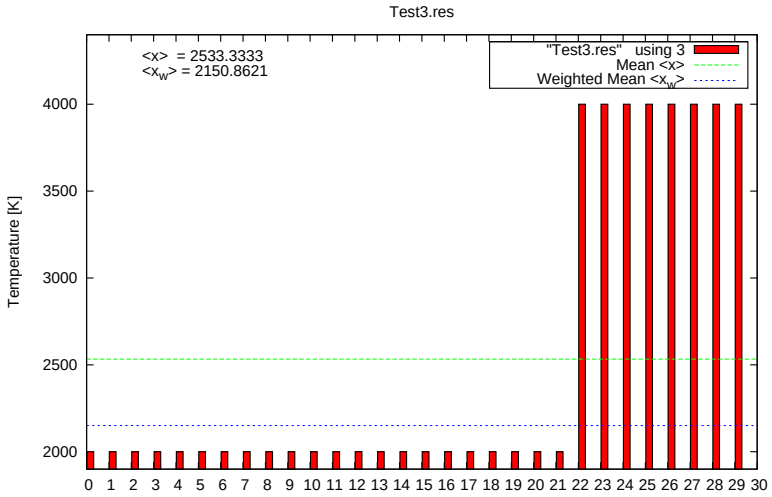

Figure 4.14: Test 3 of the weighted mean. The first twentytwo models have the same temperature of 2000 K, the last eight models have a temperature of of 4000 K. So the weighted mean is smaller than the mean. The difference is about 383 K.

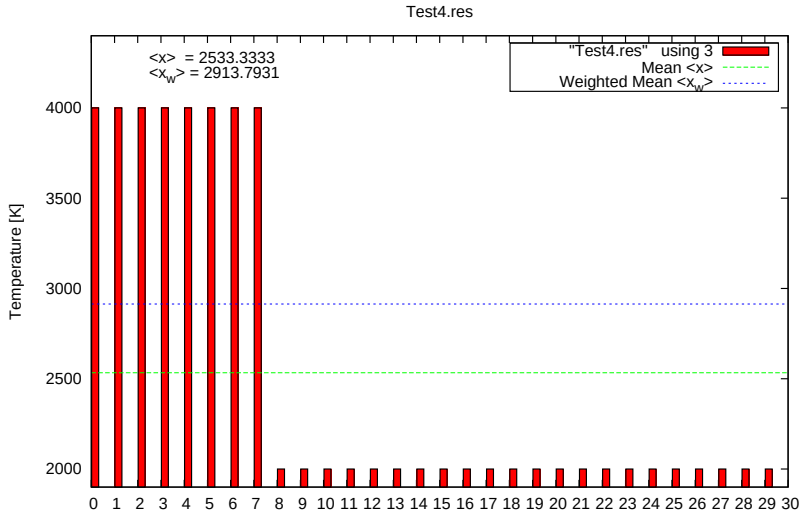

Figure 4.15: Test 4 of the weighted mean. The first eight stars have a temperature of 4000 K. So the weighted mean is higher than the mean. The difference is about 380 K.

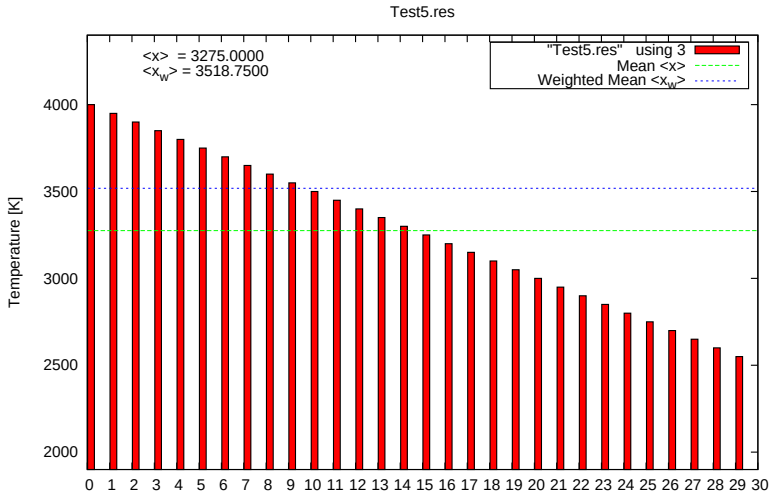

Figure 4.16: Test 5 of the weighted mean. The temperature is decreasing from 4000 K to 2550 K in steps of 50 K for each model. The weighted mean is higher and the difference is about 243 K.

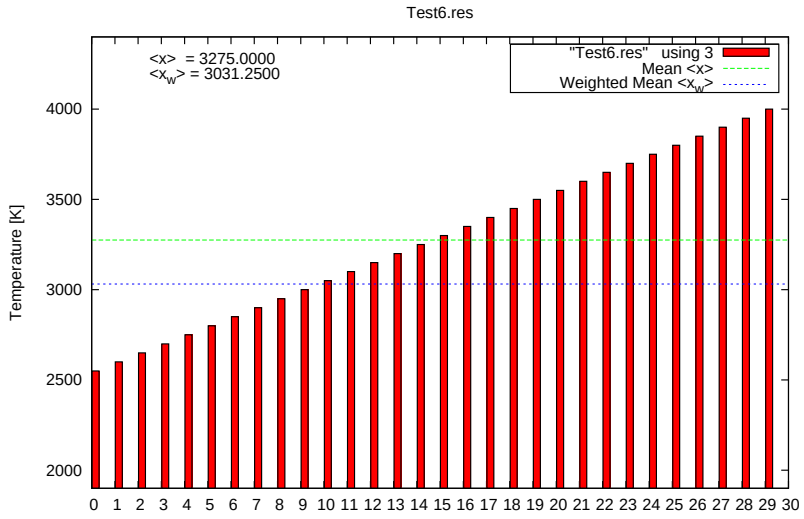

Figure 4.17: Test 6 of the weighted mean. The temperature is increasing from 2550 K to 4000 K in steps of 50 K. The weighted mean is smaller and the difference is about 244 K. Note that the mean here and in test5 is the same.

Chapter 5

New software for the AGB-community

5.1 Motivation

The motivation for writing the two software packages *AGB*StarViewer and *ComaGUI*, was to create a tool, which can handle most of the work that people in the AGB-Group of the *University of Vienna* have to do when studying stellar spectra. Learning to operate the Fortran software COMA08 developed by B.Aringer, S.Höfner, M.Gorfer is a task which takes a considerable amount of time. More specifically writing computer scripts in Bash, Pearl and Ruby which can handle many hundreds to thousands of COMA08 calculations on the servers is not trivial. *ComaGUI* is a frontend or a GUI (graphical user interface), which can operate the Fortran software COMA08. Although it is always good to learn something new, e.g. a scripting-language as Ruby, the idea behind *ComaGUI* was to remove, the heavy-informatics task from the users and to set the focus more to astronomical science. In *ComaGUI* one can import a bunch of MARCS model atmospheres and calculate synthetic model spectra. *ComaGUI* helps to select and calculate a grid of synthetic spectra, for comparison with observations. One can select a specific temperature range, e.g. from 2300 Kelvin to 4000 Kelvin, and perform calculations for a specific log(g)[1], C/O-ratio and isotopic abundances of $^{12}C/^{13}C$, for the given temperature range[2]. The main function of *AGB*StarViewer is to produce a zoomable plot of stellar spectra[3] and do chi-square fits to determine the best synthetic model spectra for an observed star spectra.

[1] Log(g) is the logarithm of the surface gravity of a star.
[2] But only for the set of input (MARCS) models which were calculated in the first place.
[3] Or any other physical data.

5.2 *AGB*StarViewer - best fit and spectra plotting software

5.2.1 Features

The software (SW) *AGB*StarViewer has the following features:

- Show two stellar spectra[4] in a plot and compare them via a chi-square fit.
- Find the best fit using several hundred synthetic spectra files and save the results to a file.
- Navigate and zoom through all plots in the order of their best fits, e.g. one can zoom into a feature like TiO and look, how the fit changes in with respect to the chi-square value[5].
- Perform a range selection, which data (bandheads) should be taken into account for the chi-square fit. This is realised by inclusion or exclusion of certain wavelength ranges[6].
- Apply one set of "Range Selection" for different stars. The selection will be corrected for different radial velocities[7].
- Show positions of atomic lines and molecules identified in the *Infrared atlas of the Arcturus spectrum, 0.9-5.3 microns* (Hinkle et al., 1995) in the plot.
- Change the scale of the plot from Å to 1/cm for direct comparison to the *Infrared atlas of the Arcturus spectrum, 0.9-5.3 microns* (Hinkle et al., 1995).
- Overplot the *OH-Atlas of the night sky* (Rousselot et al., 2000).

[4]It could show either an observed with a synthetic spectrum, or two observed spectra or compare two synthetic spectra or any other data.

[5]In this way, the software supports also the choosing of the best fit via inspection by eye.

[6]If there are several stars in the data set, each spectrum must be analysed in the same wavelength range, to ensure that the statistics will be correct.

[7]Doppler-shifts.

5.2.2 Input data

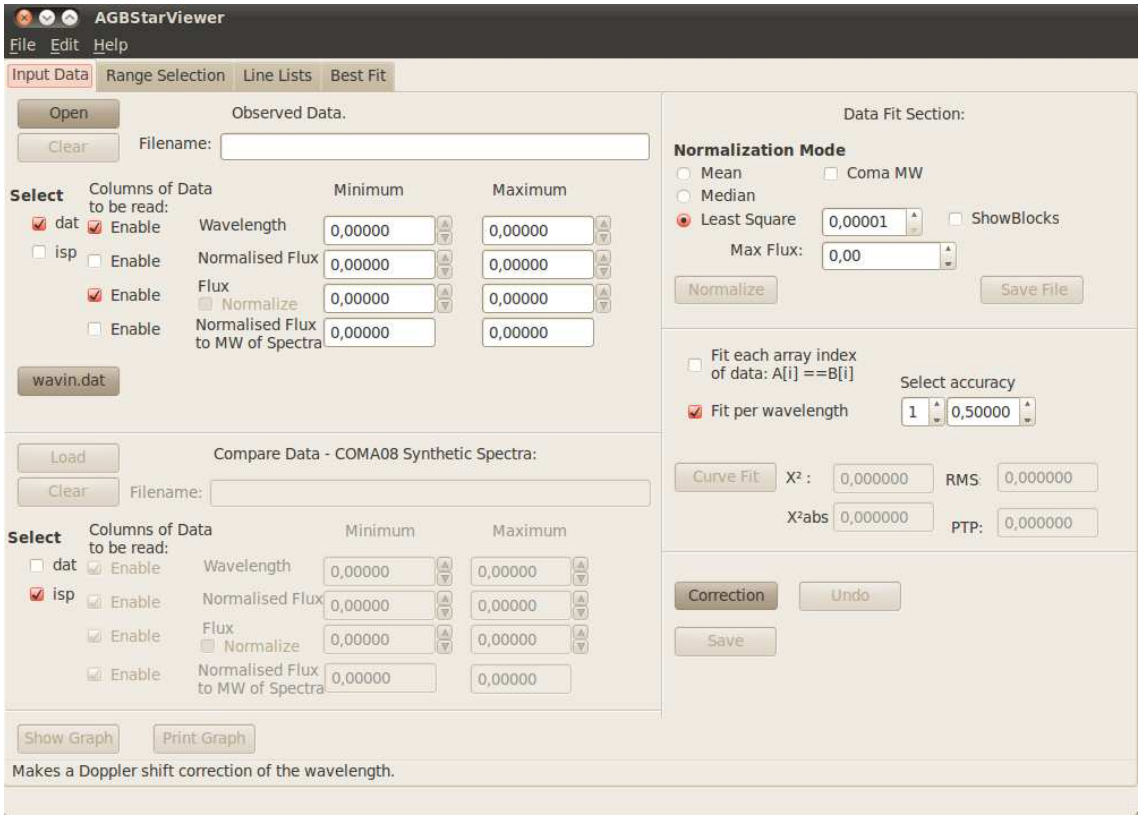

Figure 5.1: In the Tab "Input Data", section "Observed Data", two spectra can be compared in detail. One has to select the correct file format to be read. In principal other txt-file formats could be read in, too, but the columns in the other file formats must correspond to the selected check-boxes: wavelength, normalised flux, flux and the flux normalised to the mean of the spectra.

Tool tips

If one hovers over the buttons with the mouse arrow, the tool tips of the buttons will be displayed. In Fig. 5.1 the tool tip of the button "Correction" is shown as an example.

Observed data

In the section "Observed data", the reduced file from the observation should be loaded with the button "Open". It can be cleared with the button "Clear", or by simply pressing the "Open" button again and selecting a new file. The minimum and maximum values of each column will be displayed. The small up and down arrows have no function in this SW version. But they will have in future versions. The button "Wavin.dat" creates a file wavin.dat, with the correct format for COMA08. With this file, COMA08 calculates the spectrla flux at the exact wavelength positions which are given in the file wavin.dat.

Compare data

The section "Compare Data", has the same functionality as the section "Observed data". It is intended for uploading the synthetic spectrum.

File format

To load a data file into the software, one has to select the file format first. *AGB*StarViewer can read two pre-defined file formats. *.isp with four columns and *.dat with two columns of data. One can select between these two file formats with the check-box "Select". In principal the SW can read files with other filename-extensions, too. In the section: "Columns of data to be read", one has to select up to four check-boxes. Each check-box corresponds to one column of data[8] in a file. The SW does not check the validity of the data format. This has to be done by the user. A typical *.isp file has the information about it physical parameters in it filenames, like:
mxcom03_t3750_g+025_m0150_z0040_czuo0035_xi250_O+0p2dex_IACO20.isp

Listing 5.1: *.isp text file format of a synthetic spectrum. The order of the columns are: the wavelength in Å; the normalised flux; the flux and the flux normalised to the mean of the spectra.

```
15692.090    0.89673   0.129072E+38    0.104280E+01
15692.888    0.83985   0.120890E+38    0.976700E+00
15693.685    0.79392   0.114284E+38    0.923326E+00
15694.483    0.84571   0.121746E+38    0.983611E+00
15695.280    0.88187   0.126955E+38    0.102570E+01
15696.078    0.83093   0.119627E+38    0.966494E+00
```

[8]The wavelength, the normalised flux, the absolute flux and the flux normalised to the mean of the spectrum.

Listing 5.2: *.dat text-file format of the observed spectrum. It is the reduced spectrum from the former IRAF fits-file. The flux is not yet normalised here. The order of the columns are: the wavelength in Å and the flux.

```
15693.685   709.3432
15694.483   810.2981
15695.280   905.4319
15696.078   1018.041
15696.875   1025.139
15697.673   1013.231
15698.470   1006.823
15699.268   1004.141
15700.065   1010.357
```

Plot window

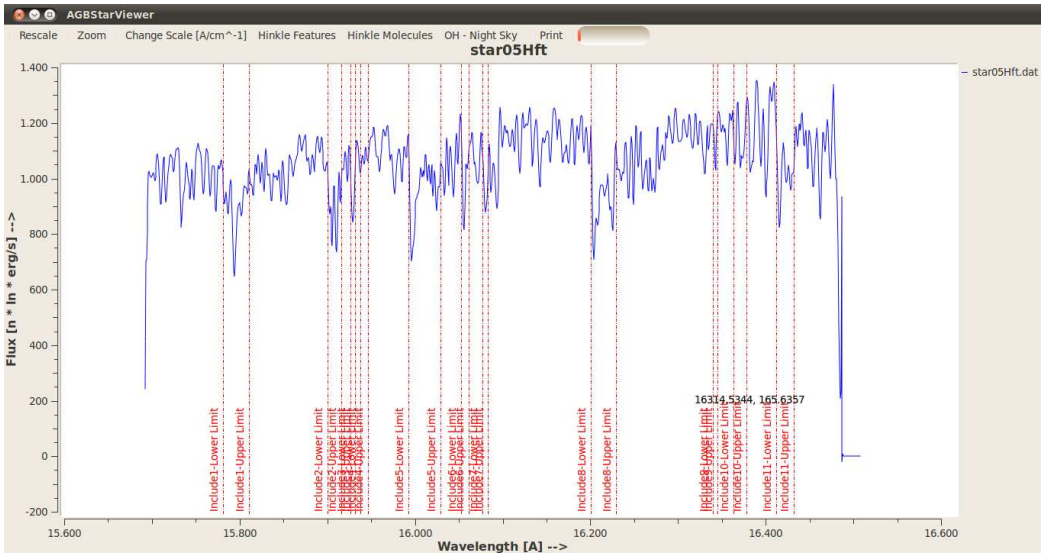

Figure 5.2: The plot window shows the data of a star. The vertical red lines are the included ranges from the tab “Range selection”.

The button “Show graph” generates a window with the plot (Fig. 5.2). It shows the flux against the wavelength. On the left side the name of the data-file is displayed as well as the window title. The plot window has several buttons. The button “Zoom” can be used to zoom into the data. With a right mouse click, the original size will be re-established. The button “Rescale”

establishes the original scale sizing. The button "Change scale" changes from Å to 1/cm, so one can compare the plot directly with the Hinkle-Atlas (Hinkle et al., 1995). The button "Hinkle-features" shows the atomic lines which were enabled in the tab "Line-Lists". That applies also to the button "Hinkle-molecules", but only for the selected molecules. The button "OH-Nightsky" shows OH-lines from Rousselot et al. (2000). The progress-bar shows the time for plotting the atomic and molecular line positions which may take a while. And with the button "Print" one can send the output to a printer or a post-script or pdf-file.

Data fit section - normalization mode

In the section "Data Fit - Normalization Mode", one can select by which method the flux shall be normalised. One can select; "mean", "median" or "least squares". The methods are described in detail in the chapter *Data fitting*. The double-spin-box next to the radio-button "Least Square" returns the result of the calculated least square. The double-spin-box "Max Flux" limits the maximal value of the flux. In a first step, it simply returns the value of the maximum flux. If there are any cosmics or high peaks in the observed data, one can select an upper limit for the maximum flux, to avoid a false normalisation. The button "Normalise", does the normalisation. The button "Save File", next to the normalisation button returns the normalised file for further manipulation, e.g. to make overview-plots in *Gnuplot*.

Data fit section - curve fit

In the section "Curve Fit", the check-box "Fit per Wavelength" is preselected. This means, it is the normal mode to perform fits. The two double-spin-boxes "Select Accuracy" allow to match the resolution of the observed data. The first spin-box sets the digits after the comma[9]. The second spin-box sets the range where a fit should be achieved, e.g. if the starting wavelength is 232338.65 Å and the range is 0.03 Å, then valid values are 23238.62 Å to 23238.68 Å. The check-box "Fit Each Array Index" should be checked if one uses wavin.dat files. In these files, the wavelength points of the synthetic spectra correspond with the wavelength points of the file of the observed spectra. In other words, wavin.dat files match the resolution of observed and synthetic spectra-files automatically. The result of a chi-square computation will be displayed in a box next to χ^2 or χ^2_{abs}. The root mean

[9]The concept of having two spin-boxes to gain a resolution of ± 0.001 Å certainly has a potential for improvement combining both functions into one single spin-box. This will be corrected in future SW-versions.

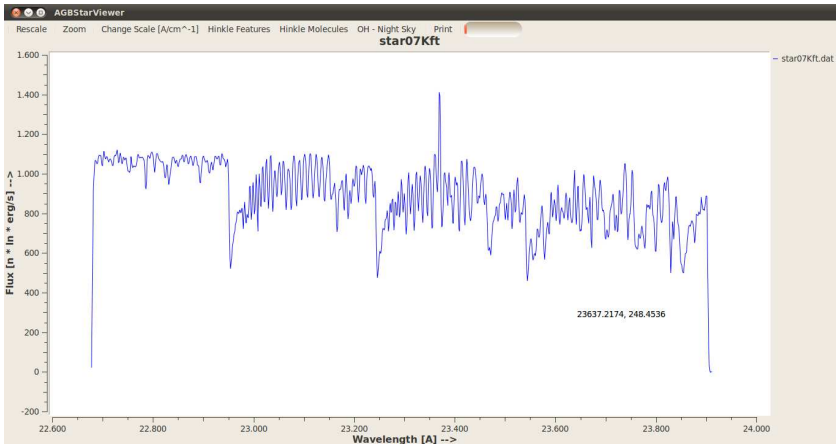

Figure 5.3: Observed data of star07K. One can see the peak in the flux reaches up to 1400 counts. A limit has to be introduced to avoid false normalisation and to avoid a false chi-square calculation. With the double-spin-box "Max Flux" one can limit this high value to a value around 1100, so that the least square will be calculated in the correct way.

square (RMS) and point to point (PTP) are not operational yet, and will be implemented in a future SW-version.

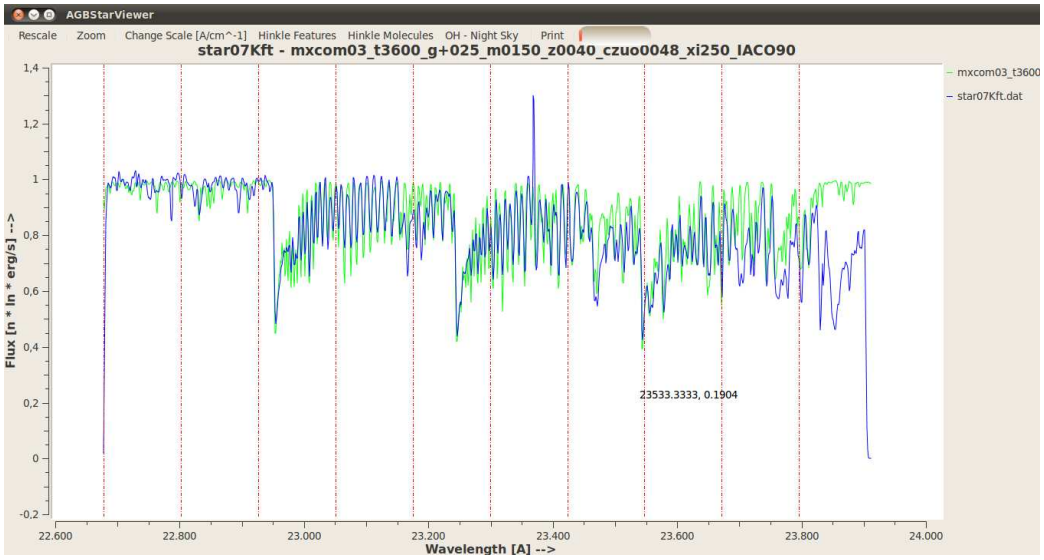

(a) Peak corrected

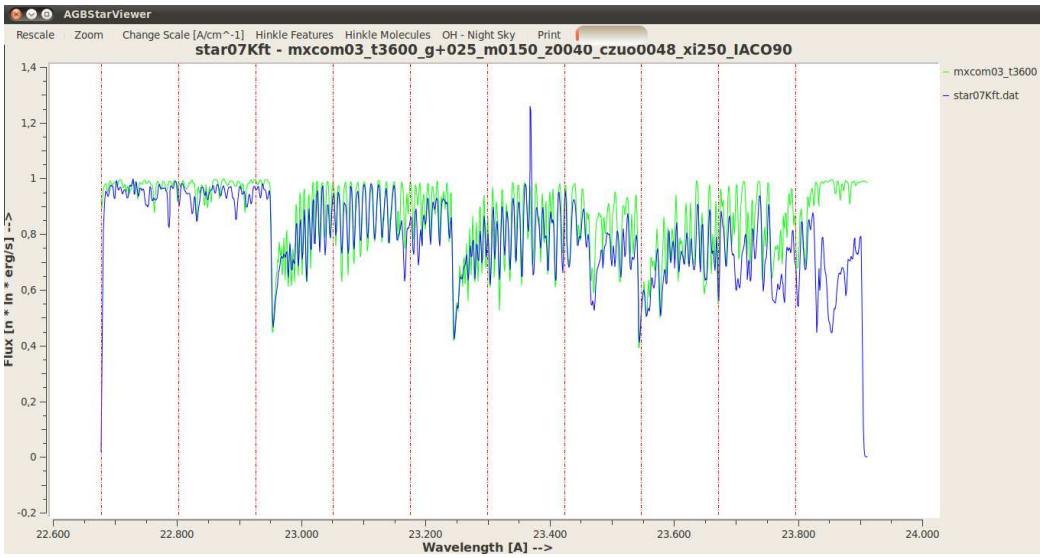

(b) Peak uncorrected

Figure 5.4: Peaks affecting normalisation. In (a) one can see least square normalisation with the peak correction selected. In (b) without limitation of the flux, one can see that the observed data (blue line) are a little bit below the synthetic ones. This will result in a false chi-square calculation. The red dotted lines in both plots show the ranges where the least squares will take its maximum value for each sub-calculation (See Chapter 4 *Data fitting/Flux normalisation/Least squares).*

5.2.3 Range selection

In the tab "Range Selection" one can set inclusions or exclusions of the data.

The range selection is a useful way to handle many observed spectra with different radial velocities. One has to include, e.g., the bandheads of a star with a Doppler shift of, say, 239 km s^{-1}. To apply this selection to other stars, the radial velocity of the first star template has to be put into the field "Original Star". Then the radial velocity of another star has to be put in the field "New Star". The button "Correct Shift" corrects the range selection for the other star. After that procedure a chi-square fit can easily be calculated for other stars.

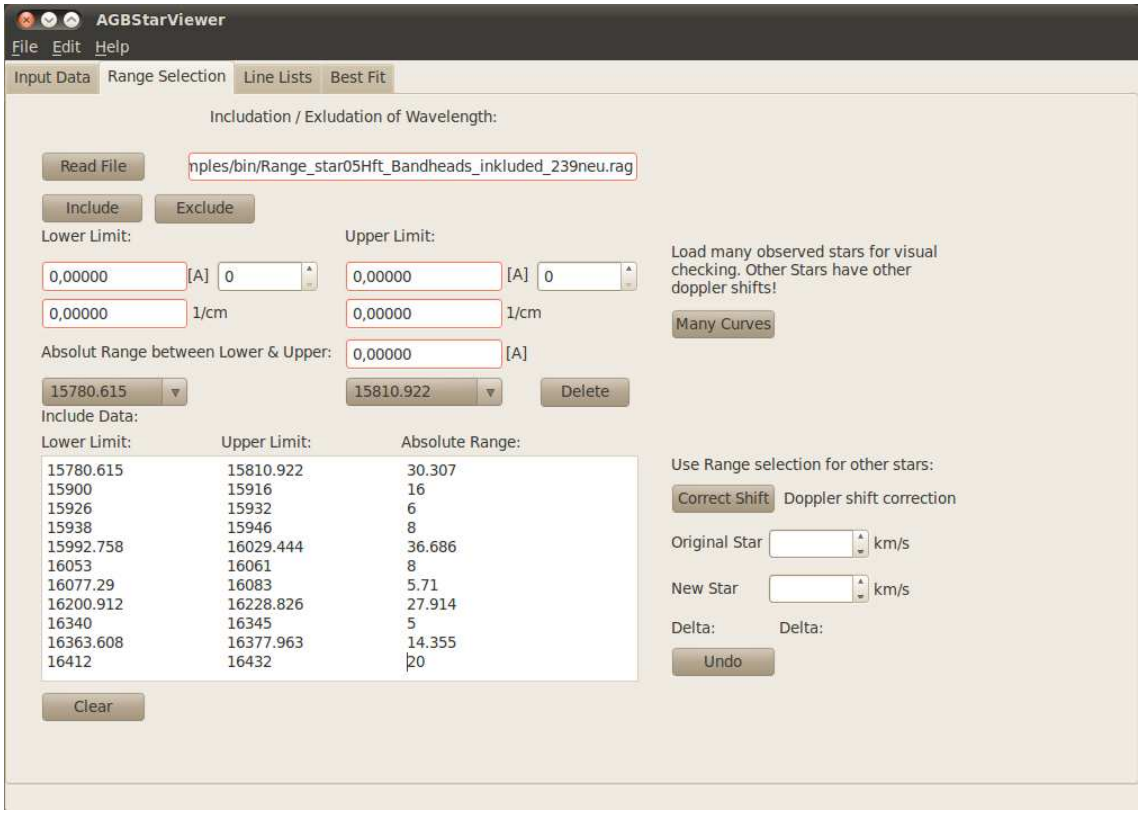

Figure 5.5: Range selection of certain wavelengths. With the tab "Range Selection" the user can basically include or exclude a set of wavelength ranges.

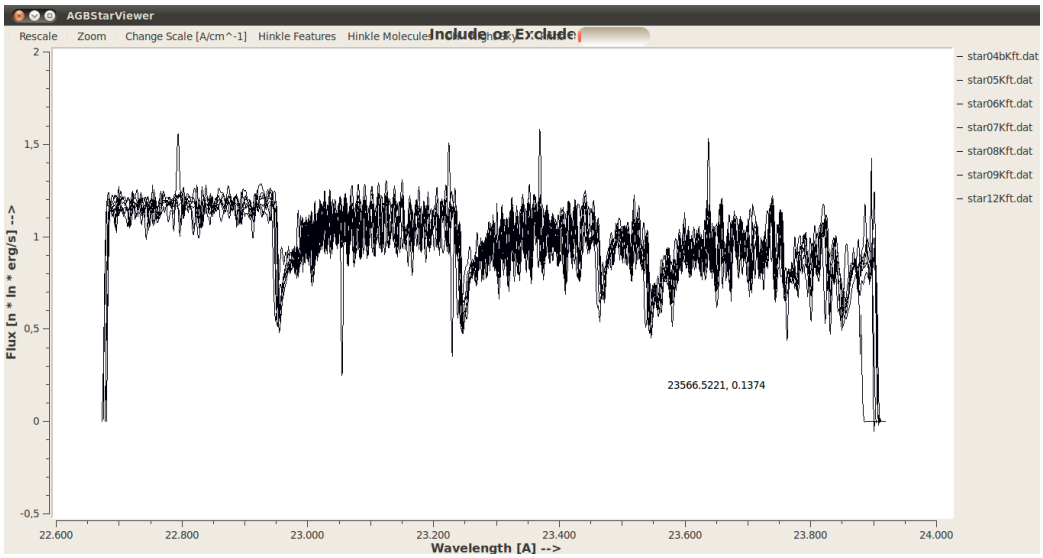

(a) All stars are displayed. Notice the several peaks.

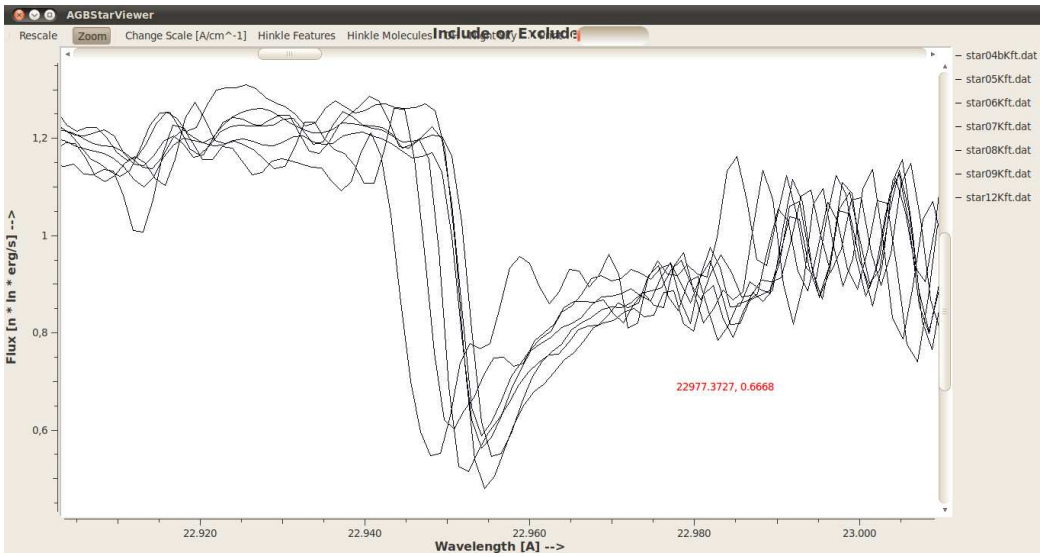

(b) Zoomed into one bandhead.

Figure 5.6: Overview of many spectra. The button "Many Curves" allows a first inspection of a set of observed spectra at once. In Sub-figure (a) one can see some peaks. Sub-figure (b) shows a zoom of one of the bandheads. One can see the different radial velocities.

The button "Many Curves" allows an inspection of a large sample of observed spectra at once. See Fig. 5.6. The button "Read File" loads a previously generated range selection. It is recommended to include the Doppler shift optional in the name of the file for reference. To create a range selection, one must first load the star data in the tab "Input". Then press the button "Include" or "Exclude". Possible settings are to either include or exclude all ranges entered. This should satisfy practical needs in most cases. If one wishes to analyse bandheads, the proper mode will be to include all of them. If one wishes to analyse the whole spectrum, but there are some unwanted peaks due to cosmic ray noises or instrumentational errors, these ranges can be excluded. If one has several data sets entered to be included, the chosen settings will be used for all of them. In Fig. 5.7, three different ways to do a selection are presented. First select the lower limit. This can be done by entering a value in the spin-box for Å or 1/cm. By pressing the button "Include" the entry will be accepted. Then enter the upper limit in the same way. The absolute range between the lower and the upper limit will be shown in the box below. To delete selections search for the wanted

Figure 5.7: Input of the range selection. To create a range selection, enter the lower and upper limit and press include or exclude.

range with the drop-down-box[10] and press the "Delete" button on the right. See Fig. 5.8. To delete all entered ranges press the "Clear" button at the

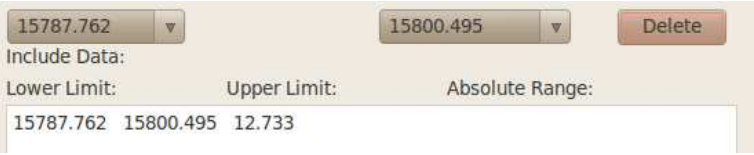

Figure 5.8: To delete ranges, select them via the drop-down-box and press the "Delete" button.

[10]The lower and upper limits are displayed there.

lower left. See Fig. 5.5. The spinbox with the up-down-arrows next to the Ångstroem spin-box, will navigate through each observed point of the spectrum. In this way one can adapt the ranges very accurate and verify them. The entered ranges will be shown in a big text-box below the input boxes. See Fig. 5.9.

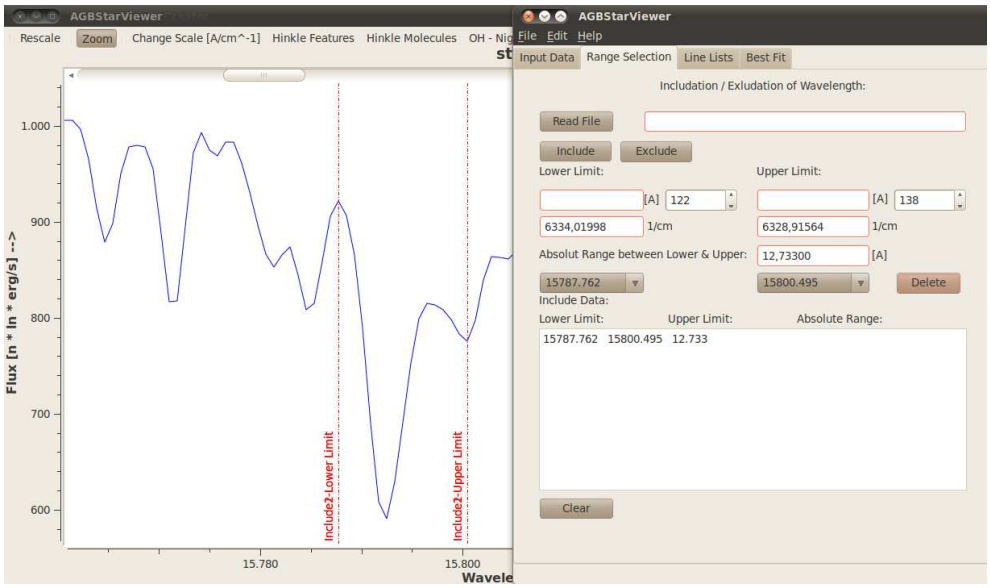

Figure 5.9: To verify selections, first zoom into the feature to be studied. By overlapping the plot window with the range selection window one can verify the selections.

File-format "rag"

The file-format used to save range selections is named "*.rag". The predefined file-name consists of the characters "Range_", the title of the loaded star in the first place and the file name extension, *.rag, for example: "Range_star04H.rag" It is a simple text-file and can also be edited with a text-editor. In the first line there is an entry: "INCLUDE" or "EXCLUDE" in upper case letters. The further lines give the ranges selected with their lower and upper wavelength limits. A appropriate name would be e.g. "Range_star04H_Bandheads_included_239kmps.rag".

5.2.4 Line lists

In the tab "Line Lists", one can select several features to be shown in a plot.

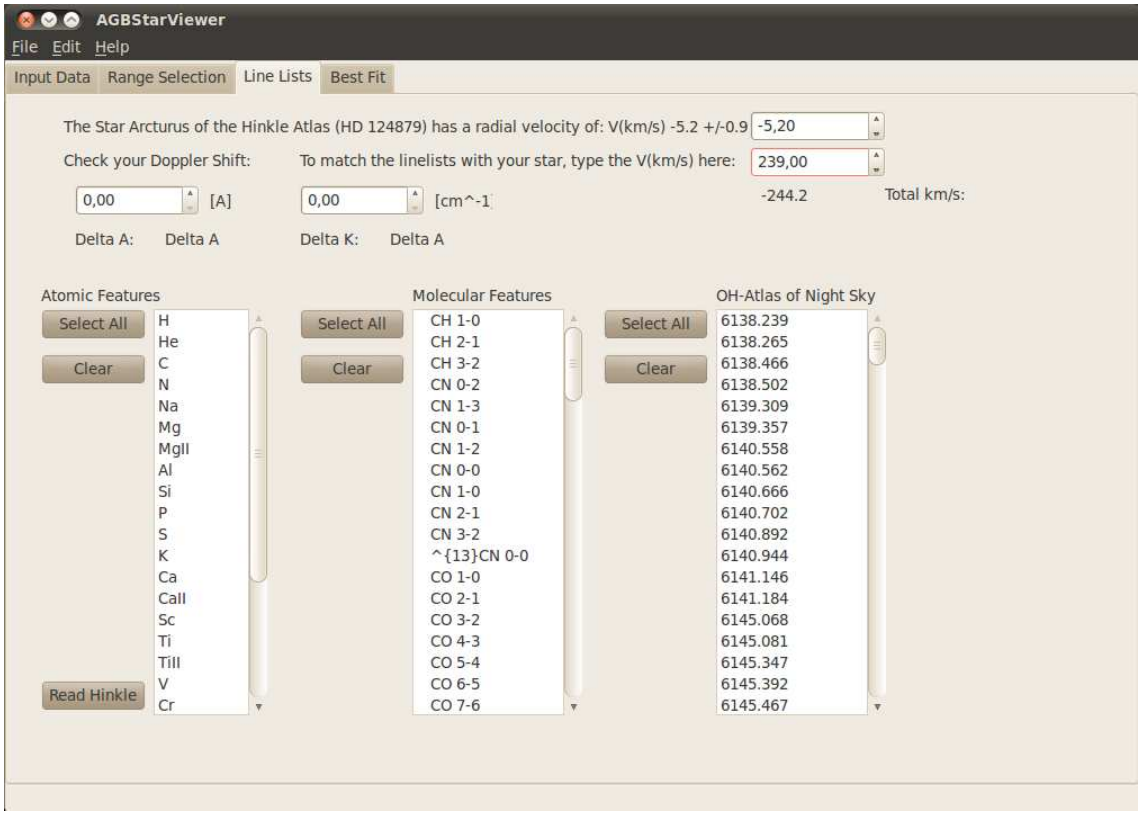

Figure 5.10: Line lists of AGBStarViewer. One can select from atomic features, molecular features (Hinkle et al., 1995) and the OH Atlas of the night sky (Rousselot et al., 2000).

Hinkle Atlas

The atomic line lists and the molecular line lists from the *Infrared atlas of the Arcturus spectrum, 0.9-5.3 microns* from Hinkle (1995), were implemented. It should help identify lines of atoms and molecules in the observed star spectra.

Atlas of OH lines

The medium resolution spectra atlas of the night-sky-OH-emission from Rousselot et al. (2000) was also included. It can be over plotted to the spectra.

The following abstract was taken from their paper:
"*The spectra cover the range 0.997 - 2.25 μm with a resolution of about 8000. Line wavelengths are computed from laboratory data and are given in vacuum. A few lines due to O_2 are also identified. This new set of data can be used to calibrate the wavelength scale of spectra obtained in the near-infrared. It can also help to distinguish between the lines due to astronomical objects and lines due to the earth atmosphere* (Rousselot et al., 2000)".

Selection of features

Before the line lists in Fig. 5.10 can be selected, one should be aware that the features were obtained from the star Arcturus, which has a radial velocities (RV) of about 5.2 km s^{-1}. So one has to match these radial velocity with the observed ones in order to compare them. Therefore, one has to enter the RV of the observed star in the double-spin-box. The difference of the two RVs will be shown below the box. See Fig. 5.10. The following two double-spin-boxes calculate a given range from Ångstroem into 1/cm or vice versa. The buttons "Select All" and "Clear" are self explaining. A multiple selection of features is possible by pressing the key "Shift + select per mouse". It is recommended to start with a few features and then zoom into the star's spectrum as seen in Fig. 5.11, to avoid a with features too crowded plot.

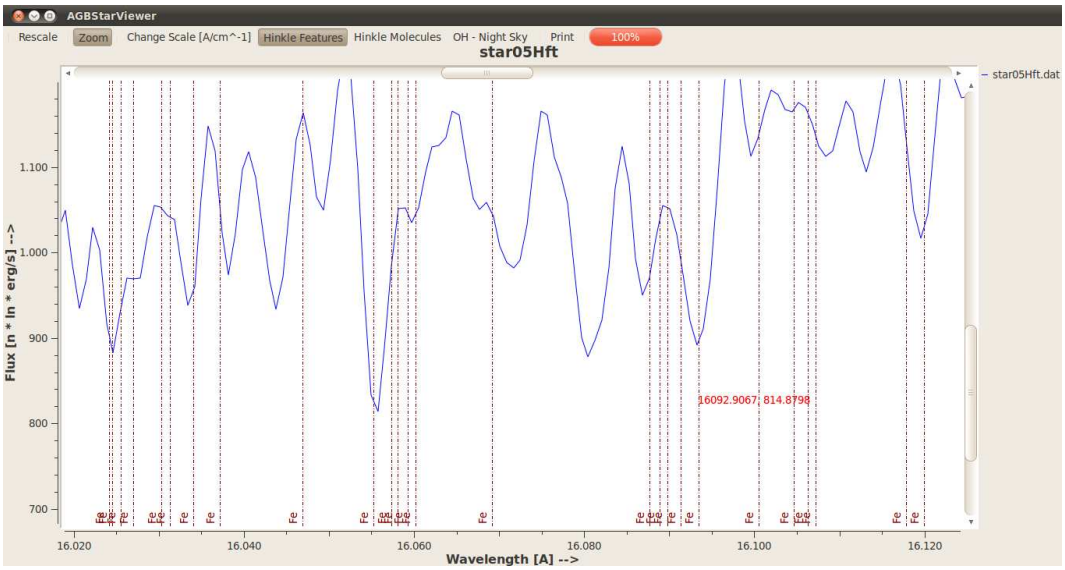

Figure 5.11: Zoomed into star05Hft. Only the lines of Fe are displayed.

5.2.5 Best fit

The tab "Best Fit" determines the best fit between the observed spectrum and many hundreds of synthetic models.

Performing a chi-square

Before one can perform a best fit, the observed file must be loaded in the tab "Input Data". Then switch to the tab "Best Fit". Via the button "Select Files", multiple files can be selected. The path to the directory will be shown next to the button "Select Files". The selected files will be shown below, in the text-box "Files". To clear them all, press the button "Clear". The spin-box "Digits", sets the precision of the output of the chi-square. The button "Best Fit" starts the fit. The check-box "Normalise" activates a normalisation which was pre-selected by mean, median or least squares in the tap "Input Data" before. One can select two Chi-square methods. χ^2 is the common chi-square which is described in "Data fitting" (section 4.5). χ^2_{abs} is for small fluxes, (see section 4.6). The calculations may take a while. The progress is shown in the progress-bar below. The result of the best-fit will be displayed in the lowest text-bar "Best-Fit Result". The value of the corresponding chi-square will be displayed in the far right. The chi-square results are sorted from the best to the poorest fit in the text-box "Chi-square Results". Below the result, one can navigate with the second "Show" button

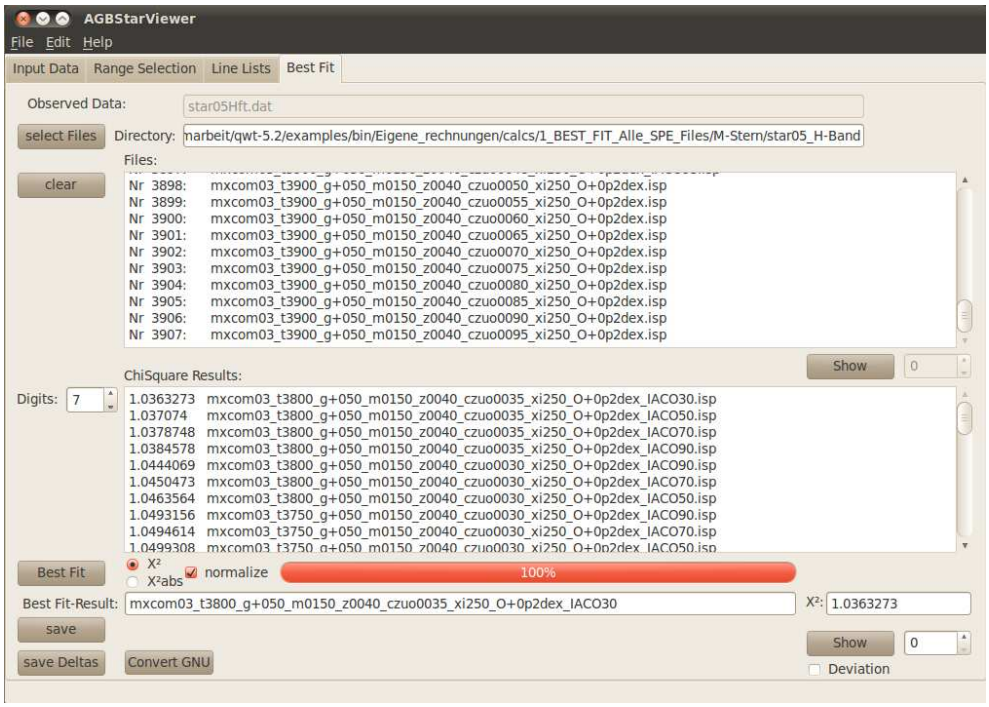

Figure 5.12: The tab "Best Fit" allows to select several hundreds of synthetic spectra in order to perform a search for the best fitting spectrum. The results are listed descending from the best chi-square value to the worst.

through the plots of the stellar spectrum sorted ascending in order of the best chi-square results.

Result files

The button "Save" below the best fit button, saves these chi-square results to two text files for further examination. The first text file is called: *Result_star05H.dat_.res* and contains the output shown in the text-box. The second text file is called *Result_star05H.dat_DataGnuplot.res* and contains the output in a data format which can be imported in *Gnuplot*. The button *Convert GNU* converts a normal result file to a *Gnuplot* supported file format in case the file was accidentally deleted[11].

[11]In the result plots the *Gnuplot* file was limited to the 30 best fit results. In case one needs more best fit results for statistics again, there is no need to run the whole chi-square process again.

Investigating spectra and bandheads

Via the first "Show" button, one can navigate using the double-spin-box next to the "Show" button through all the loaded synthetic model files in order of their file-names. One has to overlap the plot window with the tab "Best Fit" (see Fig. 5.13). Due to the fact that the file-names are ordered by the physical parameters and are also loaded in *AGB*StarViewer in this way, one can navigate through the plots of the spectra, watching to the changes in the spectrum caused by the temperature, the log(g), the C/O-ratio, and the ratio of the isotopic abundances. Especially, if one zooms into a feature and is looking for changes in the plot of the spectra due to changes in the physical parameters like the temperature. This method also works with the second button "Show", navigating through the plots ordered by their chi-square values.

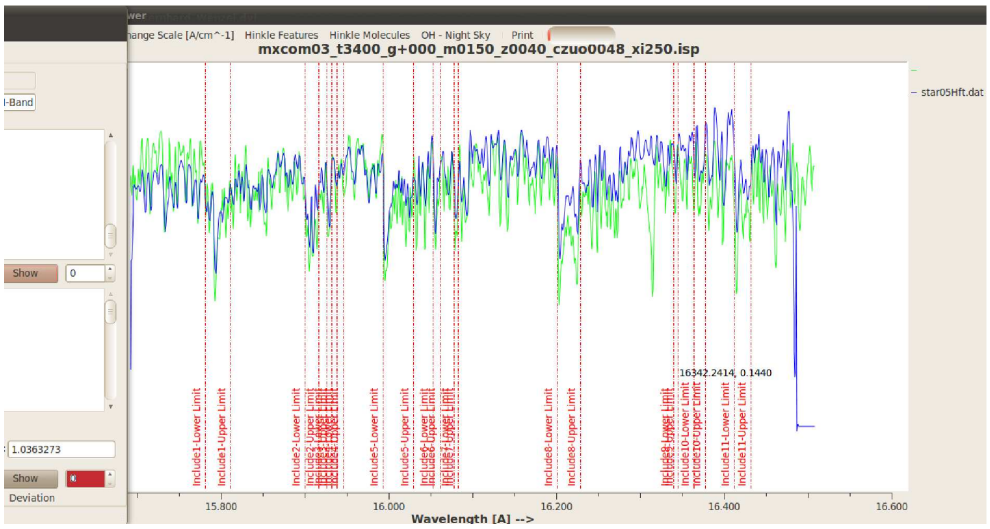

Figure 5.13: Navigation through the best fitting models. Navigate with the red marked spin-box through the synthetic stellar spectra files generated by COMA08, by overlapping the plot window with the "Best Fit" tab. The actual synthetic spectra (blue) is shown bold at the top of the plot window with the observed spectra (green). Also the range selection markers around the bandheads are shown.

5.2.6 The menu

The menus: "File", "Edit" and "Help" are not finished in this SW-version yet, but functionality will be included in future SW-developments.

5.3 *ComaGUI* - a graphical user interface for COMA08

The control file of COMA08 (*coma08.ctr*) has nearly 200 different input-parameters. The idea behind *ComaGUI* is to take care of the most common control file parameters. Therefore, the primary goal of *ComaGUI* is to manage the various calculations of the synthetic spectra. *ComaGUI* has two operational modes. It can be run on the computer where the calculations will be done, or it can generate a script in which the instructions from *ComaGUI* are put as console or terminal commands[12]. This script can be run on any target computer it was copied to and can perform many hundreds of calculations. The idea behind fitting stellar spectra is to create a grid of the parameter-space of the physical-parameters like the temperature, the logarithm of the surface gravity log(g) and the C/O ratio. The best fitting model will be found in a certain area of the grid of the parameter-space. If, e.g., the temperature is found, one can calculate a denser grid with the other parameters around the found temperature to determine the other stellar parameters. *ComaGUI* distinguishes between main jobs and subjobs. In principal, the main jobs are the given MARCS models, which will be used to calculate the first grid. The subjobs are needed to calculate the denser grid around a found temperature, e.g. varying the isotopic abundances of $^{12}C/^{13}C$.

5.3.1 Features

ComaGUI has the following features:

- The SW is designed to be working under *UNIX / Linux* environments.
- Perform COMA08 calculation tasks (jobs).
- Generate terminal scripts for COMA08 calculation tasks (jobs).
- Management and sorting of the MARCS models *mxcom*
- Select COMA08 jobs by specific MARCS models.
- Select COMA08 jobs by an *Auto Grid*[13] of specific physical parameters.

[12]Mainly BASH, AWK and SED commands for Unix/Linux were used for the script.
[13]In the auto grid mode one can select all models within certain physical ranges.

- Perform subjobs (e.g. on the isotopic abundances of $^{12}C/^{13}C$) on the last, best model calculations, to calculate a denser grid of the parameter-space to further parameters.

- Email notification when the jobs are done.

5.3.2 Input models

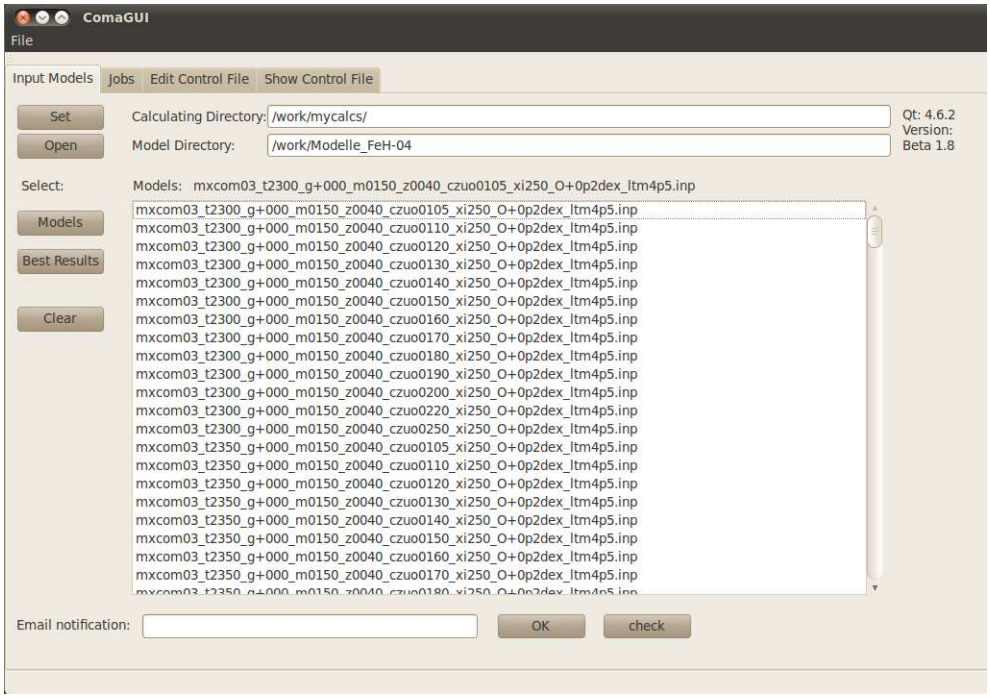

Figure 5.14: The tab "Input Models" assigns the MARCS models to *ComaGUI*. Also, the calculating and model directory can be set here.

Via the tab "Input Models" the calculating directory, the directory including the (atmospheric) MARCS models, and an email address for notifications[14] can be assigned. The models are selected with the button "Models". For this thesis there were about 1200 different MARCS models used. They were originally calculated by Michael Lederer (2009). *ComaGUI* can read MARCS models using the filename specifications given in listing 5.3. In particular *ComaGUI* recognizes the physical parameters by specific characters:

[14]The Unix program Sendmail or Mail has to be installed.

"_t" for temperature, "_g" for surface gravity, "_m" for mass, "_z" for metallicity and so on. Thus if one changes the structure of the naming of the MARCS models, *ComaGUI* will have to be adopted to! The button "Best Results" reads former *AGBS*tarViewer best fitting results. For example, if one takes the previous 30 or 50 best fit results to generate subjobs with the variation of the isotopic ratio of $^{12}C/^{13}C$ (IACO), it is more comfortable to read them into *ComaGUI* by the button "Best Results" than to select them by hand among the 1200 models.

Listing 5.3: Examples of MARCS model filenames which can be interpreted by *ComaGUI*.

```
mxcom03_t2300_g+000_m0150_z0040_czuo0105_xi250_O+0p2dex_ltm4p5.inp
mxcom03_t2350_g+000_m0150_z0040_czuo0170_xi250_O+0p2dex_ltm4p5.inp
mxcom03_t2500_g-025_m0150_z0040_czuo0170_xi250_O+0p2dex_ltm4p0
mxcom03_t2550_g+000_m0150_z0040_czuo0130_xi250_O+0p2dex_ltm4p5
mxcom03_t3000_g+000_m0150_z0040_czuo0105_xi250_O+0p2dex.inp
mxcom03_t3050_g-050_m0150_z0040_czuo0120_xi250.inp
mxcom03_t3350_g+000_m0150_z0040_czuo0150_xi250_O+0p2dex_ltm4p0.inp
mxcom03_t3350_g+025_m0150_z0040_czuo0025_xi250.inp
mxcom03_t3500_g+000_m0150_z0040_czuo0105_xi250_O+0p2dex.inp
mxcom03_t3550_g+050_m0150_z0040_czuo0075_xi250_O+0p2dex.inp
mxcom03_t3600_g+000_m0150_z0040_czuo0075_xi250_O+0p2dex.inp
mxcom03_t3650_g+050_m0150_z0040_czuo0020_xi250.inp
mxcom03_t3700_g+000_m0150_z0040_czuo0070_xi350.inp
mxcom03_t3700_g+000_m0150_z0040_czuo0075_xi250_O+0p2dex.inp
mxcom03_t3800_g+000_m0150_z0040_czuo0010_xi250_O+0p2dex.inp
mxcom03_t3900_g+050_m0150_z0040_czuo0095_xi250_O+0p2dex.inp
```

5.3.3 Jobs

Input models and creating jobs

At the tab "Jobs" (see Fig. 5.15), one can select several main-jobs for COMA08. First of all, one has to give a name to the jobs[15]. The button "Update", reads in the MARCS models from the tab "Input Models". Every input model has an unique model number for identification in the SW. Now one can create jobs either by a double click with the mouse or by the buttons "Create" or "Create All". The button "Create All" is useful if one

[15]Next to the text-line: "Select Job Name".

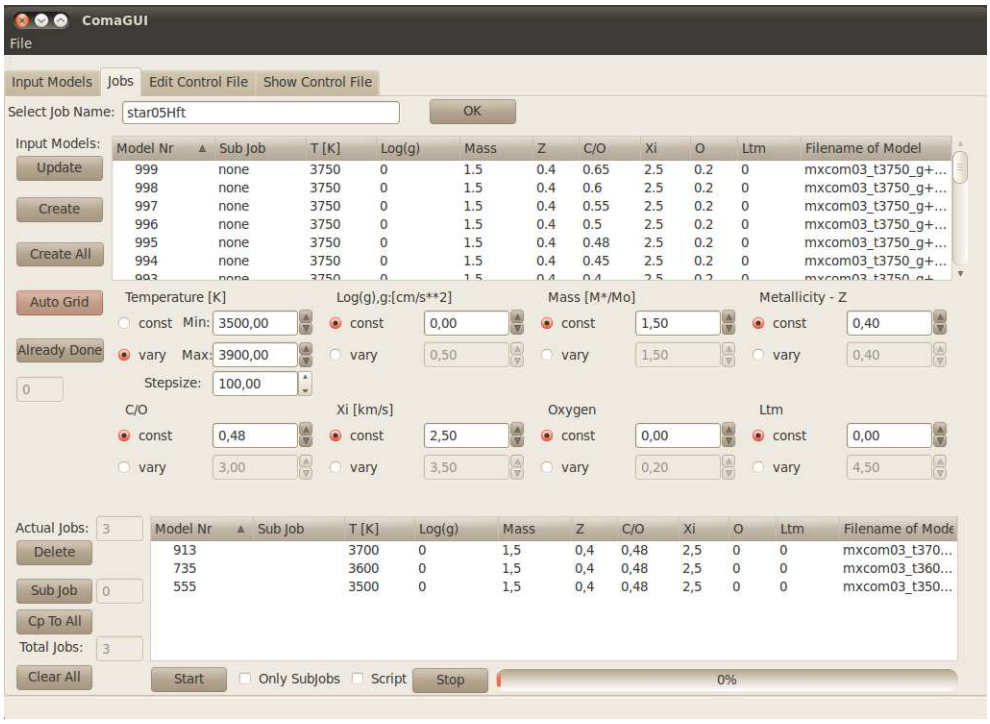

Figure 5.15: In the tab "Jobs" one can create the calculations for the synthetic spectra. The button "Auto Grid" can select various parameters with a given range e.g. take all models from 3500 K to 3900 K in steps of 50 K and so on. A parameter which is set to a constant value will only be taken from this value.

reads in the e.g. 30 former found best fitting models and do final parameter variations with them.

Sorting parameters

One nice feature is the ability to sort the MARCS models by the parameters. This can be done by clicking at the corresponding parameter columns. One can sort, e.g., the available log(g) models versus the available C/O ratios. This allows a visual check of available parameters in order to finalize the strategy for the final paramter-space of the grid.

Auto grid

The button "Auto Grid" is the most useful feature in *ComaGUI*. One can select the physical parameters to change from selectable min to max values[16], or to get all models which consists of a constant parameter, e.g. a log(g) value of 0. From the over 1200 MARCS models which were used for this thesis, a first grid was defined in this way by selecting a temperature range from 2300 K to 3900 K in steps of 100 K, a constant log(g) at 0, a constant mass, metallicity, overabundance of Oxygen, microturbulent velocity ξ (Xi), log(τ) (Ltmn)[17] and C/O-ratio. After the best temperature fit was found, the variables of log(g), C/O-ratio and Oxygen abundance were set to a wider grid-range. Every set of calculations created by the button "Auto Grid", will be put in the section "Actual Jobs". The button "Already Done"[18] reads in all completed jobs from a directory to prevent from doing calculations twice. This is possible, because the unique name of the MARCS models are containing the model parameters which the button "Already Done" can parse.

Actual jobs

"Actual Jobs", contains all scheduled jobs. The actual number of the jobs in the queue is displayed on the left. A job can be deleted by selecting it and pressing the button "Delete". Each job can have several subjobs e.g. for varying the isotopic abundances of $^{12}C/^{13}$C. Each MARCS model represents an unique set of atmospheric parameters. From the best fitting models, which were found by *AGB*StarViewer, the sub parameters of these best ones will be varied and again the best fitting combinations are determined. This will be done by selecting one actual job and pressing the button "Subjob". The number of the new subjobs will be displayed next to the model number. The button "CP to All", copies this specific subjob to all other main-jobs which are listed. This command will also overwrite all previous subjobs. The button "Clear All" clears the whole list of actual jobs. Deleting all subjobs can also be achieved by marking a parent job which has no subjobs and pressing the *CP to All* button.

[16] An example is given in the field temperature in Fig. 5.15.

[17] Ltm4p5 means log(τ) = -4.5

[18] The SW development is still going on, meaning, this particular button is still under construction.

Starting jobs

Pressing the button "Start" will perform the defined jobs. The progress-bar will indicate the progress. The button "Stop"[19] will stop the process. The check-box "Only Subjobs", prevents the SW from calculating the main-jobs again[20]. This is useful (time-saving) for the fine-tuning of the sub parameters.

Scripts

The check-box "Script", is the another useful feature of the SW *ComaGUI*. It writes the whole output to a file named *run_Jobname*. An example of the such a script can be seen in listing 5.4. I choose not to edit single characters of the control file (coma08.ctr) but instead to erase the whole line and to replace it. This method is much safer for scripting than trying to edit one of the 200 lines of the control file. An example can be seen in the first two lines of the listing with the command *sed -i*. The command *./coma/coma08 > writeToOutput.txt*, calls the Fortran program COMA08 and writes the output to the file listed after the ">", in this case writeToOutput.txt.

Listing 5.4: The output of *ComaGUI* for parent-jobs.

```
sed -i 17d coma08.ctr
sed -i '16a\* CZUO =  1.500  C/O used to change eps_C if
CHABC='PAR' * ' coma08.ctr
#echo ParentJob: Nr: 1 Model Nr.15
rm model.isp
rm model.spe
rm model.out
rm kapco.dat
rm kapnu.dat
rm sym.dat
rm syo.dat
rm filter.out
rm model.dat
ln -s /Modelle_FeH-04/mxcom03_t3450_g+000_m0150_z0040_czuo0150_
xi250_O+0p2dex_ltm4p0.inp model.dat
./coma/coma08 >  outputComa_mxcom03_t3450_g+000_m0150_z0040_
czuo0150_xi250_O+0p2dex_ltm4p0.dat
./coma/sphspec04 >> outputComa_mxcom03_t3450_g+000_m0150_z0040_
czuo0150_xi250_O+0p2dex_ltm4p0.dat
```

[19]This feature is still in development and will be solved with thread-programming, to prevent the SW from apparently freezing.

[20]Because they were already calculated by a previous grid-calculation.

```
./coma/sphread04 >> outputComa_mxcom03_t3450_g+000_m0150_z0040_
czuo0150_xi250_O+0p2dex_ltm4p0.dat
mv model.isp      mxcom03_t3450_g+000_m0150_z0040_czuo0150_xi250_
O+0p2dex_ltm4p0.isp
mv model.spe      mxcom03_t3450_g+000_m0150_z0040_czuo0150_xi250_
O+0p2dex_ltm4p0.spe
mv model.out      mxcom03_t3450_g+000_m0150_z0040_czuo0150_xi250_
O+0p2dex_ltm4p0.out
rm kapco.dat
rm kapnu.dat
rm sym.dat
rm syo.dat
mv mxcom03_t3450_g+000_m0150_z0040_czuo0150_xi250_
O+0p2dex_ltm4p0.isp /calcs/model_isp
mv mxcom03_t3450_g+000_m0150_z0040_czuo0150_xi250_
O+0p2dex_ltm4p0.spe /calcs/model_spe
mv mxcom03_t3450_g+000_m0150_z0040_czuo0150_xi250_
O+0p2dex_ltm4p0.out /calcs/model_out
mv outputComa_mxcom03_t3450_g+000_m0150_z0040_czuo0150_
xi250_O+0p2dex_ltm4p0.dat /calcs/coma_output
```

5.3.4 Subjobs

The button "Subjob" (Fig. 5.15), calls the dialogue shown in Fig. 5.16. The dialog window shows the parent-job-number at the top and the name of the MARCS model. Below, the other parameters of coma08 can be edited[21]. As seen in Fig. 5.16, the isotopic ratio $^{12}C/^{13}C$ of carbon can be set to a constant value, or to vary from, e.g., 4 to 10 in steps of 1 and from 10 to 100 in steps of 10. The sum of $^{12}C^{16}O$ and $^{13}C^{16}O$ is shown at the bottom. This number added to the other combinations of isotopes must be equal to 1.0 total. The button "Create" copies the subjob to the list above. To delete a subjob, mark the subjob in the list above and press the "Delete" button. Pressing the button "OK", accepts the changes and returns to the main window. The button "Cancel", discards the modifications.

Listing 5.5: The output of *ComaGUI* for a typical subjob.

```
echo SubJob: isotopic ratio C/O: 46
```

[21] In this SW-version only the variation of the isotopic ratio $^{12}C/^{13}C$ of carbon is implemented.

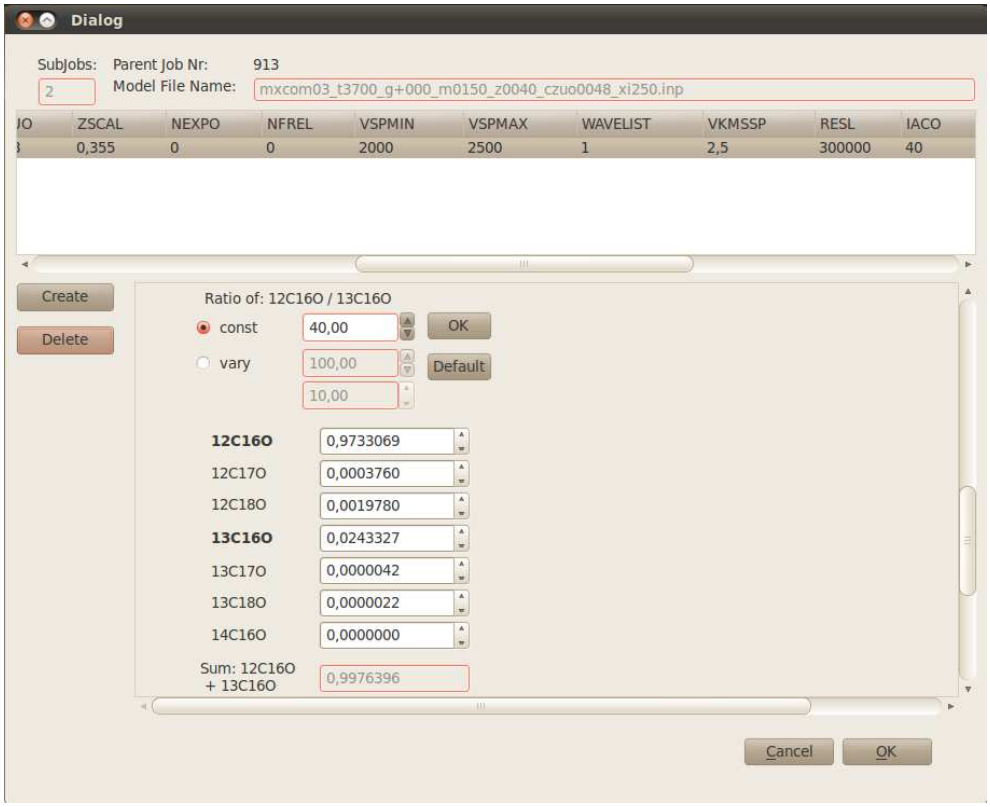

Figure 5.16: Creating subjobs varying the isotopic ratio $^{12}C/^{13}C$ of carbon. It can be set to a constant value, or to various numbers from e.g. 10 to 100 in steps of 10 or any other stepping ratio.

```
sed -i 102d coma08.ctr
sed -i '101a\* CO          0.9764132 --> 12C16O * ' coma08.ctr
sed -i 103d coma08.ctr
sed -i '102a\*             0.0003760 --> 12C17O *' coma08.ctr
sed -i 104d coma08.ctr
sed -i '103a\*             0.0019780 --> 12C18O * ' coma08.ctr
sed -i 105d coma08.ctr
sed -i '104a\*             0.0212264 --> 13C16O * ' coma08.ctr
sed -i 106d coma08.ctr
sed -i '105a\*             0.0000042 --> 13C17O * ' coma08.ctr
sed -i 107d coma08.ctr
sed -i '106a\*             0.0000022 --> 13C18O * ' coma08.ctr
sed -i 108d coma08.ctr
sed -i '107a\*             0.0000000 --> 14C16O * ' coma08.ctr
```

```
rm model.isp
rm model.spe
rm model.out
rm kapco.dat
rm kapnu.dat
rm sym.dat
rm syo.dat
rm filter.out
rm model.dat
ln -s /Modelle_FeH-04/mxcom03_t3650_g+025_m0150_z0040_czuo0010_
xi250_O+0p2dex.inp model.dat
./coma/coma08 > outputComa_mxcom03_t3650_g+025_m0150_z0040_
czuo0010_xi250_O+0p2dex_IACO46.dat
./coma/sphspec04 >> outputComa_mxcom03_t3650_g+025_m0150_z0040_
czuo0010_xi250_O+0p2dex_IACO46.dat
./coma/sphread04 >> outputComa_mxcom03_t3650_g+025_m0150_z0040_
czuo0010_xi250_O+0p2dex_IACO46.dat
mv model.isp mxcom03_t3650_g+025_m0150_z0040_czuo0010_xi250_
O+0p2dex_IACO46.isp
mv model.spe mxcom03_t3650_g+025_m0150_z0040_czuo0010_xi250_
O+0p2dex_IACO46.spe
mv model.out mxcom03_t3650_g+025_m0150_z0040_czuo0010_xi250_
O+0p2dex_IACO46.out
rm kapco.dat
rm kapnu.dat
rm sym.dat
rm syo.dat
mv mxcom03_t3650_g+025_m0150_z0040_czuo0010_xi250_O+0p2dex_
IACO46.isp /calcs/model_isp
mv mxcom03_t3650_g+025_m0150_z0040_czuo0010_xi250_O+0p2dex_
IACO46.spe /calcs/model_spe
mv mxcom03_t3650_g+025_m0150_z0040_czuo0010_xi250_O+0p2dex_
IACO46.out /calcs/model_out
mv outputComa_Kband3600bis3650_mxcom03_t3650_g+025_m0150_
z0040_czuo0010_xi250_O+0p2dex_IACO46.dat /calcs/coma_output
```

5.3.5 Control file

In the tab "Edit Control File" one can edit the single parameters of COMA08. The button 'Update" reads the actual file coma08.ctr into *ComaGUI*. The

button “Write” writes the edited values back into the file coma08.ctr. In the drop-down-box “Load predefined control file” on the upper right, one can select control files sorted by M-stars, MS-stars or C-stars in several bandwidths[22].

5.3.6 Show control file

The tab “Show Control File” lists the content of the file coma08.ctr. This is useful for double checking the SW *ComaGUI* after editing the file coma08.ctr, e.g. if something seems not to work correct, the parameters of coma08.ctr can be checked here again.

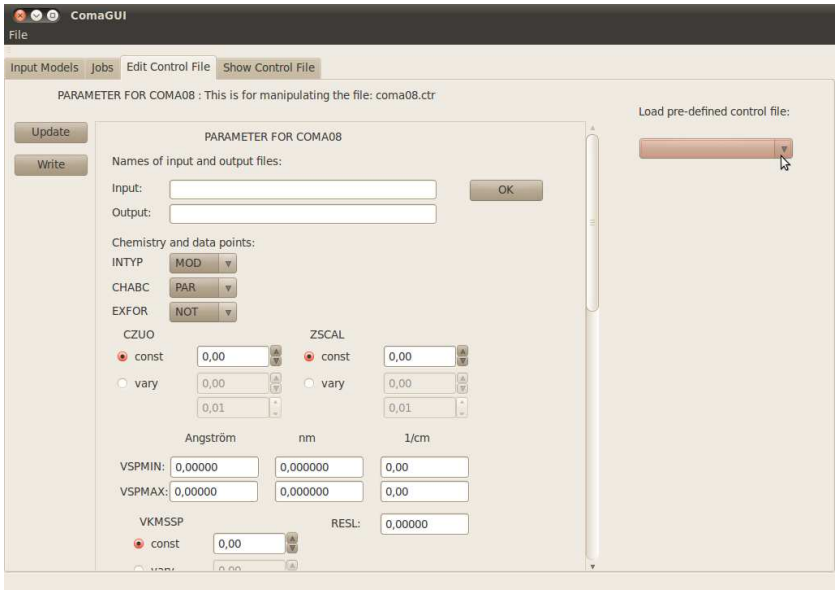

Figure 5.17: In the tab “Edit Control File” one can edit the single parameters of COMA08.

[22]This SW feature is still under construction.

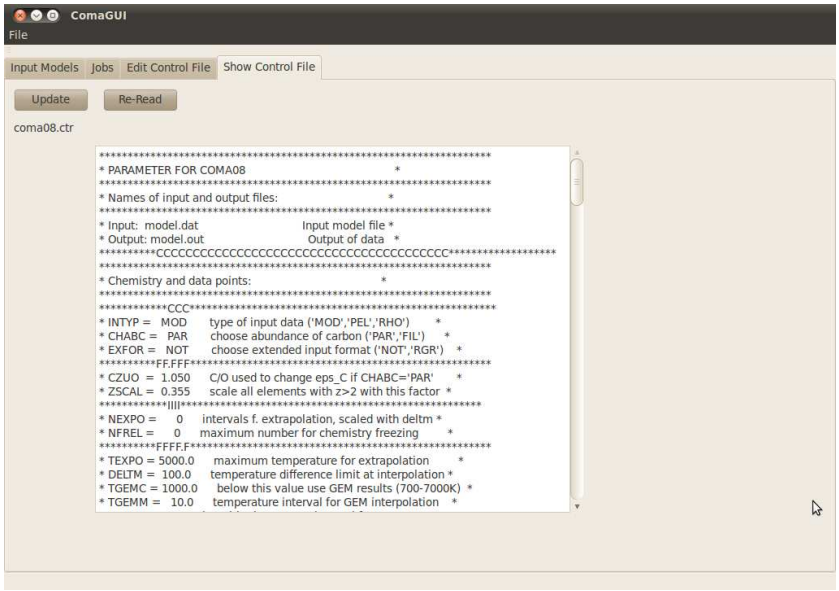

Figure 5.18: In the tab "Show Control File" one can check the edited parameters of the file coma08.ctr.

5.4 Software developing with the Qt-IDE

*AGB*StarViewer and *ComaGUI* were developed with Qt-Creator 4.6 of NOKIA.

5.4.1 Qt installation

The best and easiest way to install the Linux packages "qtcreator and qtcreator-doc" is with the synaptic packet manager. Under Ubuntu 10.04 LTS the version of these files are 1.3.1-ubuntu1.1.

Manual installation

Otherwise the free LGPL version of the integrated development environment (IDE) of Qt can be downloaded at `http://qt.nokia.com/downloads` First, download the latest file and then the file e.g. Qt 4.5 **qt-sdk-linux-x86_64-opensource-2009.04.1.bin** must be prepared for the installation process. Type **sudo chmod a+rwx qt-sdk-linux-x86_64-opensource-2009.04.1.bin**, to make the file accessible for all users logged onto a Linux system. There are example programs included which will only work properly if all users have the right to access the file.

For installing e.g. Qt 4.7 type:
sudo ./qt-sdk-linux-x86_64-opensource-2010.05.1.bin and follow the setup instructions. It will be a good idea to install the files in the directory: **/opt**
To see which changes were made in the actual release (its now Qt 4.6) see at: `http://qt.nokia.com/developer/changes/changes-4.6`

5.4.2 The project file

In the following project files **ComaGUI.pro** and **AGBStarViewer.pro** the source code files are linked. The command CONFIG += static or CONFIG += staticlib will use a static general library of the Qt4 widgets. It is much better not to use the static libraries, because the dynamic libraries will be supported and updated by the Linux-communities. By using the static libraries the project also must be declared as an *Open Source* project. AGBStarViewer and ComaGUI are using dynamic libraries but they will be put under the Open Source licence after this thesis is finished.

Listing 5.6: The *ComaGUI* project file.

```
# -------------------------------------------------
# Project created by QtCreator 2010-08-06T17:09:30
# -------------------------------------------------
TARGET = ComaGui
TEMPLATE = app
SOURCES += main.cpp \
    mainwindow.cpp \
    tab1.cpp \
    jobs.cpp \
    form.cpp \
    comacontrolfile.cpp \
    subjob.cpp \
    workspace.cpp \
    showcontrolfiles.cpp \
    classcoma08ctr.cpp \
    parentcoma08ctr.cpp \
    cjobthread.cpp \
    cmodel.cpp \
    isotopicmolecularabundances.cpp \
    aburelco.cpp \
    classparentjob.cpp \
    emailnotification.cpp
HEADERS += mainwindow.h \
    tab1.h \
    jobs.h \
    form.h \
    global.h \
    comacontrolfile.h \
    constants.h \
    subjob.h \
    workspace.h \
    showcontrolfiles.h \
    classcoma08ctr.h \
    parentcoma08ctr.h \
    cjobthread.h \
    cmodel.h \
    isotopicmolecularabundances.h \
    aburelco.h \
    classparentjob.h \
```

```
    emailnotification.h
FORMS += mainwindow.ui \
    tab1.ui \
    jobs.ui \
    form.ui \
    comacontrolfile.ui \
    subjob.ui \
    showcontrolfiles.ui \
    parentcoma08ctr.ui \
    isotopicmolecularabundances.ui \
    aburelco.ui \
    emailnotification.ui
OTHER_FILES +=
```

Listing 5.7: The *AGB*StarViewer project file.

```
#-------------------------------------------------
# Project created by QtCreator 2009-10-14T16:57:18
#-------------------------------------------------
include( ../examples.pri )

# include( libqwt.a )
TARGET = AGBStarViewer
CONFIG += qwt

# CONFIG += static
# CONFIG += staticlib
TEMPLATE = app
SOURCES += main.cpp \
    mainwindow.cpp \
    scrollzoomer.cpp \
    scrollbar.cpp \
    CData.cpp \
    CPlot.cpp \
    CMyDoubleSpinBox.cpp \
    cmyqwtplotpicker.cpp \
    cfirstmainwindow.cpp \
    tab2.cpp \
    cmylistwidget.cpp \
    mathfunctions.cpp \
    tab3.cpp \
```

```
    workspace.cpp \
    rangeselection.cpp \
    catomicfeatures.cpp \
    linelist.cpp \
    enableatomicfeature.cpp \
    cmolekularfeatures.cpp \
    ccalibration.cpp \
    hinkledopplershift.cpp \
    cmodel.cpp \
    correction.cpp \
    about_agbstarviewer.cpp
HEADERS += mainwindow.h \
    scrollzoomer.h \
    scrollbar.h \
    CData.h \
    CZoomer.h \
    CPlot.h \
    Constants.h \
    Interface.h \
    mathfunctions.h \
    nr3.h \
    CMyDoubleSpinBox.h \
    cmyqwtplotpicker.h \
    cfirstmainwindow.h \
    tab2.h \
    cmylistwidget.h \
    tab3.h \
    workspace.h \
    rangeselection.h \
    catomicfeatures.h \
    linelist.h \
    enableatomicfeature.h \
    cmolekularfeatures.h \
    ccalibration.h \
    hinkledopplershift.h \
    global.h \
    cmodel.h \
    correction.h \
    about_agbstarviewer.h
FORMS += mainwindow.ui \
    cfirstmainwindow.ui \
```

```
    tab2.ui \
    tab3.ui \
    linelist.ui \
    enableatomicfeature.ui \
    ccalibration.ui \
    hinkledopplershift.ui \
    correction.ui \
    about_agbstarviewer.ui
INCLUDEPATH += /home/user/1_Uni/Astro_Diplomarbeit/qwt-5.2/lib \ # LIBS +
# INCLUDEPATH += /home/user/1_Uni/Astro_Diplomarbeit/qwt-5.2/src \
# LIBS += /home/user/1_Uni/Astro_Diplomarbeit/qwt-5.2/lib/libqwt.a
\
    LIBS \
    += \
    -lqwt
```

5.4.3 Qwt library for technical widgets

The plots were developed with an additional library, "Qwt" of Uwe Rathman.
`http://qwt.sourceforge.net/`
The best and easiest way is to install the Linux packages "libqwt5-gt4", "libqwt5-gt4-dev", and "libqwt5-doc" with the synaptic packet installer.

Manual Installation

For a manual installation of Qwt 5.2.0 see:
`http://qwt.sourceforge.net/qwtinstall.html`
One can download the latest snapshot with the newest bug fixes (for the 5.2 release) with the command:
svn co https://qwt.svn.sourceforge.net/svnroot/qwt/branches/qwt-5.2
Be aware of write permissions during the installation process. If you are installing Qwt with root or sudo, you may have troubles with a compilation under a normal user account. Then the resulting libraries **libqwt.so**, **libqwt.so.5**,**libqwt.so.5.2**, **libqwt.so.5.2.1** must be made visible to the Linux environment.
Under Ubuntu and Debian Linux systems one has to edit: **/etc/ld.so.conf** or the file **libc.conf**[23] must be inserted the path of the directory where

[23]The names of these particular files changes often in newer Linux versions. One has to *Google* them.

libqwt.so, are to find. For example: **/home/user/qwt-5.2/lib** has to be written in ld.so.conf. In general under Linux systems you have to rebuild the library cache. One can rebuild the library cache with the command: **sudo ldconfig -v**. Please read "man ldconfig" before entering the command. One should get a huge amount of output from the console. Here one has to look for an entry like:
/home/user/qwt-5.2/lib/libqwt.so.5 → libqwt.so.5.2.1
After that one should be able to compile the widgets of Qwt.

To use the widgets from Qwt one has to make a build with the whole Qwt-Project. Open the Qwt project file: **qwt.pro** with the Qt-Creator 4.6. In Qt-Creator 4.6 one has to go to the tab "Projects" on the left side of the screen. At the tabulator "Build-Properties", click to "Build-Environment". There the following variable are to be selected:
LD_LIBRARY_PATH and paste the path to the Qwt libraries.
/opt/qtsdk-2009.03/lib/qtcreator:/home/user/qwt-5.2/lib

The variable **PATH** below has to look like:
/opt/qtsdk-2009.03/qt/bin:/usr/local/sbin:/usr/local/bin:
/usr/sbin:/usr/bin:/sbin:/bin:/usr/games:/home/user/qwt-5.2/bin
In the file ComaGui.pro the following line must be included:
include(../examples.pri). Otherwise the files of:
include <qwt_plot.h>, include <qwt_plot_marker.h>, include <qwt_plot_curve.h>, include <qwt_legend.h>, include <qwt_data.h>, include <qwt_text.h>, include <qwt_math.h>, include <math.h> cannot not be found by the Qt-Creator!

Environment variables

The Environment variables also have to be set in the Linux system. Type in the console:
export EnvironmentVariable=$EnvironmentVariable:/path/to/the/variable/

LD_LIBRARY_PATH
/opt/qtsdk-2009.04/lib/qtcreator:/path/to/the/qwt/Library/qwt-5.2/lib

PATH
/opt/qtsdk-2009.04/qt/bin:/usr/local/sbin:/usr/local/bin:/usr/sbin:/usr/bin:/sbin:/bin:/usr
5.2/bin:/PathtotheqwtLibrary/qwt-5.2/src

PWD

/home/user:/PathtotheqwtLibrary/qwt-5.2/src

QWTLIB
/lib:/PathtotheqwtLibrary/qwt-5.2/lib/:/PathToInstalledProgrammFilesFromComaView/bin/lib

5.4.4 C++ coding rules

Writing a program is like painting a picture. One has all freedom and rights to code, but practically some general common properties should be abided. These few coding rules should avoid bugs and errors during the runtime.

- Never use a variable name twice, although it is possible. This is because, the tool "Replace All" in the IDE, cannot replace another variable in the project, with the same name, by accident.
- Always use names which suggest the functionality of the function or variable. Even if they are very long names. So the program becomes more readable.
- Opening files should always be put in a "try and catch" block.
- Use small comments on programming parts which are not self-explaining.

5.5 Tools and scripts

5.5.1 Script 1

If one produces result files with a chi-square, one would typically like to compare say the best 30 results. This script reduces all result files, e.g. Star05.res, in a directory to its 30 best chi-square results. Copy the file: *reduce_to30*, in the directory with the result files and call it in a terminal with:
*./reduce_to30 *.res*

Listing 5.8: Script *reduce* for deleting file contents.

```
#! /bin/bash
# Bernhard Wenzel: reduce data to 30 best Chisquare results
# call it with: "reduce *.res" and all res's in the
# directory will be handeld.
```

```
for i in $*
do
   echo "process $i";
   #safety copy
   #cp $i ${i%.*}.bak;
   sed '31,$d' $i > neu.res
   cp neu.res ${i%.*}.res;
   rm neu.res
done
```

5.5.2 Script 2

Script *mergeSpeToWavindat* is for merging the *.spe files from coma, to a distinct wavin.dat file of a star. This is useful if one has a grid of spe-files. This grid should be calculated with a resolution of about 300 000. One must specify the radial velocity of a certain star in sphread04.ctr, before calling this script.

Listing 5.9: Script *mergeSpeToWavindat* is for merging the spe files from coma to a certain wavin.dat.

```
#! /bin/bash
# Bernhard Wenzel: Script for merging spe files to a certain
# wavin.dat. call it with: "mergeSpeToWavindat *.spe" and all
# spe's in the "work" directory of coma will be handeld.
for i in $*
do
   echo "process $i";
   # safety copy of a file
   #cp $i ${i%.*}.bak;
   rm spectrum.dat;
   ln -s $i spectrum.dat;
   ./coma/sphread04;
   mv model.isp ${i%.*}.isp;
done
```

5.5.3 Script 3

The script *eraseThisFromFilenameAndRename* is for deleting a certain string from a filename. In this example the string to delete is: *DeleteThisString*.

This is useful if one has calculated several COMA08 jobs, but with different job filenames. In order to compare these many jobs, one has to give them the same filename structure. Or delete some strings to obtain the same result, which is exactly what this script does. It was invented originally by John W. `http://forum.ubuntuusers.de/topic/suche-und-ersetzen-von-filenames-wie-mit-strg-/`

Listing 5.10: Script *eraseThisFromFilenameAndRename* is for deleting a certain string from a filename. In this example the string to delete is *DeleteThisString*. It was taken from John W. at the forum: ubuntuusers.de

```
find -maxdepth 1 -type f | while read i
do
    toDelete="${i/DeleteThisString/}"
    [[ "$i" != "$toDelete" ]] && mv "$i" "$toDelete"
done
```

5.5.4 Script 4

The script *insert_rowNumbers* inserts the row numbers in a file. This is useful if you want to process your files with external programs as Gnuplot, but your initial file had no row numbers.

Listing 5.11: Script *insert_rowNumbers* is for inserting row numbers in a file.

```
#! /bin/bash
# Bernhard Wenzel: inserts rownumbers in *.res, this is
# useful for fitting data. Call it with: "insert_rowNumbers
# *.res" and all res's in the directory will be handeld.
for i in $*
do
   echo "process $i";
   cat -n $i > new.txt
   cp new.txt ${i%.*}.res;
   rm new.txt
done
```

5.5.5 Script 5

The script *WriteResultsToLatexFileSingleRow* generates a Latex file with the final result tables.

Listing 5.12: Script *WriteResultsToLatexFileSingleRow* geberates final result tables.

```
#! /bin/bash

# Bernhard Wenzel: write FinalResultsLatex in one Data File
# call it with: "write_results_to_File *.res" and all res's
# in the directory will be handeld.

echo "write FinalResultsLatex in one Data File call it with:
 write_results_to_File *.res and all res's in the directory
will be handeld" > "FinalResultsLatex.txt"

for i in $*
do
   echo "process $i ";
   #safety copy
   #cp $i ${i%.*}.bak;

   echo "\begin{tabular}{|c||c|c|c|c|}" | tee >> "FinalResultsLatex
   echo "\hline"       | tee >> "FinalResultsLatex.txt";
   echo "\cline{2-5} "| tee >> "FinalResultsLatex.txt";
   echo "\textbf{$i}  & T [K] & Log G  & C/O & IACO  \\\ " | tee >>
   "FinalResultsLatex.txt";
   echo "\hline\hline"| tee >> "FinalResultsLatex.txt";

#  echo "Best Fit: & & & & \\\ " | tee >> "FinalResultsLatex.tx
#  echo "Mean:     & & & & \\\ " | tee >> "FinalResultsLatex.tx
#  echo "wMean:    & & & & \\\ " | tee >> "FinalResultsLatex.tx


   echo "Best Fit: & " | tee >> "FinalResultsLatex.txt";
   head -1 $i  | awk '{print $3}'  | tee >> "FinalResultsLatex.txt"
   echo "  &  " | tee >> "FinalResultsLatex.txt";
   head -1 $i  | awk '{print $4}'  | tee >> "FinalResultsLatex.txt"
   echo "  &  " | tee >> "FinalResultsLatex.txt";
   head -1 $i  | awk '{print $7}'  | tee >> "FinalResultsLatex.txt"
   echo "  &  " | tee >> "FinalResultsLatex.txt";
   head -1 $i  | awk '{print $11}'  | tee >> "FinalResultsLatex.txt
   echo " \\\ " | tee >> "FinalResultsLatex.txt";
```

```
    echo "␣" | tee >> "FinalResultsLatex.txt";

    echo "Mean:␣␣&" | tee >> "FinalResultsLatex.txt";
    ./Mean $i +03  | tee >> "FinalResultsLatex.txt";
    echo "␣␣&␣␣" | tee >> "FinalResultsLatex.txt";
    ./Mean $i +04  | tee >> "FinalResultsLatex.txt";
    echo "␣␣&␣␣" | tee >> "FinalResultsLatex.txt";
    ./Mean $i +07  | tee >> "FinalResultsLatex.txt";
    echo "␣␣&␣␣" | tee >> "FinalResultsLatex.txt";
    ./Mean $i +11  | tee >> "FinalResultsLatex.txt";
    echo "␣\\\␣" | tee >> "FinalResultsLatex.txt";

    echo "␣" | tee >> "FinalResultsLatex.txt";

    echo "wMean:␣␣&" | tee >> "FinalResultsLatex.txt";
    ./wMean $i +03  | tee >> "FinalResultsLatex.txt";
    echo "␣␣&␣␣" | tee >> "FinalResultsLatex.txt";
    ./wMean $i +04  | tee >> "FinalResultsLatex.txt";
    echo "␣␣&␣␣" | tee >> "FinalResultsLatex.txt";
    ./wMean $i +07  | tee >> "FinalResultsLatex.txt";
    echo "␣␣&␣␣" | tee >> "FinalResultsLatex.txt";
    ./wMean $i +11  | tee >> "FinalResultsLatex.txt";
    echo "␣\\\␣" | tee >> "FinalResultsLatex.txt";

    echo "\hline"| tee >> "FinalResultsLatex.txt";
    echo "\end{tabular}" | tee >> "FinalResultsLatex.txt";

    echo "␣" | tee >> "FinalResultsLatex.txt";
    echo "␣" | tee >> "FinalResultsLatex.txt";

 #  cp neu.res ${i%.*}.res;
 #  rm neu.res
done
```

Chapter 6

Results

6.1 Chi-square of all models

There were calculated about 4000 synthetic spectra in the H-band and about 8000 synthetic spectra for the K-band. The "first" 4000 calculations were applied to both the H-band and the K-band. The "second" 4000 synthetic spectra for the K-band are for a denser parameter space grid[1], because the isotopic abundance ratio of $^{12}C/^{13}C$ (IACO) is more sensitive and therefore reliable in the K-band. Since the first results for the IACO of the stars were around 4 to 50, a denser grid for the IACO values of 1 to 50 was calculated for the previous best models.

Therefore, the chi-square results over the whole model grid of the stars are better comparable together for each H-band and K-band, since all the stars have the same amount of calculated model atmospheres. In particular one can see if any of the stars break out of a normal ascending curve of the chi-square fit, which might indicate, a bad signal to noise or bad calibration of the radial velocities, or due to a lack of models or some peaks in the wavelength range due to cosmics, or just for some unforeseen problems else. In the following Figures the values of the chi-square of the stars are shown for the bandheads and the full spectra. In Fig. 6.1 the value of the best chi-squares have a range from 0.5 to 1.5. In Fig. 6.2 the chi-squares of stars 9 and 12 have not the shape of the other stars. Star12 had a smaller signal for the flux in the original fits file from the VLT. In Fig. 6.4 star09 and star12 have a bad shape in the full spectra of the H-band.

[1]See also section 4.5.1.

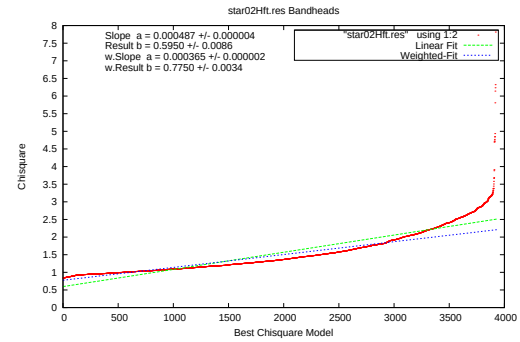

(a) H-band

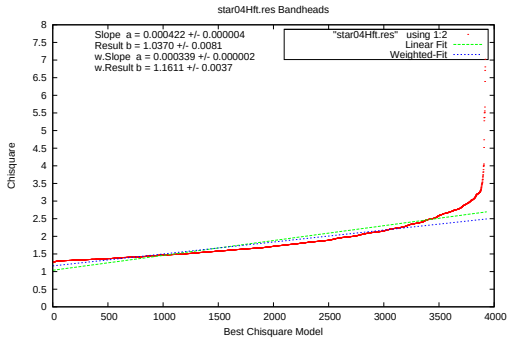

(b) H-band

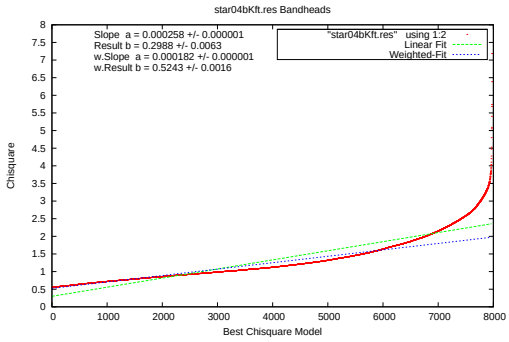

(c) K-band

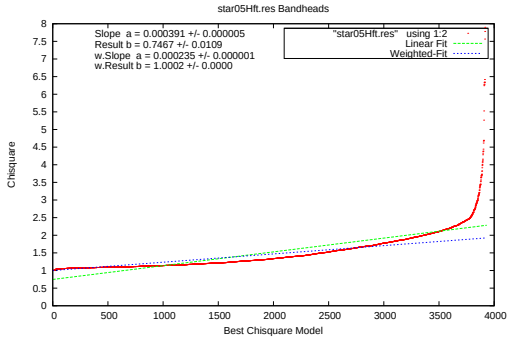

(d) H-band

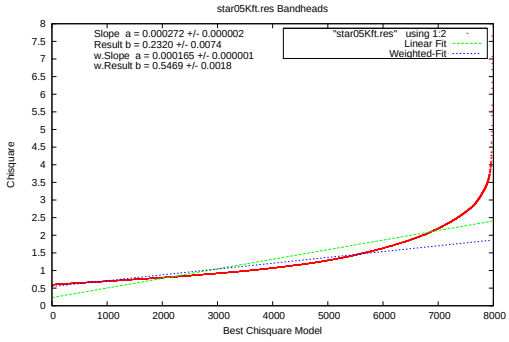

(e) K-band

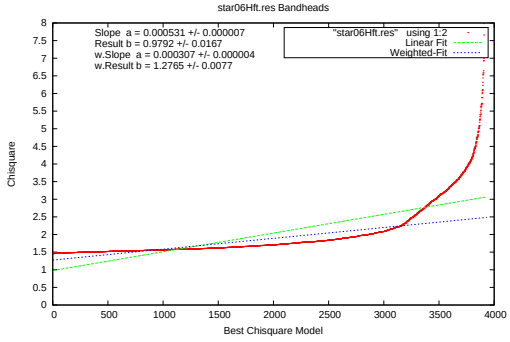

(f) H-band

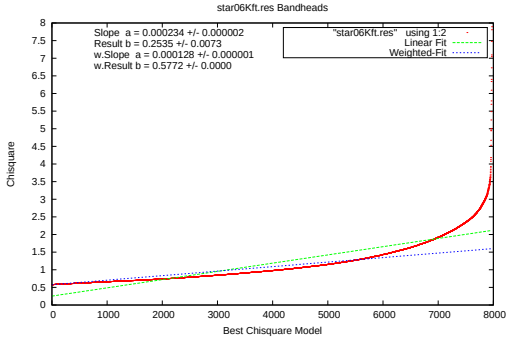

(g) K-band

Figure 6.1: Chi-square of stars 2-6 in the bandheads.

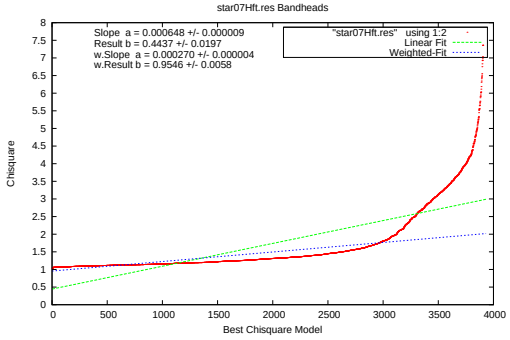

(a) H-band

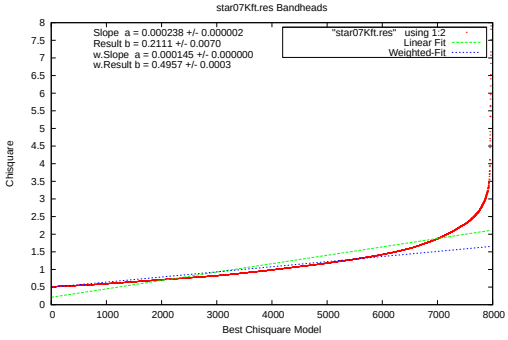

(b) K-band

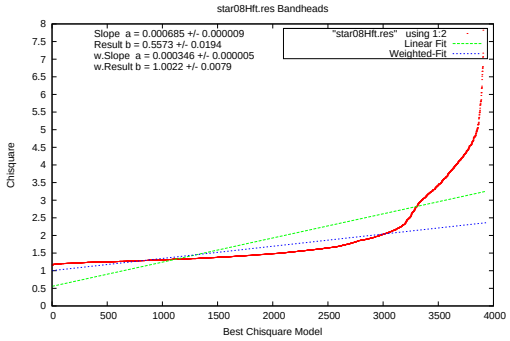

(c) H-band

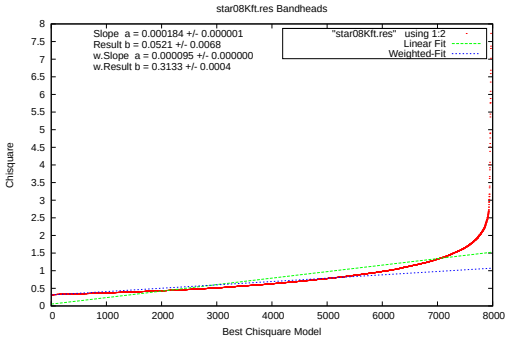

(d) K-band

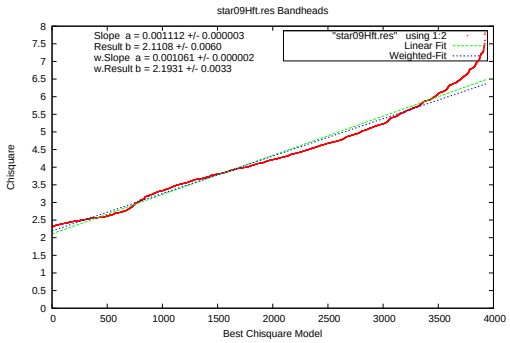

(e) H-band

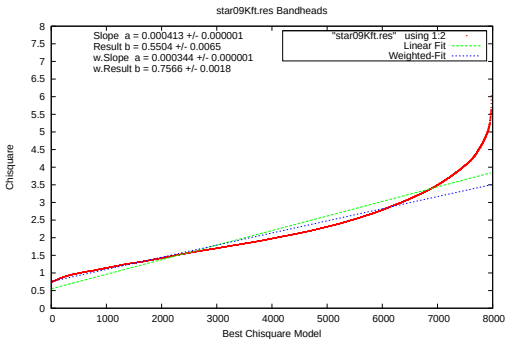

(f) K-band

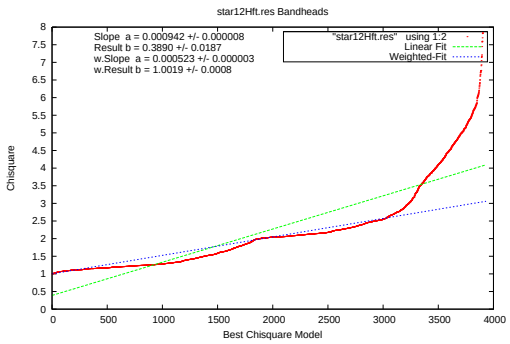

(g) H-band

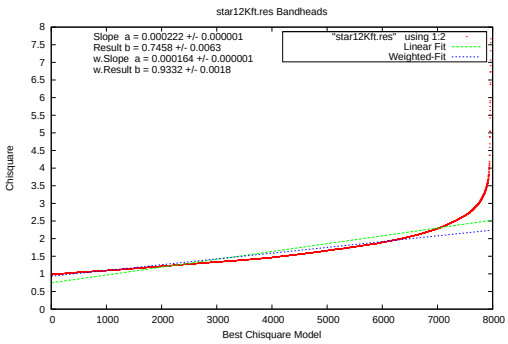

(h) K-band

Figure 6.2: Chi-square of the stars 7-12 in the bandheads.

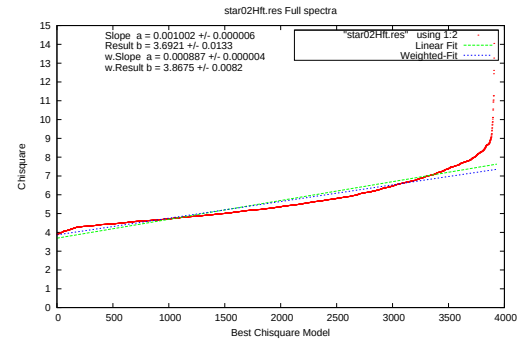

(a) H-band

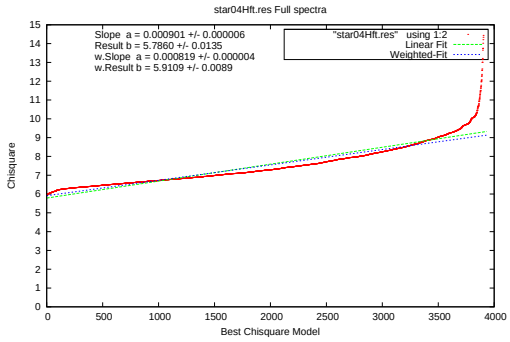

(b) H-band

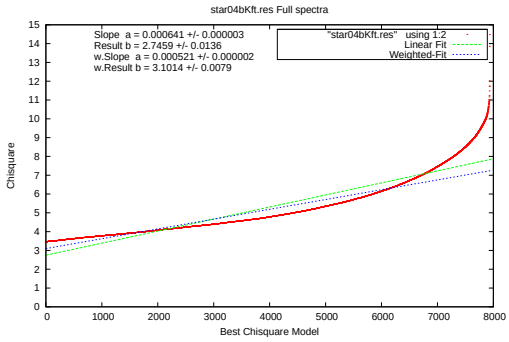

(c) K-band

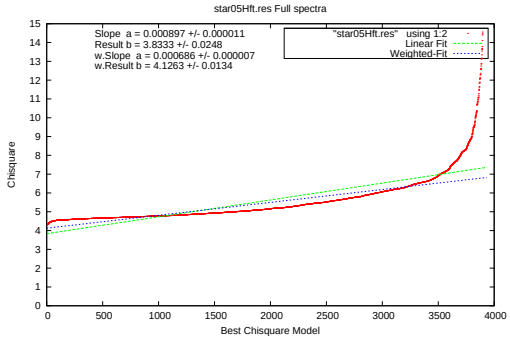

(d) H-band

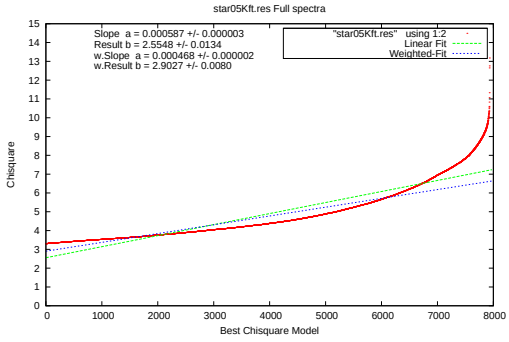

(e) K-band

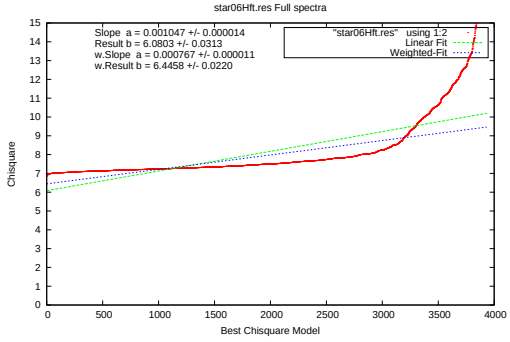

(f) H-band

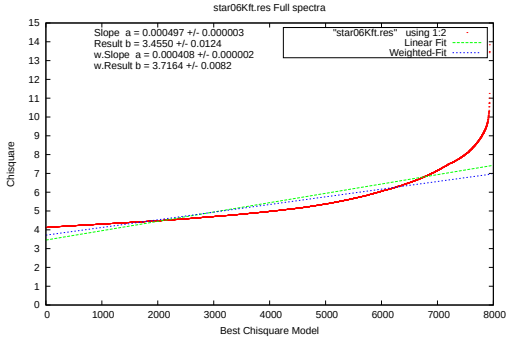

(g) K-band

Figure 6.3: Chi-square of stars 2-6 at full spectra range.

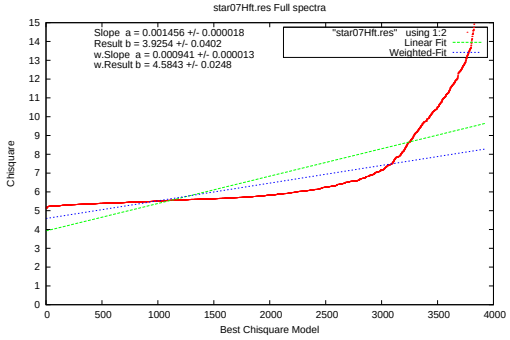

(a) H-band

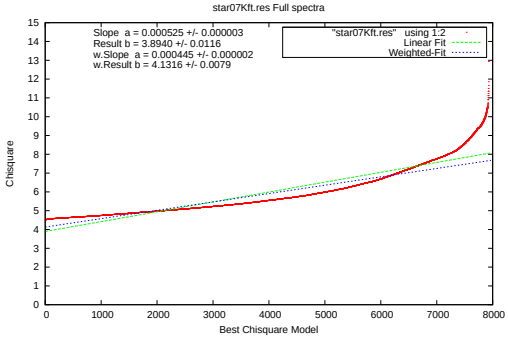

(b) K-band

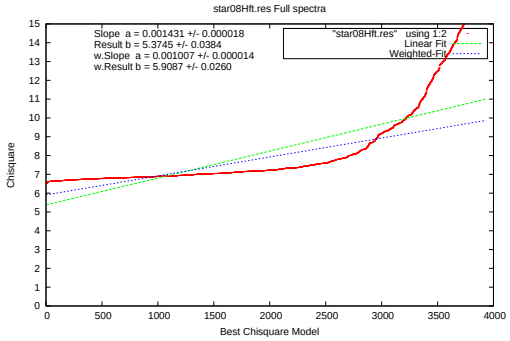

(c) H-band

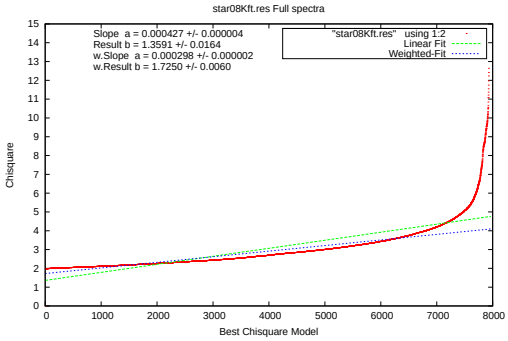

(d) K-band

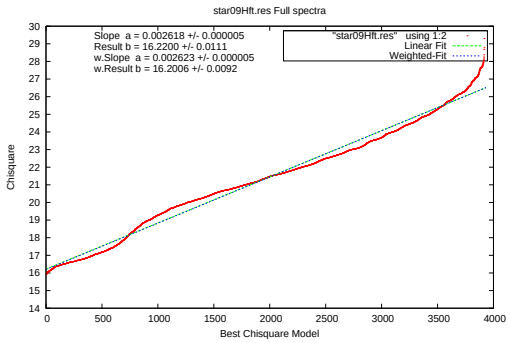

(e) H-band

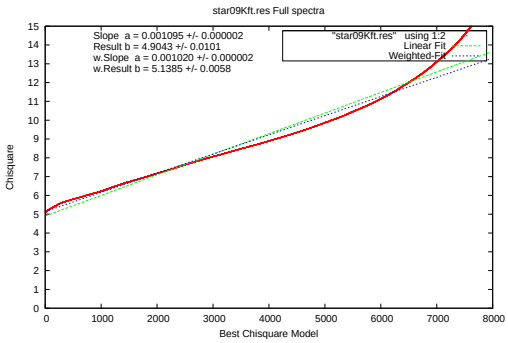

(f) K-band

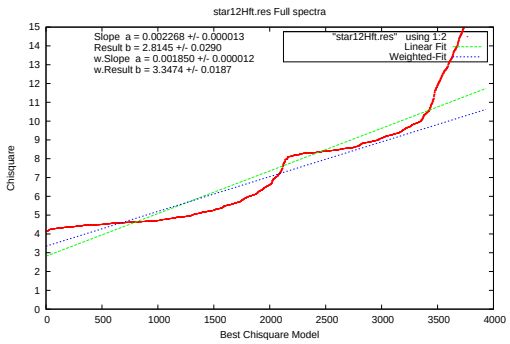

(g) H-band

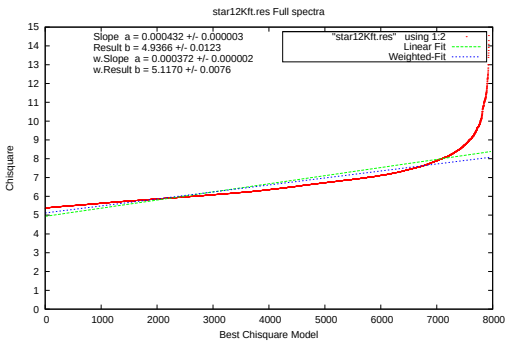

(h) K-band

Figure 6.4: Chi-square of stars 7-12 at full spectra range.

6.2 Result diagrams of parameters

In the following Figures the result diagrams of the 30 best fitting physical parameters are shown. The diagrams of the chi-square values are shown all together. As mentioned in Chapter 4 - Section *A Gnuplot visualisation problem*, the best fit in the plots is shown at number zero. The first series of plots are showing the bandheads where the plots of the physical parameters of the temperature, the log(g), the C/O-ratio, and the IACO-ratio are arranged for both the H-band and the K-band in one big plot. Then the plots of the full spectra range are shown in the same order.

The final value for the IACO was taken from the K-band. The IACO diagrams of the H-band are not very reliable due to the lack of missing prominent ^{13}C features in the H-band. For statistical investigations they are shown also in the H-band. The data from star02 in the K-band was too bad to be analysed and therefore it is missing in the diagrams.

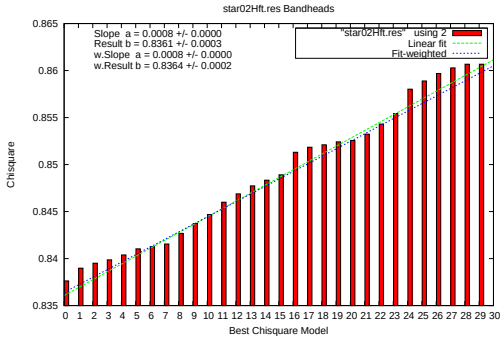

(a) H-band

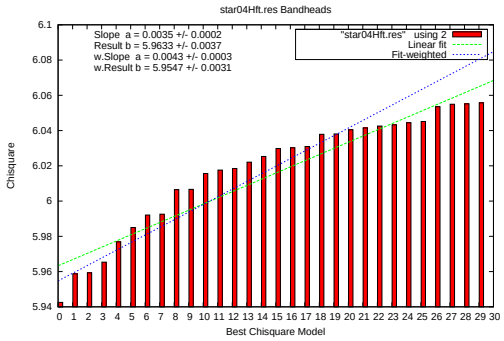

(c) H-band

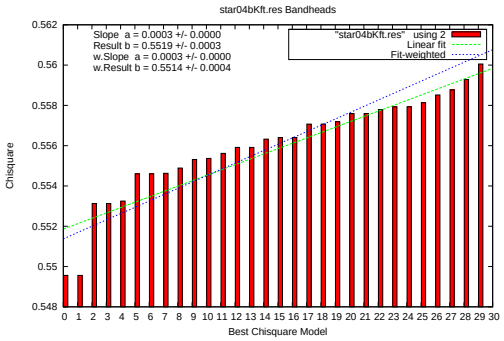

(d) K-band

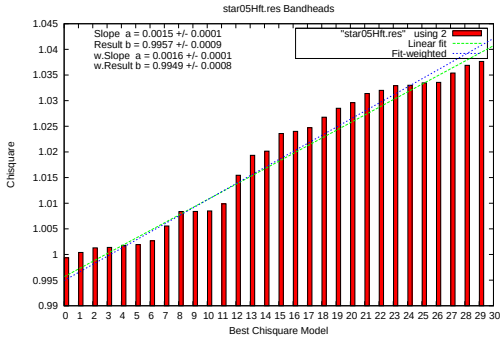

(e) H-band

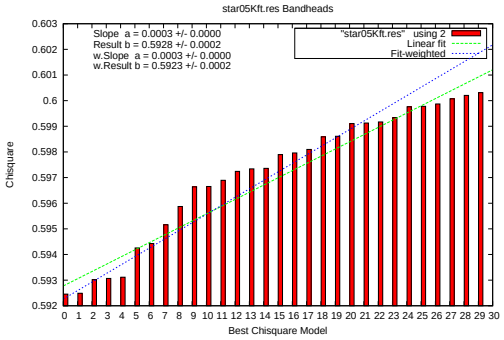

(f) K-band

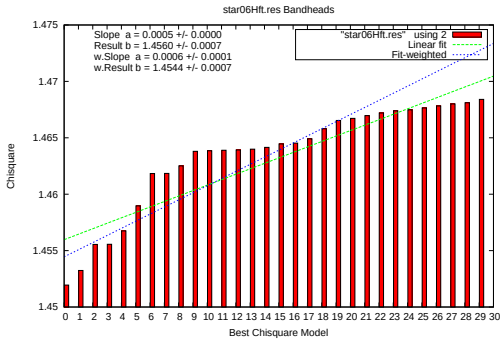

(g) H-band

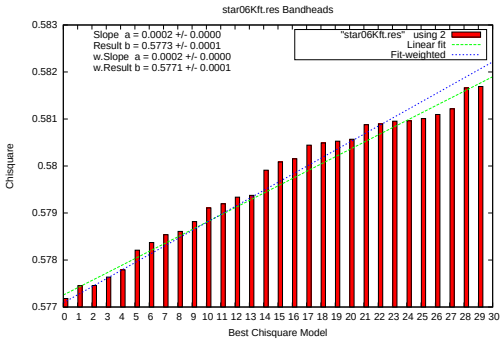

(h) K-band

Figure 6.5: Results of the bandheads of the best 30 chi-squares per star.

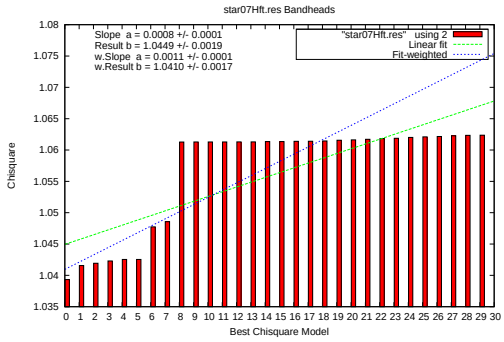

(a) H-band

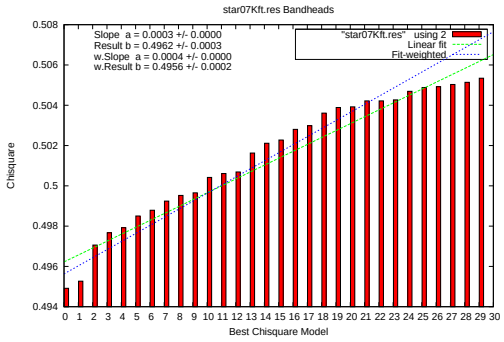

(b) K-band

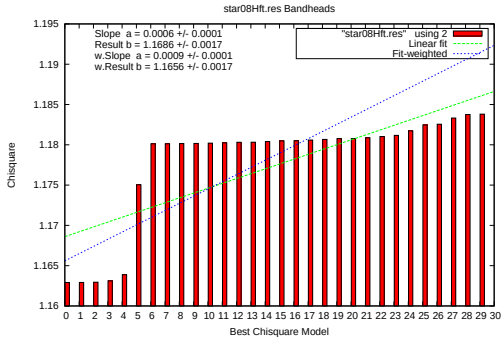

(c) H-band

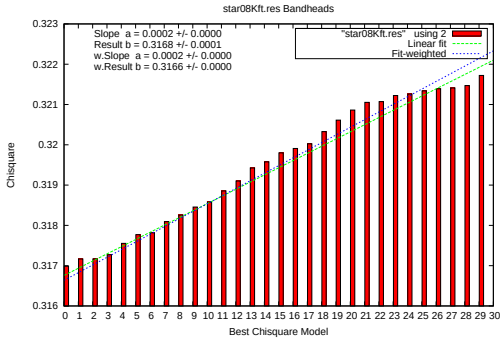

(d) K-band

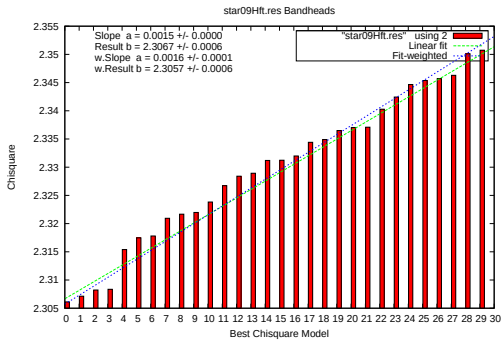

(e) H-band

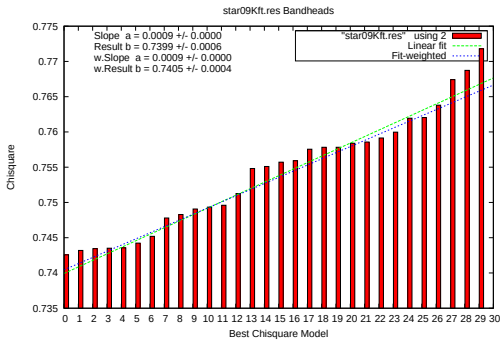

(f) K-band

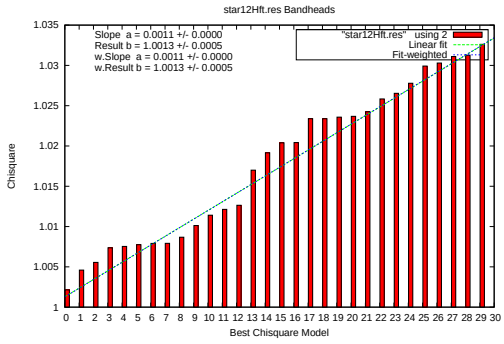

(g) H-band

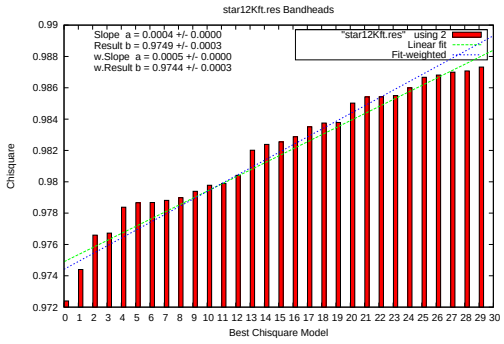

(h) K-band

Figure 6.6: Results of the bandheads of the best 30 chi-squares per star.

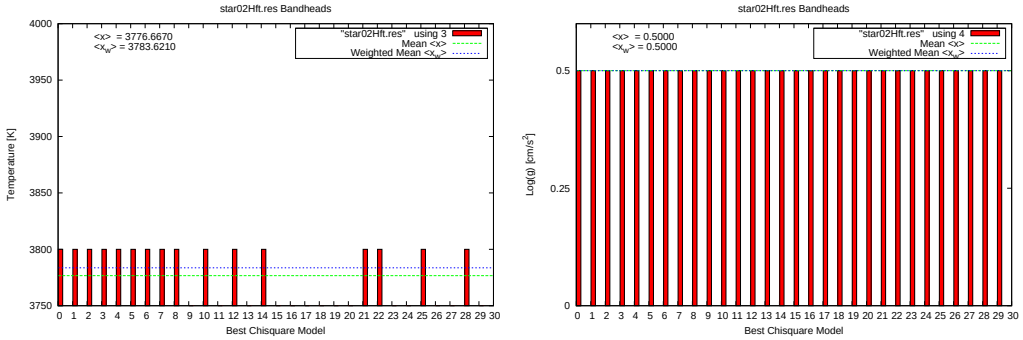

(a) H-band (b) H-band

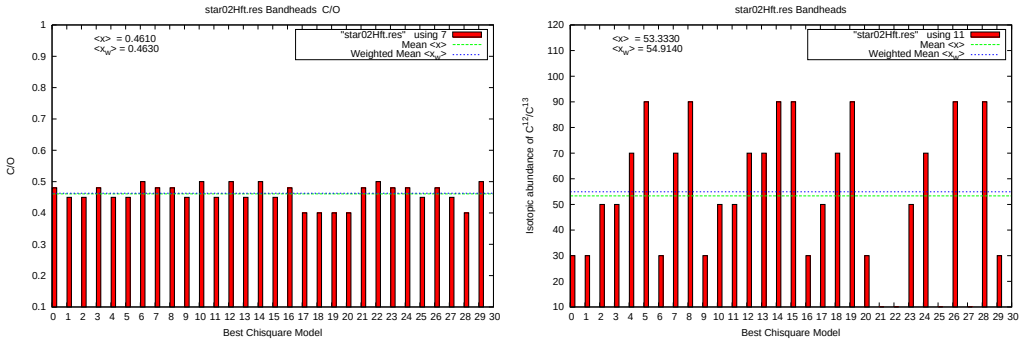

(c) H-band (d) H-band

Figure 6.7: Results of the bandheads of the 30 best models of star02.

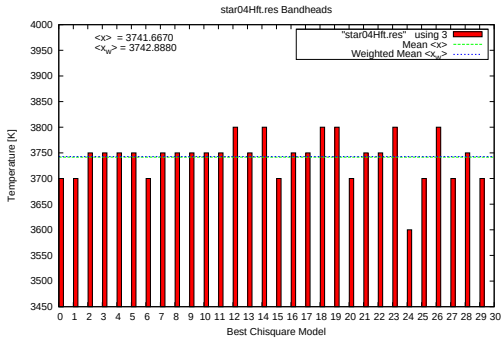

(a) H-band

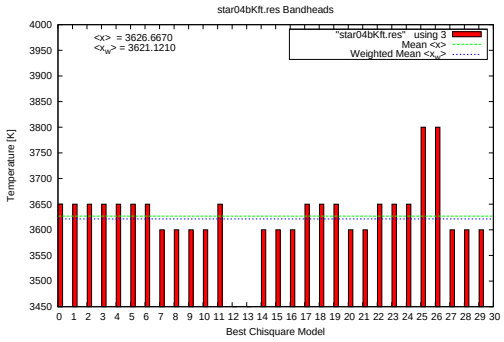

(b) K-band

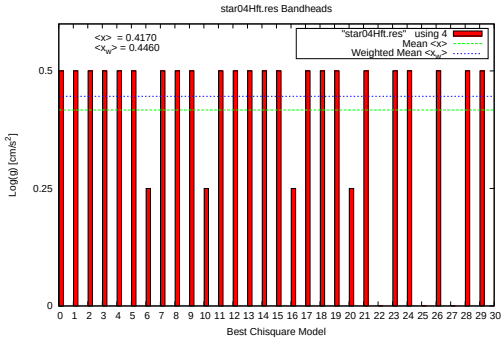

(c) H-band

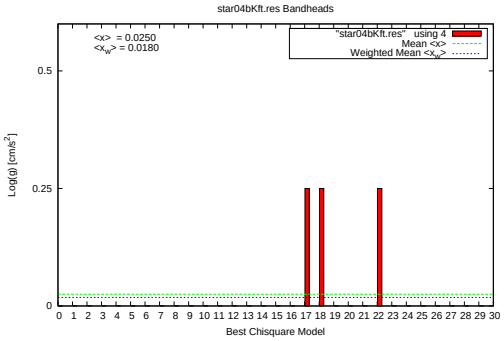

(d) K-band

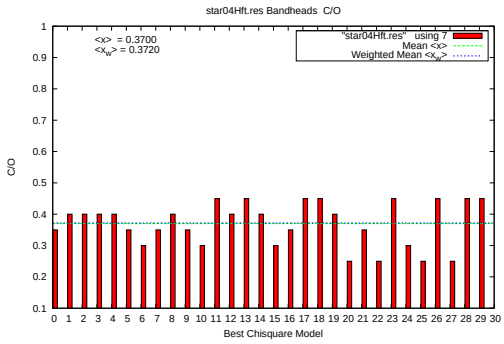

(e) H-band

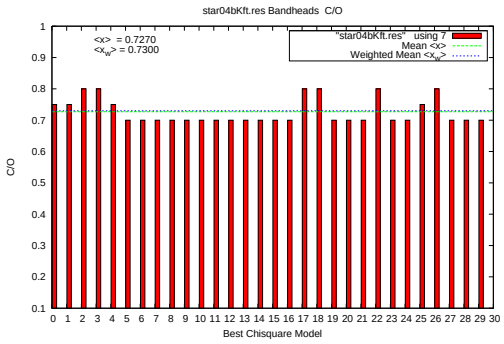

(f) K-band

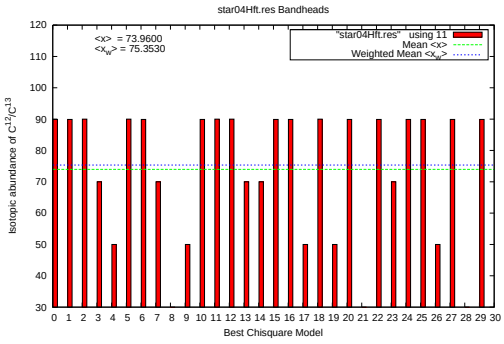

(g) H-band

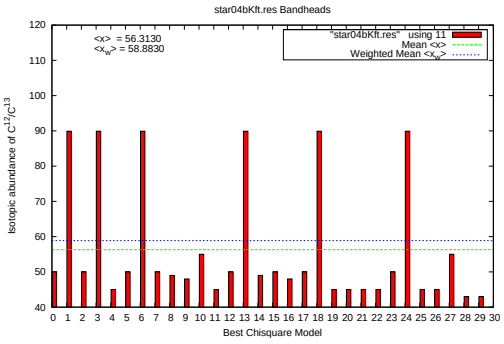

(h) K-band

Figure 6.8: Results of the bandheads of the 30 best models of star04.

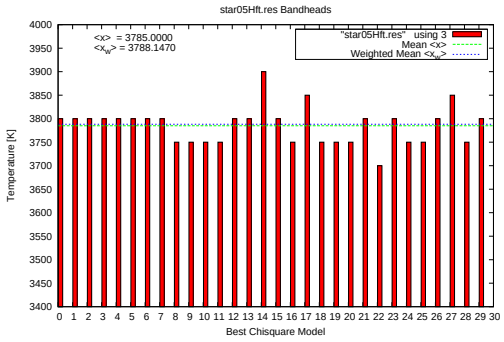

(a) H-band

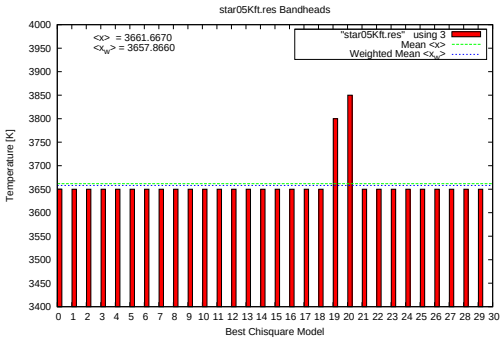

(b) K-band

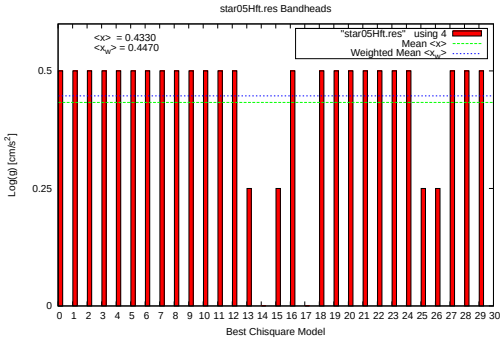

(c) H-band

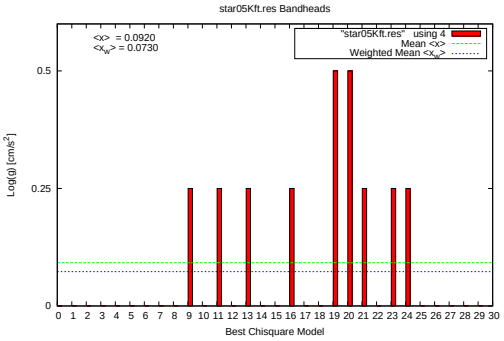

(d) K-band

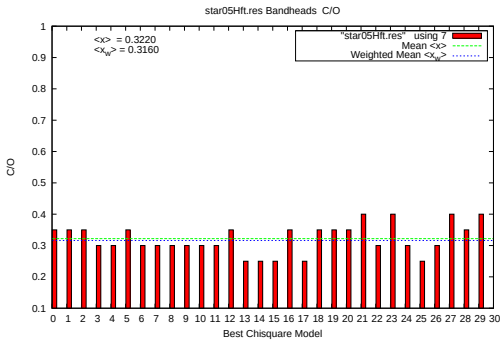

(e) H-band

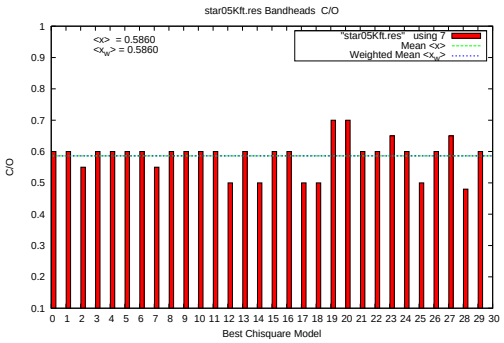

(f) K-band

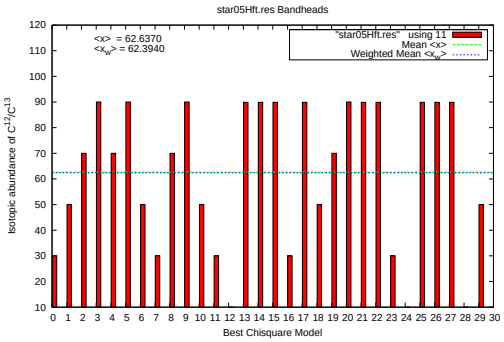

(g) H-band

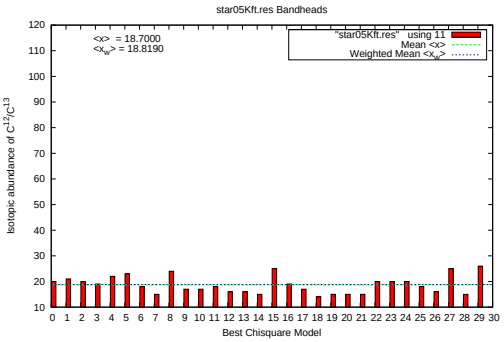

(h) K-band

Figure 6.9: Results of the bandheads of the 30 best models of star05.

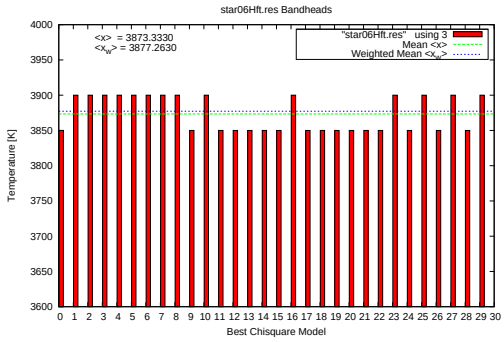

(a) H-band

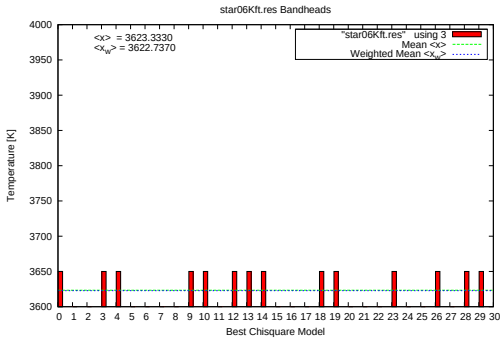

(b) K-band

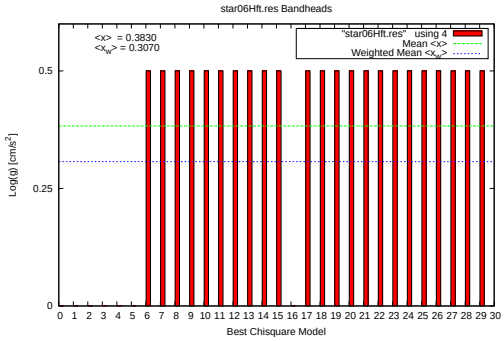

(c) H-band

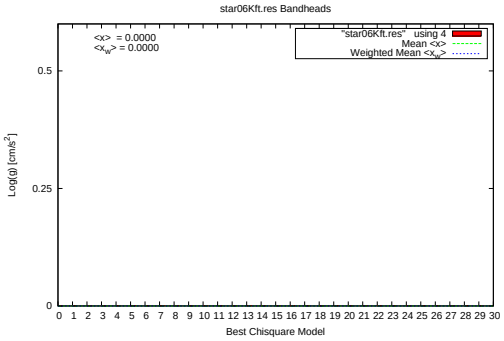

(d) K-band

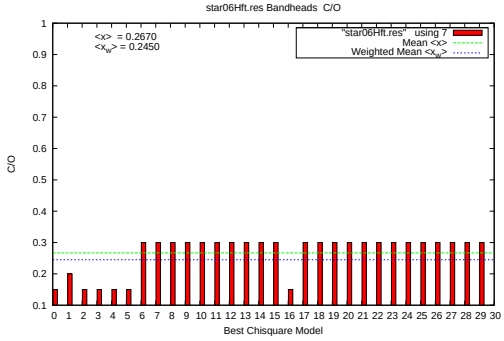

(e) H-band

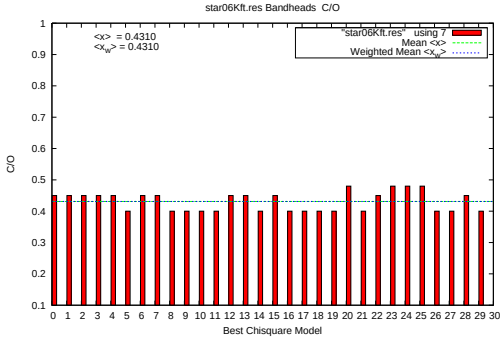

(f) K-band

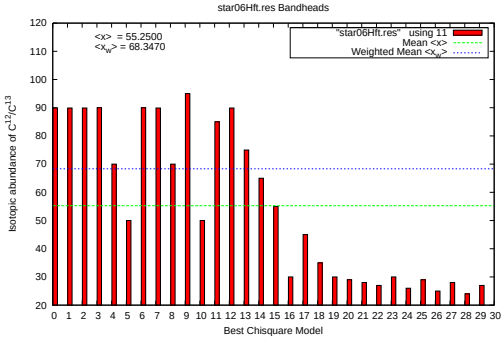

(g) H-band

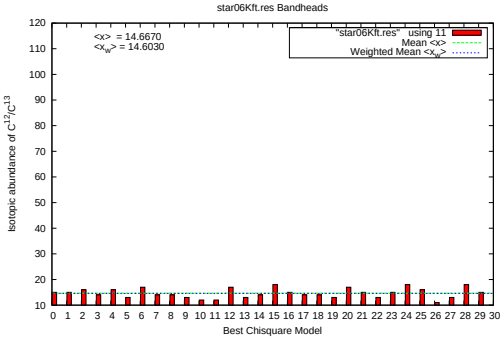

(h) K-band

Figure 6.10: Results of the bandheads of the 30 best models of star06.

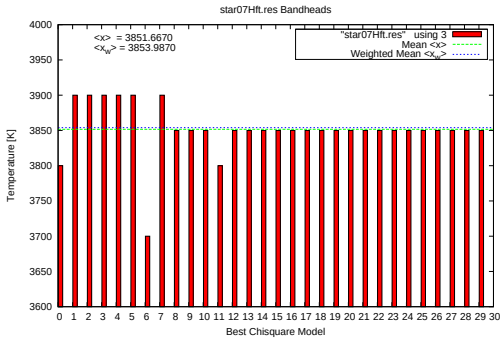

(a) H-band

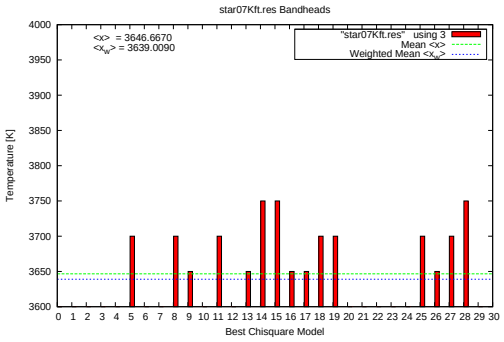

(b) K-band

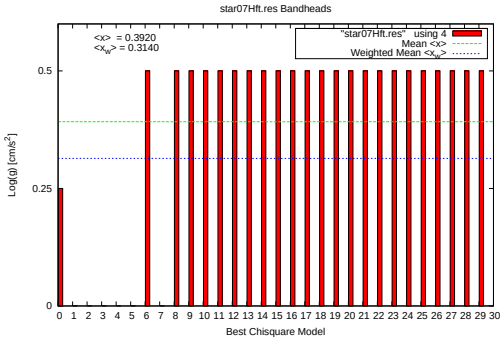

(c) H-band

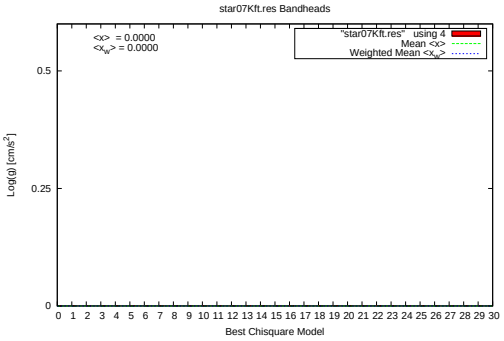

(d) K-band

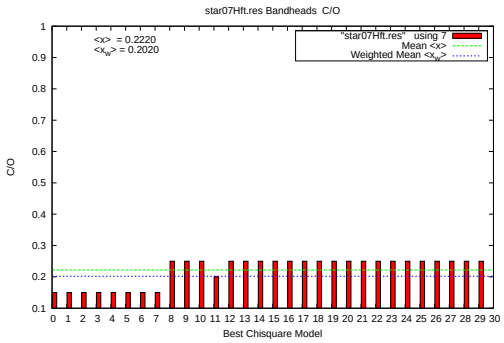

(e) H-band

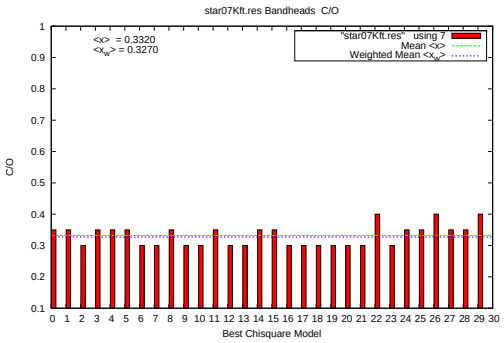

(f) K-band

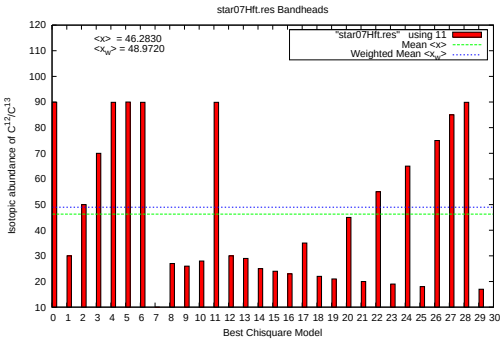

(g) H-band

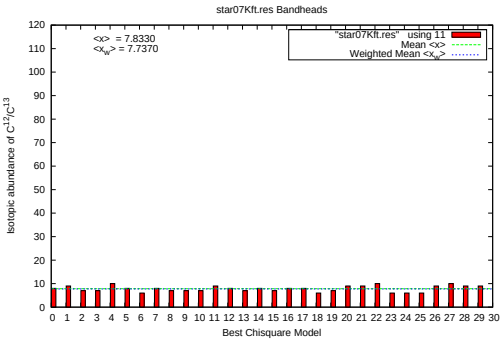

(h) K-band

Figure 6.11: Results of the bandheads of the 30 best models of star07.

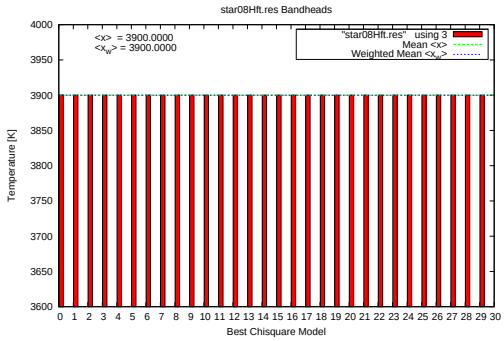

(a) H-band

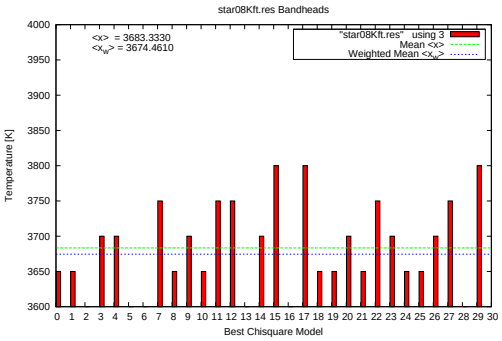

(b) K-band

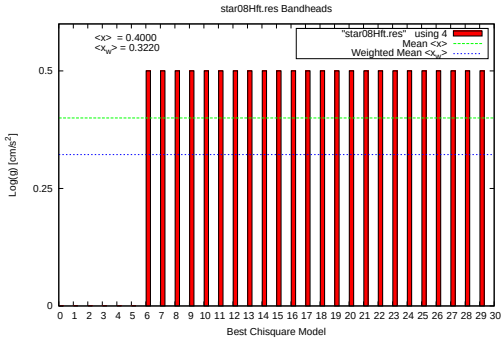

(c) H-band

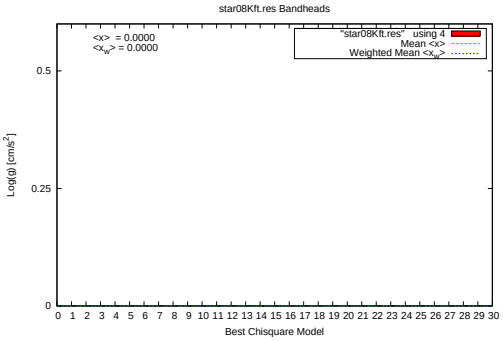

(d) K-band

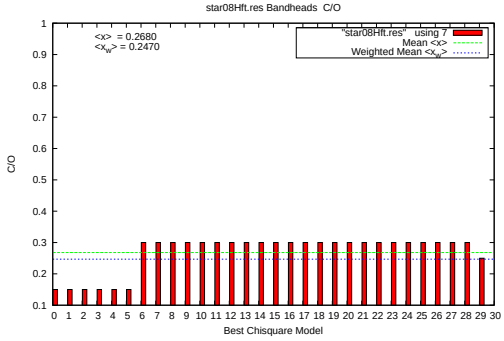

(e) H-band

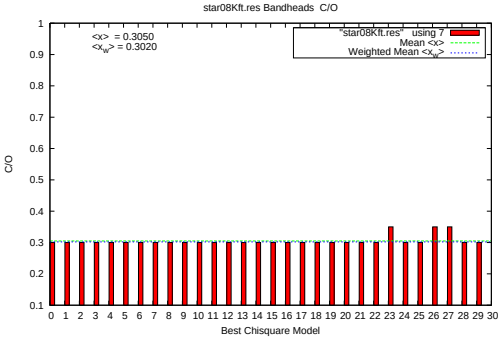

(f) K-band

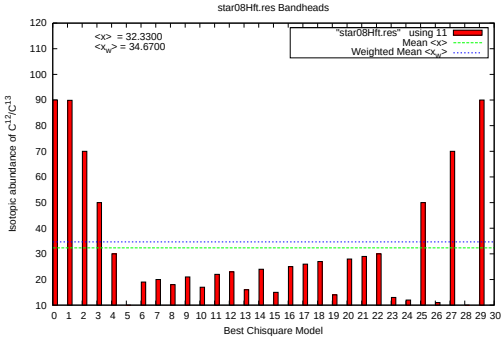

(g) H-band

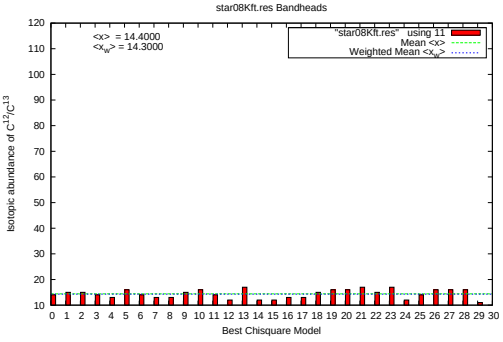

(h) K-band

Figure 6.12: Results of the bandheads of the 30 best models of star08.

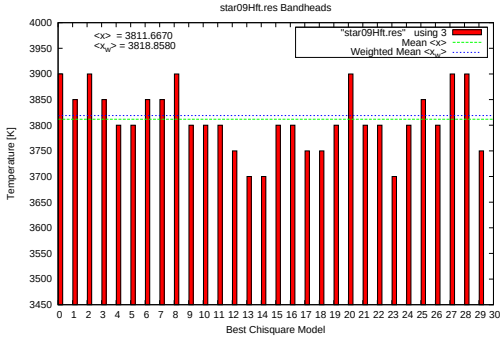

(a) H-band

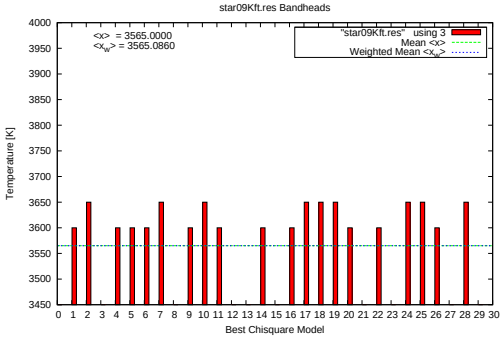

(b) K-band

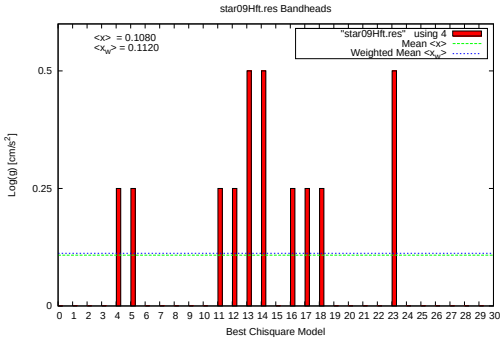

(c) H-band

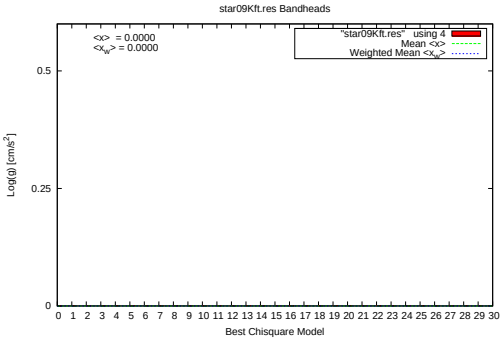

(d) K-band

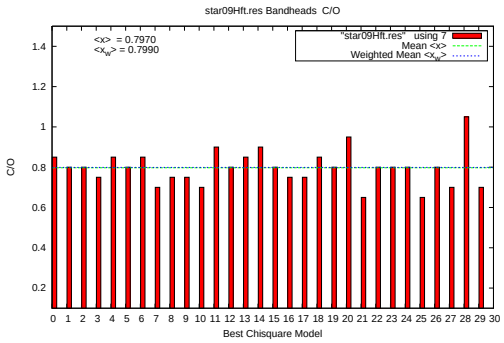

(e) H-band

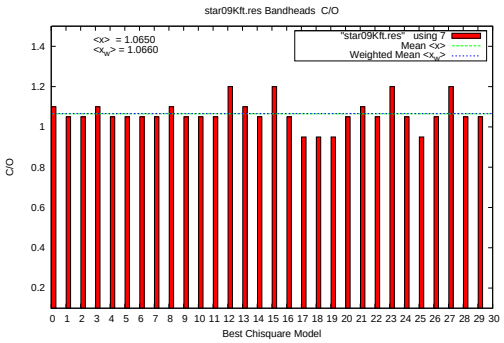

(f) K-band

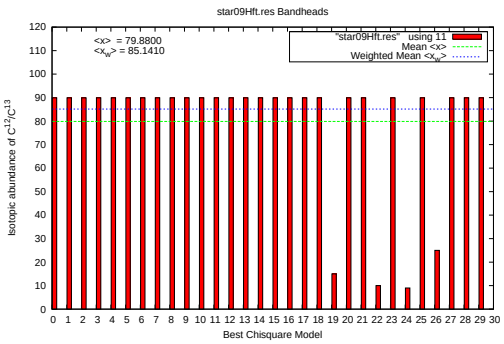

(g) H-band

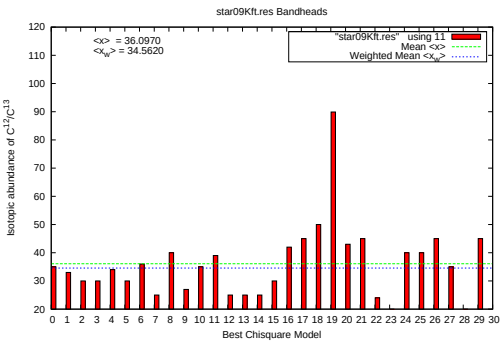

(h) K-band

Figure 6.13: Results of the bandheads of the 30 best models of star09.

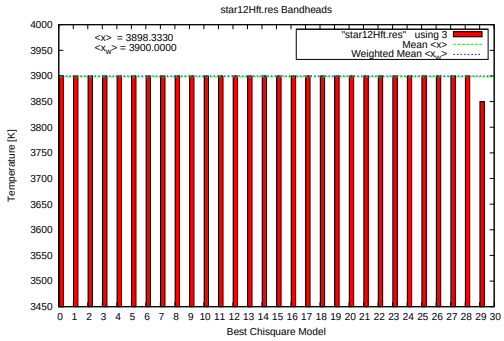

(a) H-band

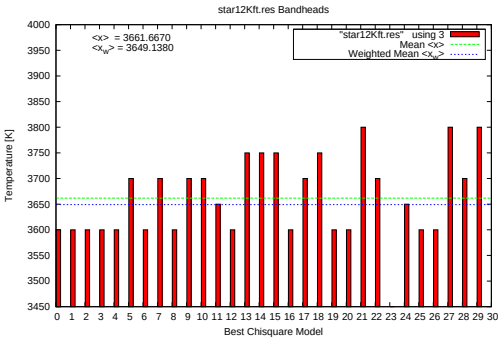

(b) K-band

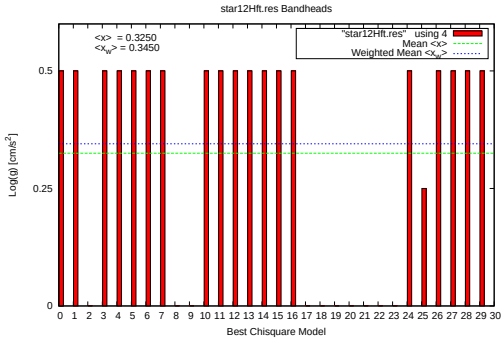

(c) H-band

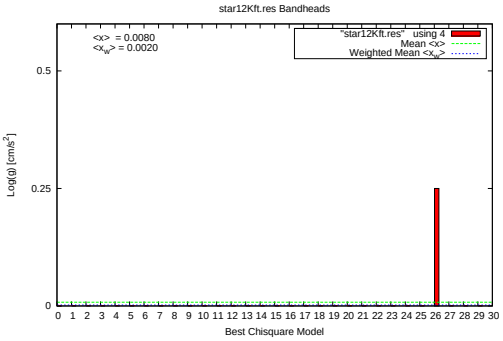

(d) K-band

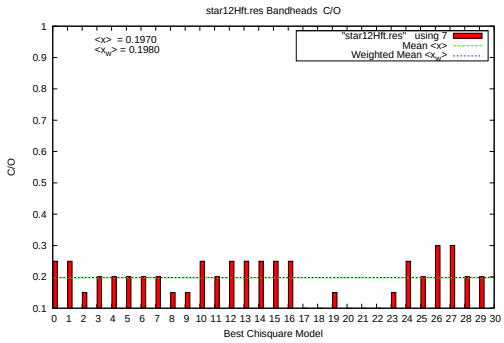

(e) H-band

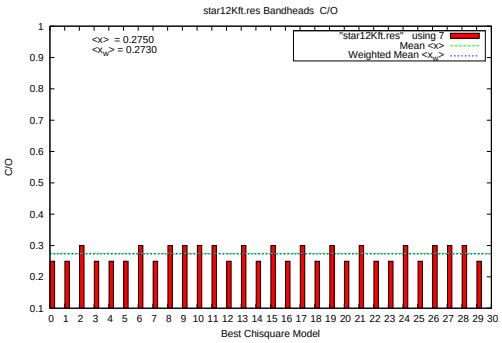

(f) K-band

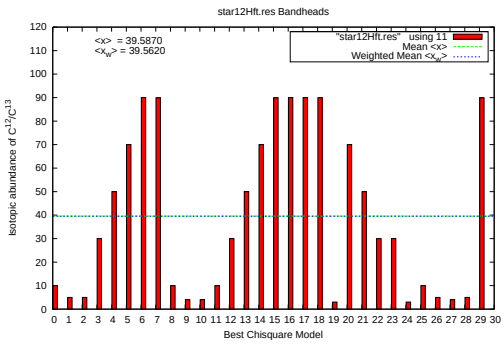

(g) H-band

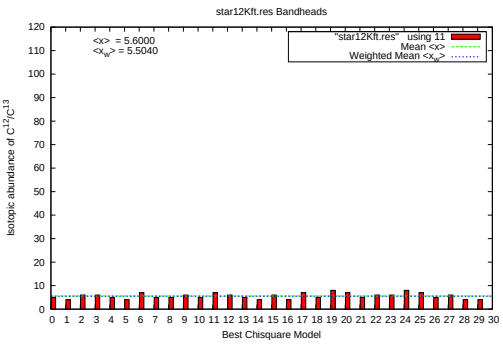

(h) K-band

Figure 6.14: Results of the bandheads of the 30 best models of star12.

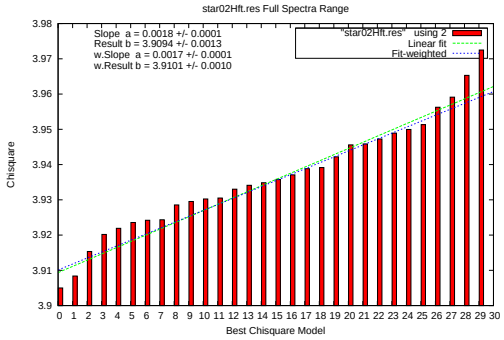

(a) H-band

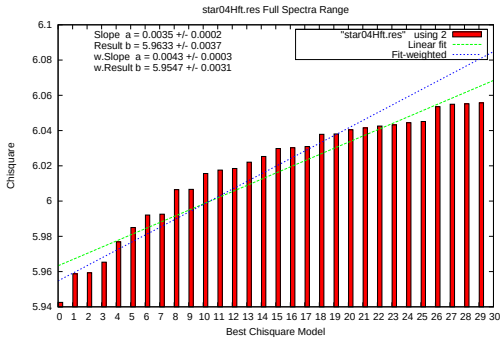

(c) H-band

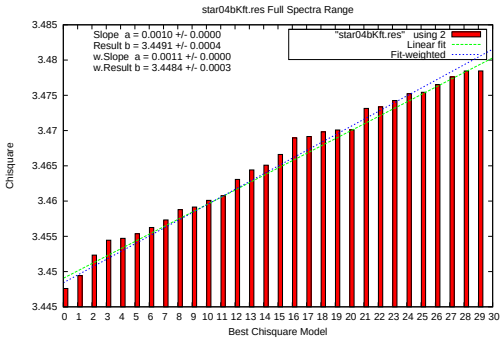

(d) K-band

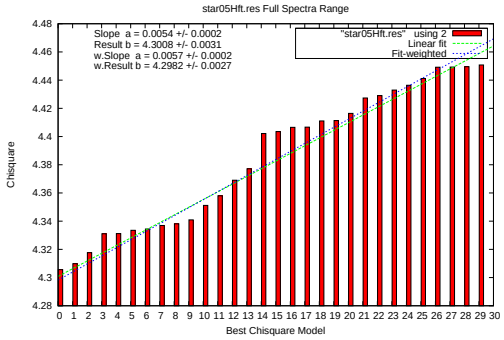

(e) H-band

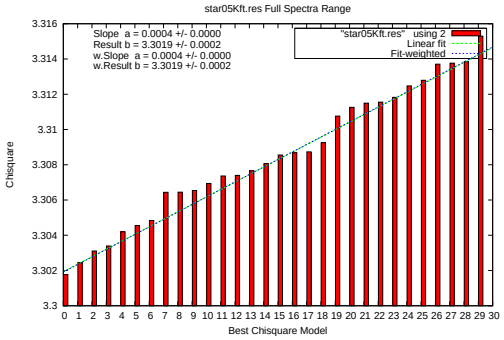

(f) K-band

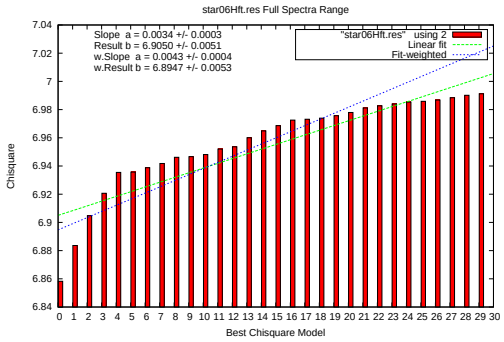

(g) H-band

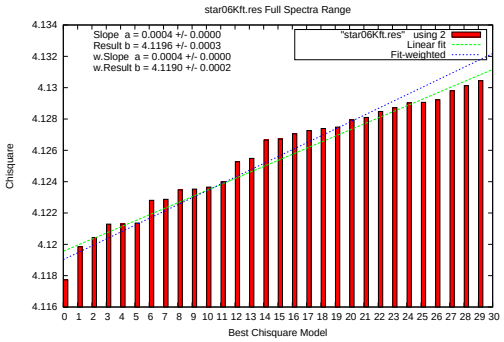

(h) K-band

Figure 6.15: Results of the full spectra of the best 30 chi-squares per star.

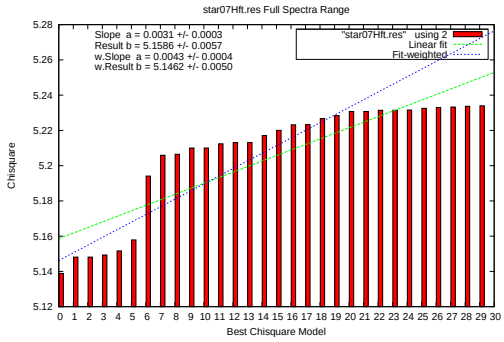

(a) H-band

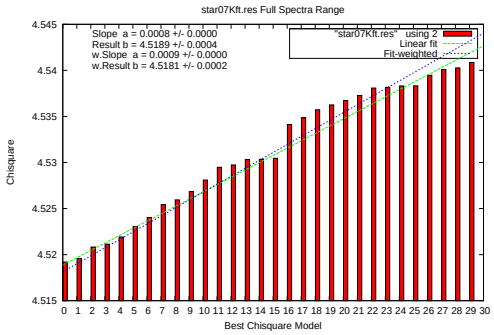

(b) K-band

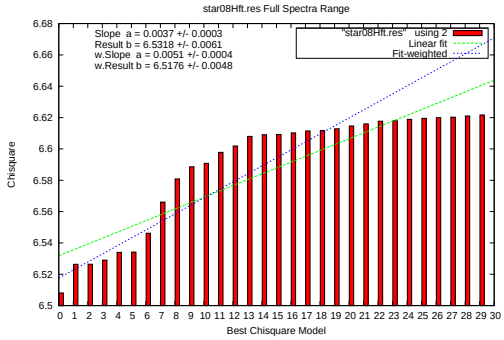

(c) H-band

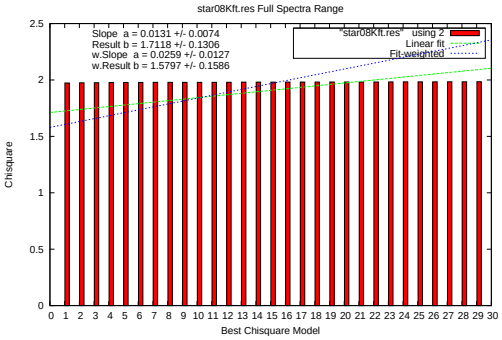

(d) K-band

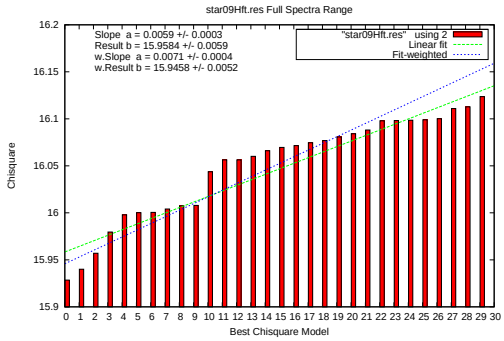

(e) H-band

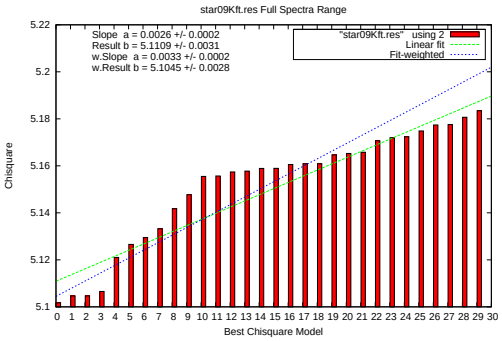

(f) K-band

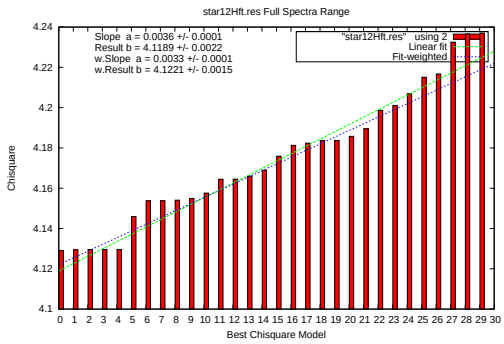

(g) H-band

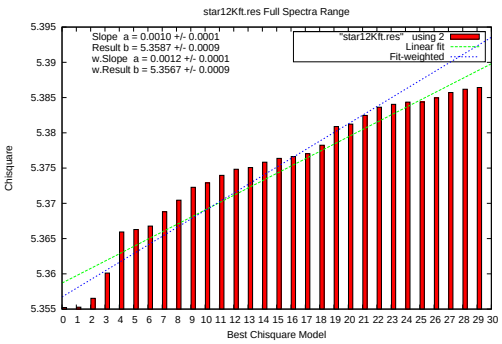

(h) K-band

Figure 6.16: Results of the full spectra of the best 30 chi-squares per star.

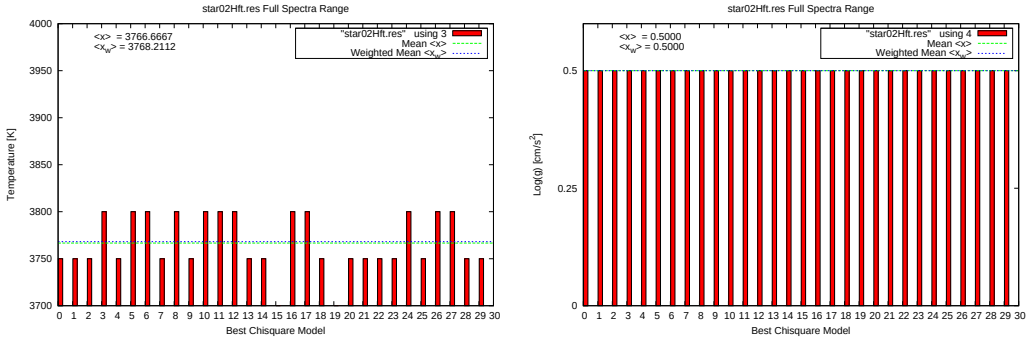

(a) H-band

(b) H-band

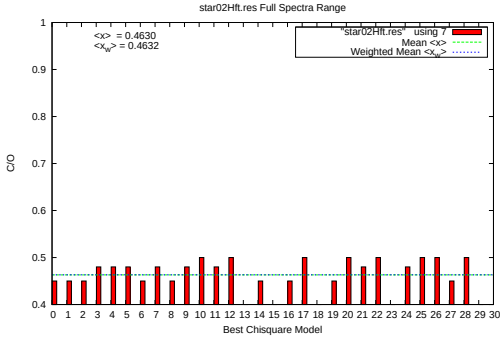

(c) H-band

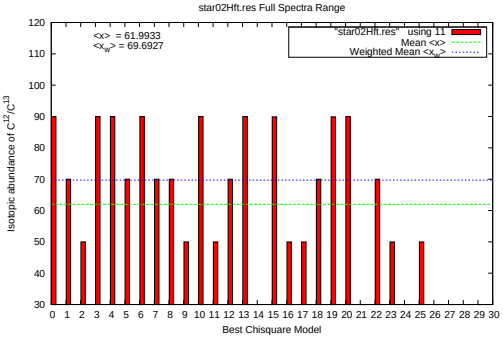

(d) H-band

Figure 6.17: Results of the full spectra of the 30 best models of star02.

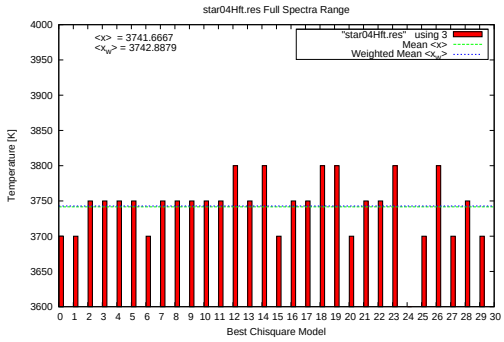

(a) H-band

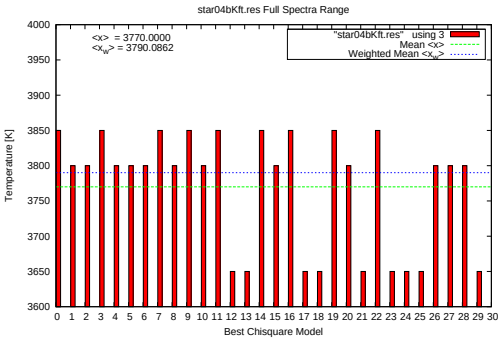

(b) K-band

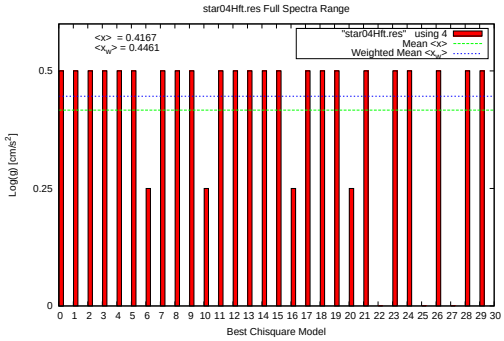

(c) H-band

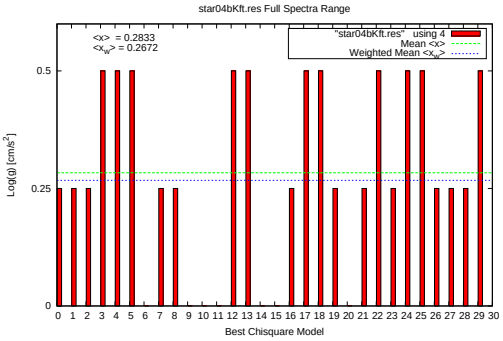

(d) K-band

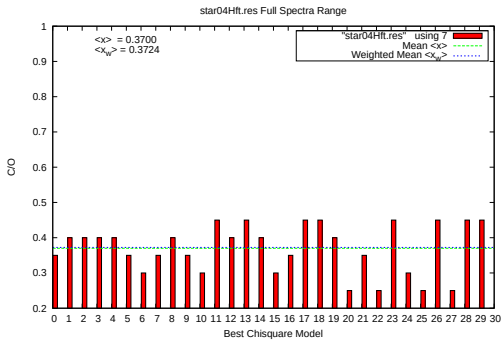

(e) H-band

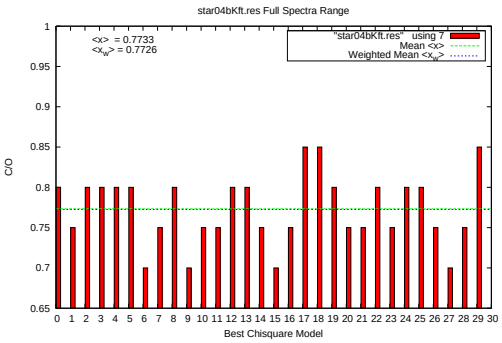

(f) K-band

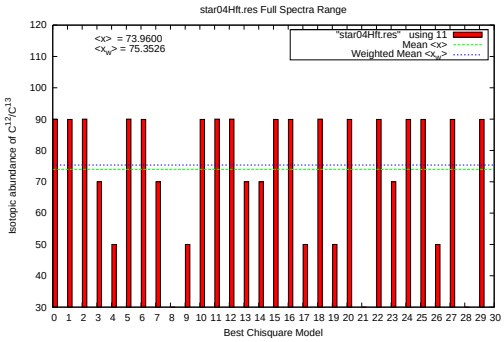

(g) H-band

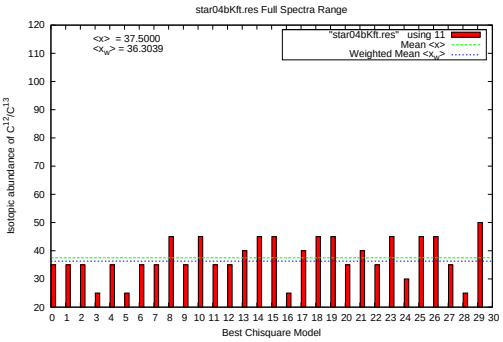

(h) K-band

Figure 6.18: Results of the full spectra of the 30 best models of star04.

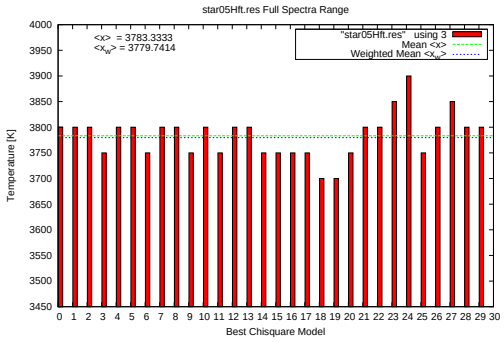

(a) H-band

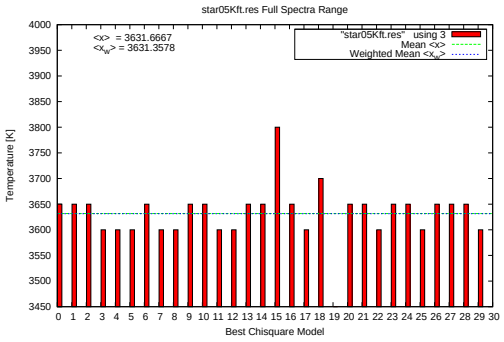

(b) K-band

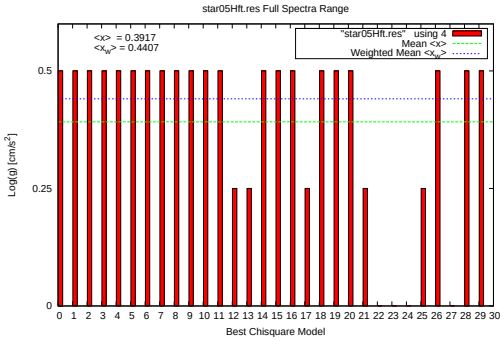

(c) H-band

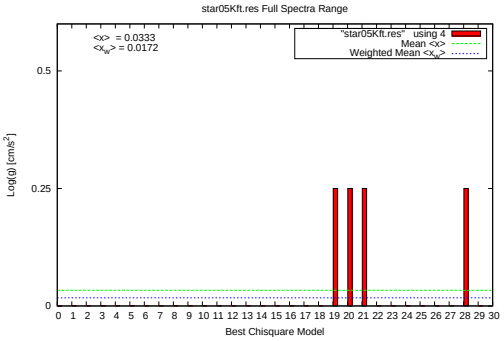

(d) K-band

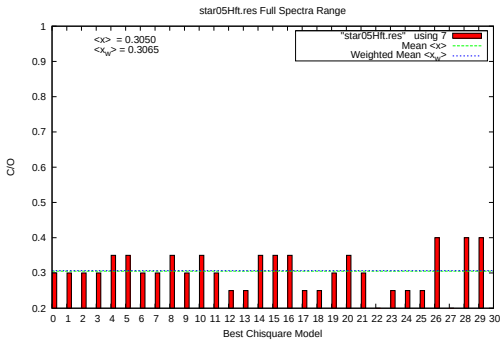

(e) H-band

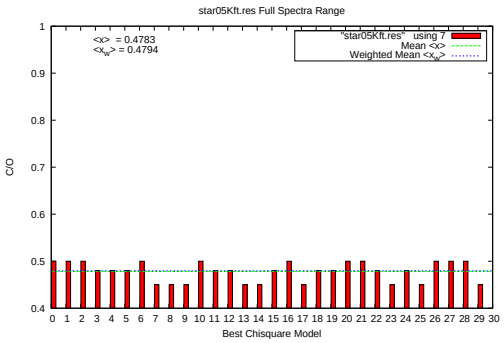

(f) K-band

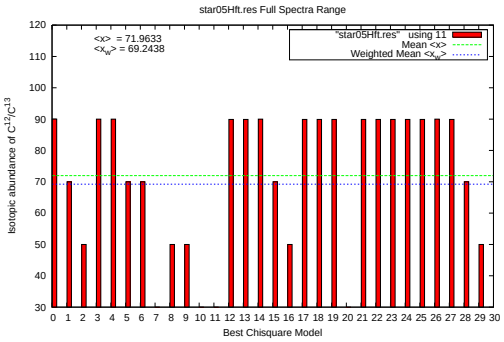

(g) H-band

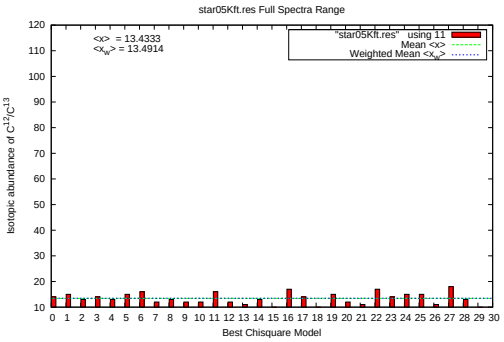

(h) K-band

Figure 6.19: Results of the full spectra of the 30 best models of star05.

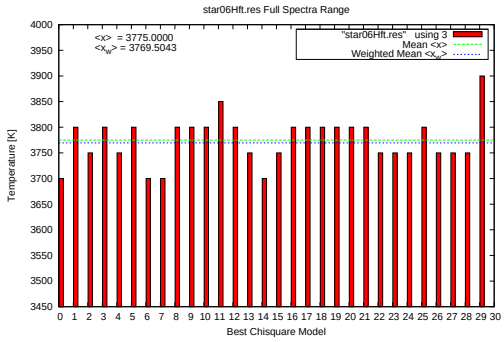

(a) H-band

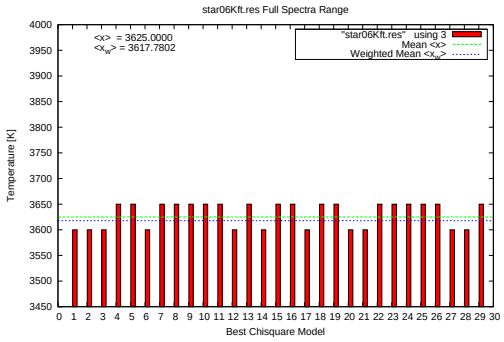

(b) K-band

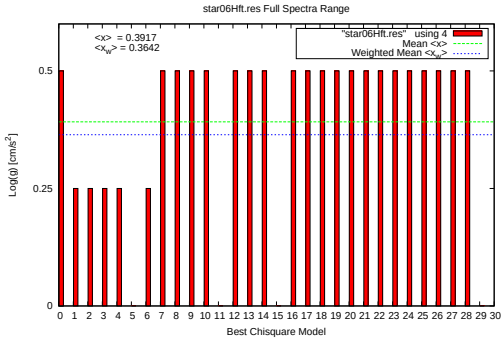

(c) H-band

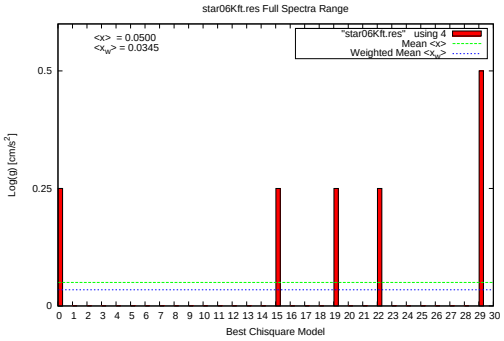

(d) K-band

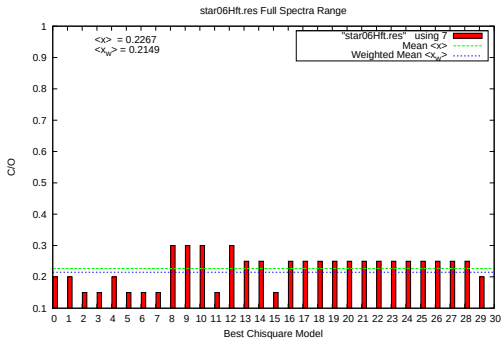

(e) H-band

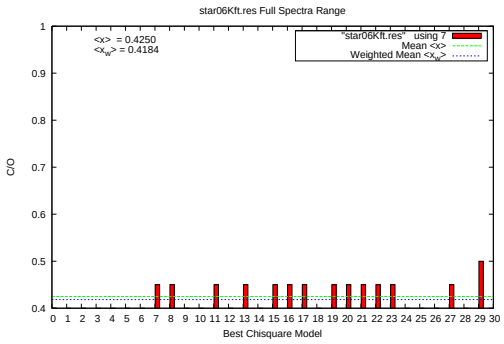

(f) K-band

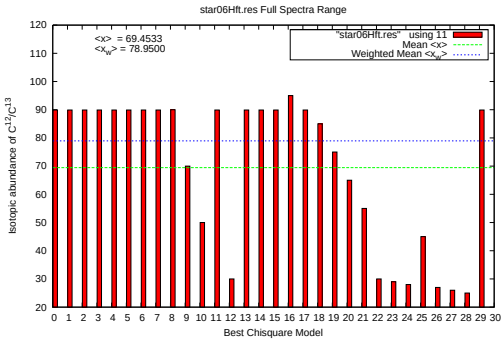

(g) H-band

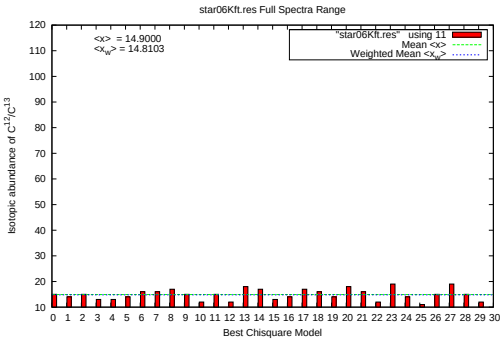

(h) K-band

Figure 6.20: Results of the full spectra of the 30 best models of star06.

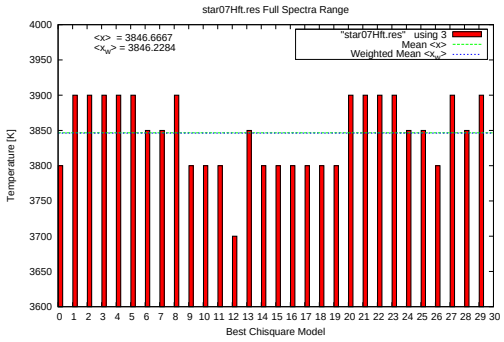

(a) H-band

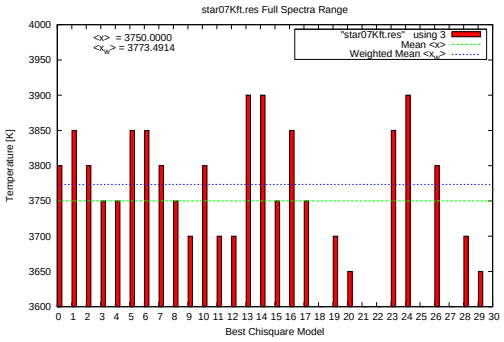

(b) K-band

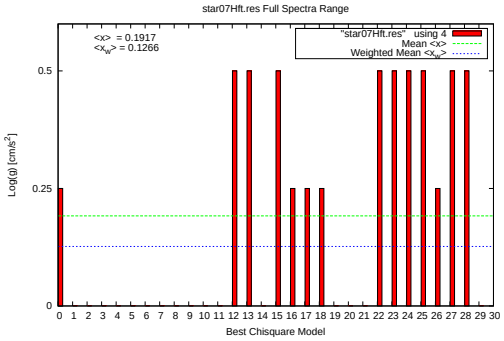

(c) H-band

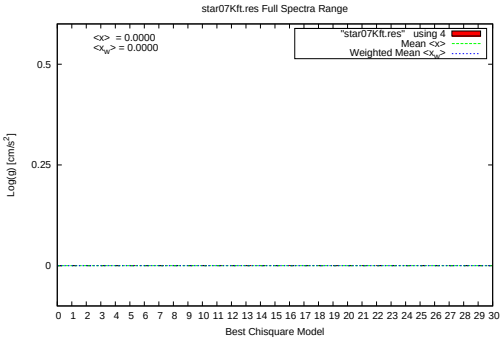

(d) K-band

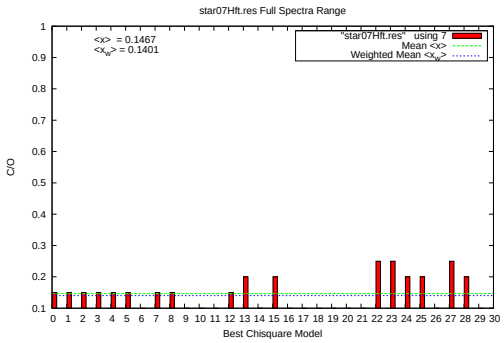

(e) H-band

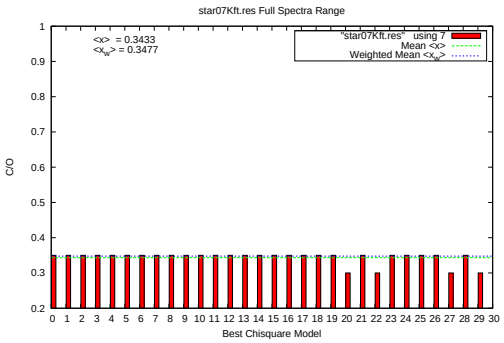

(f) K-band

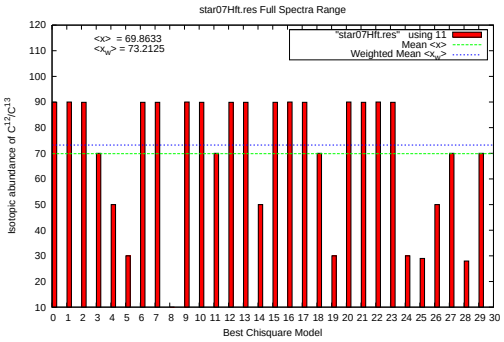

(g) H-band

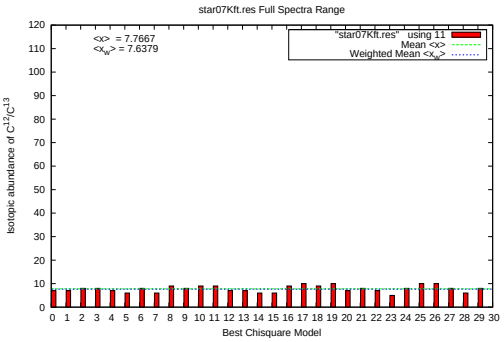

(h) K-band

Figure 6.21: Results of the full spectra of the 30 best models of star07.

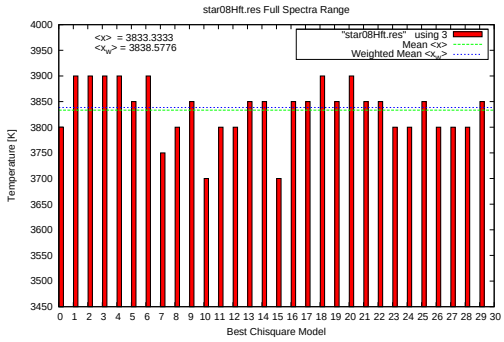

(a) H-band

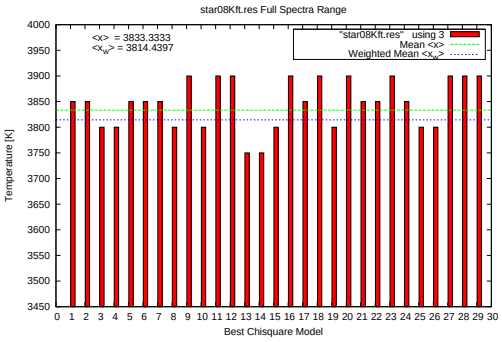

(b) K-band

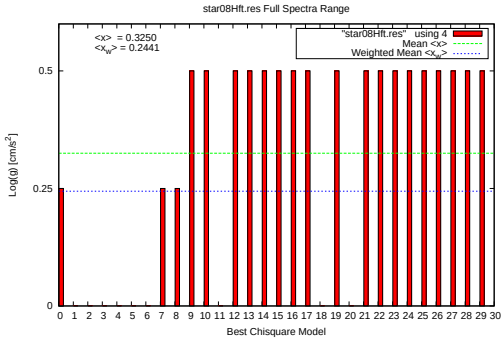

(c) H-band

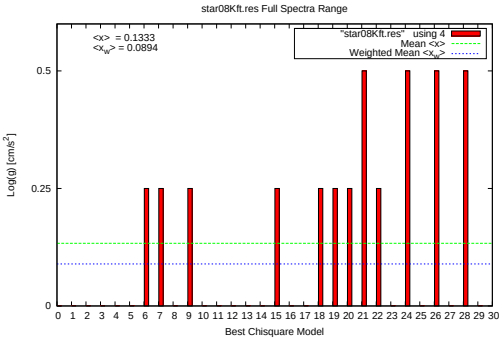

(d) K-band

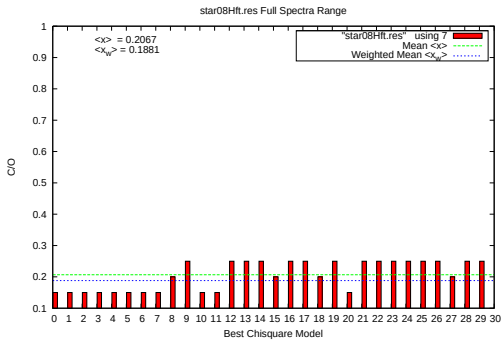

(e) H-band

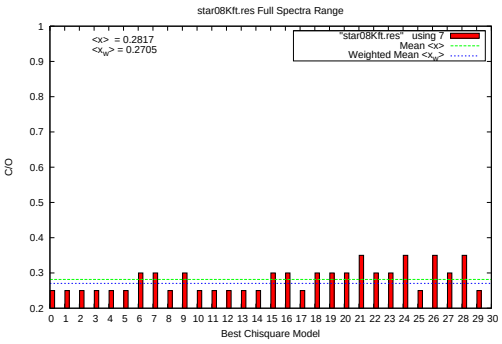

(f) K-band

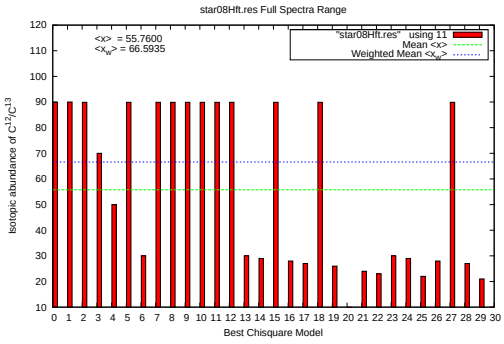

(g) H-band

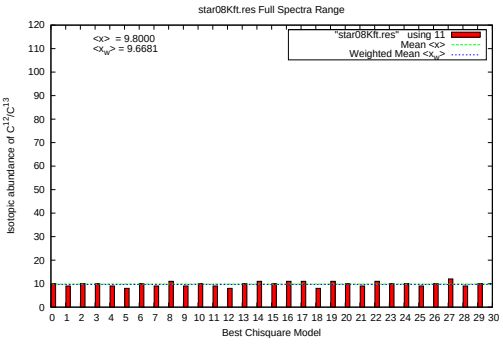

(h) K-band

Figure 6.22: Results of the full spectra of the 30 best models of star08.

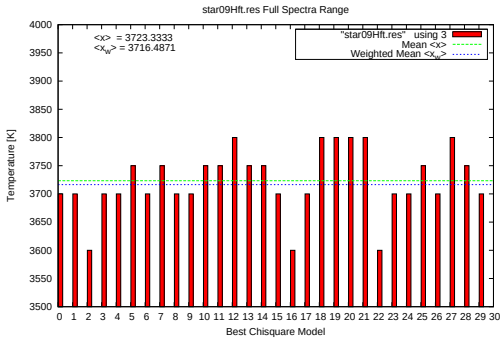

(a) H-band

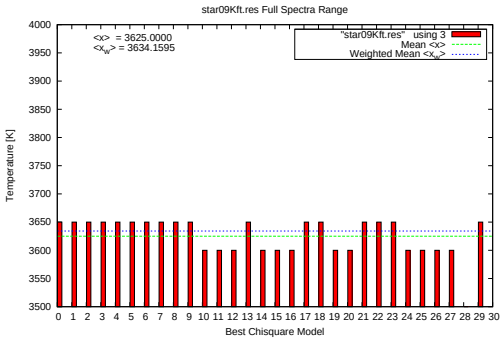

(b) K-band

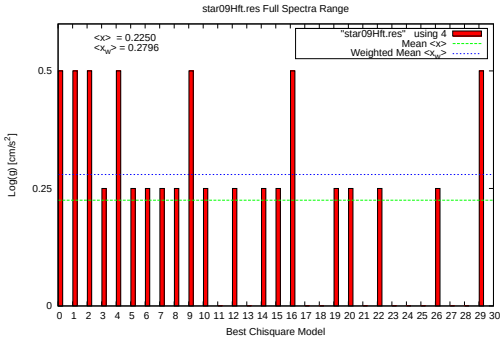

(c) H-band

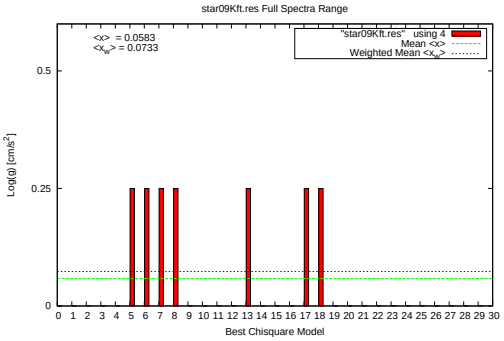

(d) K-band

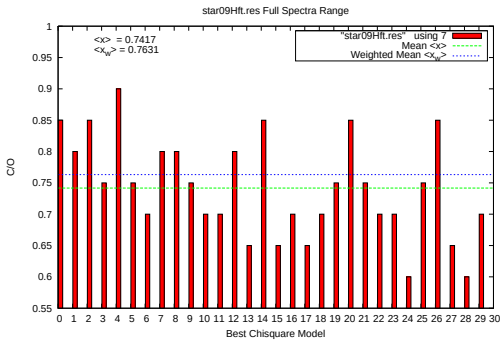

(e) H-band

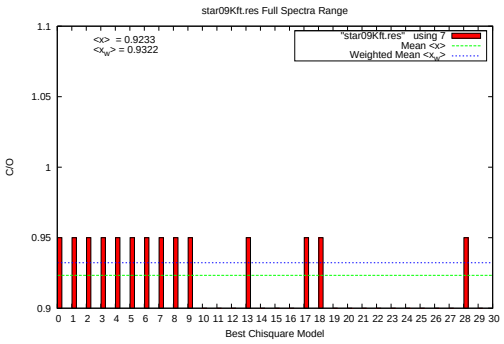

(f) K-band

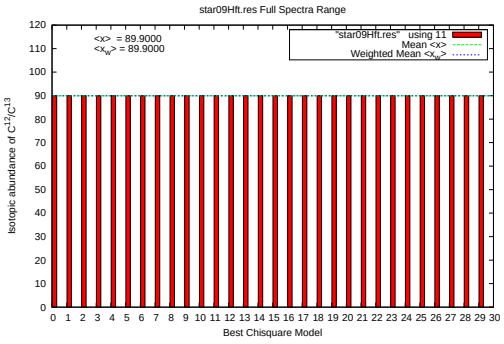

(g) H-band

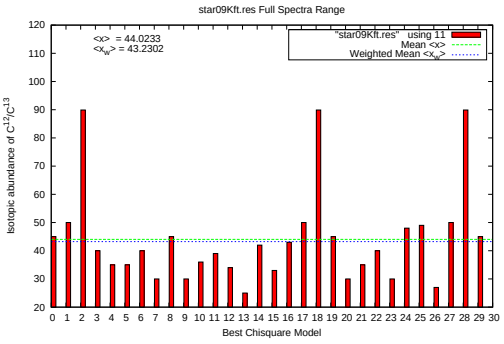

(h) K-band

Figure 6.23: Results of the full spectra of the 30 best models of star09.

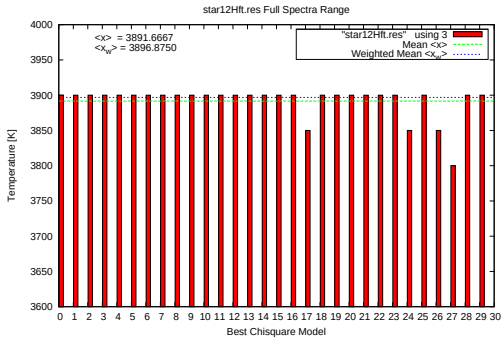

(a) H-band

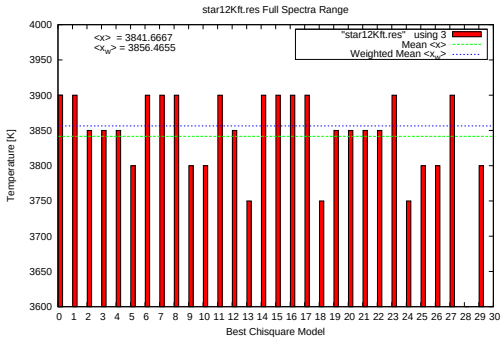

(b) K-band

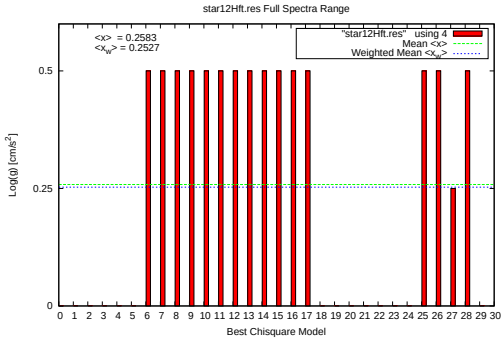

(c) H-band

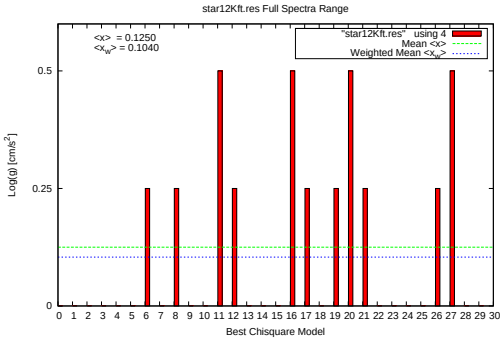

(d) K-band

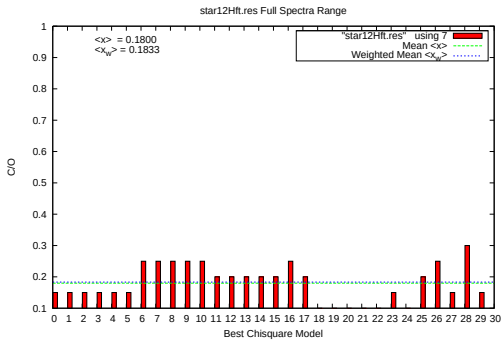

(e) H-band

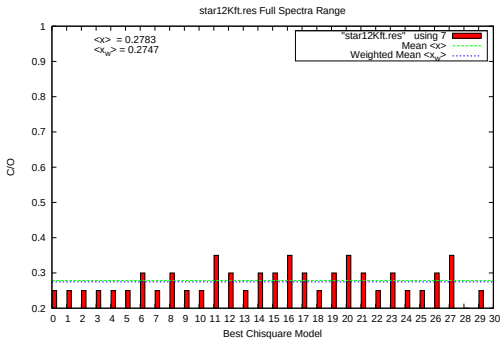

(f) K-band

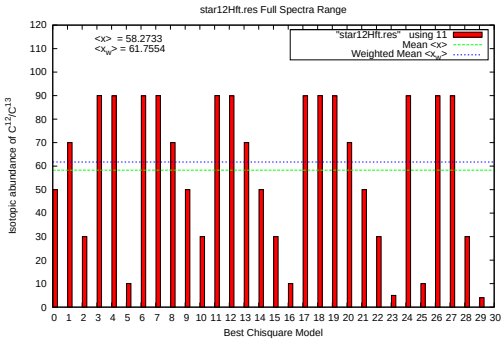

(g) H-band

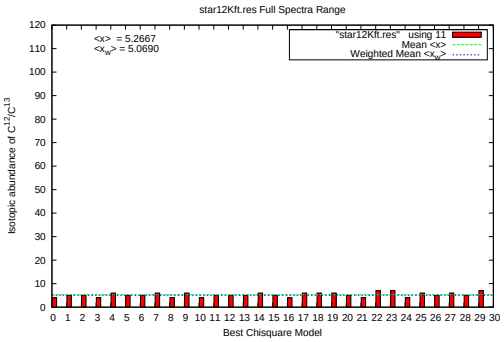

(h) K-band

Figure 6.24: Results of the full spectra of the 30 best models of star12.

6.3 Result tables

The result tables contain the best fitting parameters, the mean, the weighted mean, and the final mean which is calculated by the mean of the former three methods. See in Chapter 4.9 - *Parameter and abundance determination* for the detailed description.

The result tables are shown for each the H-band and the K-band one upon the other to gain a better comparison of the bands. The data from star02 in the K-band was too bad to be analysed and therefore it is missing in the result tables. No error is given in the result tables until now, because the errors are given in the final result tables, where only the *Final Mean* is shown.

star02Hft.res	T [K]	Log(g)	C/O	$^{12}C/^{13}C$
Best Fit:	3800	0.5	0.48	30
Mean:	3776.667	0.500	0.461	53.333
wMean:	3783.621	0.500	0.463	54.914
Final Mean:	3786.762	0.500	0.468	46.082
star04Hft.res	T [K]	Log(g)	C/O	$^{12}C/^{13}C$
Best Fit:	3700	0.5	0.35	89.9
Mean:	3741.667	0.417	0.370	73.960
wMean:	3742.888	0.446	0.372	75.353
Final Mean:	3728.185	0.454	0.364	79.738
star04Kft.res	T [K]	Log(g)	C/O	$^{12}C/^{13}C$
Best Fit:	3650	0	0.75	50
Mean:	3626.667	0.025	0.727	56.313
wMean:	3621.121	0.018	0.730	58.883
Final Mean:	3632.596	0.014	0.735	55.065
star05Hft.res	T [K]	Log(g)	C/O	$^{12}C/^{13}C$
Best Fit:	3800	0.5	0.35	30
Mean:	3785.000	0.433	0.322	62.637
wMean:	3788.147	0.447	0.316	62.394
Final Mean:	3791.049	0.460	0.329	51.677
star05Kft.res	T [K]	Log(g)	C/O	$^{12}C/^{13}C$
Best Fit:	3650	0	0.6	20
Mean:	3661.667	0.092	0.586	18.700
wMean:	3657.866	0.073	0.586	18.819
Final Mean:	3656.511	0.055	0.591	19.173
star06Hft.res	T [K]	Log(g)	C/O	$^{12}C/^{13}C$
Best Fit:	3850	0	0.15	89.9
Mean:	3873.333	0.383	0.267	55.250
wMean:	3877.263	0.307	0.245	68.347
Final Mean:	3866.865	0.230	0.221	71.166
star06Kft.res	T [K]	Log(g)	C/O	$^{12}C/^{13}C$
Best Fit:	3650	0	0.45	15
Mean:	3623.333	0.000	0.431	14.667
wMean:	3622.737	0.000	0.431	14.603
Final Mean:	3632.023	0.000	0.437	14.757

Table 6.1: Result tables of bandheads from star02 to star06.

star07Hft.res	T [K]	Log(g)	C/O	$^{12}C/^{13}C$
Best Fit:	3800	0.25	0.15	89.9
Mean:	3851.667	0.392	0.222	46.283
wMean:	3853.987	0.314	0.202	48.972
Final Mean:	3835.218	0.318	0.191	61.718
star07Kft.res	T [K]	Log(g)	C/O	$^{12}C/^{13}C$
Best Fit:	3600	0	0.35	8
Mean:	3646.667	0.000	0.332	7.833
wMean:	3639.009	0.000	0.327	7.737
Final Mean:	3628.558	0.000	0.336	7.857
star08Hft.res	T [K]	Log(g)	C/O	$^{12}C/^{13}C$
Best Fit:	3900	0	0.15	90
Mean:	3900.000	0.400	0.268	32.330
wMean:	3900.000	0.322	0.247	34.670
Final Mean:	3900.000	0.241	0.222	52.333
star08Kft.res	T [K]	Log(g)	C/O	$^{12}C/^{13}C$
Best Fit:	3650	0	0.3	14
Mean:	3683.333	0.000	0.305	14.400
wMean:	3674.461	0.000	0.302	14.300
Final Mean:	3669.265	0.000	0.302	14.233
star09Hft.res	T [K]	Log(g)	C/O	$^{12}C/^{13}C$
Best Fit:	3900	0	0.85	89.9
Mean:	3811.667	0.108	0.797	79.880
wMean:	3818.858	0.112	0.799	85.141
Final Mean:	3843.508	0.073	0.815	84.974
star09Kft.res	T [K]	Log(g)	C/O	$^{12}C/^{13}C$
Best Fit:	3450	0	1.1	35
Mean:	3565.000	0.000	1.065	36.097
wMean:	3565.086	0.000	1.066	34.562
Final Mean:	3526.695	0.000	1.077	35.220
star12Hft.res	T [K]	Log(g)	C/O	$^{12}C/^{13}C$
Best Fit:	3900	0.5	0.25	10
Mean:	3898.333	0.325	0.197	39.587
wMean:	3900.000	0.345	0.198	39.562
Final Mean:	3899.444	0.390	0.215	29.716
star12Kft.res	T [K]	Log(g)	C/O	$^{12}C/^{13}C$
Best Fit:	3600	0	0.25	5
Mean:	3661.667	0.008	0.275	5.600
wMean:	3649.138	0.002	0.273	5.504
Final Mean:	3636.935	0.003	0.266	5.368

Table 6.2: Result tables of bandheads from star07 to star12.

star02Hft.res	T [K]	Log(g)	C/O	$^{12}C/^{13}C$
Best Fit:	3750	0.5	0.45	90
Mean:	3766.667	0.500	0.463	61.993
wMean:	3768.211	0.500	0.463	69.693
Final Mean:	3761.626	0.500	0.459	73.895
star04Hft.res	T [K]	Log(g)	C/O	$^{12}C/^{13}C$
Best Fit:	3700	0.5	0.35	89.9
Mean:	3741.667	0.417	0.370	73.960
wMean:	3742.888	0.446	0.372	75.353
Final Mean:	3728.185	0.454	0.364	79.738
star04Kft.res	T [K]	Log(g)	C/O	$^{12}C/^{13}C$
Best Fit:	3850	0.25	0.8	35
Mean:	3770.000	0.283	0.773	37.500
wMean:	3790.086	0.267	0.773	36.304
Final Mean:	3803.362	0.267	0.782	36.268
star05Hft.res	T [K]	Log(g)	C/O	$^{12}C/^{13}C$
Best Fit:	3800	0.5	0.3	90
Mean:	3783.333	0.392	0.305	71.963
wMean:	3779.741	0.441	0.306	69.244
Final Mean:	3787.692	0.444	0.304	77.069
star05Kft.res	T [K]	Log(g)	C/O	$^{12}C/^{13}C$
Best Fit:	3650	0	0.5	14
Mean:	3631.667	0.033	0.478	13.433
wMean:	3631.358	0.017	0.479	13.491
Final Mean:	3637.675	0.017	0.486	13.642
star06Hft.res	T [K]	Log(g)	C/O	$^{12}C/^{13}C$
Best Fit:	3700	0.5	0.2	89.9
Mean:	3775.000	0.392	0.227	69.453
wMean:	3769.504	0.364	0.215	78.950
Final Mean:	3748.168	0.419	0.214	79.434
star06Kft.res	T [K]	Log(g)	C/O	$^{12}C/^{13}C$
Best Fit:	3450	0.25	0.4	15
Mean:	3625.000	0.050	0.425	14.900
wMean:	3617.780	0.034	0.418	14.810
Final Mean:	3564.260	0.111	0.414	14.903

Table 6.3: Result tables of full spectra range from star02 to star06.

star07Hft.res	T [K]	Log(g)	C/O	$^{12}C/^{13}C$
Best Fit:	3800	0.25	0.15	89.9
Mean:	3846.667	0.192	0.147	69.863
wMean:	3846.228	0.127	0.140	73.213
Final Mean:	3830.965	0.189	0.146	77.659
star07Kft.res	T [K]	Log(g)	C/O	$^{12}C/^{13}C$
Best Fit:	3800	0	0.35	7
Mean:	3750.000	0.000	0.343	7.767
wMean:	3773.491	0.000	0.348	7.638
Final Mean:	3774.497	0.000	0.347	7.468
star08Hft.res	T [K]	Log(g)	C/O	$^{12}C/^{13}C$
Best Fit:	3800	0.25	0.15	89.9
Mean:	3833.333	0.325	0.207	55.760
wMean:	3838.578	0.244	0.188	66.594
Final Mean:	3823.970	0.273	0.182	70.751
star08Kft.res	T [K]	Log(g)	C/O	$^{12}C/^{13}C$
Best Fit:	3450	0	0.25	10
Mean:	3833.333	0.133	0.282	9.800
wMean:	3814.440	0.089	0.270	9.668
Final Mean:	3699.258	0.074	0.267	9.823
star09Hft.res	T [K]	Log(g)	C/O	$^{12}C/^{13}C$
Best Fit:	3700	0.5	0.85	89.9
Mean:	3723.333	0.225	0.742	89.900
wMean:	3716.487	0.280	0.763	89.900
Final Mean:	3713.273	0.335	0.785	89.900
star09Kft.res	T [K]	Log(g)	C/O	$^{12}C/^{13}C$
Best Fit:	3650	0	0.95	45
Mean:	3625.000	0.058	0.923	44.023
wMean:	3634.159	0.073	0.932	43.230
Final Mean:	3636.386	0.044	0.935	44.085
star12Hft.res	T [K]	Log(g)	C/O	$^{12}C/^{13}C$
Best Fit:	3900	0	0.15	50
Mean:	3891.667	0.258	0.180	58.273
wMean:	3896.875	0.253	0.183	61.755
Final Mean:	3896.181	0.170	0.171	56.676
star12Kft.res	T [K]	Log(g)	C/O	$^{12}C/^{13}C$
Best Fit:	3900	0	0.25	4
Mean:	3841.667	0.125	0.278	5.267
wMean:	3856.466	0.104	0.275	5.069
Final Mean:	3866.044	0.076	0.268	4.779

Table 6.4: Result tables of full spectra range from star07 to star12.

6.4 Final result tables

In the final result tables only the *Final Mean* is shown for the H-band and the K-band.

6.4.1 Bandheads

	T [K]	Log(g)	C/O	$^{12}C/^{13}C$
star02Hft.res	3787	0.50	0.47	46
star04Hft.res	3728	0.45	0.36	80
star04Kft.res	3633	0.01	0.74	55
star05Hft.res	3791	0.46	0.33	52
star05Kft.res	3657	0.06	0.59	19
star06Hft.res	3867	0.23	0.22	71
star06Kft.res	3632	0.00	0.44	15
star07Hft.res	3835	0.32	0.19	62
star07Kft.res	3629	0.00	0.34	8
star08Hft.res	3900	0.24	0.22	52
star08Kft.res	3669	0.00	0.30	14
star09Hft.res	3844	0.07	0.82	85
star09Kft.res	3527	0.00	1.08	35
star12Hft.res	3899	0.39	0.22	30
star12Kft.res	3637	0.01	0.27	5
Error	± 50 K	± 0.25	± 0.05	± 1

Table 6.5: The *Final Mean* results of the bandheads.

6.4.2 Full spectra

	T [K]	Log(g)	C/O	$^{12}C/^{13}C$
star02Hft.res	3762	0.50	0.46	74
star04Hft.res	3728	0.45	0.36	80
star04Kft.res	3803	0.27	0.78	36
star05Hft.res	3788	0.44	0.30	77
star05Kft.res	3638	0.02	0.49	14
star06Hft.res	3748	0.42	0.21	79
star06Kft.res	3564	0.11	0.41	15
star07Hft.res	3831	0.19	0.15	78
star07Kft.res	3774	0.00	0.35	7
star08Hft.res	3824	0.27	0.18	71
star08Kft.res	3699	0.07	0.27	10
star09Hft.res	3713	0.34	0.79	90
star09Kft.res	3636	0.04	0.94	44
star12Hft.res	3896	0.17	0.17	57
star12Kft.res	3866	0.08	0.27	5
Error	± 50 K	± 0.25	± 0.05	± 1

Table 6.6: The final results of the full spectra.

6.4.3 Difference

In Table 6.7 the difference between the full spectra and the bandheads is shown. The values of the full spectra were subtracted with the values from the bandheads. In the most cases the values of the differences are smaller than the given error.

	T [K]	Log(g)	C/O	$^{12}C/^{13}C$
star02Hft.res	-25	0.00	-0.01	28
star04Hft.res	0	0.00	0.00	0
star04Kft.res	171	0.25	0.05	-19
star05Hft.res	-3	-0.02	-0.03	25
star05Kft.res	-19	-0.04	-0.11	-6
star06Hft.res	-119	0.19	-0.01	8
star06Kft.res	-68	0.11	-0.02	0
star07Hft.res	-4	-0.13	-0.05	16
star07Kft.res	146	0.00	0.01	0
star08Hft.res	-76	0.03	-0.04	18
star08KHft.res	30	0.07	-0.03	-4
star09Hft.res	-130	0.26	-0.03	5
star09Kft.res	110	0.04	-0.14	9
star12Hft.res	-3	-0.22	-0.04	27
star12Kft.res	229	0.07	0.00	-1
Error	$\pm$ 50 K	$\pm$ 0.25	$\pm$ 0.05	$\pm$ 1

Table 6.7: Difference between bandheads and the full spectra. Note that many values are smaller than the given error.

6.4.4 Mean between bandheads and fullspectra

	T [K]	Log(g)	C/O	$^{12}C/^{13}C$
star02Hft.res	3774	0.50	0.46	60
star04Hft.res	3728	0.45	0.36	80
star04Kft.res	3718	0.14	0.76	46
star05Hft.res	3789	0.45	0.32	64
star05Kft.res	3647	0.04	0.54	16
star06Hft.res	3808	0.32	0.22	75
star06Kft.res	3598	0.06	0.43	15
star07Hft.res	3833	0.25	0.17	70
star07Kft.res	3702	0.00	0.34	8
star08Hft.res	3862	0.26	0.20	62
star08Kft.res	3684	0.04	0.28	12
star09Hft.res	3778	0.20	0.80	87
star09Kft.res	3582	0.02	1.01	40
star12Hft.res	3898	0.28	0.19	43
star12Kft.res	3751	0.04	0.27	5
Error	± 50 K	± 0.25	± 0.05	± 1

Table 6.8: The mean between bandheads and the full spectra.

6.5 C/O versus $^{12}C/^{13}C$

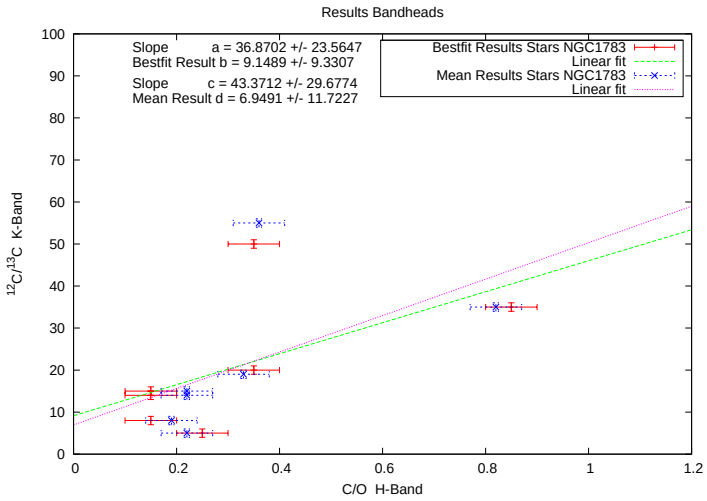

(a) Bandheads

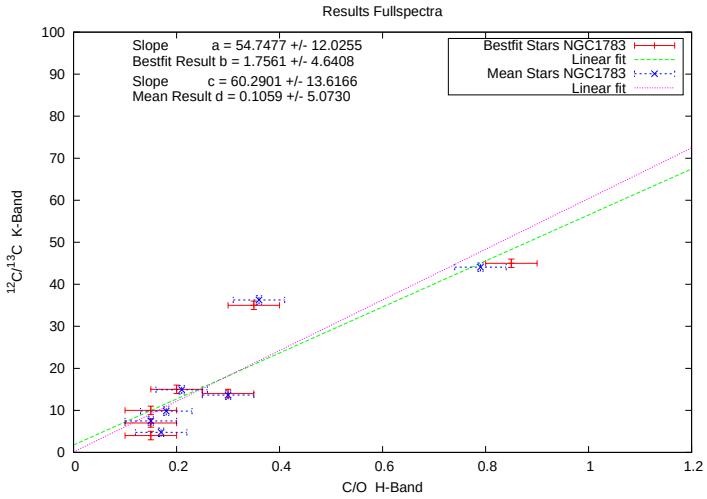

(b) Fullspectra range

Figure 6.25: Here, the "best fit" and the "final mean" results of the bandheads and the full spectra for the C/O-ratio versus the isotopic abundance of $^{12}C/^{13}C$ of the AGB-stars in NGC 1783 are shown. The C/O-ratio values were taken only from the H-band and the IACO values were taken only from the K-band. Note that the slope of the final-mean values is slightly higher than the best-fit values.

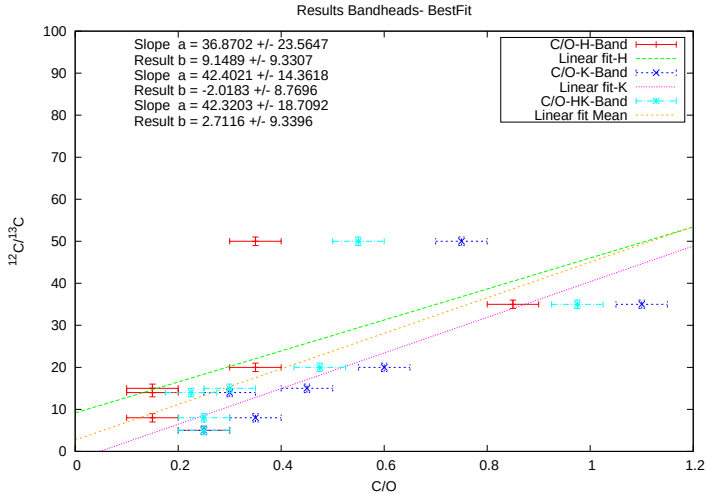

(a) Bandheads

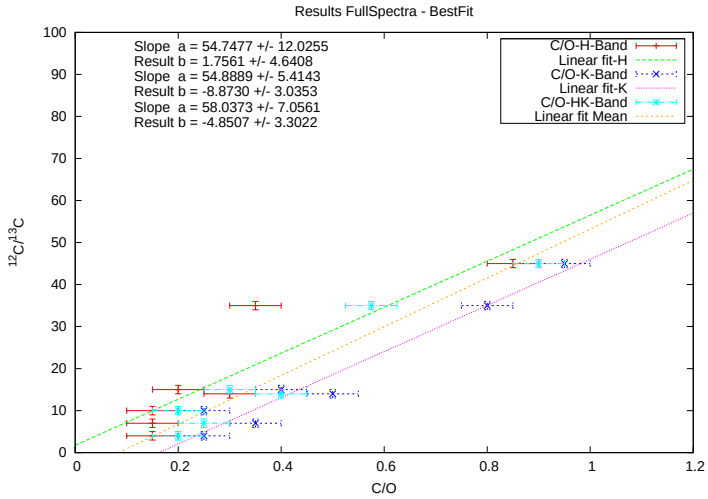

(b) Fullspectra range

Figure 6.26: Here only the "best fit" results of the bandheads and the full spectra for the C/O-ratio versus the isotopic abundance of $^{12}C/^{13}C$ of the AGB-stars in NGC 1783 are shown. Red crosses and green fit: the C/O-ratio was taken from the H-band. Blue crosses and red fit: the C/O-ratio was taken experimental from the K-band, which is shifted nearly parallel. (Normally the C/O ratio is taken only from the H-band.) The IACO was taken only from the K-band in both cases. The orange fit is the mean of both H- and K-band

	Best Fit		Final Mean	
Star	C/O H-band	$^{12}C/^{13}C$ K-band	C/O H-band	$^{12}C/^{13}C$ K-band
Star07	0.15	8	0.19	8
Star06	0.15	15	0.22	15
Star08	0.15	14	0.22	14
Star12	0.25	5	0.22	5
Star05	0.35	20	0.33	19
Star04	0.35	50	0.36	55
Star02	0.48	-	0.47	-
Star09	0.85	35	0.82	35

Table 6.9: Results listed with ascending C/O-ratios from the bandheads.

	Best Fit		Final Mean	
Star	C/O H-band	$^{12}C/^{13}C$ K-band	C/O H-band	$^{12}C/^{13}C$ K-band
Star07	0.15	7	0.15	7
Star08	0.15	10	0.18	10
Star12	0.15	4	0.17	5
Star06	0.2	15	0.21	15
Star05	0.3	14	0.30	14
Star04	0.35	35	0.36	36
Star02	0.45	-	0.46	-
Star09	0.85	45	0.79	44

Table 6.10: Results listed with ascending C/O-ratios from the full spectra.

6.6 Measuring individual bandheads

Since the K-band is very sensitive to the isotopic abundances of $^{12}C/^{13}C$, a permutation of the bandheads for the chi-square fit to find out which bandheads are more sensitive to the isotopic ratios, but also to the temperature, log(g) and the C/O-ratio was done. Representative results are shown for star05 in the K-band.

Number	Bandhead	Lower limit [Å]	Upper limit [Å]	Sum [Å]
1	^{12}CO 2-0 head	22951.762	22988.084	36.322
2	^{12}CO 3-1 head	23243.546	23272.604	29.058
3	^{13}CO 2-0 head	23465.109	23483.270	18.161
4	^{12}CO 4-2 head	23542.595	23566.810	24.215
5	^{13}CO 3-1 head	23758.104	23783.529	25.425

Table 6.11: Included ranges in the K-band. Total: 133.181 Å.

6.6.1 Single bandheads K-band

For each chi-square fit only one of the five bandheads of Table 6.11 was taken into account. The five results were named from bandhead 1 to bandhead 5.

6.6.2 Combination of bandheads K-band

Combination 1 consists of bandhead 1 and bandhead 3. These are the ^{12}CO 2-0 head and the ^{13}CO 2-0 head. Combination 2 consists of bandhead 2 and bandhead 5 (Table 6.11). These are the ^{12}CO 3-1 head and the ^{13}CO 3-1 head.

6.6.3 Single bandheads H-band

In the H-band there are much more bandheads. The candidates according to Table 6.12 would be: the CO-bandheads 1, 4, 5, 8, 11 and the OH-bandheads 2, 3, 6, 7, 9, 10.

6.6.4 Combination of bandheads H-band

Combination 1 consists of the CO-bandheads 1, 5, 8, 11.
Combination 2 consists of the OH-bandheads 2, 3, 6, 7, 9, 10.
Combination 3 consists of the bandheads 2, 7.

Number	Bandhead	Lower limit [Å]	Upper limit [Å]	Sum [Å]
1	^{12}CO 4-1 head	15780.62	15810.92	-30.31
2	OH 2-0 P1e 13.5 OH 2-0 P1f 13.5 OH 2-0 P2f 12.5	15900	15916	-16
3	OH 3-1 P1e 8.5 OH 3-1 P1f 8.5	15926	15932	-6
4	^{13}C^{12}O, Fe, V	15938	15946	-8
5	^{12}CO 5-2 head	15992.76	16006.32	-13.56
6	OH 3-1 P2e 8.5 OH 3-1 P2f 8.5	16052	16061	-9
7	OH 2-0 P2e 13.5 OH 2-0 P2f 13.5	16077.29	16083	-5.71
8	CO 6-3 head	16200.91	16228.83	-27.91
9	OH 3-1 P2e 10.5 OH 3-1 P2f 10.5 OH 4-2 P1e 5.5 OH 4-2 P1f 5.5	16340	16345	-5
10	OH 3-1 P2f 10.5 OH 3-1 P2e 10.5 OH 4 -2 P1e 5.5 OH 4-2 P1f 5.5	16363.61	16377.96	-14.35
11	Fe + ^{12}CO 7-4 head	16412	16432	-20

Table 6.12: Included ranges in the H-band. Total: 154.844 Å. The bandheads are numbered from bandhead 1 to bandhead 11. The synthetic spectra in the range of bandhead 4 is very ^{12}C/^{13}C sensitive.

Combination 4 consists of the bandheads 3, 6.
Combination 5 consists of the bandheads 9, 10 (see Table 6.12).

6.6.5 Result tables

Bandhead1.res	T [K]	Log(g)	C/O	$^{12}C/^{13}C$
Best Fit:	3900	0	0.6	89.9
Mean:	3866.667	0.167	0.673	67.673
wMean:	3876.078	0.147	0.661	76.404
Final Mean:	3880.915	0.105	0.645	77.993
Bandhead2.res	T [K]	Log(g)	C/O	$^{12}C/^{13}C$
Best Fit:	3650	0	0.55	4
Mean:	3711.667	0.000	0.499	43.277
wMean:	3729.634	0.000	0.502	51.058
Final Mean:	3697.100	0.000	0.517	32.778
Bandhead3.res	T [K]	Log(g)	C/O	$^{12}C/^{13}C$
Best Fit:	3450	0	0.25	15
Mean:	3570.000	0.017	0.377	21.100
wMean:	3552.371	0.013	0.379	21.731
Final Mean:	3524.124	0.010	0.335	19.277
Bandhead4.res	T [K]	Log(g)	C/O	$^{12}C/^{13}C$
Best Fit:	3500	0	1.5	89.9
Mean:	3516.667	0.000	1.110	39.217
wMean:	3495.151	0.000	1.286	46.527
Final Mean:	3503.939	0.000	1.299	58.548
Bandhead5.res	T [K]	Log(g)	C/O	$^{12}C/^{13}C$
Best Fit:	3450	0	0.25	4
Mean:	3565.000	0.117	0.322	4.400
wMean:	3561.638	0.112	0.314	4.231
Final Mean:	3525.546	0.076	0.295	4.210

Table 6.13: Result table of individual bandheads K-band.

Combination1.res	T [K]	Log(g)	C/O	$^{12}C/^{13}C$
Best Fit:	3850	0	0.7	35
Mean:	3703.333	0.092	0.612	32.633
wMean:	3712.608	0.103	0.624	32.718
Final Mean:	3755.314	0.065	0.645	33.450
Combination2.res	T [K]	Log(g)	C/O	$^{12}C/^{13}C$
Best Fit:	3600	0	0.48	8
Mean:	3560.000	0.017	0.467	8.167
wMean:	3555.065	0.009	0.465	8.287
Final Mean:	3571.688	0.009	0.471	8.151

Table 6.14: Result table of combinations in the K-band.

Bandhead01.res	T [K]	Log(g)	C/O	$^{12}C/^{13}C$
Best Fit:	3550	0.5	0.1	89.9
Mean:	3560.000	0.417	0.374	77.943
wMean:	3542.134	0.453	0.396	78.526
Final Mean:	3550.711	0.457	0.290	82.123
Bandhead02.res	T [K]	Log(g)	C/O	$^{12}C/^{13}C$
Best Fit:	3900	0.5	0.48	15
Mean:	3840.000	0.442	0.550	38.983
wMean:	3862.177	0.461	0.533	36.428
Final Mean:	3867.392	0.468	0.521	30.137
Bandhead03.res	T [K]	Log(g)	C/O	$^{12}C/^{13}C$
Best Fit:	3850	0	0.9	89.9
Mean:	3771.667	0.333	0.656	77.267
wMean:	3768.211	0.301	0.691	78.377
Final Mean:	3796.626	0.211	0.749	81.848
Bandhead04.res	T [K]	Log(g)	C/O	$^{12}C/^{13}C$
Best Fit:	3900	0.5	0.2	1
Mean:	3820.000	0.392	0.276	2.600
wMean:	3831.681	0.402	0.274	2.330
Final Mean:	3850.560	0.431	0.250	1.977
Bandhead05.res	T [K]	Log(g)	C/O	$^{12}C/^{13}C$
Best Fit:	3600	0	1.2	89.9
Mean:	3783.333	0.467	0.610	36.890
wMean:	3777.802	0.436	0.671	32.064
Final Mean:	3720.378	0.301	0.827	52.951
Bandhead06.res	T [K]	Log(g)	C/O	$^{12}C/^{13}C$
Best Fit:	3700	0.5	0.15	89.9
Mean:	3650.000	0.500	0.133	42.973
wMean:	3643.534	0.500	0.117	41.998
Final Mean:	3664.511	0.500	0.134	58.291

Table 6.15: Result table of individual bandheads 1 to 6 in the H-band.

Bandhead07.res	T [K]	Log(g)	C/O	$^{12}C/^{13}C$
Best Fit:	3850	0.25	0.45	89.9
Mean:	3820.000	0.008	0.347	33.797
wMean:	3827.371	0.016	0.354	32.612
Final Mean:	3832.457	0.091	0.384	52.103
Bandhead08.res	T [K]	Log(g)	C/O	$^{12}C/^{13}C$
Best Fit:	3700	0.5	0.2	89.9
Mean:	3790.000	0.400	0.262	62.930
wMean:	3787.177	0.360	0.248	73.588
Final Mean:	3759.059	0.420	0.236	75.473
Bandhead09.res	T [K]	Log(g)	C/O	$^{12}C/^{13}C$
Best Fit:	3900	0.5	0.1	6
Mean:	3853.333	0.500	0.100	9.300
wMean:	3868.211	0.500	0.100	8.248
Final Mean:	3873.848	0.500	0.100	7.849
Bandhead10.res	T [K]	Log(g)	C/O	$^{12}C/^{13}C$
Best Fit:	3900	0.5	0.45	10
Mean:	3900.000	0.433	0.357	11.867
wMean:	3900.000	0.458	0.364	10.791
Final Mean:	3900.000	0.464	0.390	10.886
Bandhead11.res	T [K]	Log(g)	C/O	$^{12}C/^{13}C$
Best Fit:	3900	0.5	0.35	1
Mean:	3863.333	0.383	0.258	3.600
wMean:	3864.978	0.410	0.280	2.802
Final Mean:	3876.104	0.431	0.296	2.467

Table 6.16: Result table of individual bandheads 7 to 11 in the H-band.

Combination01.res	T [K]	Log(g)	C/O	$^{12}C/^{13}C$
Best Fit:	3750	0.5	0.3	90
Mean:	3768.333	0.383	0.337	68.627
wMean:	3772.953	0.414	0.338	68.073
Final Mean:	3763.762	0.432	0.325	75.567
Combination02.res	T [K]	Log(g)	C/O	$^{12}C/^{13}C$
Best Fit:	3900	0.5	0.48	89.9
Mean:	3851.667	0.450	0.398	67.470
wMean:	3859.375	0.469	0.411	67.309
Final Mean:	3870.347	0.473	0.429	74.893
Combination03.res	T [K]	Log(g)	C/O	$^{12}C/^{13}C$
Best Fit:	3900	0.5	0.48	15
Mean:	3830.000	0.425	0.551	43.547
wMean:	3853.017	0.443	0.541	45.526
Final Mean:	3861.006	0.456	0.524	34.691
Combination04.res	T [K]	Log(g)	C/O	$^{12}C/^{13}C$
Best Fit:	3750	0.5	0.35	10
Mean:	3768.333	0.500	0.367	40.000
wMean:	3764.009	0.500	0.354	34.914
Final Mean:	3760.781	0.500	0.357	28.305
Combination05.res	T [K]	Log(g)	C/O	$^{12}C/^{13}C$
Best Fit:	3900	0.5	0.2	15
Mean:	3900.000	0.500	0.217	19.900
wMean:	3900.000	0.500	0.213	18.601
Final Mean:	3900.000	0.500	0.210	17.834

Table 6.17: Result table of combinations in the H-band.

6.6.6 Final results tables

	T [K]	Log(g)	C/O	$^{12}C/^{13}C$
Star05Hft.res	3791	0.46	0.33	52
Bandhead01.res	3551	0.46	0.29	82
Bandhead02.res	3867	0.47	0.52	30
Bandhead03.res	3797	0.21	0.75	82
Bandhead04.res	3851	0.43	0.25	2
Bandhead05.res	3720	0.30	0.83	53
Bandhead06.res	3665	0.50	0.13	58
Bandhead07.res	3832	0.09	0.38	52
Bandhead08.res	3759	0.42	0.24	75
Bandhead09.res	3874	0.50	0.10	8
Bandhead10.res	3900	0.46	0.39	11
Bandhead11.res	3876	0.43	0.30	2
Combination01.res	3764	0.43	0.33	76
Combination02.res	3870	0.47	0.43	75
Combination03.res	3861	0.46	0.52	35
Combination04.res	3761	0.50	0.36	28
Combination05.res	3900	0.50	0.21	18
Error	± 50 K	± 0.25	± 0.05	± 1

Table 6.18: Final result table of individual bandheads in the H-band. Note that the isotopic abundances of $^{12}C/^{13}C$-ratio was taken from the K-band and has in the H-band experimental status because of only one single ^{13}CO feature in bandhead 4.

	T [K]	Log(g)	C/O	$^{12}C/^{13}C$
Star05Kft.res	3657	0.06	0.59	19
Bandhead01.res	3881	0.11	0.65	78
Bandhead02.res	3697	0.00	0.52	33
Bandhead03.res	3524	0.01	0.34	19
Bandhead04.res	3504	0.00	1.30	59
Bandhead05.res	3526	0.08	0.30	4
Combination01.res	3755	0.07	0.65	33
Combination02.res	3572	0.01	0.47	8
Error	± 50 K	± 0.25	± 0.05	± 1

Table 6.19: Final result table of individual bandheads in the K-band. Note that the C/O-ratio was taken from the H-band and has in the K-band experimental status. Combination 1 consists of bandheads 1 and 3, combination 2 consists of bandheads 2 and 5.

6.6.7 Results of parameters of individual bandheads K-band

In the following Figures, as in Chapter 6.2 - *Result diagrams of parameters* the result diagrams of the 30 best fitting physical parameters of the individual bandheads are shown. As mentioned in Chapter 4 - Section *A Gnuplot visualisation problem*, the best fit in the plots is shown at number zero. The diagrams of the chi-square values, the physical parameters of the temperature, the log(g), the C/O-ratio, and the IACO-ratio are shown all together, to obtain a direct comparison.

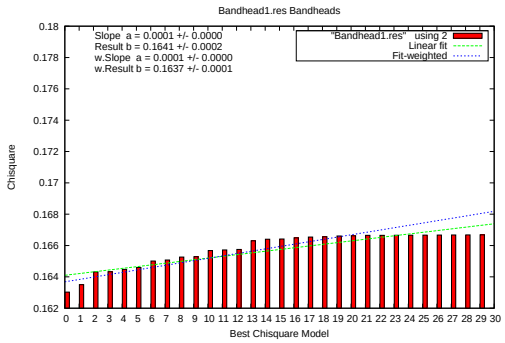

(a) ^{12}CO 2-0 head

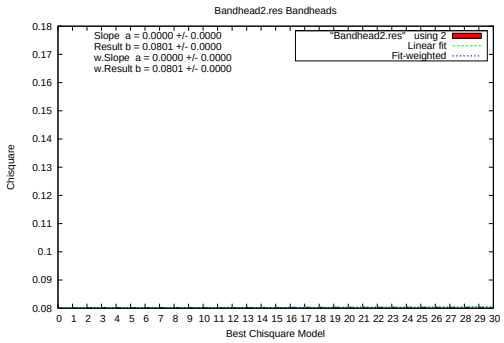

(b) ^{12}CO 3-1 head

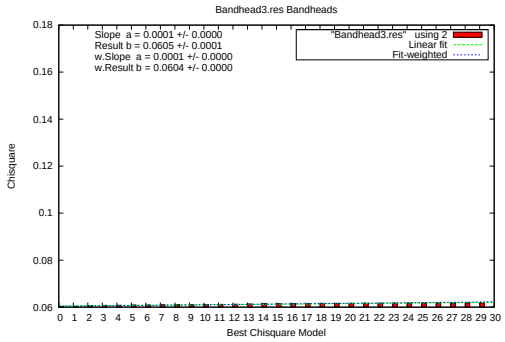

(c) ^{13}CO 2-0 head

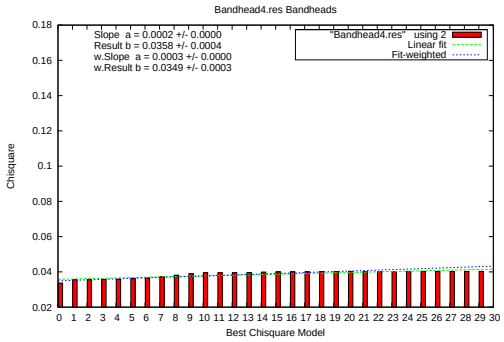

(d) ^{12}CO 4-2 head

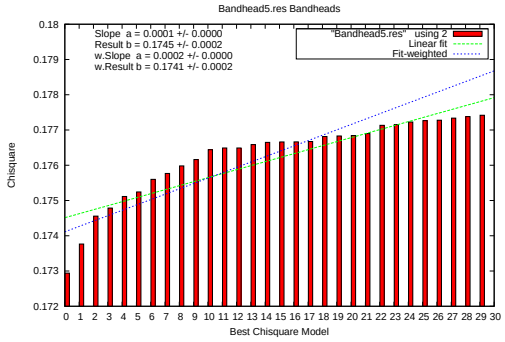

(e) ^{13}CO 3-1 head

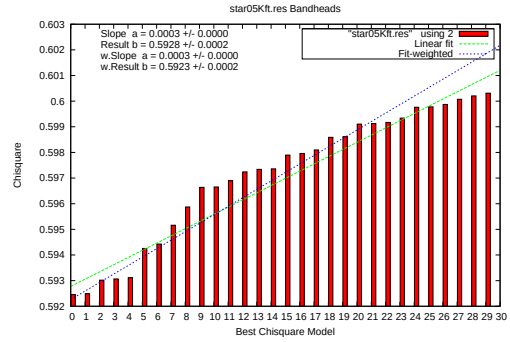

(f) K-band all bandheads

Figure 6.27: Results of individual bandheads in the K-band of star05 of the best 30 chi-squares. On the lower right the result of all included bandheads is shown, where the chi-square has a value of 0.6 instead of the 0.18 limit of the plots of the single bandheads.

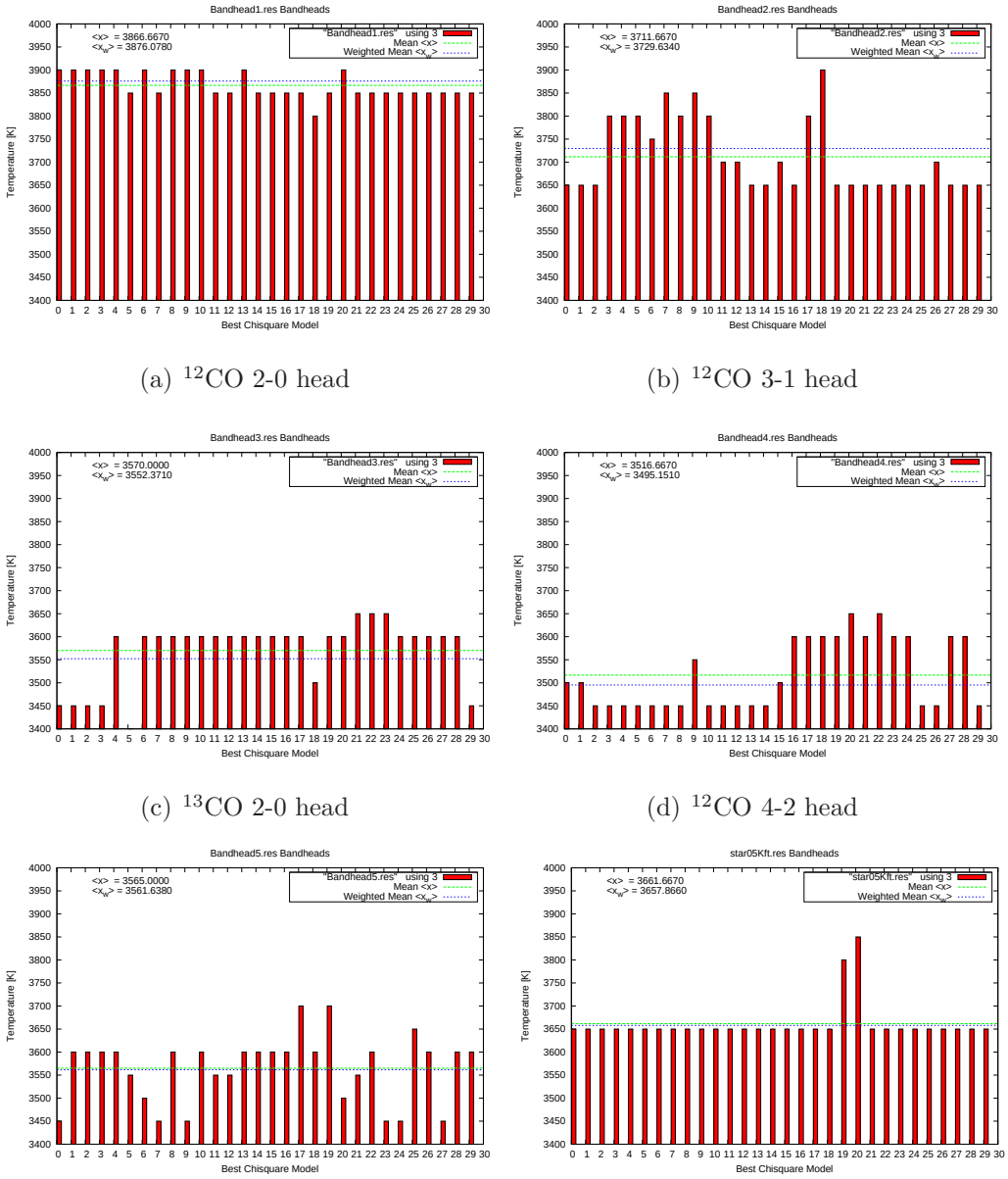

(a) ^{12}CO 2-0 head

(b) ^{12}CO 3-1 head

(c) ^{13}CO 2-0 head

(d) ^{12}CO 4-2 head

(e) ^{13}CO 3-1 head

(f) K-band all bandheads

Figure 6.28: Results of individual bandheads in the K-band of star05 of the best 30 temperatures. Note the temperature of all bandheads in subfigure (f).

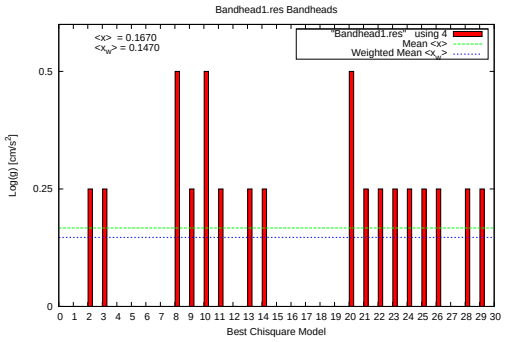

(a) ^{12}CO 2-0 head

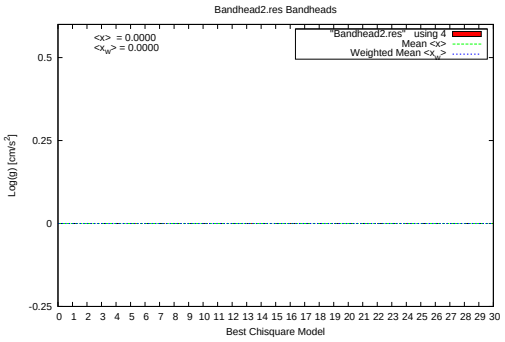

(b) ^{12}CO 3-1 head

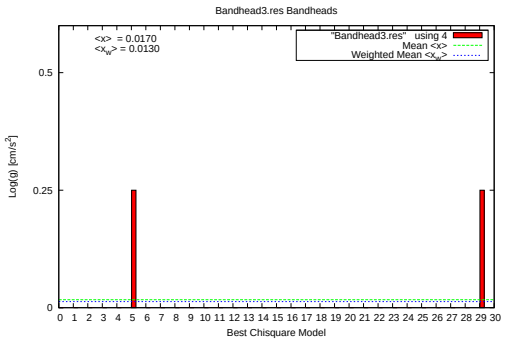

(c) ^{13}CO 2-0 head

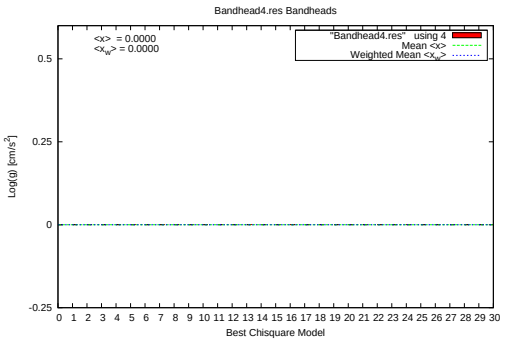

(d) ^{12}CO 4-2 head

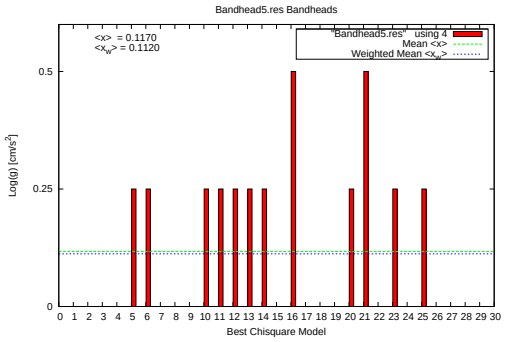

(e) ^{13}CO 3-1 head

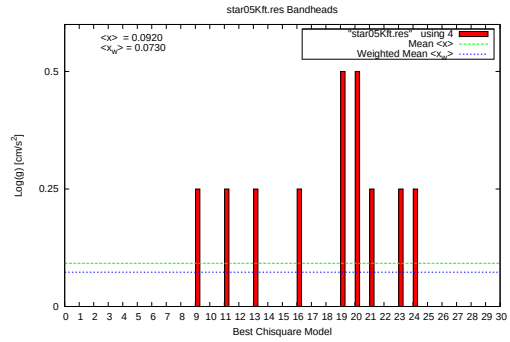

(f) K-band all bandheads

Figure 6.29: Results of individual bandheads in the K-band of star05 of the best 30 log(g). On the lower right the result of all included bandheads is shown in subfigure (f).

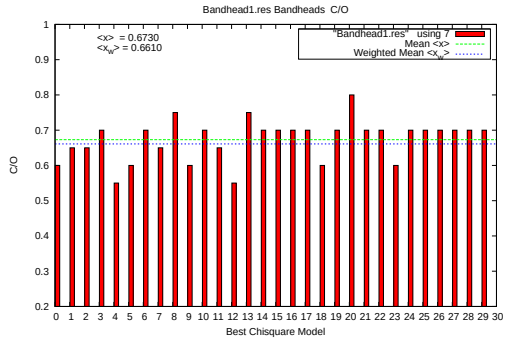

(a) ^{12}CO 2-0 head

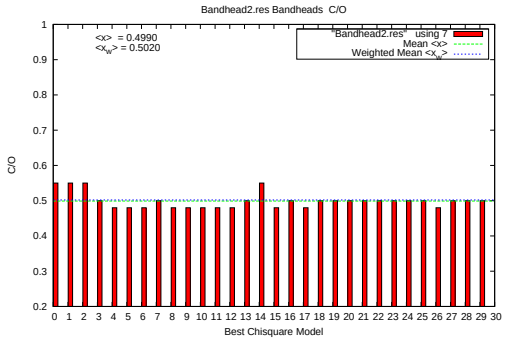

(b) ^{12}CO 3-1 head

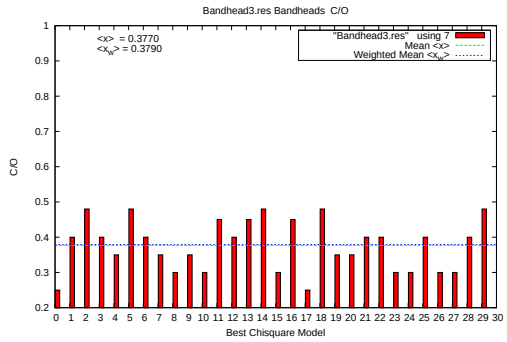

(c) ^{13}CO 2-0 head

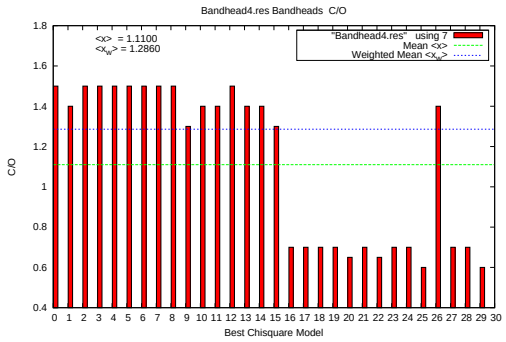

(d) ^{12}CO 4-2 head

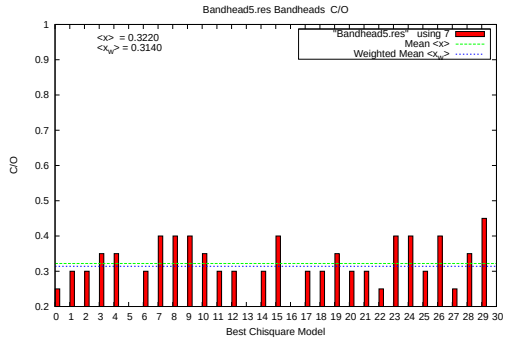

(e) ^{13}CO 3-1 head

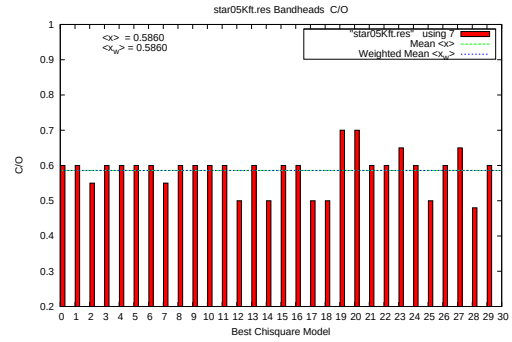

(f) K-band all bandheads

Figure 6.30: Results of individual bandheads in the K-band of star05 of the best 30 C/O-ratios. On the lower right the result of all included bandheads is shown. Note in subfigure (d) the rising of the C/O-ratio to a value of 1.5.

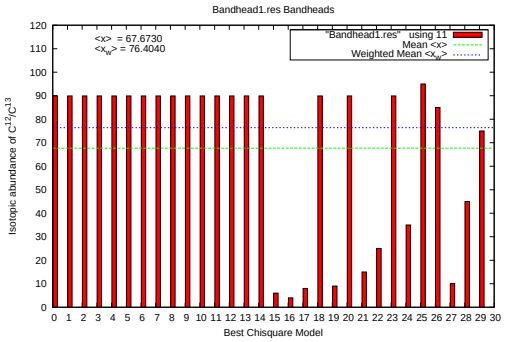

(a) ^{12}CO 2-0 head

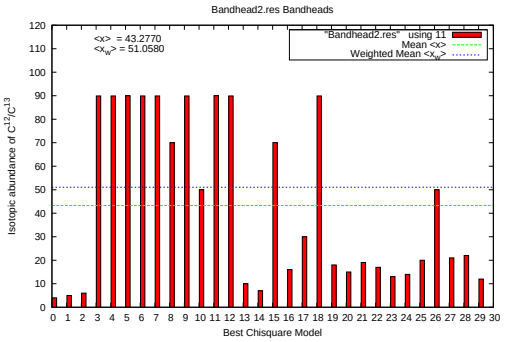

(b) ^{12}CO 3-1 head

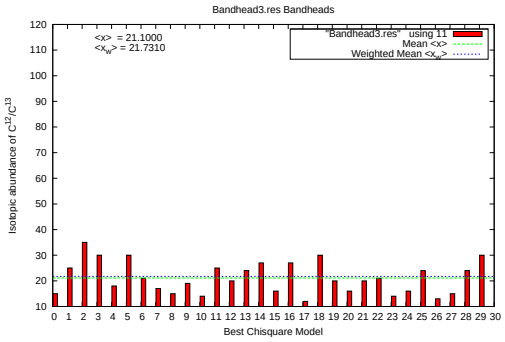

(c) ^{13}CO 2-0 head

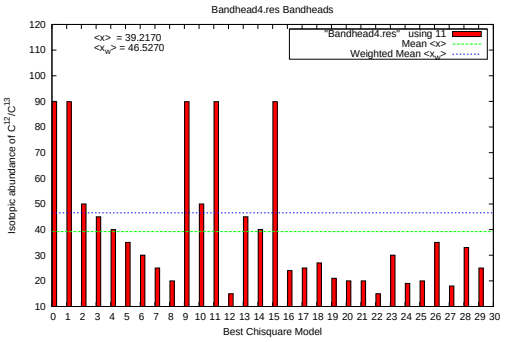

(d) ^{12}CO 4-2 head

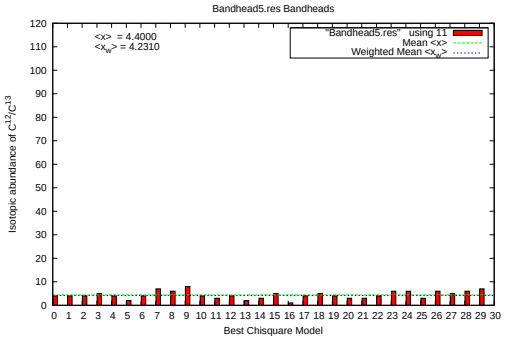

(e) ^{13}CO 3-1 head

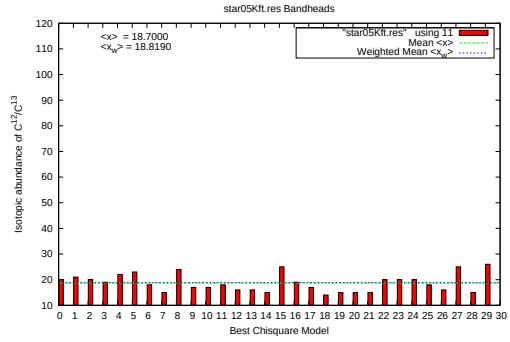

(f) K-band all bandheads

Figure 6.31: Results of individual bandheads in the K-band of star05 of the best 30 isotopic abundances of ^{12}C/^{13}C. On the lower right the result of all included bandheads is shown. Note that the bandheads in subfigure (c) and (e) seem to affect the result of all bandheads included in subfigure (f) much.

6.6.8 Results of combinations of bandheads K-band

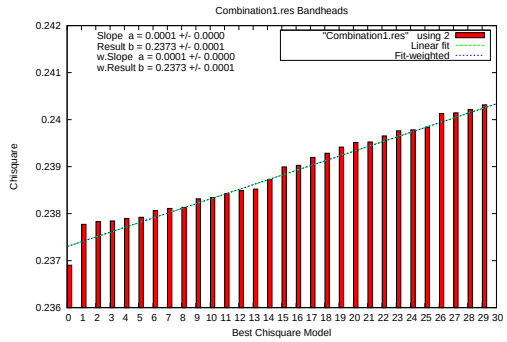

(a) chi-square

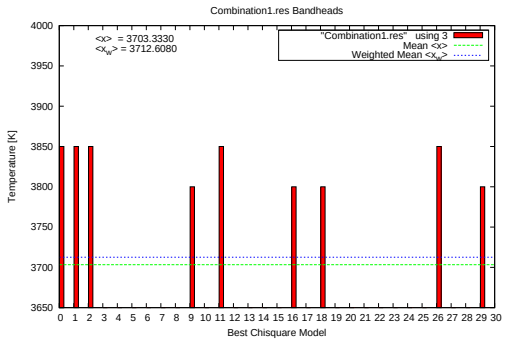

(b) temperature

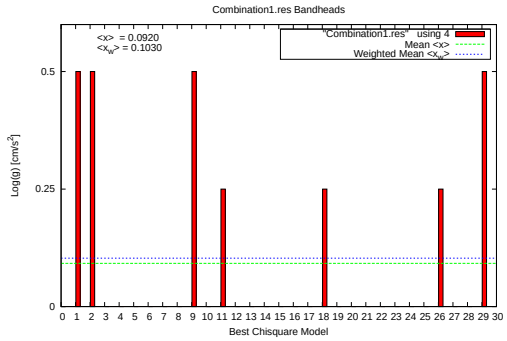

(c) Log(g)

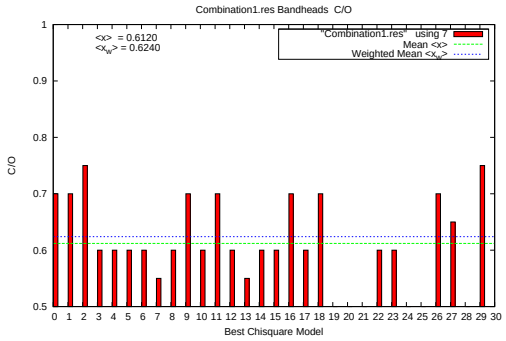

(d) C/O

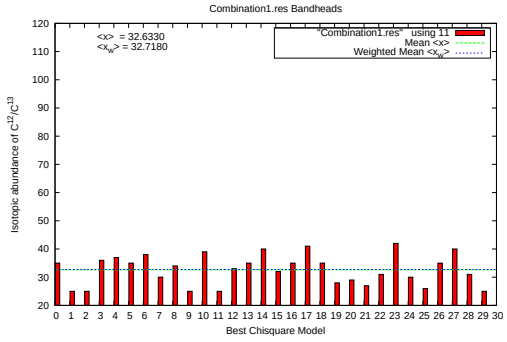

(e) $^{12}C/^{13}C$

Figure 6.32: Results of combination 1 (^{12}CO 2-0 head and ^{13}CO 2-0 head) of the K-band bandheads of star05 of the best 30 fits. Compare these figures with Fig. 6.9.

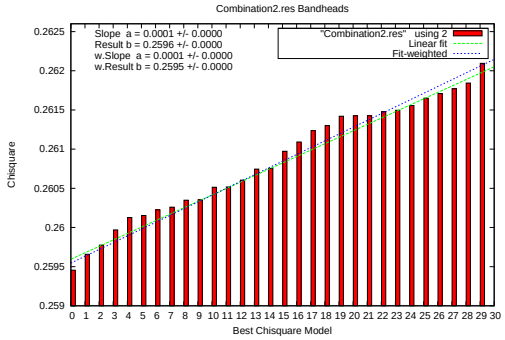

(a) chi-square

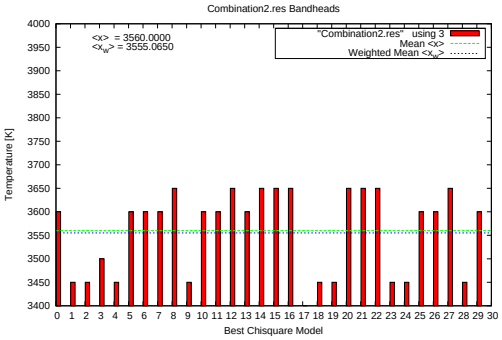

(b) temperature

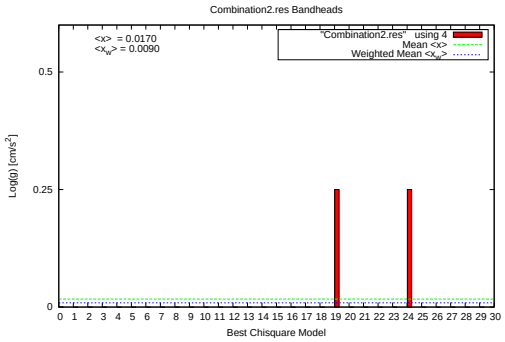

(c) Log(g)

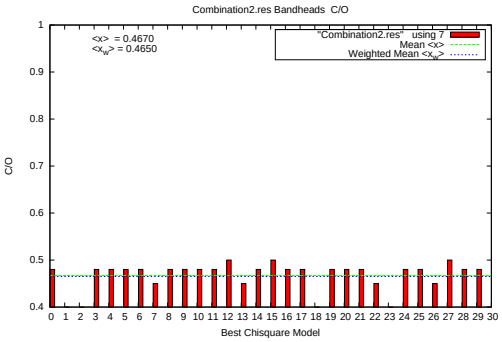

(d) C/O

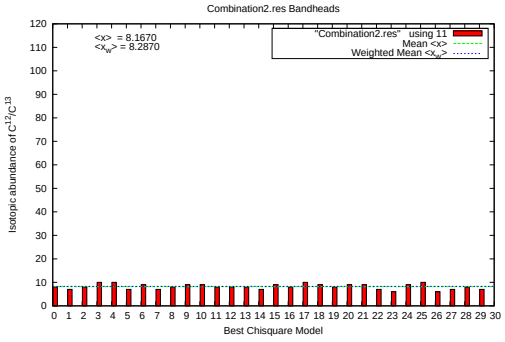

(e) $^{12}C/^{13}C$

Figure 6.33: Results of combination 2 (^{12}CO 3-1 head and ^{13}CO 3-1 head) of the K-band bandheads of star05 of the best 30 fits. Compare these figures with Fig. 6.9.

6.6.9 Results of parameters of individual bandheads H-band

In the following Figures, as in Chapter 6.2 - *Result diagrams of parameters* the result diagrams of the 30 best fitting physical parameters of the individual bandheads in the H-band are shown. As mentioned in Chapter 4 - Section *A Gnuplot visualisation problem*, the best fit in the plots is shown at number zero. The diagrams of the chi-square values, the physical parameters of the temperature, the log(g), the C/O-ratio, and the IACO-ratio are shown all together, to obtain a direct comparison.

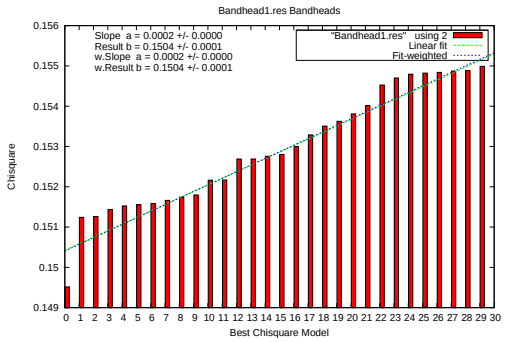

(a) ^{12}CO 4-1 head

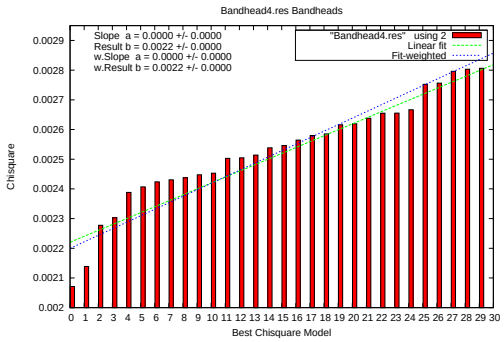

(b) V, Fe,^{13}C^{12}O

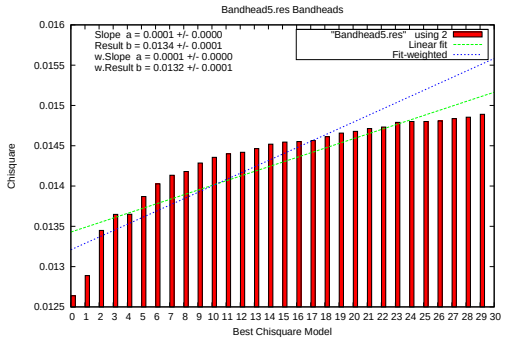

(c) ^{12}CO 5-2 head

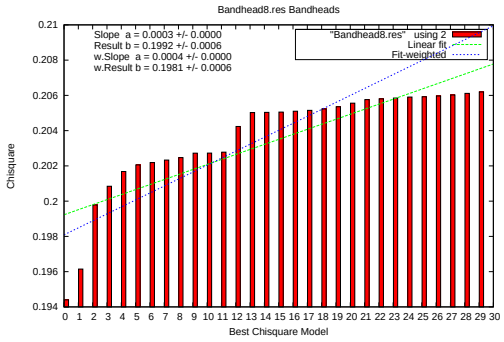

(d) CO 6-3 head

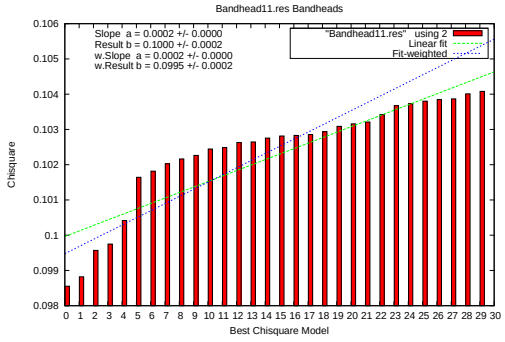

(e) Fe + ^{12}CO 7-4 head

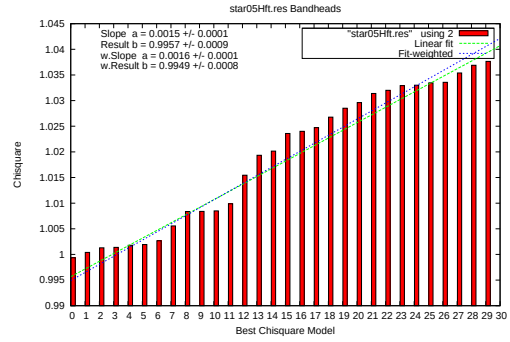

(f) H-band all bandheads

Figure 6.34: Results of individual bandheads in the H-band of star05 of the best 30 chisquares. Note the chi-square of all bandheads in subfigure (f).

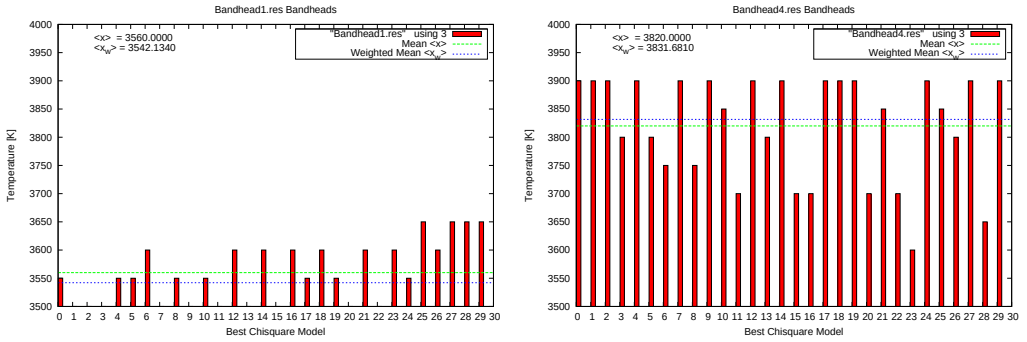

(a) ^{12}CO 4-1 head

(b) V, Fe,^{13}C^{12}O

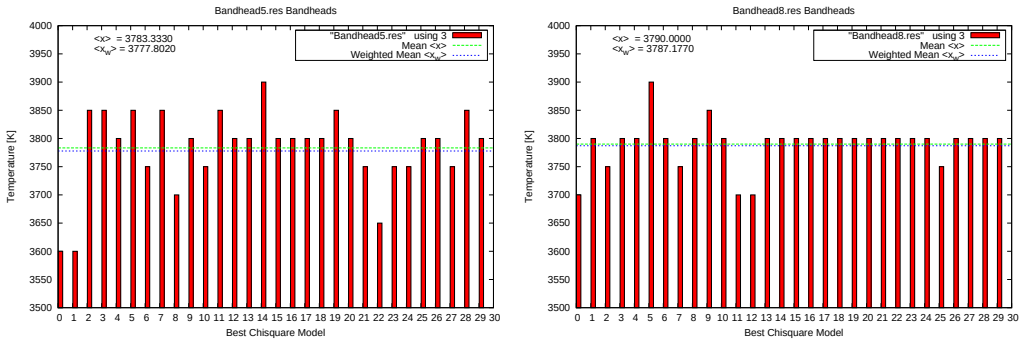

(c) ^{12}CO 5-2 head

(d) CO 6-3 head

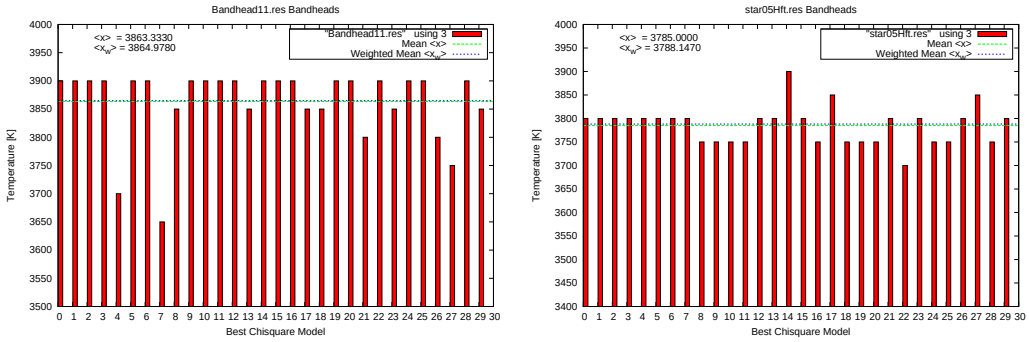

(e) Fe + ^{12}CO 7-4 head

(f) H-band all bandheads

Figure 6.35: Results of individual bandheads in the H-band of star05 of the best 30 temperatures. Note the temperature of all bandheads in subfigure (f).

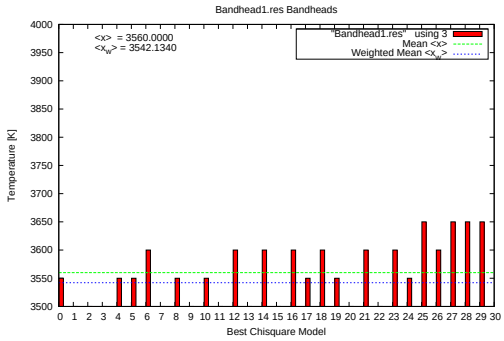

(a) ^{12}CO 4-1 head

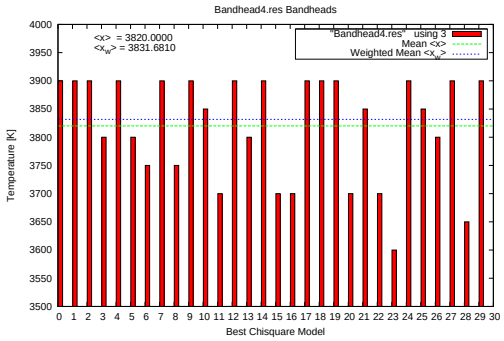

(b) V, Fe,^{13}C^{12}O

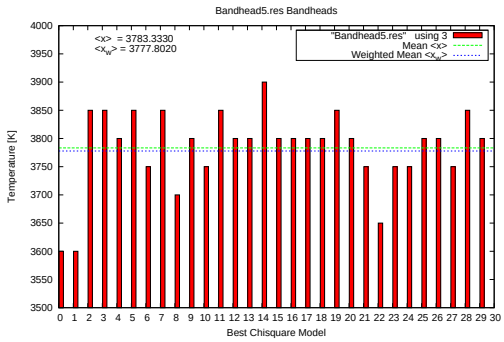

(c) ^{12}CO 5-2 head

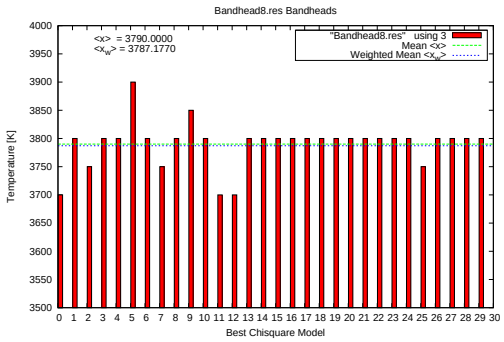

(d) CO 6-3 head

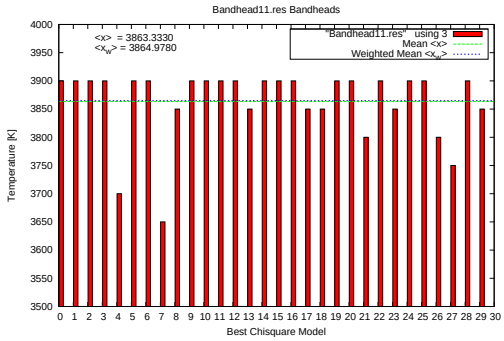

(e) Fe + ^{12}CO 7-4 head

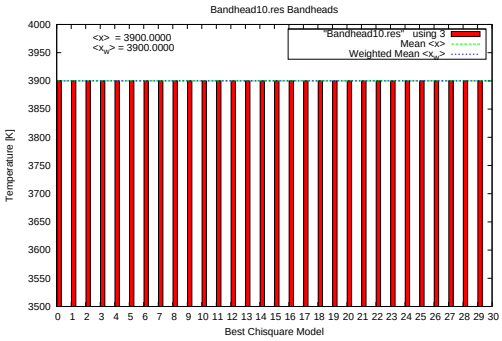

(f) H-band all bandheads

Figure 6.36: Results of individual CO bandheads in the H-band of star05 of the best 30 temperatures. Note the temperature of all bandheads in subfigure (f).

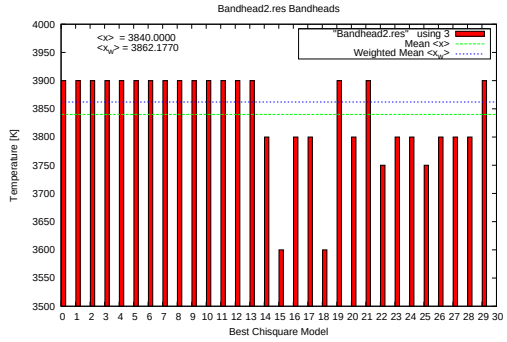

(a) OH 2-0 P1e 13.5, P1f 13.5, P2f 12.5

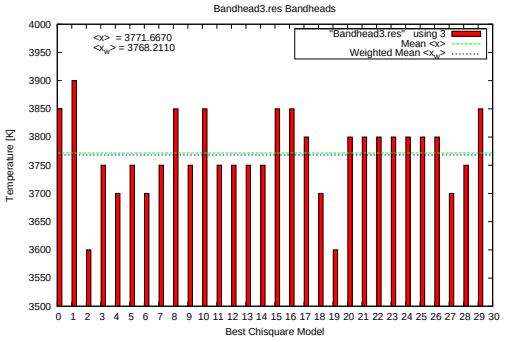

(b) OH 3-1 P1e 8.5, P1f 8.5

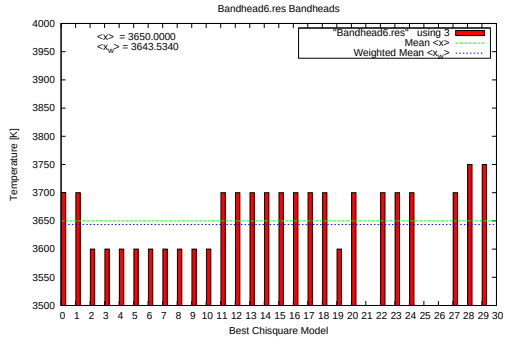

(c) OH 3-1 P2e 8.5, P2f 8.5

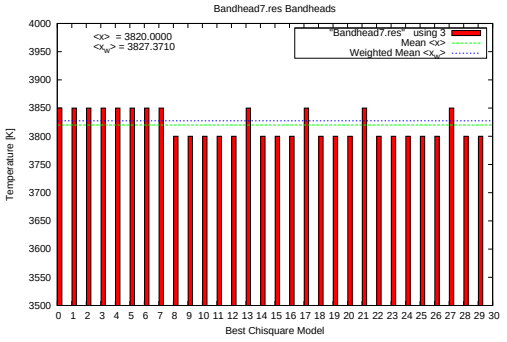

(d) OH 2-0 P2e 13.5, P2f 13.5

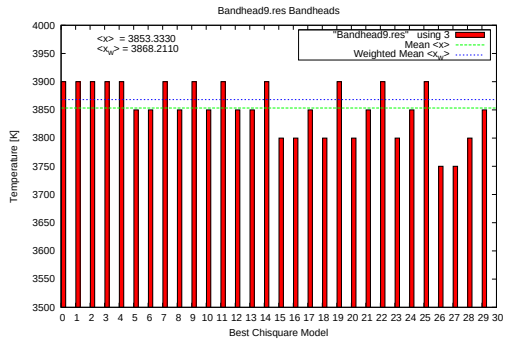

(e) OH 3-1 P2e 10.5, P2f 10.5, OH 4-2 P1e 5.5, P1f 5.5

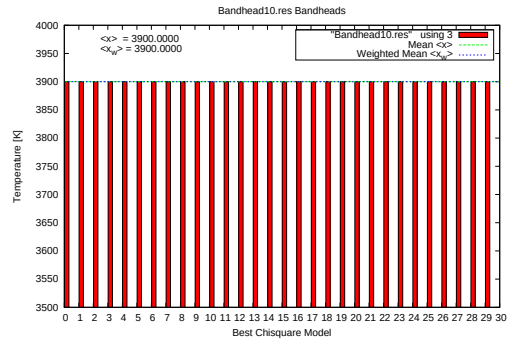

(f) OH 3-1 P2e 10.5, P2f 10.5, OH 4-2 P1e 5.5, P1f 5.5

Figure 6.37: Results of individual OH bandheads in the H-band of star05 of the best 30 temperatures.

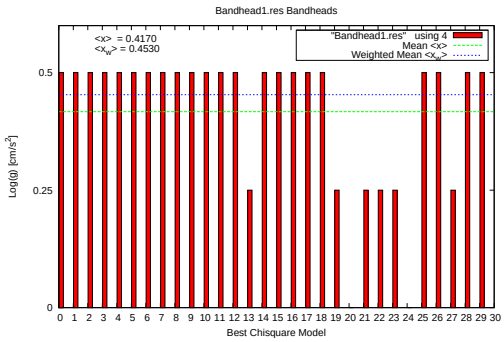

(a) ^{12}CO 4-1 head

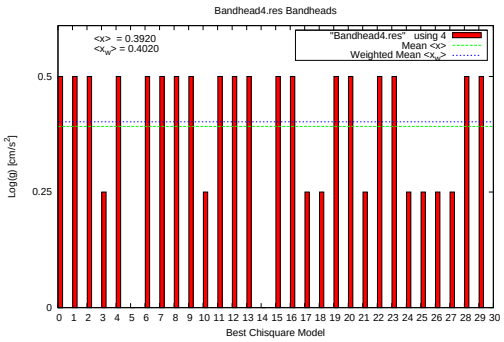

(b) V, Fe,^{13}C^{12}O

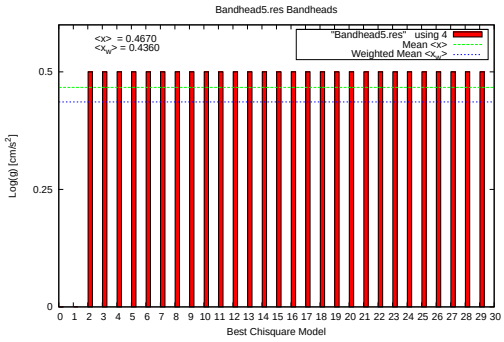

(c) ^{12}CO 5-2 head

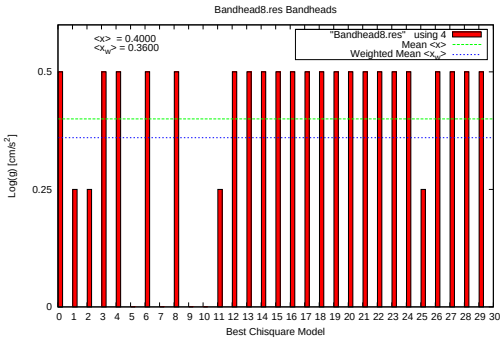

(d) CO 6-3 head

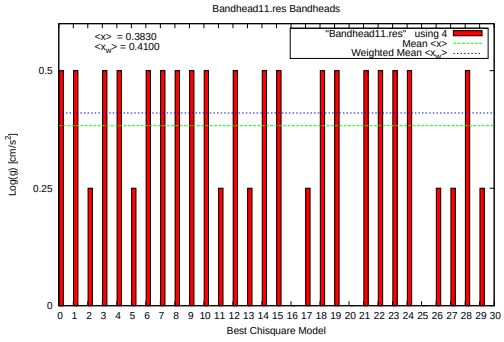

(e) Fe + ^{12}CO 7-4 head

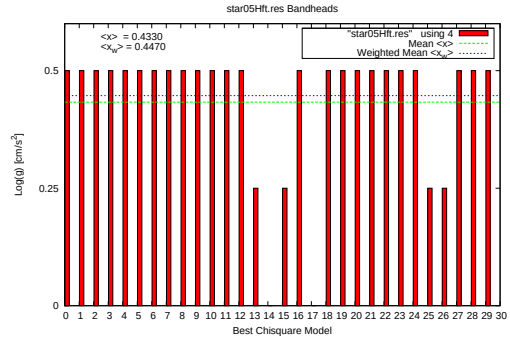

(f) H-band all bandheads

Figure 6.38: Results of individual bandheads in the H-band of star05 of the best 30 log(g). Note the log(g) of all bandheads in subfigure (f).

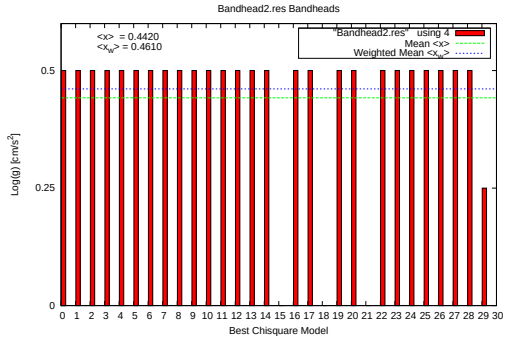

(a) OH 2-0 P1e 13.5, P1f 13.5, P2f 12.5

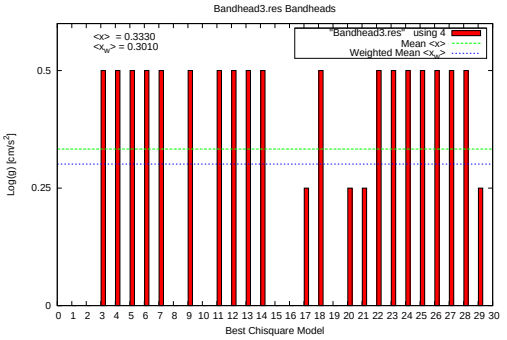

(b) OH 3-1 P1e 8.5, P1f 8.5

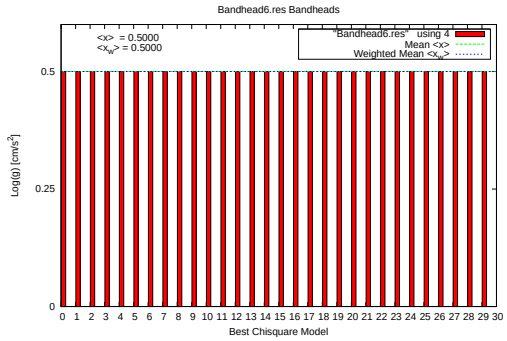

(c) OH 3-1 P2e 8.5, P2f 8.5

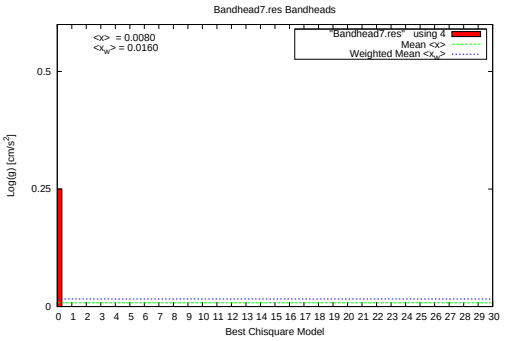

(d) OH 2-0 P2e 13.5, P2f 13.5

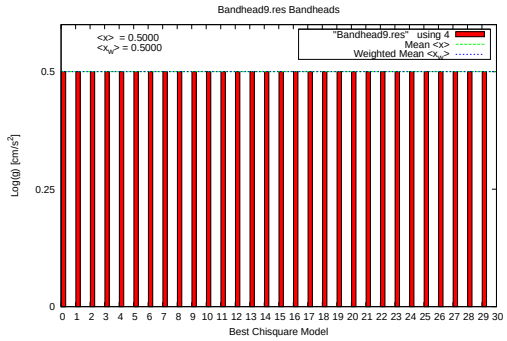

(e) OH 3-1 P2e 10.5, P2f 10.5, OH 4-2 P1e 5.5, P1f 5.5

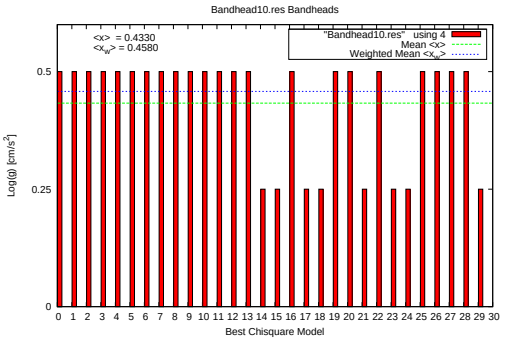

(f) OH 3-1 P2e 10.5, P2f 10.5, OH 4-2 P1e 5.5, P1f 5.5

Figure 6.39: Results of individual OH bandheads in the H-band of star05 of the best 30 log(g).

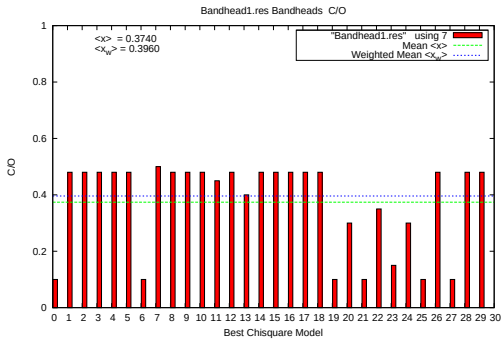

(a) ^{12}CO 4-1 head

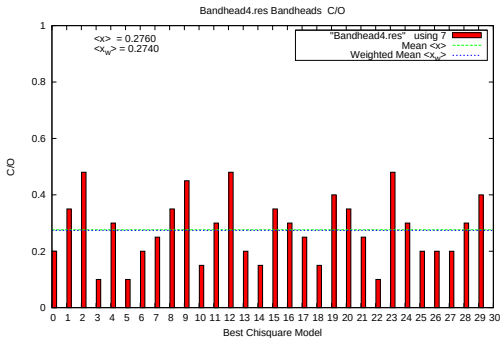

(b) V, Fe,^{13}C^{12}O

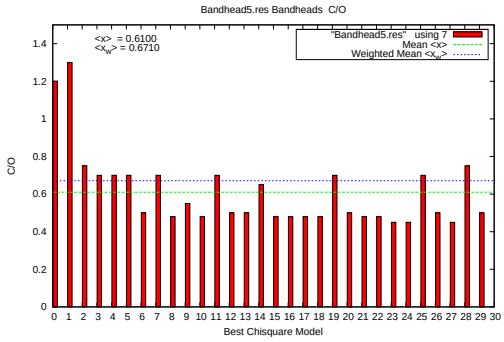

(c) ^{12}CO 5-2 head

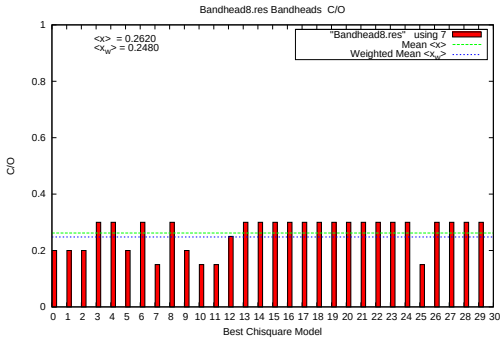

(d) CO 6-3 head

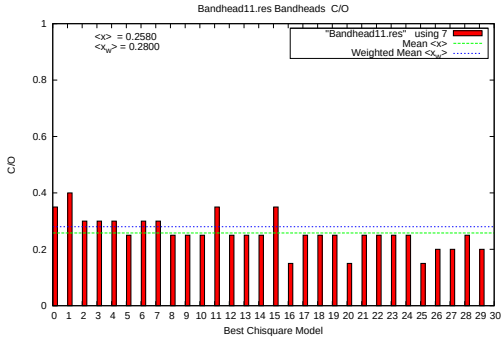

(e) Fe + ^{12}CO 7-4 head

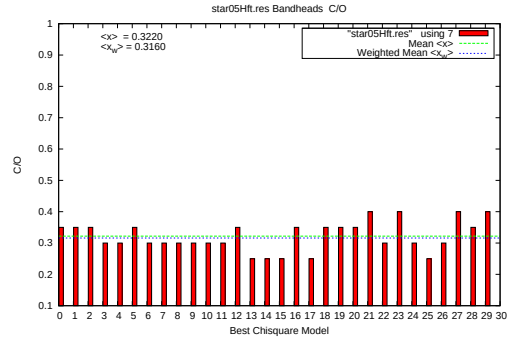

(f) H-band all bandheads

Figure 6.40: Results of individual bandheads in the H-band of star05 of the best 30 C/O-ratios. Note the C/O-ratio of all bandheads in subfigure (f).

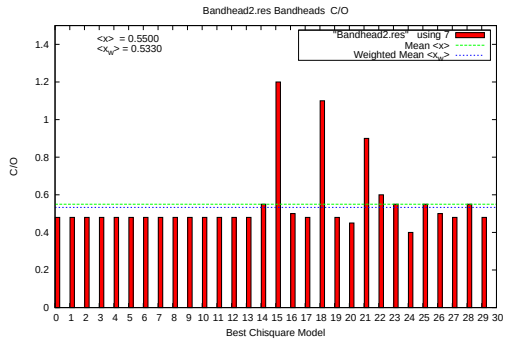

(a) OH 2-0 P1e 13.5, P1f 13.5, P2f 12.5

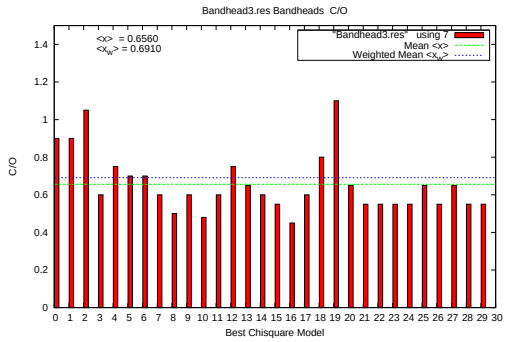

(b) OH 3-1 P1e 8.5, P1f 8.5

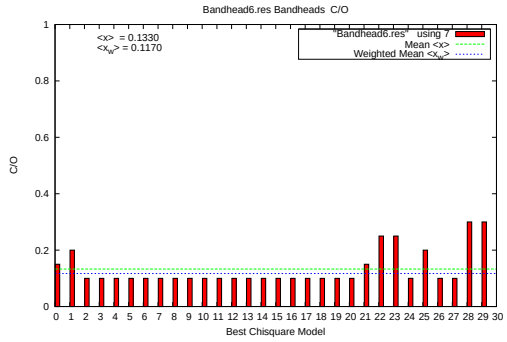

(c) OH 3-1 P2e 8.5, P2f 8.5

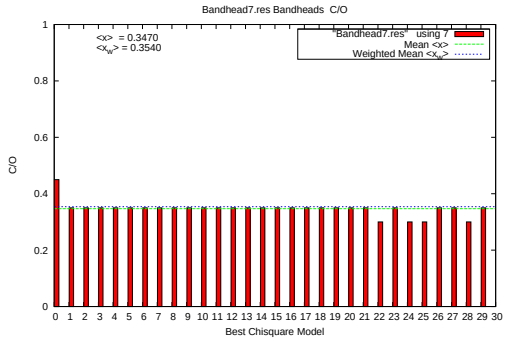

(d) OH 2-0 P2e 13.5, P2f 13.5

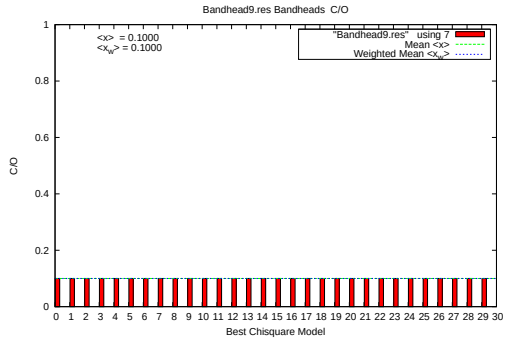

(e) OH 3-1 P2e 10.5, P2f 10.5, OH 4-2 P1e 5.5, P1f 5.5

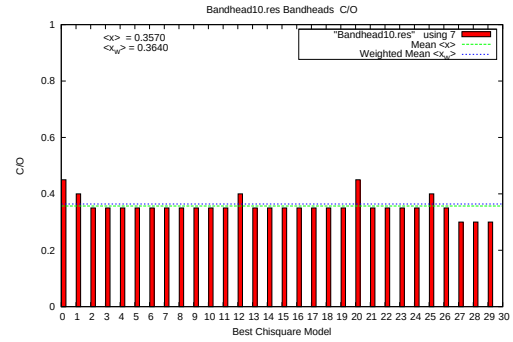

(f) OH 3-1 P2e 10.5, P2f 10.5, OH 4-2 P1e 5.5, P1f 5.5

Figure 6.41: Results of individual OH bandheads in the H-band of star05 of the best 30 C/O.

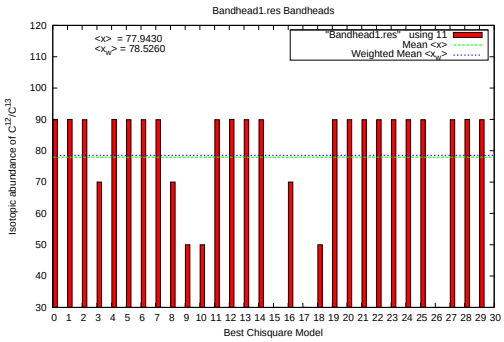

(a) ^{12}CO 4-1 head

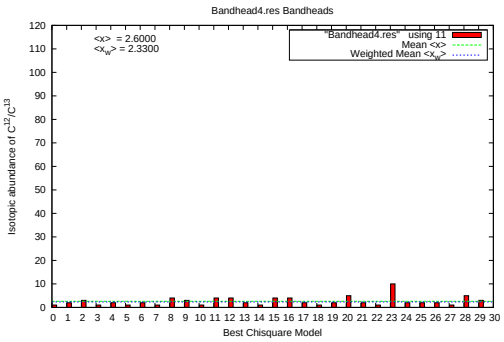

(b) V, Fe,^{13}C^{12}O

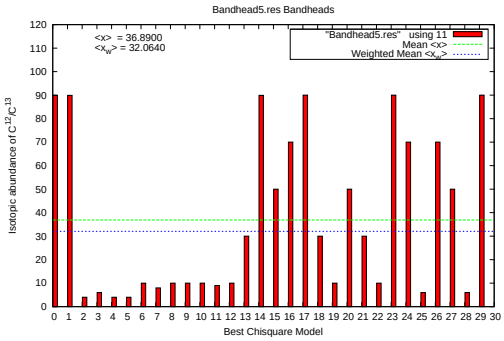

(c) ^{12}CO 5-2 head

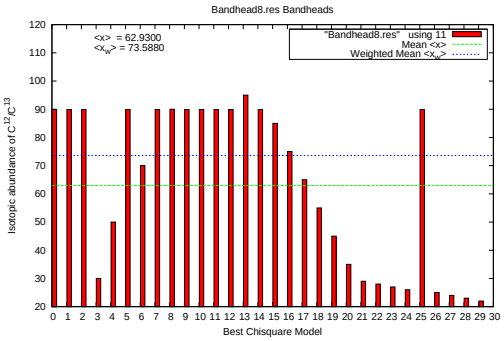

(d) CO 6-3 head

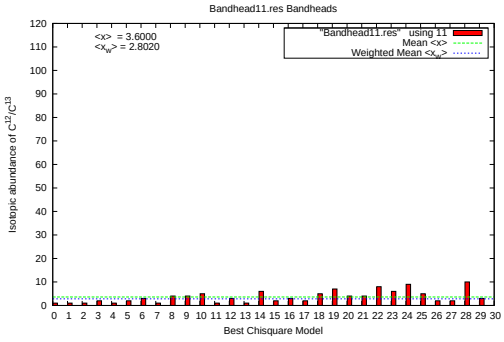

(e) Fe + ^{12}CO 7-4 head

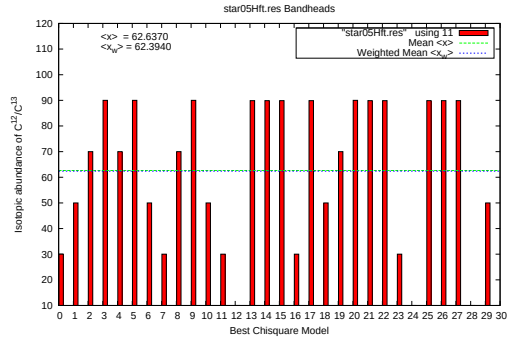

(f) H-band all bandheads

Figure 6.42: Results of individual bandheads in the H-band of star05 of the best 30 IACO. Note that there are no known ^{13}C bandheads in the H-band. So the correctness of these diagrams can be questioned.

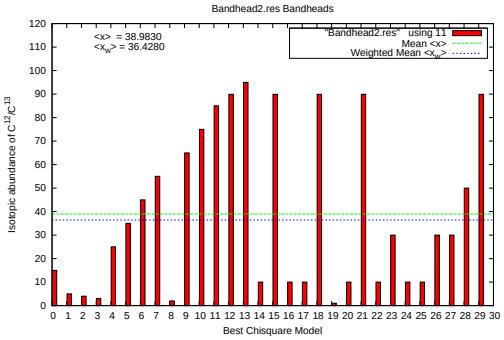

(a) OH 2-0 P1e 13.5, P1f 13.5, P2f 12.5

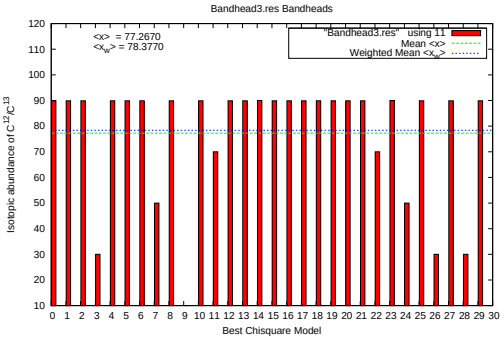

(b) OH 3-1 P1e 8.5, P1f 8.5

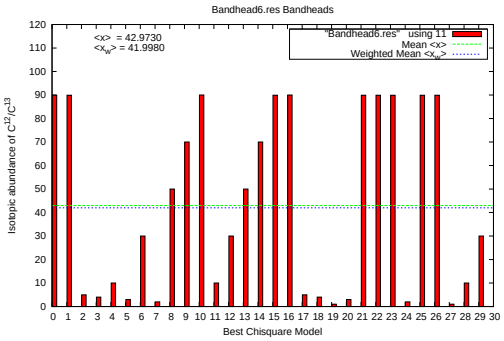

(c) OH 3-1 P2e 8.5, P2f 8.5

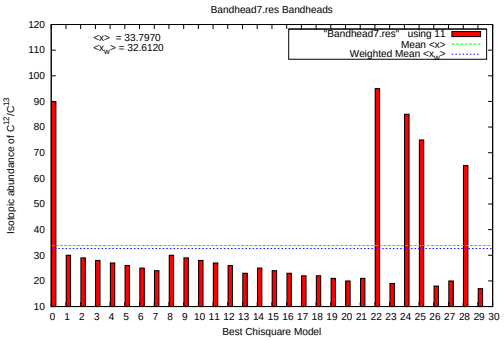

(d) OH 2-0 P2e 13.5, P2f 13.5

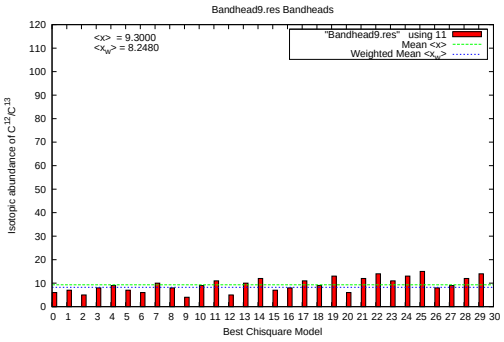

(e) OH 3-1 P2e 10.5, P2f 10.5, OH 4-2 P1e 5.5, P1f 5.5

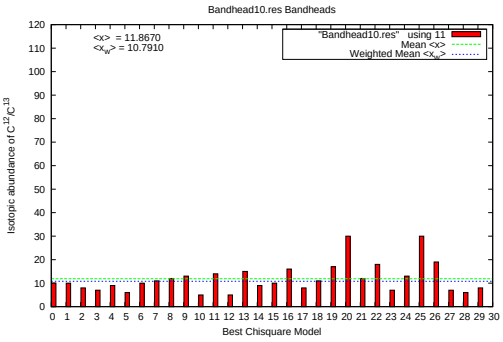

(f) OH 3-1 P2e 10.5, P2f 10.5, OH 4-2 P1e 5.5, P1f 5.5

Figure 6.43: Results of individual OH bandheads in the H-band of star05 of the best 30 $^{12}C/^{13}O$.

6.6.10 Results of combinations of bandheads H-band

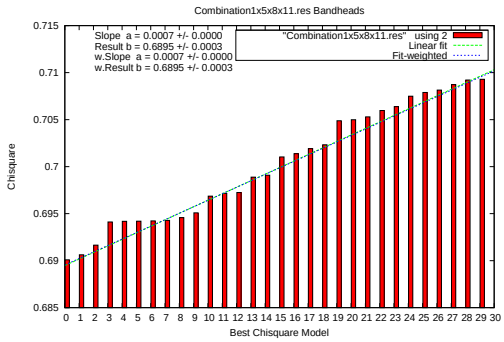

(a) chi-square

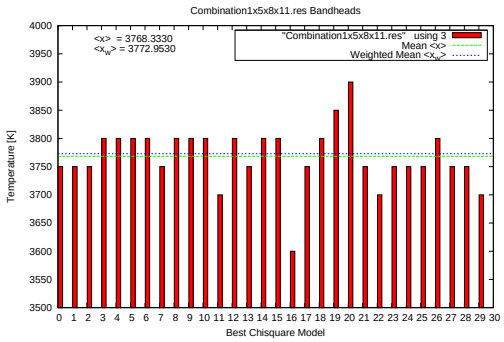

(b) temperature

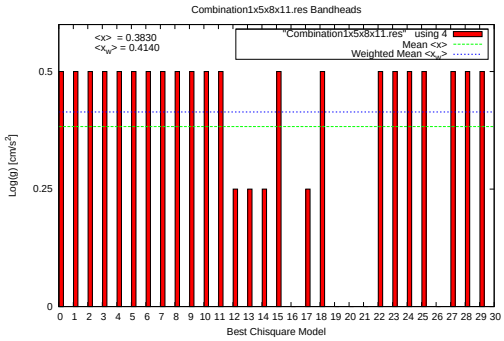

(c) Log(g)

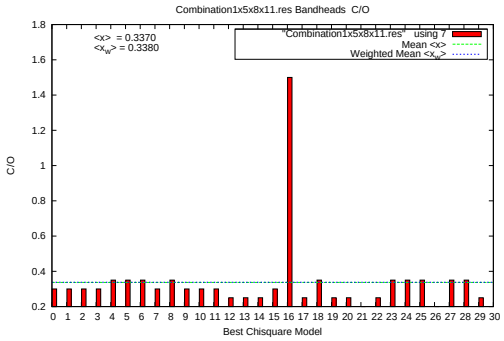

(d) C/O

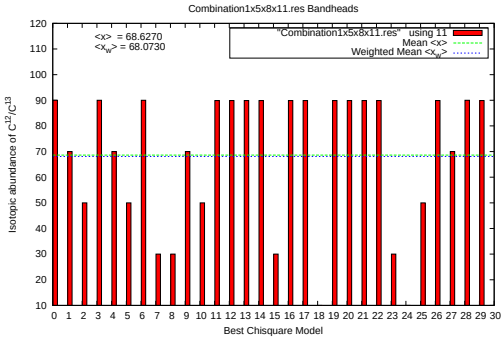

(e) $^{12}C/^{13}C$

Figure 6.44: Results of combination 1 of all the H-band ^{12}CO bandheads 1, 5, 8, 11 of star05 of the best 30 fits. Compare these figures with Fig. 6.9.

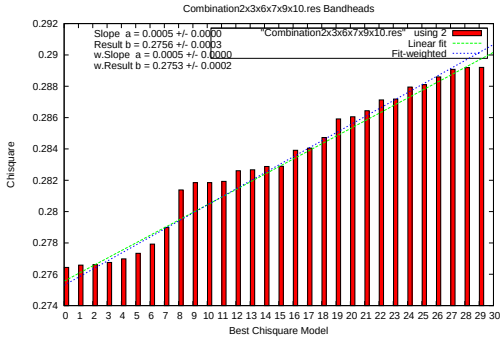

(a) chi-square

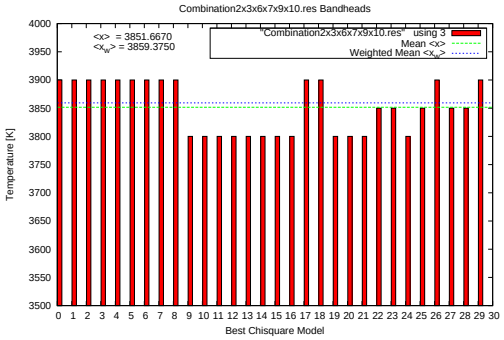

(b) temperature

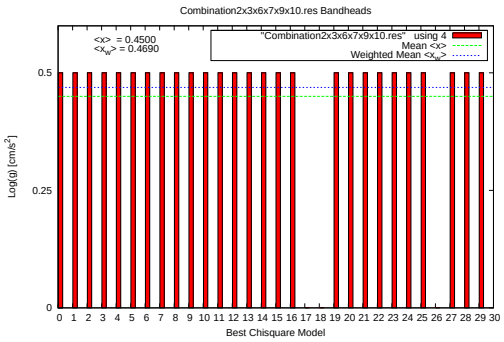

(c) Log(g)

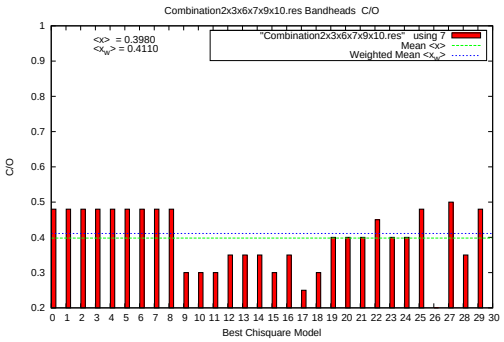

(d) C/O

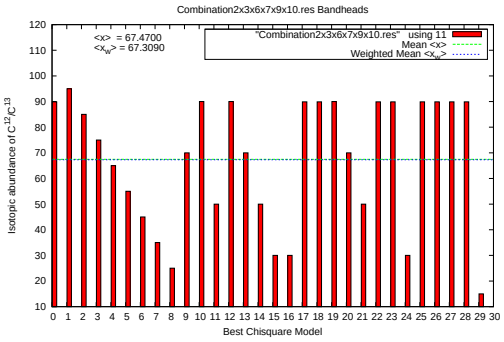

(e) $^{12}C/^{13}C$

Figure 6.45: Results of combination 2 of all the H-band OH bandheads 2, 3, 6, 7, 9, 10 of star05 of the best 30 fits. Compare these figures with Fig. 6.9.

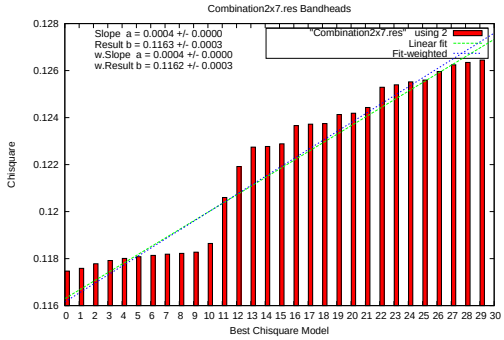

(a) chi-square

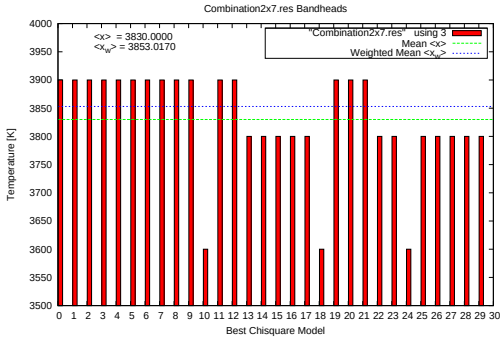

(b) temperature

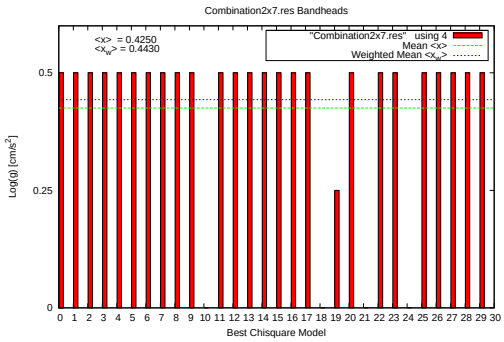

(c) Log(g)

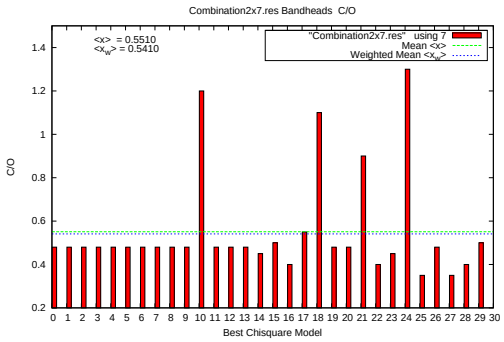

(d) C/O

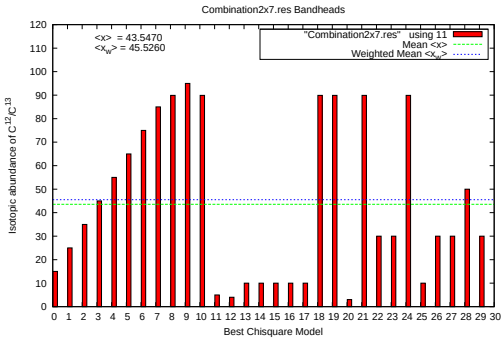

(e) $^{12}C/^{13}C$

Figure 6.46: Results of combination 3 of all the H-band OH bandheads 2, 7 of star05 of the best 30 fits. Compare these figures with Fig. 6.9.

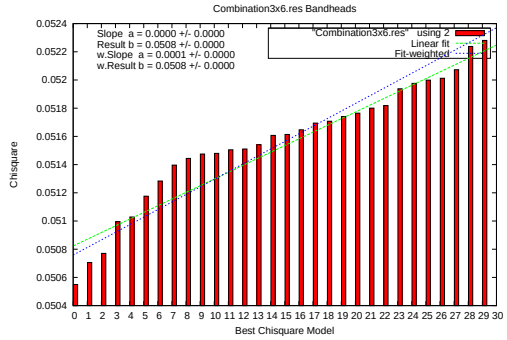

(a) chi-square

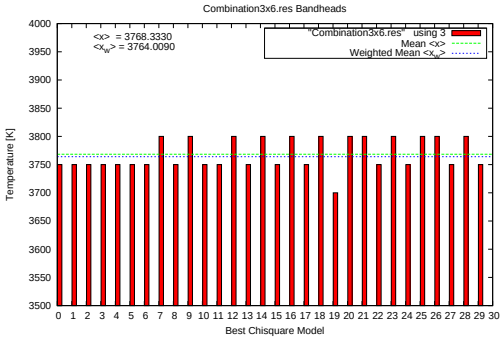

(b) temperature

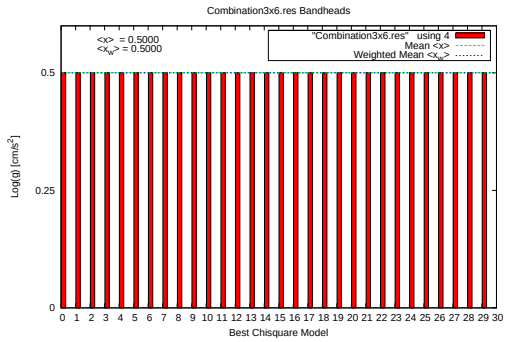

(c) Log(g)

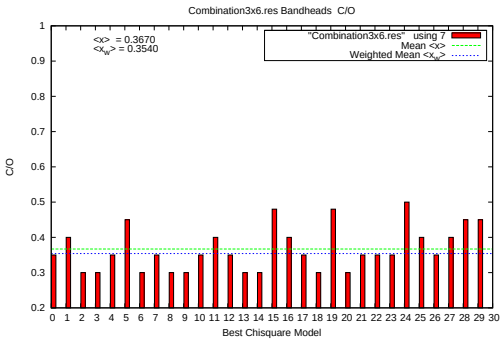

(d) C/O

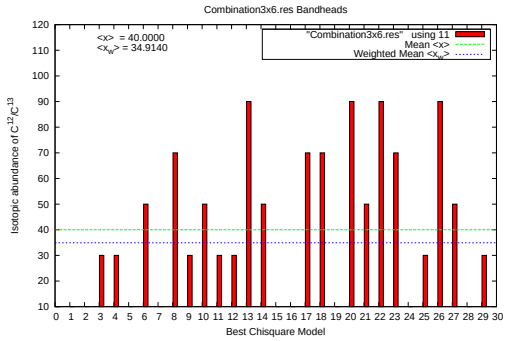

(e) $^{12}C/^{13}C$

Figure 6.47: Results of combination 4 of all the H-band OH bandheads 3, 6 of star05 of the best 30 fits. Compare these figures with Fig. 6.9.

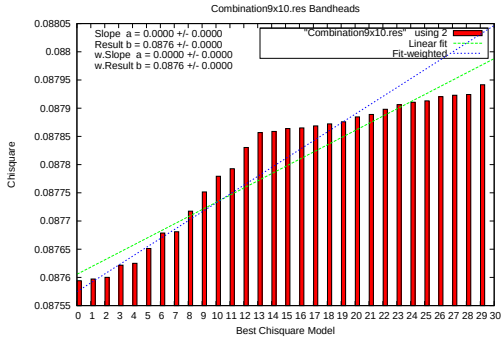

(a) chi-square

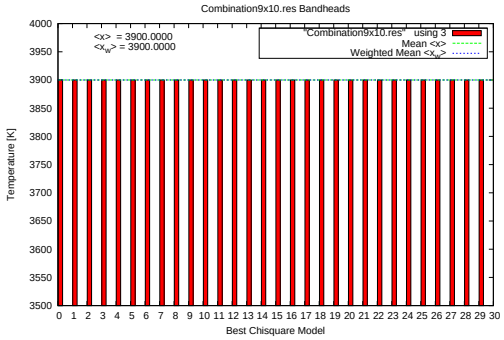

(b) temperature

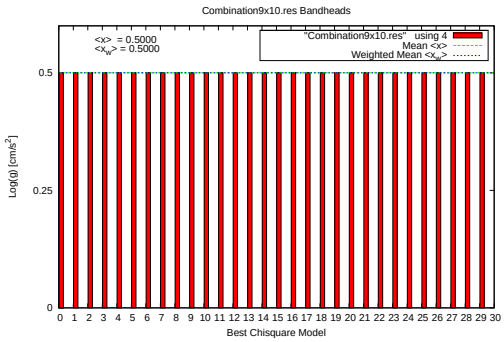

(c) Log(g)

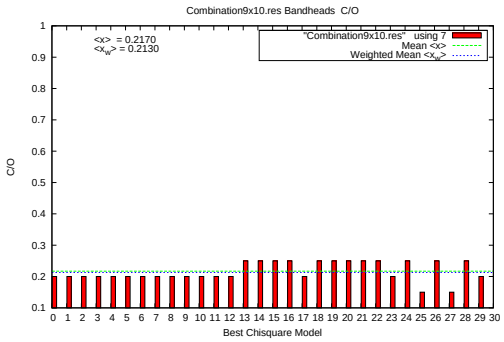

(d) C/O

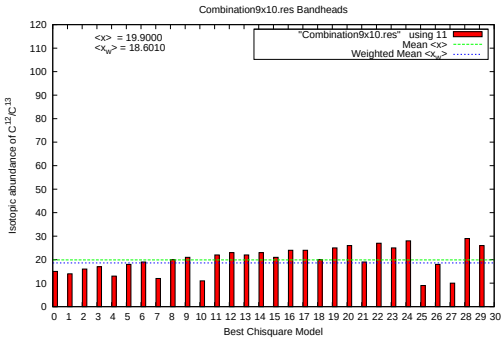

(e) $^{12}C/^{13}C$

Figure 6.48: Results of combination 5 of all the H-band OH bandheads 9, 10 of star05 of the best 30 fits. Compare these figures with Fig. 6.9.

Chapter 7

Conclusions

7.1 Radial velocity v_r

The radial velocities v_r (see Table 2.5) are determined to:

- Mean of v_r of all stars H-band: 210.06 ± 16.19 km s^{-1}
- Mean of v_r of all stars K-band: 206.78 ± 31.72 km s^{-1}
- Mean of v_r of H-band and K-band: 213.15 ± 15.33 km s^{-1}

Star09 has a v_r = 228.05 km s^{-1} which is slightly higher than of the other stars but it is within the range of the sigma of ± 15.33 km s^{-1}. Star05 has a radial velocity of v_r = 241.32 km s^{-1} which is significantly higher than the maximum of 228.48 km s^{-1} and therefore the membership of the star to the cluster can be questioned.

7.2 Bandheads versus full spectral range

The final results of the physical parameters determined in the bandheads is shown in Table 6.5 and for the full spectral range it is shown in Table 6.6. The difference of the results are shown in Table 6.7 and the mean of the bandheads and the full spectral range are shown in Table 6.8. In some cases the difference of the bandheads versus the full spectral range of a physical parameter is smaller than the given error, e.g. the temperature difference for star02H, star04H, star05H+K, star07H, star08K, star12H is smaller than Δ T = ± 50 K. The situation for the log(g) and the C/O-ratio is even better. Nearly all stars have a difference which is smaller than the error. Only the results for the isotopic abundances of $^{12}C/^{13}C$ differ a lot more than the

error in the two spectral ranges.

Additionally, the mean of the results of the bandheads and the full spectral range is given in Table 6.8 for both the H-band and the K-band. In principal, all parameters from Table 6.7 where the difference is smaller than the given error could be taken to investigate the parameters in greater detail. Here exemplary the temperature of star05 is in good agreement with respect to the temperature which was derived only from the bandheads. The mean temperature derived from the full spectral range and the bandheads in the H-band is 3789 K which is close to the result of 3791 K of the bandheads in the H-band. And the mean of the full spectral range and the bandheads in the K-band is 3647 K which is close to the result of 3657 K of the bandheads in the K-band.

7.3 C/O versus $^{12}C/^{13}C$

Since the H-band has only one faint $^{13}C^{12}O$ feature in bandhead 4, which is blended with Iron and Vanadium, the isotopic abundances of $^{12}C/^{13}C$ were taken only from the K-band, and the C/O-ratio was taken from the H-band as it was done by Lederer et al. (2009) and Lebzelter et al. (2008b). Most stars which measurements are based only on the bandheads (see Fig. 6.25) have a final mean of $^{12}C/^{13}C < 20$ except for star04 with $^{12}C/^{13}C = 55$ and for star09 with $^{12}C/^{13}C = 35$ (see Table 6.9). Using the full spectral range (see Table 6.10) the situation is quite similar. All stars have a final mean value of $^{12}C/^{13}C < 20$ except star04 with $^{12}C/^{13}C = 36$ and star09 with $^{12}C/^{13}C = 44$. In Fig. 6.25 the slope using the final mean is slightly larger than the slope of the best fitting model. For the bandheads the value of the final mean slope is about 8 times higher, and for the full spectra the value of the final mean slope is about 5 times higher, than for the best fitting model.

In Fig. 6.26 the C/O-ratio was also experimentally determined in the K-band (red line). The mean of the C/O-ratio of the H-band and K-band is plotted with an orange line. The $^{12}C/^{13}C$-ratio was only taken from the K-band. The green fit is identical with the fits in Fig. 6.25 since the C/O-ratio was taken from the H-band. Note that in Fig. 6.26 (b) the C/O-ratio of the K-band (red fit) of the full spectra is shifted nearly parallel but has the same slope as the green fit of the H-band. The parallel C/O shift of the K-band (red line) to the H-band (green line) could indicate a general tendency. It is interesting whether this shift can be found in other samples, too. Due to the dredge up of ^{12}C, an increased C/O ratio should be accompanied by an

increased isotopic abundance ratio (Lebzelter et al., 2008b). This expected correlation of the C/O-ratio and the isotopic abundances of $^{12}C/^{13}C$ is shown in Fig. 6.25 and Fig. 6.26.

7.4 Measuring individual bandheads

The idea to study the single bandheads was to see if it is possible to derive the C/O-ratio and the isotopic abundances of $^{12}C/^{13}C$ with less observations. Meaning with only a few specific bandheads and features, since the K-band has a coverage of total 1238.57 Å and the H-band has a total coverage of 815.87 Å. The calculations for over 2054.44 Å take a significant amount of computing time. So with less spectral coverage on the VLT, one can observe more stars and compute synthetic spectra more quickly.

For this study star05 was chosen because it has good observed data and a small chi-square value. The results of the individual bandheads are listed in Table 6.19 for the K-band and in Table 6.18 for the H-band.

	T [K]	Log(g)	C/O	$^{12}C/^{13}C$
star05Hft.res	3791	0.46	0.33	52
star05Kft.res	3657	0.06	0.59	19
Error	± 50 K	± 0.25	± 0.05	± 1

Table 7.1: The *Final Mean* results of star05. Note that the C/O-ratio is more reliably in the H-band and $^{12}C/^{13}C$ is more reliably in the K-band.

7.4.1 The temperatures

A comparison of Table 7.1 (*Final Mean* values) with Table 6.19 and Fig. 7.1 for the individual bandheads in the K-band shows that the temperatures for the single features vary around the final mean result. Fig. 7.1 shows that bandhead 2, combination 1 and 2 represent the found temperature of star05 by the 30 best chi-squares in the K-band best. The mean of the temperatures in the K-band (bandhead 1 to 5) in Table 6.19 is 3626 K which is close to the value of 3657 K which is found by the 30 best fitting models with the chi-square method. Therefore, the final mean of the temperature (3657 K) of star05K of the 30 best fitting chi-squares is a good representation of all included features. But the question is, which bandheads or features are really reliable for the determination of the effective temperature of the

star. In Fig. 7.1 the bandheads 3, 4, 5 and the combination 2 are within the same range of approx 3500 K to 3550 K ± 50 K. So if bandheads 1, 2 and combination 1 would be excluded for the 30 best fitting models, the result of the final mean would be around 3500 K ± 50 K. This leads to the question, why bandhead 1, 2 and combination 1 have high temperatures from 3755 K to 3881 K while the other bandheads in the K-band have temperatures near 3500 K. This needs to be investigated in future works in depth.

The situation in the H-band is better. In Fig. 7.5 most bandheads and combinations have high temperatures. Only bandheads 1 and 6 have temperatures below and bandhead 10 and combination 5 are a bit above the errorbars of the final mean temperature of 3791 K.

7.4.2 The Log(g)

The logarithm of the surface gravity is shown in Fig. 7.2 for the K-band and in Fig. 7.6 for the H-band. The final mean of the Log(g) in the K-band is around zero and in the H-band around 0.5. Only bandhead 3 and 7 in the H-band are outliers but are still in the range of the errorbars. While the single results for the K-band and the H-band have all a good agreement within the errorbars, the question remains why the H-band has a log(g) which value is nearly 0.5 higher than in the K-band, and which band represents the real log(g). Another question is, is the log(g) in the H-band always higher with a factor of about 0.5. Since the log(g) of the MARCS models were only calculated with ± 0.25, the errorbars are quite big. A further discussion of these questions is beyond the scope of this thesis, but will be provided in a future work. It would be also better to have a denser grid for the log(g) for future calculations.

7.4.3 The C/O-ratio

In Lebzelter et al. (2008b) the C/O-ratio was taken from the H-band. The C/O-ratios are shown in Fig. 7.3 for the K-band and in Fig. 7.7 for the H-band. In the H-band bandhead 2, 3, 5 and combination 3 have much higher C/O-ratio values, and bandheads 6, 9 and combination 5 have values below the errorbars of the final C/O-ratio of star05 in the H-band. The C/O-ratio found by the chi-square method of star05 is C/O = 0.33. The mean of all bandheads in the H-band of Table 6.10 is C/O = 0.38 and if bandheads 2, 3, and 5 are excluded the mean is C/O = 0.26. Experimentally we looked for the C/O-ratio in the K-band which is C/O = 0.59 determined by the chi-square. A major outlier of the C/O-ratios in Fig. 7.7 is bandhead 4 with

a value of C/O = 1.30. In Table 6.19 the mean of the bandheads of the C/O-ratio is 0.62 and if bandhead 4 is excluded the mean of the C/O-ratio is C/O = 0.45 which is still higher than the found C/O-ratio of C/O = 0.33 in the H-band.

7.4.4 The $^{12}C/^{13}C$-ratio

In Lebzelter et al. (2008b) the $^{12}C/^{13}C$-ratio was taken from the K-band. In Fig. 7.4 the $^{12}C/^{13}C$-ratio is shown for the K-band and in Fig. 7.8 it is shown experimentally for the H-band. In the K-band, bandhead 1 and 4 (^{12}CO 2-0 and ^{12}CO 4-2) are major outliers with values of $^{12}C/^{13}C$ = 78 and 59. The mean of all single ratios would be $^{12}C/^{13}C$ = 39 which is close to the value of combination 1 which is $^{12}C/^{13}C$ = 33. If bandheads 1 and 4 would be excluded the mean of the $^{12}C/^{13}C$-ratio will be 19, which is exact the found value of star05 in the K-band.

We looked also at the $^{12}C/^{13}C$-ratio derived from the H-band which was determind by the chi-square approach to $^{12}C/^{13}C$ = 52. In Fig. 7.8 the $^{12}C/^{13}C$-ratio varies from close to 10 to over 80. In Table 6.18 the mean of all bandheads is $^{12}C/^{13}C$ = 41. The mean of bandheads 2, 4, 9, 10 and 11 is $^{12}C/^{13}C$ = 11 and combination 5 has a value of 18 which is close to the ratio of 19 found in the K-band. Maybe bandheads 2, 4, 9, 10 11 or combination 3, 4 and 5 can be a reliable source to determine the $^{12}C/^{13}C$-ratio also in the H-band.

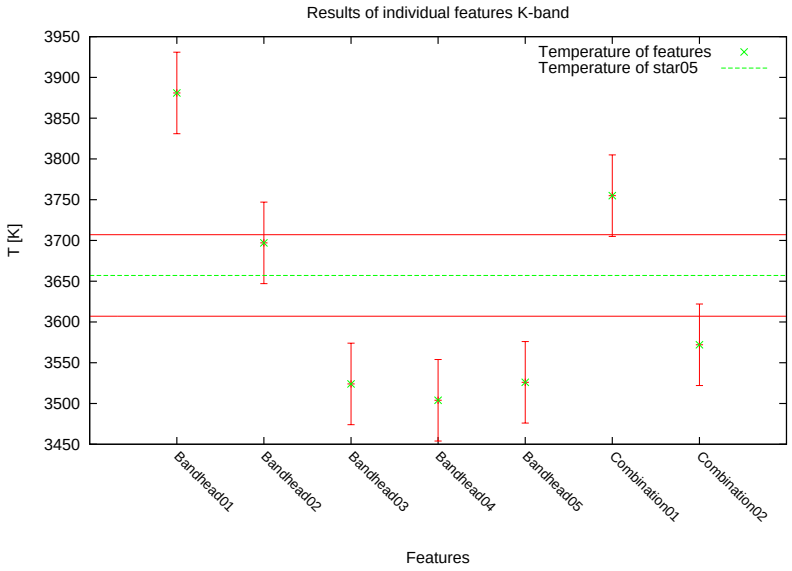

Figure 7.1: Final results of individual features of star05's temperature for the K-band.

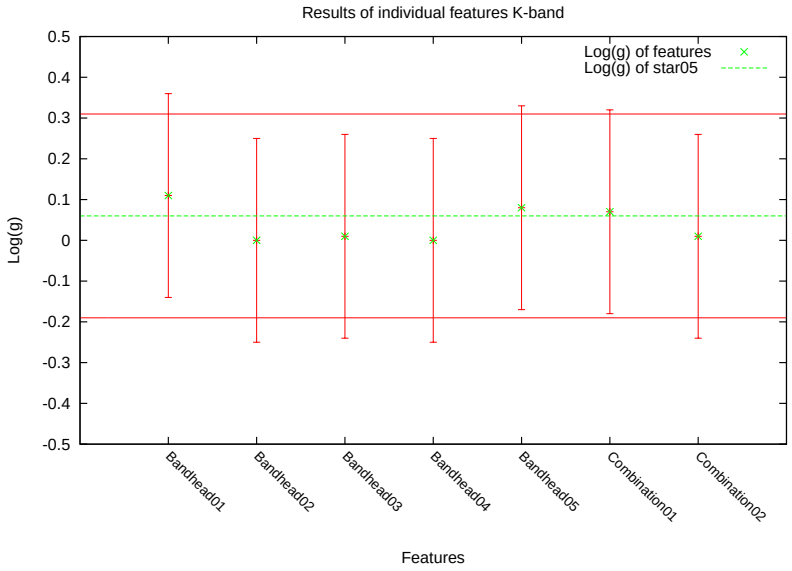

Figure 7.2: Final results of individual features of star05's log(g) for the K-band.

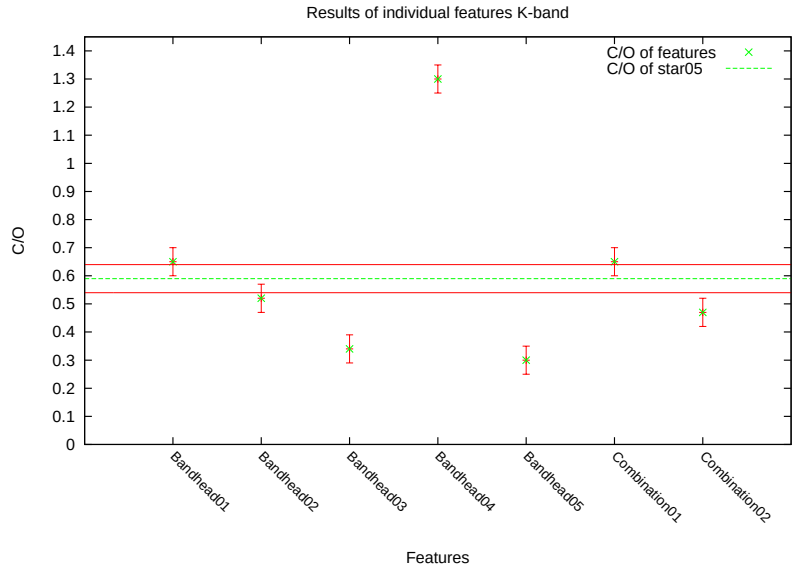

Figure 7.3: Final results of individual features of star05's C/O-ratio for the K-band.

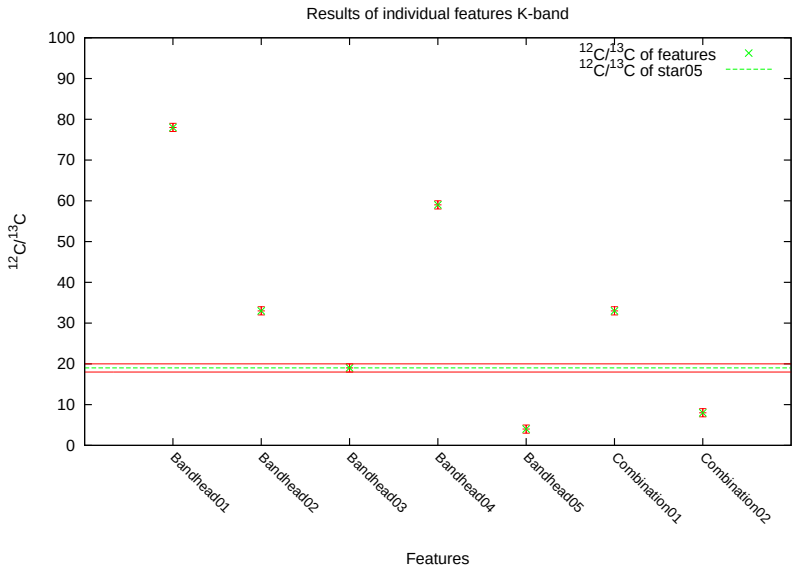

Figure 7.4: Final results of individual features of star05's $^{12}C/^{13}C$-ratio for the K-band.

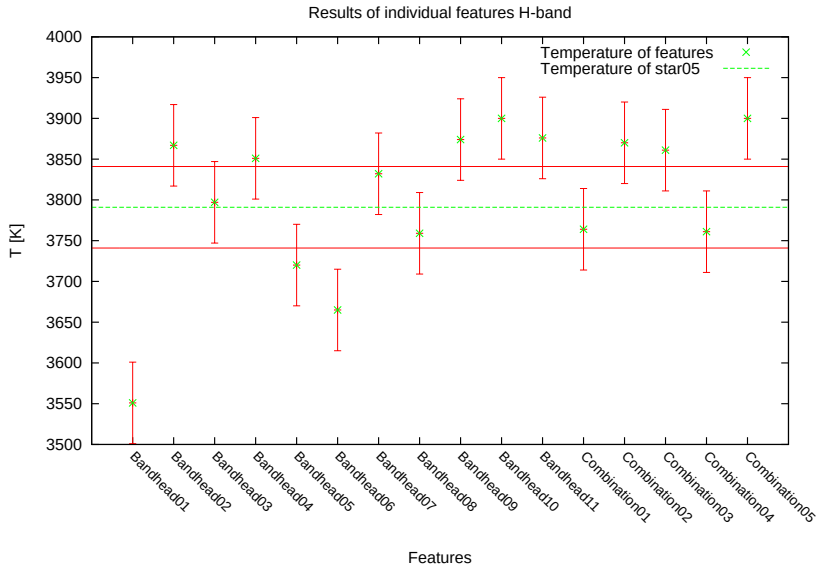

Figure 7.5: Final results of individual features of star05's temperature for the H-band.

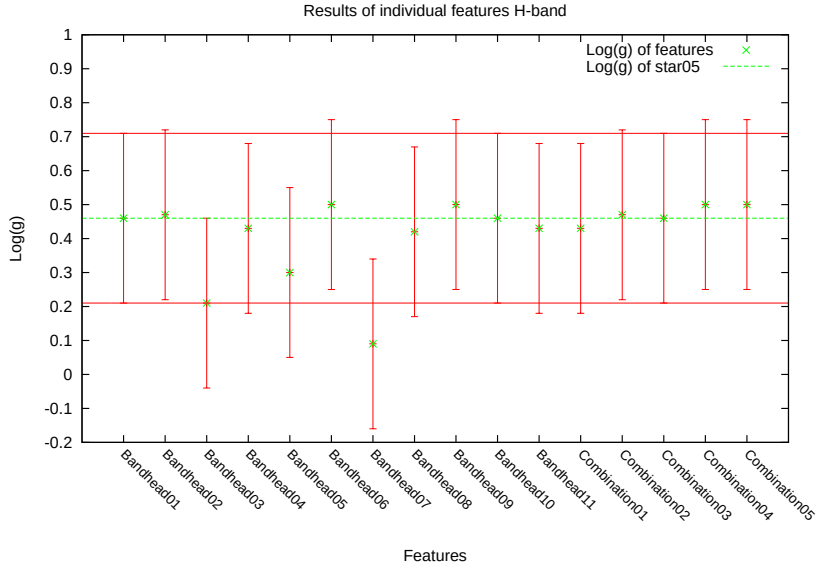

Figure 7.6: Final results of individual features of star05's log(g) for the H-band.

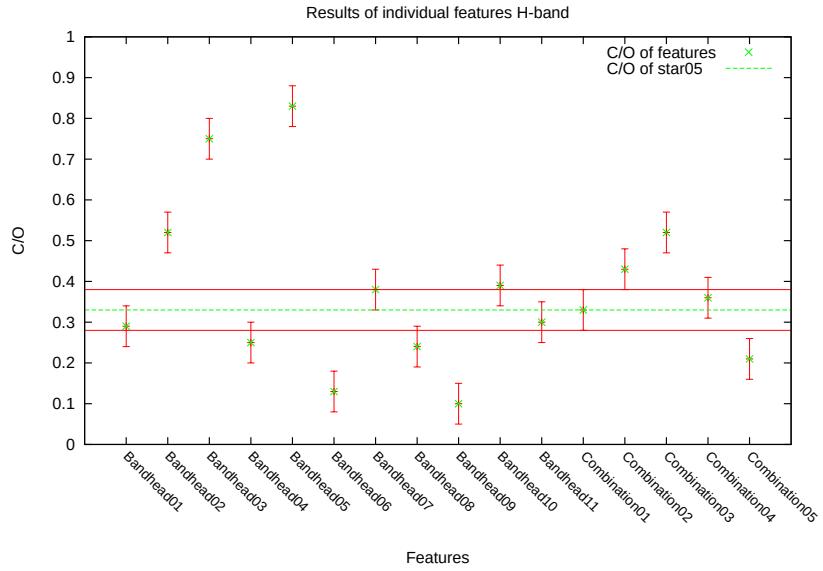

Figure 7.7: Final results of individual features of star05's C/O-ratio for the H-band.

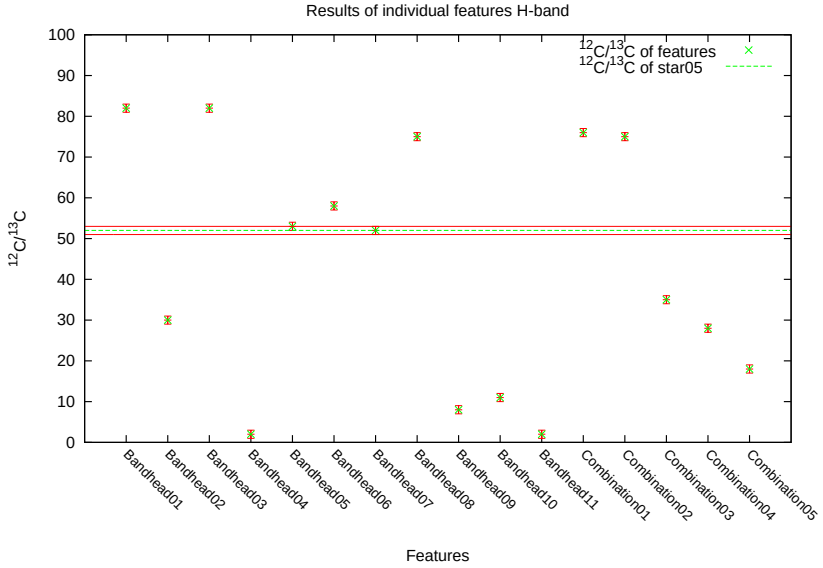

Figure 7.8: Final results of individual features of star05's $^{12}C/^{13}C$-ratio for the H-band.

Chapter 8

Future aspects and outline

8.1 General considerations

8.1.1 Extension of the best fitting models

In this thesis less than the best one percent of calculations (the 30 best fits) were taken to investigate the observed spectra. It would be interesting to which number the best fitting models could be extended, since there were calculated nearly 4000 synthetic spectra for the H-band and 8000 synthetic spectra for the K-band. Maybe the best three or five percent of the calculated models can be taken for investigation. That would be nearly 200 to 400 model spectra.

8.1.2 The membership of star05

Since the radial velocity of star05 is higher than one sigma, the membership of the star to the cluster NGC 1783 should be investigated again in more detail.

8.1.3 Finding a result function depending on transitions and wavelength range

In the study of measuring individual bandheads, we showed that different bandheads have different impacts on the determination of the physical parameters. A correlation of the impact of the various transitions (^{12} CO 4-1, 5-2, 6-3, 7-4) of the bandheads would be interesting. Also a correlation of the absolute included spectra (Å) of the bandheads would be nice to have. This means that the function of the impact to the physical parameters could

be depending on different transitions and of the included wavelength range per bandhead-transition.

8.1.4 A comparison of this thesis to the paper of Lebzelter et al. (2008b)

Lebzelter et al. (2008b) took the C/O-ratio from the H-band and used this to determine the $^{12}C/^{13}C$-ratio in the K-band. This method of the structured combinations of the two steps, first to investigate the H-band and then take the found parameter from the H-band to investigate the K-band should be studied in more detail also for our data set in a forthcoming paper.

8.2 *ComaGUI*

A needed feature would be a function which can update the already calculated models to create a diagram of the parameter space. The management of the calculations is currently by the user. Sometimes it is not possible to avoid duplicate calculations which were already done. Therefore *ComaGUI* should rebuild an internal parameter space and update it with already done calculations, to save computing time and avoid calculating models twice.

Chapter 9

Appendix

9.1 Abstract

The goal of this master thesis is the determination of element abundances in cold red giants, namely AGB-stars in the globular cluster NGC 1783. This globular cluster is located in the Large Magellanic Cloud (LMC) and was chosen because of its well known stellar parameters. The determination of the C/O-ratio and the isotopic abundance of ^{12}C/^{13}C are primary goals. During the AGB evolution, the third dredge-up (3DUP) brings freshly produced ^{12}C and s-process elements into the stellar atmosphere of a star. Subsequently a heavy mass-loss process, which occurs during the AGB evolution, also enriches the interstellar material with heavy elements. With observed data from the VLT / ISAAC instrument of ESO and COMARCS, MARCS and COMA model atmospheres, we have measured the C/O-ratio and the isotopic abundance of ^{12}C/^{13}C.

For this purpose, a "best fit and spectra plotting" software was developed. The software is called *AGB*StarViewer and is able to compare two spectra, namely the observed one and the synthetic model spectra. The best fit from several hundred synthetic models can be obtained with a chi-square technique.

Another software called *ComaGUI* was also developed. *ComaGUI* is a graphical user interface, which is a front-end for COMA08[1]. It can also generate shell-scripts for semi-remote operating.

[1]COMA08 is a Fortran software developed by B. Aringer, S. Höfner and M. Gorfer.

9.2 Zusammenfassung

Das Ziel dieser Magisterarbeit ist die Bestimmung der Elementhäufigkeiten von AGB Sternen, wobei kühle Riesen untersucht werden. Mit Hilfe von Beobachtungsdaten der ESO-VLT/ISAAC soll das C/O-Verhältnis und das Isotopenverhältnis von $^{12}C/^{13}C$, von *Asymptotic Giant Branch* (AGB) Sternen bestimmt werden. Die Beobachtungsdaten stammen von einem Kugelsternhaufen (NGC 1783) in der Großen Magellanschen Wolke. Mit Hilfe von Modellatmosphären und synthetischen Spektren, welche mit MARCS und COMA berechnet werden, wurde durch einen Vergleich der Spektren, das C/O-Verhältnis und das Isotopenverhältnis von $^{12}C/^{13}C$ bestimmt.
Während der AGB-Phase bringt der sogenannte *Third Dredge-Up* (3DUP) frische, durch Nukleosynthese produzierte Elemente an die Oberfläche der Sternatmosphäre. Ein starker Massenverlust, welcher durch Pulsation und Staubbildung getrieben wird, reichert das Interstellare Medium mit schweren Elementen an.
Zu diesem Zweck wurde eine "Best-Fit und Spektren-Visualisierungs-Software", *AGB*StarViewer, entwickelt. Sie kann zwei Sternspektren miteinander vergleichen oder Chi-quadrat Fits mit vielen hundert gerechneten Sternspektren druchführen.

Als zweite Software wurde *ComaGUI* entwickelt, welche ein graphisches User Interface (GUI) bzw. ein Frontend für die Software COMA08[2] ist. Sie kann entweder am Computer direkt eingesetzt werden, oder sie kann Shell-Skripte erzeugen, welche über den SSH[3] Dienst an die jeweiligen Server kopiert werden und quasi eine semi-remote Steuerung der Modell-Rechnungen ermöglichen.

[2]COMA08 wurde von Aringer, Höfner und Gorfer in Fortran geschrieben.

[3]Secure Shell: Ist ein Netzwerkprotokoll für verschlüsselte Verbindungen über das Internet zu einem Server.

List of Figures

List of Tables

Bibliography

Anders, E. and Grevesse, N., 1989, *Geochim. Cosmochim. Acta* **53**, 197

Aringer, B., *The SiO Molecule in the Atmospheres and Circumstellar Envelopes of AGB Stars*, 2000, *Ph.D. thesis*, University of Vienna, Institute of Astronomy

Aringer, B., Girardi, L., Nowotny, W., Marigo, P. and Lederer, M. T., 2009, *A& A* **503**, 913

Aringer, B., Kerschbaum, F. and Jörgensen, U. G., 2002, *A& A* **395**, 915

Bartsch, H., *Taschenbuch Mathematischer Formeln*, 2004, Fachbuchverlag Leipzig, Hanser Verlag, 2004, 20.Auflage

Becker, S. A., 1981, *ApJ* **248**, 298

Becker, S. A. and Iben, Jr., I., 1980, *ApJ* **237**, 111

Bernath (ed.), 2005, *Spectra of atoms and molecules*

Bica, E., Bonatto, C., Dutra, C. M. and Santos, J. F. C., 2008, *MNRAS* **389**, 678

Biermann, L., 1951, *ZAp* **29**, 274

Bonatto, C. and Bica, E., 2010, *MNRAS* **403**, 996

Busso, M., Wasserburg, G. J., Nollett, K. M. and Calandra, A., 2007, *ApJ* **671**, 802

Cantiello, M., Hoekstra, H., Langer, N. and Poelarends, A. J. T., Thermohaline Mixing in Low-mass Giants: RGB and Beyond, 2007, in R. J. Stancliffe, G. Houdek, R. G. Martin, & C. A. Tout (ed.), *Unsolved Problems in Stellar Physics: A Conference in Honor of Douglas Gough*, Vol. 948 of *American Institute of Physics Conference Series*, p. 73

Castellani, V., Degl'Innocenti, S., Marconi, M., Prada Moroni, P. G. and Sestito, P., 2003, *A& A* **404**, 645

Chabrier, G., The Initial Mass Function: from Salpeter 1955 to 2005, 2005, in E. Corbelli, F. Palla, & H. Zinnecker (ed.), *The Initial Mass Function 50 Years Later*, Vol. 327 of *Astrophysics and Space Science Library*, p. 41

Charbonnel, C., 1995, *ApJ* **453**, L41

Cohen, J. G., 1982, *ApJ* **258**, 143

Cristallo, S., Straniero, O., Lederer, M. T. and Aringer, B., 2007, *ApJ* **667**,

489
Denissenkov, P. A., Pinsonneault, M. and MacGregor, K. B., 2008, *ApJ* **684**, 757
Deutsch, A. J., 1956, *ApJ* **123**, 210
Eggleton, P. P., Dearborn, D. S. P. and Lattanzio, J. C., 2008, *ApJ* **677**, 581
Feast, M. W., 1963, *MNRAS* **125**, 367
Frogel, J. A., Mould, J. and Blanco, V. M., 1990, *ApJ* **352**, 96
Frogel, J. A., Persson, S. E. and Cohen, J. G., 1980, *ApJ* **239**, 495
Gautschy-Loidl, R., Höfner, S., Jørgensen, U. G. and Hron, J., 2004, *A& A* **422**, 289
Girardi, L., Chiosi, C., Bertelli, G. and Bressan, A., 1995, *A& A* **298**, 87
Glass, I. S. and Evans, T. L., 1981, *Nature* **291**, 303
Goorvitch, D. and Chackerian, Jr., C., 1994, *ApJS* **91**, 483
Grevesse, N. and Noels, A., 1993, *Physica Scripta Volume T* **47**, 133
Groenewegen, M. A. and Marigo, P. (eds.), 2003, *Asymptotic giant branch stars*
Gustafsson, B., Towards a Satisfactory Understanding of AGB-Star Atmospheres?, 2007, in F. Kerschbaum, C. Charbonnel, & R. F. Wing (ed.), *Why Galaxies Care About AGB Stars: Their Importance as Actors and Probes*, Vol. 378 of *Astronomical Society of the Pacific Conference Series*, p. 60
Gustafsson, B., Bell, R. A., Eriksson, K. and Nordlund, A., 1975, *A& A* **42**, 407
Gustafsson, B., Edvardsson, B., Eriksson, K., Jørgensen, U. G., Nordlund, Å. and Plez, B., 2008, *A& A* **486**, 951
Habing, H. J. and Olofsson, H. (eds.), 2003, *Asymptotic giant branch stars*
Herwig, F., 2000, *A& A* **360**, 952
Herwig, F., 2005, *ARA& A* **43**, 435
Herwig, F. and Austin, S. M., 2004, *ApJ* **613**, L73
Herwig, F., Blöcker, T. and Driebe, T., 2000, *Mem. Soc. Astron. Italiana* **71**, 745
Herzberg, G., *Molecular spectra and molecular structure. Vol.1: Spectra of diatomic molecules*, 1950
Hill, V., François, P., Spite, M., Primas, F. and Spite, F., 2000, *A& A* **364**, L19
Hinkle, K., Wallace, L. and Livingston, W. C., *Infrared atlas of the Arcturus spectrum, 0.9-5.3 microns*, 1995
Höfner, S., 2008, *A& A* **491**, L1
Höfner, S., Gautschy-Loidl, R., Aringer, B. and Jørgensen, U. G., 2003, *A& A* **399**, 589
Jeans, J. H., *Astronomy and cosmogony*, 1928

Jørgensen, U. G. (ed.), 1994, *Molecules in the Stellar Environment*, Vol. 428 of *Lecture Notes in Physics, Berlin Springer Verlag*

Jørgensen, U. G., Molecular databases., 1995, in S. J. Adelman & W. L. Wiese (ed.), *Astrophysical Applications of Powerful New Databases*, Vol. 78 of *Astronomical Society of the Pacific Conference Series*, p. 179

Jørgensen, U. G., Cool star models., 1997, in E. F. van Dishoeck (ed.), *IAU Symposium*, Vol. 178 of *IAU Symposium*, p. 441

Jørgensen, U. G., Johnson, H. R. and Nordlund, A., 1992, *A& A* **261**, 263

Joyce, R. R., Observing With Infrared Arrays, 1992, in S. B. Howell (ed.), *Astronomical CCD Observing and Reduction Techniques*, Vol. 23 of *Astronomical Society of the Pacific Conference Series*, p. 258

Karakas, A. I., Current Status of Stellar Evolutionary Models for AGB Stars, 2011, in F. Kerschbaum, T. Lebzelter, & R. F. Wing (ed.), *Why Galaxies Care about AGB Stars II: Shining Examples and Common Inhabitants*, Vol. 445 of *Astronomical Society of the Pacific Conference Series*, p. 3

Karakas, A. I., Lattanzio, J. C. and Pols, O. R., 2002, *pasa* **19**, 515

Kupka, F. G., Ryabchikova, T. A., Piskunov, N. E., Stempels, H. C. and Weiss, W. W., 2000, *Baltic Astronomy* **9**, 590

Lattanzio, J. and Wood, P. (eds.), 2003, *Asymptotic giant branch stars*

Lattanzio, J. C. and Boothroyd, A. I., Nucleosynthesis of elements in low to intermediate mass stars through the AGB phase, 1997, in E. K. Zinner & T. J. Bernatowicz (ed.), *American Institute of Physics Conference Series*, Vol. 402 of *American Institute of Physics Conference Series*, p. 85

Lebzelter, T., Lederer, M. T., Cristallo, S., Hinkle, K. H., Straniero, O. and Aringer, B., 2008a, *A& A* **486**, 511

Lebzelter, T., Lederer, M. T., Cristallo, S., Hinkle, K. H., Straniero, O. and Aringer, B., 2008b, *Astronomy and Astrophysics* **486**, 511

Lederer, M., *Third dredge-up in cluster AGB stars: observational constraints and improved opacity data for models*, 2009, *Ph.D. thesis*, University of Vienna, Institute of Astronomy

Lederer, M. T., Lebzelter, T., Cristallo, S., Straniero, O., Hinkle, K. H. and Aringer, B., 2009, *Astronomy and Astrophysics* **502**, 913

Lloyd Evans, T., 1980a, *MNRAS* **193**, 87

Lloyd Evans, T., 1980b, *MNRAS* **193**, 97

Lloyd Evans, T., 1983, *MNRAS* **204**, 985

Lloyd Evans, T., 1984, *MNRAS* **208**, 447

Loidl, R., Lançon, A. and Jørgensen, U. G., 2001, *A& A* **371**, 1065

Maeder, A. and Zahn, J.-P., 1998, *A& A* **334**, 1000

Moorwood, A., Cuby, J.-G., Biereichel, P., Brynnel, J., Delabre, B., Devillard, N., van Dijsseldonk, A., Finger, G., Gemperlein, H., Gilmozzi, R., Herlin, T., Huster, G., Knudstrup, J., Lidman, C., Lizon, J.-L., Mehrgan,

H., Meyer, M., Nicolini, G., Petr, M., Spyromilio, J. and Stegmeier, J., 1998, *The Messenger* **94**, 7
Mucciarelli, A., Origlia, L. and Ferraro, F. R., 2007, *AJ* **134**, 1813
Nollett, K. M., Busso, M. and Wasserburg, G. J., 2003, *ApJ* **582**, 1036
Palacios, A., Charbonnel, C., Talon, S. and Siess, L., 2006, *A& A* **453**, 261
Reimers, D., 1975, *Memoires of the Societe Royale des Sciences de Liege* **8**, 369
Rejkuba, M., 2004, *A& A* **413**, 903
Renzini, A. and Voli, M., 1981, *A& A* **94**, 175
Rey, S.-C., Yoon, S.-J., Lee, Y.-W., Chaboyer, B. and Sarajedini, A., 2001, *AJ* **122**, 3219
Rousselot, P., Lidman, C., Cuby, J.-G., Moreels, G. and Monnet, G., 2000, *Astronomy and Astrophysics* **354**, 1134
Salpeter, E. E., 1952, *ApJ* **115**, 326
Schönberg, M. and Chandrasekhar, S., 1942, *ApJ* **96**, 161
Schwarzschild, M., *Structure and evolution of the stars.*, 1958
Schwarzschild, M. and Härm, R., 1965, *ApJ* **142**, 855
Stancliffe, R. J. and Glebbeek, E., 2008, *MNRAS* **389**, 1828
Sweigart, A. V. and Mengel, J. G., 1979, *ApJ* **229**, 624
Talon, S. and Charbonnel, C., 2008, *A& A* **482**, 597
Tsuji, T., 1966, *PASJ* **18**, 127
Vassiliadis, E. and Wood, P. R., 1993, *ApJ* **413**, 641
Wasserburg, G. J., Boothroyd, A. I. and Sackmann, I.-J., 1995, *ApJ* **447**, L37
Weigert, A., 1966, *ZAp* **64**, 395
Windsteig, W., Dorfi, E. A., Hoefner, S., Hron, J. and Kerschbaum, F., 1997, *A& A* **324**, 617
Wood, P. R., 1979, *ApJ* **227**, 220
Zahn, J.-P., 1992, *A& A* **265**, 115

9.3 Urheberrechte und Quellenangaben

9.4 Danksagung / Acknowledgement

Mein Dank gilt:

Meinen Betreuern Doz. Dr. Thomas Lebzelter und Dr. Bernhard Aringer für die kompetente fachliche Betreuung dieser Arbeit sowie all unseren anderen Professoren, die uns bisher begleitet haben. Thomas ich möchte dir danken für deine Unterstützung, deine Ratschläge und unsere gute Zusammenarbeit. Als ich mich damals nach einem Diplom-Thema umgesehen habe, hat mir Denise einmal gesagt, das ihr Betreuer in puncto Kompetenz, Hilfestellung und vor allem bez. Fairness in der Zusammenarbeit exzellent ist! Lieber Thomas, das bist du. Auch danke ich dir das du meine Arbeit über die Osterfeiertage korrigiert hast und ich sie dann von dir daheim abholen durfte. Das war heuer quasi der Osterhase für mich!

Lieber "Dotore" Aringer, auch Dir danke ich für die vielen Hilfestellungen per Email und Ratschläge bez. COMA. Auch danke für deine Geduld wenn ich mal öfter das gleiche gefragt habe und das du dir immer Zeit genommen hast für die ausführliche Beantwortung meiner Fragen. Auch danke ich für das Exemplar deiner Diss., die in Sachen COMA sehr wertvoll für mich war. Ohne deine Hilfe wäre diese Arbeit nicht so glatt über die Bühne gegangen (Auch bez. dem Korrektur-Lese-Marathon)!

Ich danke der AGB-Gruppe, wo die Zusammenarbeit so ist wie man sie sich sonst wo nur wünschen kann. Es gibt kaum jemanden von dem ich nicht etwas gelernt habe, oder in irgend einer Art Hilfestellungen bekommen habe!

Allen voran / among all: Denise Lorenz and Claudia Paladini. Really, i do not know what i might have done without both of you. You were there when my motivation sometimes went to -273 K. You helped me with my first talks and presentations and gave me support otherwise with the AGB-stars. Beneath, it is always nice to keep chatting and drinking cups of coffee with you!

Michael Lederer danke ich für den Post-Support bez. Skripte, Emails und Erklärungen. Auch danke ich für das Exemplar Deiner Dissertation. Da ich ja ähnliches gemacht habe, war sie in vielen Bereichen ein Wegweiser für mich!

Walter Nowotny-Schipper danke ich für seine lustige Art und für einen Account auf seinem Rechner Mira zum Rechnen von Sternspektren, als die AGB an ihre Leistungsgrenzen kam und ich meine Diplomarbeit sonst nicht in der

Zeit, bezüglich der Rechnungen, fertig machen hätte können.

Dem Stefan Uttenthaler danke ich für Hilfestellungen bez. der richtigen "Papers" zu Beginn meiner Arbeit. Und vor allem für die Idee meine Spektren zuerst mit hoher Auflösung zu rechnen und danach mit Sphread auf den jeweiligen Stern umzulegen. Brav wie ich war, hätte ich alle Spektren für jeden Stern einzeln gerechnet (-;

Roland Ottensamer danke ich für die Hilfe bei Latex und der Lösung aller Computerprobleme dieses Universums. (Keine Angst, es soll ja ca 10^{500} parallel Universen geben...)

Josef Hron danke ich für den immer währenden Kuchen Support, für die moderaten Kaffee Preise und seine lustigen Kommentare.

Thomas Posch danke ich für die Bestellung des Buches: C++ Programmierung mit Qt 4. Es hat mir zu Beginn meiner SW-Entwicklung sehr geholfen.

Andreas Chwatal danke ich für ein beratendes Gespräch zu Studienbeginn gleich auch Physik mit zu belegen. Physik hat sich als genauso cool wie Astronomie erwiesen! Und für einen Abend bez. Informatik Strategien einen eventuell automatisierten Chi-square in meine Software einzubauen.

Thomas Lebzelter, Bernhard Aringer und Nigel Michell danke ich nochmals für das Korrekturlesen.

Andreas Ruhs danke ich für seine Offenheit und Ehrlichkeit. Als ich meinen Job gekündigt hatte um Musik und Astronomie zu studieren, war mir sein Ausspruch: "Na mit der Kombination kannst du dann maximal als *Sternsinger* gehen...", immer wieder eine Motivation, wenn es bei den Mathematik Vorlesungen grauslich wurde.

Danke auch an den Verein Kuffner-Sternwarte und allen meinen dortigen Freunden. Es war ca. 1998 als ich noch zur Abendschule ging und noch irgend ein Hobby nebenbei brauchte. Da es eines sein musste das man im Dunkeln machen konnte, bin ich zum Astronomie Verein gekommen und habe tatsächlich 6 Jahre später meinen Job gekündigt, um mir meinen Traum, ein Astronomie Studium zu absolvieren, zu verwirklichen. Ich habe das damals beim Sommerfest 2004 bekanntgegeben und mir sind die vielen positiven Reaktionen aller Anwesenden noch heute in Erinnerung. Ich danke allen

recht herzlich die an mich geglaubt haben.

Danke an meine Familie (Mutti, Vati und Claudia), die mich immer größtmöglich unterstützt hat. Die Essenspakete, auch die von meiner Oma, haben meine Studentenkost immer wieder abwechslungsreich ergänzt. Auch meinem Vater danke ich dafür, das er als ich ihm sagte das ich kündigen werde um Musik und Astronomie zu studieren nach kurzem innehalten gemeint hatte: "Du hast immer die richtigen Entscheidungen getroffen, also mach es!", und mir seinen Sanktus gegeben hatte.

Meinem letzten Chef danke ich für sein aufmunterndes Gespräch bei der Kündigung, das ich:"Wohl einen Knall habe, ein hoffnungsloser Fall sei, eine gescheiterte Existenz sein werde, ein arbeitsloser Akademiker den mit 35∼40 keiner mehr will, weil ich dann schon alt sein werde, dann als ein Taxifahrer und Kellner arbeiten würde (Er selbst trinkt wohl nix und geht im Regen zu Fuß nach Hause..), usw. usf. sein werde. Aber wenn ichs mir anders überlege und nach einem Jahr zurück komme würd er mich noch nehmen...". Im Nachhinein war das Gespräch ur lustig.

Der Republik Österreich und der Universität Wien danke ich für die zur Verfügungsstellung der Mittel und Einrichtungen bzw. die Möglichkeit, auch im zweiten Bildungsweg ein Studium zu absolvieren. Ich hoffe das ich davon einmal etwas an die Allgemeinheit zurückgeben kann.

Und last but not least, danke an alle meine Freunde die mich durch die schönsten Jahre meines Lebens, bei Astronomie und Physik begleiten und begleitet haben. Es sind zu viele um alle aufzuzählen, You know who you are!

Und ganz besonders Dir, meine liebe Barbara, möchte ich danke sagen, für die schöne Zeit die wir gemeinsam gehabt haben und die wir noch haben werden. Das Leben mit Dir ist um so vieles schöner geworden. Und die nächste Diplomarbeit wird ein bissi entspannter, ich versprechs (-;

Ansonsten kann ich nur sagen: “Der Weg ist das Ziel!”

Rock ’N’ Roll!!! Love, Peace and the Universe.

The Master[4] of the Universe (-;
Bernhard

Die Arbeit wurde mit Ubuntu Linux: Jaunty 9.04 und Lucid 10.04 und dem freien Latex-Editor TexMaker 1.9.9 erstellt. Die Plots wurden mit dem freien Plotprogramm *“GNUPlot”* 4.4.3 erstellt.

[4]Thesis

9.5 Curriculum vitae

Personal details

Name:	Bernhard Wenzel
Day of birth:	19.03.1977
Place of birth:	Vienna
E-mail:	bernhard.wenzel@gmx.at
Home address:	Dornbacherstraße 74/1/3 1170, Vienna

Univ. address: Bernhard Wenzel
Institute for Astrophysics
Türkenschanzstr. 17
A-1180 Vienna, Austria

Education

1983 - 1987	Elementary school
1987 - 1992	Primary school
1991 - 1992	Technical college (TGM)
1992 - 1995	Apprenticeship at Telekom Austria: Telephone-Technician / Telephone-Installation-Fitter
1996 - 2001	Technical college (night school) at HTL-Schellingasse: Electronics and Computer Engineering

University of Vienna

2004 - 2008	Astronomy: BSc - Astrophysical Computing with GRAPE
2004 - 2008	Pre-degree in Physics
2008 - ongoing	Physics: Master
2008 - 2012	Astronomy: Master with focus on: • Extragalactic Astrophysics and Cosmology. • Starformation and Structure of the Stars including our Sun. • Methods of Astronomy and Astrophysics. • Computational Astrophysics.

Programming skills

C (real time systems), C++, C++ GUI-Interfaces with Qt 4.7, Fortran, Numerical Recipies, Pascal, Visual C++, Microsoft Foundation Classes, HTML, XML, Scripts, BASH, OO and Unified Modelling Language, Linux/Unix, Windows, Opensource, LateX, Gnuplot, Origin, Mathematica, Office, Internet Networks and Security.

Additional skills
Communication and Intercourse 1, Advance your Creativity, Brain Training, Thinking in Objective Goals.

Teaching experience
2011 - ongoing: Night school www.Henriettenplatz.at: Teaching Computer - Science.
2008 - 2011 University of Vienna: Assistant for practical training in physics.
2009 - 2010 University of Vienna: Tutorial for physics freshman.

Working experience
2003 - 2004 Bosch Automotive DSA-Vienna:
Software developing for diesel vehicles for AUDI / VW, motor diagnosis, programming of diagnostic routines, costumer advisory, EDV-support.

2001 - 2003 BEKO-Engineering (Computer Engineering):
Electronic and software development for micro controllers, project management, cost estimations of electronic devices.

1995 - 2001 Telekom Austria:
Technician for Customer advisory and customer care (Selling products, installing telephones and trouble shooting), project management for internet services and commissioning of new products (ADSL, XDSL, ISDN).

Scientific Memberships
ÖGAA - Österreichische Gesellschaft für Astronomie und Astrophysik
(Austrian Society for Astronomy and Astrophysics)
Kuffner-Sternwarte.at

Conferences
2010 august LOC - “Why Galaxies Care About AGB Stars II” - Vienna
2010 april ÖGAA - “Meeting” - Graz
2012 april ÖGAA - “Meeting” - Vienna

Private
Music, Nature, Kuffner-Observatory and University-Observatory (guidances), Hoppy-Astronomy with a 10” Newton telescope, E-guitar, Heavy-Metal.